

https://dspace.org/

The measurement of longitudinal residual stresses in unidirectional glass fibre reinforced plastic

Reid, Robert Grant

2010-03-23T09:11:37Z
http://hdl.handle.net/10539/7756

Downloaded from a DSpace repository. https://dspace.org/

The Measurement of Longitudinal Residual Stresses in Unidirectional Glass Fibre Reinforced Plastic

Robert Grant Reid

A thesis submitted to the Faculty of Engineering and the Built Environment, University of the Witwatersrand, Johannesburg, in fulfilment of the requirements for the degree of Doctor of Philosophy.

Johannesburg, June 2009

Declaration

I declare that this thesis is my own, unaided work, except where otherwise acknowledged. It is being submitted for the degree of Doctor of Philosophy in the University of the Witwatersrand, Johannesburg. It has not been submitted before for any degree or examination at any other university.

Signed this ___ day of _____ 20___

_____

Robert Grant Reid.

To Carla

Acknowledgements

I would like to thank the following people:

Professor Dave Chandler for his supervision.

Professor Ratnam Paskaramoorthy and Dr Jim Huston for their advice and encouragement.

The Research Committee of the School of Mechanical, Industrial and Aeronautical Engineering for funding that allowed aspects of this work to be presented at ICCM-16 in Kyoto.

Ian Schwartz, Ian Campbell and Kamil Midor for their interest and advice.

Mr Jimmy Nicholl for the manufacture of the test fixture.

My partner, Carla, and my parents, Brian and Margaret, for their unwavering support.

Abstract

A wide range of experimental methods exist for estimating residual stresses. None of these methods is suitable, however, for finding the longitudinal residual stresses that exist in an unloaded unidirectional laminate of glass fibre reinforced plastic.

This work presents a method that enables these stresses to be measured. The method exploits the substantial reduction in the modulus of a thermoset matrix above its glass transition temperature, T_g. Restraint forces between the fibres and the matrix are thereby relaxed. The variation in the longitudinal residual strain of the fibres with temperature is estimated by gradually heating the laminate above the matrix T_g whilst monitoring the apparent longitudinal thermal expansion of the laminate.

The longitudinal residual strains in the fibres can be estimated without any knowledge of the fibre or matrix properties. The consistancy of the measured residual strains is improved, however, if the known coefficient of thermal expansion of the fibre is incorporated into the strain calculations. In some situations, the accuracy of the residual strains can be further improved if temperature-dependent material properties for the matrix are also used.

The longitudinal residual stress is easily calculated using Hooke's Law once the residual strains are known. This approach is simple and very convenient because it requires no knowledge of any matrix properties. The accuracy of the residual stress measurements can be improved by considering Poisson's stresses, however, but this is not always possible.

The dramatic reduction in matrix modulus during each test prevents the use of standard methods and so a method to obtain the necessary strain measurements is developed. Strain-gauges cannot be used and an approach based on dilatometry is used instead. Displacement measurements taken between the ends of a specimen give erroneous results, however, and so it is necessary to use reference points that are located within the specimen length.

Three sets of specimens were manufactured that differ in their longitudinal residual

stress. The fibres in two specimen sets were significantly strained during manufacture of the specimens. The stresses in one of these sets were subsequently relaxed through an annealing process. No substantial fibre preloading was used during the manufacture of the third specimen set.

Residual strains are measured in the fibres of the three specimen sets. The general form of the measured strain responses agrees well with the form required by the theoretical basis of the method. The results are also compared with strains predicted using the assumption of linear viscoelasticity in the matrix. The correlation is good except in the case of the annealed specimens. Since these specimens were subjected to non-linear creep during the manufacturing process, it is probable that the discrepancies reflect a deficiency in the theory rather than errors in the measured results.

The residual stresses at ambient conditions are calculated for the three specimen sets. It is not possible to estimate the Poisson's stresses in the annealed specimens, but these stresses do not significantly affect the longitudinal stresses in the other specimen sets. Although the measured residual stresses are small, the corresponding strains in the matrix are rather large.

Published Work

Aspects of this thesis have been published in the following references:

- R.G. Reid and R. Paskaramoorthy. Measurement of residual stress in unidirectional GFRP. In *16th International Conference on Composite Materials*, Kyoto, July 2007.
- R.G. Reid and R. Paskaramoorthy. A novel method to measure residual stresses in unidirectional GFRP. *Composite Structures*, 88(3): 388-393, 2009

Contents

Declaration **i**

Acknowledgements **iii**

Abstract **iv**

Published Work **vi**

Contents **vii**

List of Figures **xvi**

List of Tables **xxii**

List of Abbreviations **xxiv**

List of Symbols **xxv**

1 Introduction **1**

2 Objectives **7**

3 Literature survey **8**

3.1 Methods that monitor the elastic response to the release of residual stresses 8

3.1.1 Layer removal 9
3.1.2 Sachs' method 10
3.1.3 Hole drilling 11
3.1.4 Ring-core method 15
3.1.5 Deep hole drilling 16
3.1.6 Incremental slitting method 18
3.1.7 Contour method 21
3.1.8 Sectioning method 21
3.1.9 Radial cutting method 23
3.1.10 Matrix removal methods 23
3.1.11 Micro-indentation methods 26
3.2 Methods that measure the apparent failure strength 28
3.2.1 First ply failure method 28
3.3 Methods that rely on changes in the material structure 30
3.3.1 X-ray diffraction 30
3.3.2 Neutron diffraction 31
3.3.3 Raman spectroscopy 31
3.3.4 Photoelasticity 33
3.3.5 Acoustic waves 35
3.4 Methods that measure the elastic response to temperature changes . 36
3.4.1 Measurement of curvature 36
3.4.2 Cure referencing method 38

3.4.3 Local heating methods 39

3.5 Proposed new method 40

4 Basis for proposed method **43**

4.1 Finding the residual strain in the fibres 46

4.2 Calculation of residual stress 52

5 Experimental Technique **56**

5.1 Basic equipment 56

5.1.1 Oven 56

5.1.2 Temperature sensor 57

5.1.3 Data logger 57

5.1.4 Computer 57

5.1.5 Power supply 58

5.1.6 GFRP specimens 58

5.2 Measurements using strain gauges 59

5.2.1 Introduction 59

5.2.2 Additional equipment 60

5.2.2.1 Strain gauges 60

5.2.2.2 Specimens 60

5.2.2.3 Wheatstone Bridge 61

5.2.2.4 Strain amplifier 61

5.2.3 Experimental method 62

5.2.3.1 Precautions 63

5.2.4 Results 63
5.2.4.1 Cast resin 64
5.2.4.2 Reinforced specimens 65
5.2.5 Discussion 66
5.2.5.1 Pure resin 66
5.2.5.1.1 Specimen 1 66
5.2.5.1.2 Specimen 2 68
5.2.5.2 Reinforced specimens 70
5.2.6 Conclusions 73
5.3 Initial approach using a dilatometer 73
5.3.1 Introduction 73
5.3.2 Additional equipment 76
5.3.2.1 Specimens 76
5.3.2.2 Displacement transducer 77
5.3.2.3 Target 78
5.3.2.4 Test rig 79
5.3.2.4.1 Frame 80
5.3.2.4.2 Restraints 81
5.3.3 Experimental method 84
5.3.3.1 Attachment of target 85
5.3.3.2 Mounting of the specimen in the test rig 85
5.3.3.3 Test procedure 86

5.3.3.4 Precautions 87
5.3.4 Calibration 87
5.3.5 Results 89
5.3.6 Discussion 92
5.3.6.1 Pure resin 92
5.3.6.2 Reinforced specimens 95
5.3.7 Conclusions 99
5.4 Final design 100
5.4.1 Introduction 100
5.4.2 Modifications to equipment 101
5.4.2.1 Spacing blocks 101
5.4.2.2 Grips 102
5.4.2.3 Target 104
5.4.2.4 Rotational restraints 106
5.4.3 Experimental method 107
5.4.3.1 Mounting of target 107
5.4.3.2 Mounting of the specimen in the test rig 108
5.4.3.3 Cooling of oven 109
5.4.3.4 Test procedure 110
5.4.3.5 Precautions 112
5.4.4 Calibration 112

6 Results **114**

6.1 Response to thermal loading 114

6.1.1 Cast resin 114

6.1.2 Reinforced specimens 114

6.2 Residual strains 118

6.2.1 Residual strains obtained without knowledge of matrix properties 118

6.2.2 Residual strains obtained by considering matrix properties . 121

6.3 Residual stresses 127

6.3.1 Residual stresses obtained without knowledge of matrix properties 127

6.3.2 Residual stresses obtained by considering matrix properties . 128

6.4 Comparison between experiment and theory 130

7 Discussion **136**

7.1 Accuracy of measured strains 136

7.1.1 Pure resin 136

7.1.2 Reinforced specimens 139

7.1.3 Comparison with theory 142

7.2 Residual strains 144

7.2.1 Residual strains obtained without any knowledge of the matrix properties 145

7.2.2 Residual strains obtained with knowledge of the matrix properties 149

7.2.3 Comparison with theory 150

7.3 Residual stresses at 25°C 159

8 Conclusions **162**

9 Recommendations **165**

REFERENCES **166**

A Prediction of the longitudinal thermal expansion of unidirectional GFRP **184**

A.1 Theoretical derivation 184

A.2 Application to published data 190

B Calculation of residual stresses **194**

B.1 Elastic analysis 194

B.1.1 Thermal stresses 194

B.1.1.1 Temperature independent material properties 194

B.1.1.2 Temperature dependent material properties 199

B.1.2 Polymerization shrinkage stresses 202

B.1.3 Preload stresses 205

B.1.4 Combined thermal, shrinkage and preload stresses 209

B.2 Accounting for stress relaxation 210

C Calculation of strain gauge results **212**

C.1 Temperature 212

C.2 Strain 212

C.2.1 Thermal strain of AISI 4340 steel 213

C.2.2 Strain of specimen relative to AISI 4340 214

C.2.3 Overall strain 215

D Calibration of test rig **216**

D.1 Thermal strain of reference materials 216

D.1.1 Aluminium 217

D.1.2 Copper 218

D.1.3 Graphite 219

D.2 Calculation of coefficients C_1 to C_5 for the initial rig 220

D.3 Accuracy of calibration of the initial test rig 221

D.4 Calculation of coefficients C_1 to C_5 for the final rig 221

D.5 Accuracy of calibration of the final test rig 222

E Shear-lag analysis **224**

E.1 Analysis of laminate with maximum fibre dispersion 226

E.1.1 Ambient temperature 227

E.1.2 Elevated temperatures 228

E.2 Analysis of laminate with minimum fibre dispersion 229

E.2.1 Fibre volume fraction within each roving bundle 229

E.2.2 Volume fraction of roving bundles within specimen 231

E.2.3 Diameter of fibre bundles 232

E.2.4 Ambient temperature 233

E.2.5 Elevated temperature 234

E.3 Selection of results for design purposes 236

F Calculation of residual fibre strain **238**

F.1 Matrix strain between T_0 and T_2 239

F.2 Matrix modulus at T_2 241

F.3 Calculation of $\Delta\epsilon$ 244

G Calculation of measured longitudinal stress at 25°C **248**

G.1 Material properties 248

G.2 Effect of different loads 253

G.2.1 Thermal strains 253

G.2.2 Strains arising as laminate is heated from the cure temperature to the post-cure temperature 255

G.2.3 Preload strains 256

G.2.4 Relaxation strains 258

G.3 Unloaded specimens 259

G.3.1 Residual fibre stresses at 25°C 259

G.3.2 Comparison between theoretical predictions and experiment . 261

G.3.3 Residual matrix stresses and strains at 25°C 262

G.4 Preloaded specimens 264

G.4.1 Residual stresses at 25°C 264

G.4.2 Comparison between theoretical predictions and experiment . 266

G.4.3 Residual matrix stresses and strains at 25°C 269

G.5 Annealed specimens 270

G.5.1 Residual stresses at 25°C 271

List of Figures

4.1 Temperature variation of modulus in Derakane 411-350 44

4.2 Illustrative longitudinal thermal response of EPON 828/E-glass laminate 46

4.3 Extrapolation of the linear response at high temperatures defines the locus of zero fibre stress 47

4.4 Variation in the residual strain in the fibre with temperature 48

4.5 Corrected locus of zero fibre stress 50

4.6 Corrected variation of residual fibre strain 50

5.1 Schematic layout of Wheatstone bridge connections 62

5.2 Apparent strain in cast resin - Gauges affixed with cyanoacrylate . . 64

5.3 Comparison between apparent strains obtained from specimens with different strain-gauge adhesives 65

5.4 Apparent strain in glass fibre reinforced specimens 66

5.5 Position of displacement sensor relative to target 77

5.6 Spread of electric field lines 79

5.7 Configuration of specimen and measurement system 79

5.8 Test rig including specimen 80

5.9 Configuration of test frame 81

5.10 Cross-section through a jaw of the "knife-edge" grips 82

5.11 Specimen positioned within clamping jaws 82

5.12 Configuration of grip assembly on backing plate 83

5.13 Tensioned carbon threads attached to specimen - Spacing legs are not shown in the interests of clarity 84

5.14 Comparison between reference thermal strains and calibrated measurements 89

5.15 Measured strain in cast resin as a function of temperature 90

5.16 Measured strain in unloaded specimens as a function of temperature 90

5.17 Measured strain in preloaded specimens as a function of temperature 91

5.18 Measured strain in annealed specimens as a function of temperature 91

5.19 Locus of zero stress in glass fibres 93

5.20 Residual strain in glass fibres of unloaded specimens 93

5.21 Residual strain in glass fibres of preloaded specimens 94

5.22 Residual strain in glass fibres of annealed specimens 94

5.23 Surface roughness profile on the end face of preloaded specimens . . 98

5.24 Final configuration of test frame 101

5.25 Fitment of spacer blocks around sensor 102

5.26 Configuration of grip assembly 102

5.27 Steel ball positioned between tightening screw and sliding jaw 104

5.28 Configuration of target support 105

5.29 Target assembly mounted on specimen 106

5.30 Rods used to provide rotational restraint 107

5.31 Arrangement of rods providing rotational restraint - Front spacing legs are omitted for clarity 107

5.32 Effect of rate of oven cooling on measurement linearity 110

5.33 Comparison between reference thermal strains and calibrated measurements 113

6.1 Measured strain in cast resin as a function of temperature 115

6.2 Comparison of the measured thermal strain of cast resin obtained using the final test rig and strain gauges 115

6.3 Measured strain in unloaded specimens 116

6.4 Measured strain in preloaded specimens 116

6.5 Measured strain in annealed specimens 117

6.6 Comparison between measured strains in different specimen types . . 117

6.7 Locus of zero stress in glass fibre 119

6.8 Residual strain in glass fibres of unloaded specimens 119

6.9 Residual strain in glass fibres of preloaded specimens 120

6.10 Residual strain in glass fibres of annealed specimens 120

6.11 Comparison between residual strains in glass fibres of different specimen types 121

6.12 Improved method of finding the locus of zero stress in the glass fibre 122

6.13 Residual strain in glass fibres of unloaded specimens 122

6.14 Residual strain in glass fibres of preloaded specimens 123

6.15 Residual strain in glass fibres of annealed specimens 123

6.16 Comparison between residual strains in glass fibres of different specimen types 124

6.17 Residual strain in glass fibres of unloaded specimens 125

6.18 Residual strain in glass fibres of preloaded specimens 126

6.19 Residual strain in glass fibres of annealed specimens 126

6.20 Comparison between residual strains in glass fibres of different specimen types 127

6.21 Comparison between predicted residual strain variation and experimental data - Unloaded specimens 132

6.22 Comparison between predicted strain variation and experimental data - Unloaded specimens 132

6.23 Comparison between predicted residual strain variation and experimental data - Preloaded specimens 133

6.24 Comparison between predicted strain variation and experimental data - Preloaded specimens 134

6.25 Comparison between predicted residual strain variation and experimental data - Annealed specimens 135

6.26 Comparison between predicted strain variation and experimental data - Annealed specimens 135

7.1 Hypothetical changes to matrix modulus 155

7.2 Predicted response of unloaded specimens when using manufacturer's data for CTE 157

A.1 Predicted longitudinal CTE for unidirectional GFRP 185

A.2 Development of thermal strains in GFRP 187

A.3 Illustrative thermal strains in polymer matrix 187

A.4 Properties of EPON 828 cured with Jeffamine D400 190

A.5 Illustrative longitudinal thermal response of EPON 828/E-glass laminate 193

B.1 Variation in ratio between radial and longitudinal stresses in the fibres 197

B.2 Increase in fibre stress relative to that found using Hooke's Law . . . 199

B.3 Variation in ratio between radial and longitudinal stress in the fibres 207

B.4 Increase in fibre stress relative to that found using Hooke's Law . . . 208

D.1 Comparison of measured strains with reference strains 221

D.2 Comparison of measured strains with reference strains 223

E.1 Fibre within hexagonal unit cell 230

F.1 Definition of ϵ_{0-2} and s_{0-2} 239

F.2 Correlation between measured strains and fitted curves 240

F.3 Correlation between measured matrix modulus and fitted curve . . . 241

F.4 Temperature variation of tan δ in Derakane 411-350 243

F.5 Residual strain in glass fibres of unloaded specimens 245

F.6 Residual strain in glass fibres of preloaded specimens 246

F.7 Residual strain in glass fibres of annealed specimens 246

G.1 Correlation between measured modulus and fitted curves 250

G.2 Correlation between measured strain and fitted curves 253

G.3 Response of the fibre strain to changes in matrix and laminate properties 254

G.4 Variation of $\frac{A_1}{A_3}$ as function of temperature and ΔT_{shift} 255

G.5 Response of the fibre strain to changes in matrix and laminate properties 257

G.6 Comparison between predicted residual strain variation and experimental data 263

G.7 Comparison between predicted strain variation and experimental data 263

G.8 Comparison between predicted residual strain variation and experimental data 268

G.9 Comparison between predicted strain variation and experimental data 268

G.10 Comparison between predicted residual strain variation and experimental data 272

G.11 Comparison between predicted residual strain variation and experimental data 272

G.12 Comparison between predicted residual strain variation and experimental data 273

List of Tables

5.1 Coefficients of thermal expansion of pure resin 65

5.2 Apparent coefficients of thermal expansion of reinforced resin 65

5.3 Coefficients of thermal expansion at temperatures $\leqslant$50℃ 92

5.4 Coefficients of thermal expansion at temperatures $\geqslant$120℃ 92

6.1 Coefficients of thermal expansion from 25℃ to 50℃ 118

6.2 Coefficients of thermal expansion from 115℃ to 140℃ 118

6.3 Residual strain in glass fibres at 25℃ 124

6.4 T_0 and $\Delta\epsilon$ 125

6.5 Residual strain in glass fibres at 25℃ 127

6.6 Residual strains and stresses at 25℃ in longitudinal direction 128

6.7 Residual strains and stresses at 25℃ 130

A.1 Elastic constants used in calculation of CTE 185

A.2 Storage modulus vs. temperature 191

A.3 Variations in thermal strain and effective thermal expansion 192

C.1 Coefficients of thermal expansion for AISI 4340 steel 213

C.2 Thermal expansion of AISI 4340 steel 213

D.1 Coefficients of thermal expansion for Aluminium 1100 217

D.2 Thermal expansion of Aluminium 1100 217

D.3 Coefficients of thermal expansion for Copper C10200 218

D.4 Thermal expansion of Copper C10200 218

D.5 Best-fit calibration coefficients for the initial test rig 221

D.6 Best-fit calibration coefficients for the final test rig 222

F.1 T_0 and $\Delta\epsilon$ 245

F.2 Residual strain in glass fibres at 25℃ 247

G.1 Elastic constants of E-glass fibre 253

List of Abbreviations

$\mu\epsilon$	Micro-strain (Strain$\times 10^6$)
BNC	Bayonette Nut Coupling
CT	Compact Tension
CTE	Coefficient of Thermal Expansion
DHD	Deep Hole Drilling
DIC	Digital Image Correlation
DMA	Dynamic Mechanical Analysis
EAC	Environmentally Assisted Cracking
EDM	Electric Discharge Machining
EDWM	Electric Discharge Wire Machining
ESPI	Electronic Speckle Pattern Interferometry
GFRP	Glass Fibre Reinforced Plastic
HDT	Heat Distortion Temperature
LDH	Layered Double Hydroxides
RH	Relative Humidity
T_g	Glass transition Temperature
TMA	ThermoMechanical Analysis
UPS	Uninterruptable Power Supply

List of Symbols

α	Coefficient of thermal expansion (CTE)
α_{c_L}	Longitudinal CTE of composite laminate
$\alpha_{c_{L_0 1}}$	Effective longitudinal CTE of composite laminate between temperatures T_0 and T_1
$\alpha_{c_{L_1 2}}$	Effective longitudinal CTE of composite laminate between temperatures T_1 and T_2
α_f	CTE of fibre
α_{f_L}	Longitudinal CTE of fibre
α_{f_T}	Transverse CTE of fibre
$\alpha_{m_{01}}$	Effective CTE of matrix between temperatures T_0 and T_1
$\alpha_{m_{02}}$	Effective CTE of matrix between temperatures T_0 and T_2
α_{st}	CTE of steel
β	γ/r
γ	A measure of the ratio of shear stiffness to longitudinal stiffness in a unidirectional laminate
$\Delta\epsilon$	Offset between the strain of the composite at the relaxation temperature and the strain of unstressed glass fibre
$\Delta\epsilon_{cal}$	Change in calibrated strain
ΔT	Change in temperature
ΔT_{cal}	Change in temperature during calibration procedure

ΔT_{shift}	Temperature offset for time-temperature equivalence
ΔV_{cal}	Change in voltage during calibration procedure
ϵ	Strain
ϵ_{0-1}	Strain in composite between temperatures T_0 and T_1
ϵ_{0-2}	Strain in composite between temperatures T_0 and T_2
ϵ_{1-2}	Strain in composite between temperatures T_1 and T_2
ϵ_{θ}	Residual circumferential strain of fibre
$\epsilon_{al_{thermal}}$	Free thermal strain of aluminium
$\epsilon_{cu_{thermal}}$	Free thermal strain of copper
ϵ_{f}	Longitudinal fibre strain
$\epsilon_{f_{0-1}}$	Longitudinal strain of fibre between temperatures T_0 and T_1
$\epsilon_{f_{mech}}$	Longitudinal fibre strain resulting from mechanical loading
$\epsilon_{f_{thermal}}$	Free longitudinal thermal strain of fibre
$\epsilon_{graphite_{thermal}}$	Free thermal strain of graphite
ϵ_{m}	Longitudinal matrix strain
$\epsilon_{m_{0-1}}$	Longitudinal strain of matrix between temperatures T_0 and T_1
$\epsilon_{m_{mech}}$	Longitudinal matrix strain resulting from mechanical loading
$\epsilon_{m_{thermal}}$	Free longitudinal thermal strain of matrix
ϵ_{max}	Calibrated strain at maximum amplifier output
$\epsilon_{measured}$	Measured strain
ϵ_{r}	Residual radial strain of fibre
$\epsilon_{relative}$	Free thermal expansion of graphite relative to that of steel

$\epsilon_{st_{thermal}}$	Free thermal strain of steel
$\epsilon_{x_{measured}}$	Measured strain in x direction
$\epsilon_{x_{relative}}$	Free thermal expansion of graphite in x direction relative to that of steel
$\epsilon_{y_{measured}}$	Measured strain in y direction
$\epsilon_{y_{relative}}$	Free thermal expansion of graphite in y direction relative to that of steel
ϵ_z	Residual longitudinal strain of fibre
ϵ_{z_p}	Residual longitudinal strain of fibre caused by fibre preload
ϵ_{z_s}	Residual longitudinal strain of fibre caused by polymerization shrinkage
ϵ_{z_t}	Residual longitudinal strain of fibre caused by thermal loading
κ	Average ratio between transverse stresses and longitudinal stresses over a temperature range
$\mu_\circ$	Poisson's ratio of calibration material
ν	Poisson's ratio
ν_f	Poisson's ratio of isotropic fibre
$\nu_{f_{LT}}$	Longitudinal Poisson's ratio of fibre
$\nu_{f_{TT}}$	Transverse Poisson's ratio of fibre
ν_m	Poisson's ratio of matrix
σ_0	Average longitudinal stress applied to unidirectional laminate
σ_f	Longitudinal fibre stress
σ_{f_∞}	Longitudinal fibre stress far removed from a fibre break
σ_θ	Circumferential residual stress applied to fibre
σ_m	Longitudinal matrix stress

σ_r	Radial residual stress applied to fibre
σ_z	Longitudinal residual stress applied to fibre
σ_{z_p}	Longitudinal residual stress applied to fibre by fibre preload
σ_{z_s}	Longitudinal residual stress applied to fibre by polymerization shrinkage
σ_{z_t}	Longitudinal residual stress applied to fibre by thermal loading
$[A]$	A matrix similar to a compliance matrix
$\bar{A}$	Effective cross-sectional area of a roving bundle
$A_\circ$	Cross-sectional area of a fibre
A_1	A constant with units of stress
$A_1(S)$	A_1 evaluated at shrinkage state S
$A_1(S,T)$	A_1 evaluated at shrinkage state S and temperature T
$A_1(S,T_1)$	A_1 evaluated at shrinkage state S and temperature T_1
$A_1(T)$	A_1 evaluated at temperature T
$A_1(T_1)$	A_1 evaluated at temperature T_1
A_3	A constant with units of stress
$A_3(S)$	A_3 evaluated at shrinkage state S
$A_3(S,T)$	A_3 evaluated at shrinkage state S and temperature T
$A_3(S,T_1)$	A_3 evaluated at shrinkage state S and temperature T_1
$A_3(T)$	A_3 evaluated at temperature T
$A_3(T_1)$	A_3 evaluated at temperature T_1
A_Δ	One sixth of the area of a hexagon enclosing a fibre cross-section

A_g	Cross-sectional area of all glass fibres within a fibre bundle
$C_{0...10}$	Coefficients in a series fitted to experimental data
d	Fibre diameter
$\bar{D}$	Effective diameter of a roving bundle
E	Modulus of elasticity
$\bar{E}_b$	Effective longitudinal modulus of a fibre bundle
E_c	Longitudinal modulus of elasticity of composite laminate
E_f	Modulus of elasticity of fibre
E_{f_L}	Longitudinal modulus of elasticity of fibre
E_{f_T}	Transverse modulus of elasticity of fibre
E_m	Modulus of elasticity of matrix
E_{m_1}	Modulus of elasticity of matrix at temperature, T_1
E_{m_2}	Modulus of elasticity of matrix at temperature, T_2
g_p	Gain factor for longitudinal stress relative to that calculated using Hooke's Law. Stresses arise from fibre prestrain.
$g_s^{'}$	Gain factor for longitudinal stress relative to that calculated using Hooke's Law. Stresses arise from polymerization shrinkage, matrix properties are temperature and cure state dependent.
g_t	Gain factor for longitudinal stress relative to that calculated using Hooke's Law. Stresses arise from thermal loading, matrix properties are temperature independent.
$g_t^{'}$	Gain factor for longitudinal stress relative to that calculated using Hooke's Law. Stresses arise from thermal loading, matrix properties are temperature dependent.
$\bar{G}_b$	Effective shear modulus of a fibre bundle
G_f	Shear modulus of fibre

G_m	Shear modulus of matrix
k_p	Ratio of the transverse stresses and longitudinal residual stresses arising from fibre prestrain
k_t	Ratio of the transverse stresses and longitudinal residual stresses arising from thermal loads
K	Transverse sensitivity of strain gauge
l	Length of each side of a hexagon enclosing a fibre cross section
L	Fibre length
P	Prestrain applied to fibre
$\Re$	Aspect ratio of fibre ($\frac{L}{d}$)
r	Fibre radius
S	Polymerization shrinkage
S_{11}	Term in a compliance matrix
S_{12}	Term in a compliance matrix
t	Tex value of a fibre bundle
T	Temperature
T_0	Strain-free temperature
T_1	An arbitrary temperature
T_2	Another arbitrary temperature, relaxation temperature
$T_{post-cure}$	Post-cure temperature
V	Voltage
$\bar{V}_b$	Volume fraction of homogeneous fibre bundles
V_f	Fibre volume fraction
$V_{f_{max}}$	Maximum possible fibre volume fraction

V_m	Matrix volume fraction
$\bar{V}_m$	Volume fraction of matrix around homogeneous fibre bundles
z	Longitudinal position along fibre
z_{99}	Position along fibre where longitudinal stress reaches 99% of far-field stress

1 Introduction

A composite consists of two or more macroscopically distinct materials acting together in combination. One constituent provides the structural strength and stiffness and is known as the reinforcing phase. The material in which it is embedded is known as the matrix.[1] Natural examples of composite materials that have been exploited by mankind include wood, bone and leather. Since earliest recorded times, however, composite materials have also been developed to satisfy particular needs. Examples include the use of straw to reinforce clay bricks and sticks to reinforce mud walls. The development of composite materials began to accelerate when thermosetting resin systems with useful mechanical and adhesive properties became available between the two World Wars. When glass fibre became commercially available around the time of the Second World War it could be combined with these resin systems to produce the first modern composite: glass fibre reinforced plastic (GFRP). The technology has advanced tremendously, and resin systems currently used include polyester, vinyl-ester, epoxy, polymide and silicone.[1] Fibres include a wide range of glass, boron, carbon, aramid and quartz.[2]

In recent years, the fibre reinforced plastics industry has grown rapidly. In 2006 the global market, including suppliers and composite applications, was approximately US$ 50 billion.[3] The corrosion segment is the third largest, after transport and construction, accounting for approximately 12% of this total.[4] Applications within this market are very broad and include as a sample; treatment of water and waste, processing of chemicals, manufacture of foodstuffs, processing of pulp and paper, refining of precious metals and flue gas desulphurization systems in coal-fired power stations. Fibre reinforced plastics are used in these applications because their inherent corrosion resistance allows superior performance at lower cost than obtainable using traditional, high-nickel alloys. Savings are attainable in material cost, manufacturing ease when building complex shapes and installation cost.[4]

Although the use of carbon fibres is growing rapidly,[2] glass fibre is still by far the most commonly used reinforcement material in fibre reinforced plastics. In 2006,

approximately 163 000 metric tons of fibres were used worldwide in the manufacture of composites with E-glass fibre making up 80% of this total.[2] The main reason that glass fibre is so dominant in the market is its comparatively low cost. Analysis of Roberts's[2] data reveals that the average cost of carbon fibre is approximately 26 times greater per unit mass than that of E-glass fibre. The density of E-glass fibre is significantly higher than that of carbon fibre and so the cost per unit volume is even greater. Unless performance requirements demand the use of an advanced fibre, E-glass is the reinforcement of choice.

The corrosion market consequently makes extensive use of E-glass fibre for structural purposes. In most corrosion equipment the resin system used in the structural laminate is vinyl-ester[5] because it is regarded as a good compromise between polyester and epoxy resins. Although polyester resins are cheaper, vinyl-ester resins are less brittle and have better corrosion and thermal properties.[6] Vinyl ester resins are also significantly more affordable than epoxy resins.[6] In all but the least demanding applications, the structural laminate is protected from corrosion by means of a liner. The liner is usually a resin rich laminate comprising a veil of C-glass or synthetic fibre backed by a few layers of chopped strand mat[i].

Damage to the liner can, however, expose the underlying structural laminate to the corrosive medium. Although GFRP displays exceptional resistance to corrosion, it is susceptible to environmentally assisted cracking (EAC). This mode of failure is characterized by the flat nature of the fracture surface which in all cases propagates through fibres or fibre bundles at right angles to the fibre direction.[7] This contrasts with the fracture of GFRP in air which displays debonding, delamination and fibre pullout.[7]

The rate of crack growth in GFRP depends on the crack tip stress intensity in a power-law relationship.[8] Since the crack tip stress intensity is proportional to the overall tensile stress, it is apparent that the rate of crack growth is significantly dependent on the applied stress. The rate of crack growth depends also on the type of resin system, although it has been found that the chemical resistance of the resin system is not significant in this regard. Instead, it is the mechanical properties of the resin system that have an effect on the rate of crack growth by determining the extent to which the stresses acting on the fibres at the crack tip are modified through plasticity.[7,8] The corrosive medium does not appear to gain access to the fibres through diffusion, but rather by flowing through microcracks in the matrix that arise as a result of stress intensification ahead of the crack tip.[9]

[i] In more demanding applications a thermoplastic liner such as high density polyethylene can be used. In extremely corrosive environments, the liner is often some form of fluoroplastic.

Because the rate at which EAC progresses in GFRP is heavily dependent on the applied tensile stress, design codes used for corrosion applications limit the stress and consequent strains through the use of large design factors[ii]. These codes, however, only consider the effects of mechanical loading. Residual stresses are not considered. These stresses are typically small, but, because of the low stresses stipulated by the design codes, they can be comparable with those arising from mechanical loads. The overall stress state is therefore misrepresented if the residual stresses are not considered, potentially increasing the risk of failures associated with EAC.

Residual stresses arise at three size scales, all of which must be considered when determining the overall state of stress. At the macro- or structural-scale, residual stresses arise as a result of one part of the structure acting against another. This can occur when one component experiences different thermal strains from another, or as a result of external constraints. At the meso- or laminate-scale, residual stresses arise through individual laminae experiencing different unconstrained thermal and hygroscopic strains from those of adjacent laminae. This effect can arise from temperature and moisture variation through the laminate thickness and from changes in material properties or orientation from lamina to lamina. At both the macro- and meso-scales, the fibres and matrix are strained equally, and consequently, the effects of residual stresses at these scales are indistinguishable from mechanical stresses[iii]. This is not true at the micro- or lamina-scale. At this scale, stresses in the fibre and matrix act against each other even if the lamina appears unloaded at larger size scales. The residual stresses in this situation arise from differences in the unconstrained thermal and hygroscopic strains of the fibres and the matrix. Additional residual stresses can be set up at this scale through polymerization cure shrinkage of the matrix. Residual stresses are set up both aligned with, and perpendicular to, the fibre direction. The fibres are, however, able to significantly limit the free movement of the resin system in a direction aligned with their length. The stresses in this direction are consequently significantly larger than those perpendicular to the fibre direction. The magnitude of the latter stresses is therefore of little concern, especially since these stresses are not aligned in a direction that promotes environmentally assisted cracking of the laminate.

The residual stresses at the micro-scale exist in conjunction with the overall stress

[ii] BS-4994[10] specifies a minimum allowable design factor of 8 while simultaneously limiting the strain to a maximum of 2000 $\mu\epsilon$ or 0.1% of the strain to failure of the unreinforced resin system whichever is the smaller. ASME/ANSI RTP-1[11] specifies a minimum allowable design factor of 8 in the liner.

[iii] It follows that residual stresses at the macro- and meso-scales should be considered in the design of corrosion resistant GFRP structures, especially if they increase the tensile stress in the liner.

state arising from both the mechanical loading and the macro- and meso-scale residual stresses and they therefore modify the overall stress state. Tensile residual stresses at the micro-scale that tend to assist in opening microcracks in the polymer matrix ahead of the crack could be expected to promote the flow of corrosive media to the glass fibres, potentially increasing the rate of crack growth. This scenario is frequently encountered because corrosion equipment is usually cured at room temperature and then subjected to post-cure at elevated temperatures in order to improve the chemical resistance of the resin system.[12] In this case, the comparatively high thermal contraction of the resin system when the laminate cools to room temperature is largely prevented by the relatively stiff fibres. In addition, the fibres can also inhibit the free shrinkage of the resin caused by the additional polymerization reactions during post-cure. The resin system is thus loaded in tension while the fibres are placed into compression. The tensile stress in the resin must, to some degree, make it more susceptible to microcracking. On the other hand, the reduction in tensile stress in the fibres reduces their tendency to fracture. The increased percolation of corrosive media to the fibres may therefore be offset by the longer time required for flaws of critical size to develop in the fibres.

The relationship between micro-scale residual stresses and the rate of EAC in GFRP has not, however, been studied to any great extent. An investigation into this issue requires measurement of both the micro-scale residual stresses and the rate of EAC. Since unidirectional fibre reinforcement defines the simplest possible laminate, specimens of this configuration should be studied first. While investigations into EAC in laminated composites have employed a number of different techniques, most work has concentrated on using compact tension (CT) specimens to correlate the rate of EAC with stress intensity.[8, 13–15] Good results have been obtained using this approach, but it is perhaps not necessary, in an investigation into the effect of micro-scale residual stresses, to consider a wide range of nominal stress intensities. A simpler, and still illuminating, study can be performed by merely determining, for different micro-scale residual stresses, the nominal threshold stress intensity below which EAC ceases.

The threshold stress intensity can be readily found by controlling the displacement rather than the load applied to appropriate specimens. As a crack propagates across a specimen loaded in bending, for instance, its elastic stiffness is reduced. As a consequence, the bending moment reduces with crack length for a fixed displacement.[16] Even though the stress intensity increases with crack length for a given moment,[17] the reduction in moment with crack length is sufficient to ensure that the stress intensity also reduces with crack length. One way of exploiting this phenomenon

is to fabricate GFRP specimens with differing levels of micro-scale residual stress and, after initiating cracks at the specimen edges, to apply a bending deflection such that the cracks are on the tensile surfaces. The specimens are then immersed in a corrosive medium so that EAC commences. The stress intensity factor reduces as the crack length grows, and, after sufficient time has passed, the rate of crack growth is minimal. The corresponding stress intensity factor can then be taken as an estimation of the threshold below which EAC does not occur.

It is, of course, also necessary to determine the micro-scale residual stresses at the completion of such a test[iv]. An experimental method of estimating these stresses is therefore required. The requirements of this experimental method are defined by those of the EAC investigation. The method must allow the longitudinal residual stresses in a unidirectional GFRP specimen to be found after it has been immersed in a corrosive medium for some time. Individual specimens used to obtain residual stress measurements must be obtainable from those used in the EAC investigation. This means that the requirements for the specimens used in the residual stress measurements are identical to those of the specimens used in the EAC investigation. The specimens must therefore be representative of laminates used in corrosion applications in industry. Most corrosion structures are cured at room-temperature and are then subjected to post-cure to improve their corrosion resistance. The post-cure process is accordingly necessary in the manufacture of the specimens. Modifications to the resin system, fibre or interface material could interfere with the processes involved in EAC and are consequently not permitted. The specimens must therefore be manufactured from the standard fibres and resin systems used in industrial environments. In addition, since real structures contain fibres in the form of bundles, these are necessary in the specimens and hence single fibre model composites cannot be used. This requirement allows elastic interaction between the fibres of a bundle to occur as a crack grows through it. To facilitate interpretation of the experimental results obtained from the EAC investigation, the fibre bundles should be uniformly distributed within the specimens. This requirement implies that the overall volume fraction of the specimen cannot be very low and, in addition, the minimum thickness should be several times larger than the minimum dimension of the bundle.

[iv]It should be recognized that each specimen is immersed in the corrosive medium for a considerable period. During this time, moisture diffuses into the laminate causing the residual stress state to change.

The minimum specifications of the experimental technique can now be summarized. The technique must:

- be able to estimate the micro-scale residual stresses in the longitudinal direction of unidirectional GFRP.
- accommodate long-term immersion of specimens in a corrosive medium prior to testing.
- not require modification of commercially available fibres and resin systems.
- be applicable to laminates manufactured with thermoset resins that cure at room-temperature and which are subsequently subjected to a post-cure treatment.
- allow fibre bundles to be thoroughly dispersed throughout the specimen volume.

Not only do these requirements ensure that the relationship between micro-scale residual stresses and the EAC can be investigated, but if a significant link is found, they enable these stresses to be assessed for the particular resin systems and cure cycles used in specific industrial applications. Meeting these specifications by using low-cost and freely available equipment would thus be advantageous.

Many methods are available for measuring residual stresses, but, as discussed in Chapter 3, none are able to satisfy the requirements listed above. It is therefore necessary to devise an alternative technique. It is the purpose of the present work to develop such a technique.

2 Objectives

The development of an experimental method to estimate the micro-scale residual stresses in the longitudinal direction of a unidirectional GFRP laminate is the sole objective of this work.

The method is intended for use in an investigation into the effects of residual stresses on the rates of EAC and so it must:

- be applicable to specimens that have been immersed in a corrosive medium for a considerable period.
- not be dependent on modification of the standard fibres and resin systems used in industrial applications.
- enable testing of specimens manufactured using room-temperature curing thermoset resins.
- be unaffected by the post-curing of specimens at elevated temperatures.
- allow testing of specimens within which fibre bundles are uniformly distributed throughout the thickness.

3 Literature survey

A wide range of experimental methods for measuring residual stresses exist. They can be split into four approaches:

- Methods that monitor the elastic response to the release of residual stresses.
- Methods that measure changes to the apparent failure strength.
- Methods that rely on changes in the material structure.
- Methods that measure the elastic response to temperature changes.

Each of these approaches contains within it a number of techniques, with their own individual benefits and disadvantages. Before it can be stated that a measurement technique that meets the objectives of this work has not been presented in the literature, it is necessary to consider the applicability of each of these techniques in turn. Even if it transpires that they cannot be directly applied, it is possible that variants and combinations of current techniques might be found to be applicable.

The following section consequently considers every method of residual stress measurement found by the author in the literature. If a particular method is found to be unsuitable for the objectives of this work, possible variations are considered with a view to overcoming the deficiencies.

3.1 Methods that monitor the elastic response to the release of residual stresses

Methods that monitor the elastic response of a laminate to the release of residual stresses are probably the most widely used of the residual stress measurement techniques. A variety of methods for releasing residual stresses within a laminate are

consequently available. These include layer removal, Sachs' method, hole drilling, the ring-core method, deep hole drilling, the incremental slitting method, the contour method, the sectioning method, the radial cutting method, matrix removal methods and micro-indentation techniques. Each of these methods is discussed in the following sections.

3.1.1 Layer removal

The layer removal method involves the removal of thin layers of material from one surface of a plate. The internal stresses that were originally present in this layer are thus eliminated and the plate consequently curves to restore force equilibrium. By measuring the strain and curvature of the laminate as successive layers are removed, it is possible to derive the stress profile through the original laminate.

The method was originally developed by Treuting and Read[18] for metallic plates with through-thickness variations in residual stress. When applied to composite laminates, removal of the layers can be achieved by machining processes,[19–21] splitting with a knife[22] or by placing separation films within a laminate during cure.[23, 24] If separation films are used, the laminate can be sequentially parted at the films without the use of significant force. This makes the technique easier to use and provides more reproducible data than machining.[24] This is presumably because the method inherently separates the laminate between plies and does not introduce additional residual stresses during the removal of material.

The layer removal method cannot be applied to measuring the micro-scale residual stresses in a unidirectional GFRP laminate. Each layer that is removed has a thickness far larger than the fibre diameter and consequently it is not possible to remove either matrix material or fibres individually. The material removed thus contains both constituents. Since the micro-scale stresses acting in the fibre and matrix are in mutual equilibrium, removal of the layer is equivalent to removing an unstressed layer of material and no bending response results[i].

[i] If the method was to be attempted, it is quite possible that some bending response would be measured. This would not be the result of releasing micro-scale residual stresses, but rather the result of releasing meso-scale residual stresses resulting from a non-uniform stress profile through the thickness of the laminate. Such a profile could be caused by the cooling rate varying through the thickness, or even by machining stresses arising from the layer removal process.

3.1.2 Sachs' method

Sachs' method[25] is very similar to the layer removal method except that it is applied to rods and tubes rather than plates. The technique allows axial, circumferential and radial residual stresses to be determined.

The method involves progressively removing "tubes" of material from the centre of a circular section. As each radial increment is removed, the residual stresses within this material are released and the remaining material responds elastically. The response is typically measured using strain gauges aligned axially and circumferentially on the outer surface of the section.

A variant of the method allows for removal of material from the outer surface of tubes. In this case, the strain gauges are positioned on the inner surface of the tube. This approach can be used to complement the original method.[26, 27]

Although originally developed for axisymmetric residual stress states, Sachs' method has been extended[28, 29] to allow measurement of non-axisymmetric residual stresses.

Sachs' method has been widely used on components made from isotropic materials. The residual stress distribution has been measured in autofrettaged steel tubing,[27] cold drawn steel bar,[30] quenched stainless-steel tubing,[26] case hardened steel rod[31] and cold expanded holes in aluminium alloy.[32–34] Residual stresses in plasma sprayed ceramic coatings[35] and alumina-steel joints[36] have also been measured. Material removal methods such as drilling,[30, 31] boring,[26, 29, 33–35] electric discharge machining (EDM),[32, 37] etching[35] and electro-chemical machining[38] have been used in these investigations.

It appears that Sachs' method has not been applied to fibre reinforced plastic tubes even though the original work has been extended to include orthotropic materials with principal axes aligned with the axes of the cylindrical coordinate system.[38–40] These works have been used in the measurement of the residual stresses in cold-drawn Cu 1.8 wt% Be rods[37] and pilgered Zircaloy-4(R) tubes,[38] but it appears that an extension that allows for lamination[41] has not seen application in any experimental investigation.

Although these analysis techniques can be applied to measuring the residual stresses in laminated composite tubes, Sachs' method cannot be used to find the micro-scale residual stresses in a unidirectional GFRP laminate. The reason for this is identical to that preventing the use of the layer removal process for this purpose -

the technique does not have the resolution to discriminate between fibre stresses and matrix stresses. Since these stresses are in a state of mutual equilibrium, removal of a layer cannot elicit an elastic response in the remaining structure.

3.1.3 Hole drilling

The hole drilling method, sometimes referred to as the "Centre Hole Drilling Method", involves drilling a hole normal to a surface. This causes the residual stresses in the material near the hole to relax to some extent. The changes in measured surface strain can then be related to the original in-plane residual stresses. When measuring uniform through-thickness residual stresses it is usual to drill completely through the material using the "Through-hole Method"[ii]. When measuring residual stresses that vary through the thickness, the hole is drilled in successive depth increments using a technique known as the "Incremental Hole Drilling Method".

The method was first proposed and used by Mathar[43] on isotropic materials. The theoretical basis for relating measured strains to residual stresses in orthotropic materials was developed by Bert and Thompson[44] using an approximate calculation procedure. An exact formulation for uniform through-thickness residual stresses in a limited class of orthotropic materials was then developed by Schajer and Yang.[45] Measurement of the residual stresses in orthotropic composite laminates has been performed[46,47] using the incremental hole drilling method and the approximate analysis of Bert and Thompson. Recently, an exact formulation of the through-hole method that enables the measurement of uniform through-thickness residual stresses in a generic orthotropic laminate has been published.[48] This method can also consider the effects of macro-scale residual stresses acting on symmetric orthotropic laminates.

The hole drilling method is most widely used with strain gauges. It is clearly very important that the gauges are correctly positioned relative to the hole. For this reason, special strain gauge rosettes are specified in the ASTM E-837[42] standard that improve the accuracy of alignment. In addition, calibration factors that enable the strains measured with these gauges to be related to the residual stresses are presented with each new analytical technique.

[ii] The ASTM E-837[42] standard allows for the drilling of a blind hole when dealing with thick components.

Although not as widely used, optical methods[iii] have an advantage over strain gauges in that positioning of the hole is less important. A technique has been developed[52] that allows residual stresses in orthotropic materials to be determined using moiré interferometry for any alignment of moiré gratings[iv]. This method uses a least squares approach based on the measured strain over the full field. It is consequently not sensitive to localized errors in measurement and yields accurate results.[52] Dual-beam shearography yields the complete state of in-plane strain directly. The axes of symmetry in the measured fringe pattern correspond to the axes of the principal stresses and so are immediately known. Despite this advantage over moiré interferometry, the use of quantitative residual stress measurement using shearography in combination with the hole-drilling technique in orthotropic materials seems limited. It appears that qualitative measurements only[53] have been obtained on composite panels. In an effort to speed up measurements, micro-indentation (whereby a small indent is pressed into the measurement surface) has been used instead of the hole drilling process.[53] Again, this process has yielded qualitative measurements only.

Current methods of analysing the measurements obtained using the hole drilling method all assume that the material within a single ply is homogeneous. They are consequently unable to resolve the micro-scale residual stresses within a heterogeneous ply. Fibres are, however, necessarily cut when a hole is drilled into a composite laminate. As a consequence, residual stress at the cut is released and an elastic response in the adjoining material occurs. It is therefore potentially feasible to use the hole drilling technique for the purpose of measuring micro-scale residual stress in GFRP. The region over which a significant elastic response occurs is, however, extremely small. The stresses in the fibre return to their far-field values over a few fibre diameters.[54] Since the maximum diameter of E-glass fibres available for reinforcement purposes is generally less than 27 μm,[55] this implies that measurements must be taken within a very small distance of the edge of the hole.

The very localized response to the fibre break presents problems if strain gauges

[iii] It is outside the scope of this work to give a detailed explanation of the optical strain measurement techniques. It is appropriate, however, to point out that these techniques have advantages in that they are full field, have excellent sensitivity and are non-contact. With appropriate use of microscopy they can give provide high-resolution images of the strain field over very small regions. The optical methods that are widely used in strain measurement include the moiré fringe and interferometry methods, electronic speckle pattern interferometry (ESPI) and shearography. Further details on the moiré techniques, ESPI, and shearography can be found in the review articles of McKelvie,[49] Petzing[50] and Hung[51] respectively.

[iv] Prior to the development of this method it was necessary to align the gratings with the directions of principal stress. Since the directions of the principal stresses are not known prior to testing, these methods were not of much practical use.

are used. The smallest commercially available gauges are far larger than the area over which the elastic response occurs. This means that the measured output is low because most of the gauge is not strained by the response. In addition, a "dead zone" at each end of the active gauge length exists where the conducting material of the gauge reverses direction. Since the "dead zone" has a finite width, the active gauge length must be offset from the edge of the hole. Since this is where most of the elastic response occurs, the measured response is reduced even further. If special gauges of extremely small size were developed to get around the problem of sensitivity, they would simply introduce another problem caused by self-heating. GFRP is not a good conductor of heat, and so the localized heating effect of such a small gauge would become an important issue.

Fibre optic Bragg gratings[v] have been used for measuring residual stresses in a composite laminate in a modified version of the hole drilling method.[57] In this case the Bragg gratings were embedded within the laminate. Since they have no self-heating effect they offer a means of avoiding this problem associated with strain gauges. Unfortunately the lengths of fibre Bragg gratings are similar to those of strain gauges and are thus too long to be useful for measuring stress relief around individual fibre breaks. In addition, the fibres used to transmit the optical signal have a stiffness which, at a minimum, is comparable to those of the fibres in the GFRP laminate. The analysis method used to interpret the measured response must therefore accommodate the stiffening effect of the transducer[vi]. The effective stiffness of the transducer depends on the compliance of the material between the transducer and the fibre break. Since it is unlikely that the compliance of this material could be controlled in every installation, it seems improbable that reliable measurements of the stress relief associated with a fibre break could be made.

The use of optical methods appears to offer far more promise than the use of bonded transducers. These methods do not affect the localized elastic response at the edge of the hole. In addition, by employing the use of microscopy it is possible to get high resolution over extremely small areas. These benefits are, however, completely negated by two significant problems that are prevalent irrespective of the instrumentation technique used.

[v] It is outside the scope of this work to discuss the use of fibre optic methods in strain measurement. It is worth mentioning however that these techniques allow strain to be measured at multiple locations using a single optical fibre. The comparatively small diameter of the optical fibre allows embedded application in composite laminates. Details regarding the application of Bragg gratings can be found in the review article of Rao.[56]

[vi] Given the extremely small dimensions of the region over which strains must be measured, this issue would probably also be significant for strain gauges.

The first significant problem arises from the introduction of residual stresses when drilling the hole. Mechanical methods of drilling must generate stresses that, if a hole is to be created, exceed the yield strength of the matrix material. As a consequence, residual stresses are introduced into the matrix material by the hole drilling process. If the hole is carefully drilled[vii] these stresses do not extend over a wide area but even the most carefully drilled hole must have residual stresses at its edge. This is precisely the region where the elastic response resulting from the release of micro-scale residual stresses is most prevalent. The measured strains thus comprise those resulting from the release of residual stress superimposed on those caused by the hole drilling process. It is not possible to separate the two sets of strains from each other, and hence the elastic response of the structure to the release of micro-scale residual stress cannot be determined if mechanical drilling methods are used. Electric discharge machining (EDM) can be used to minimized the residual stresses introduced by making the hole, but only if the fibres and matrix are conductive. Unfortunately neither the fibre nor the matrix in GFRP satisfies this criterion and so this option is not available.

It might potentially be possible to avoid the introduction of residual stresses during hole drilling by using the micro-indentation process.[53] In this case, the indenter could be used to fracture a single glass fibre without introducing additional residual stresses into the surrounding matrix. The stresses in the fibre would be released and strains in the surrounding material could be monitored. Interpretation of the strain measurements would then, however, be complicated by another significant problem related to the heterogeneity of the material at small scales.

The stresses in the fibres and matrix return to their far-field stresses over a few fibre diameters. This means that the strain response to the release of residual stresses must be measured over a very small distance. GFRP is, however, heterogeneous at small scales. This requires that any method of relating the measured strains to the residual stresses must take account of the micro-structure of the test region. Only the in-plane structure of the test region is visible, while the structure beneath the surface also influences the measured response. Thus, even if a new method was developed that could take account of the heterogeneity of the material, problems would remain with its implementation since not all the necessary structural information is readily available.

It can therefore be seen that the hole-drilling method, and variations thereof, cannot be directly used or adapted for use in finding the micro-scale residual stresses in

[vii] The use of an abrasive jet is problematic in this situation due to the different erosion rates of the glass fibres and polymer matrix.

unidirectional GFRP.

3.1.4 Ring-core method

The ring-core method is a variant of the hole drilling technique. Rather than releasing residual stresses by means of drilling a hole and then measuring the elastic response of the surrounding material, this approach releases stress by cutting an annular groove into the surface of a part containing residual stress. The elastic response is then measured on the end of the core within the groove by means of a strain gauge rosette. By incrementally increasing the depth of the groove, it is possible to determine the stress variation through the thickness.[58] The through-thickness stresses can be determined by monitoring the change in core length with increasing groove depth.[59, 60]

The ring-core method has a number of advantages over the hole drilling method:

- The measured response is significantly larger because the strains are more fully relaxed.
- No stress concentration effects occur within the annulus and so the technique can measure residual stresses up to the yield stress of the material[viii].
- The strain relaxation on the end of the separated core is fairly uniform. As a consequence, the method is less sensitive to errors in the positioning of the strain gauge rosette.

Despite these advantages over conventional hole drilling, the method seems not to have been widely applied. This is possibly because the method was protected by patent until 1988.[58] It has though, been applied to large cast steel parts and forgings,[58] forged aluminium parts,[61] welds in stainless steel[62] and hot rolled laminates of stainless and carbon steel.[63] In metallic structures of this kind, current methods of cutting the annular groove employ the use of EDM since no additional residual stresses are introduced[ix].

[viii] As a consequence of stress concentration effects around the hole, the hole drilling method can only be used where the residual stresses are less than half of the yield stress.[42]

[ix] Earlier methods made use of milling in which case a central hole was sometimes drilled to guide the tool.[58] If a central hole was drilled, strain rosettes intended for use with the hole drilling method were applied around the central hole.[58, 61]

Recent developments using interferometry have allowed the method to make use of grooves of far smaller diameter than possible with strain gauges. This approach can thus be applied in regions with high stress gradients such as laser welds[64] and ultrasonic spot welds.[65]

The ring-core method does not appear to have been used on fibre reinforced plastics. This is quite possibly because the standard hole drilling technique can be readily applied to these materials. The use of EDM is also not practical because composite materials are either non-conducting or are poor conductors of electricity. This complicates the cutting of the annular groove.

Since fibres are cut when the groove is created, the elastic response of the neighbouring material can potentially be monitored to determine the magnitude of the micro-scale residual stresses. The ring-core method, though, is simply a variant of the hole-drilling method. Consequently it suffers from the same problems, described in section 3.1.3, which prevent the use of the hole drilling method for measuring the micro-scale residual stress state in unidirectional glass fibre reinforced plastic.

3.1.5 Deep hole drilling

Deep hole drilling (DHD) is a technique that allows the resolution of residual stresses through even very thick parts. The method requires that a narrow diameter hole is drilled through a part containing residual stresses. The diameter of the hole is then measured very accurately (typically using an air gauge) as a function of both depth and angular position within the hole. The residual stresses are then released by coaxially removing a core of larger diameter from around the hole. The release of residual stress causes the shape of the reference hole to change. The diameter of the hole is then remeasured at the same angular positions and depths as in the original measurements using the same equipment. Changes in the shape of the hole are then related to the residual stresses that existed prior to drilling the hole.

It is assumed that the introduction of the reference hole has negligible affect on the residual stress state, and that cutting of the core allows residual stresses around the hole to relax completely.[66] The core is further assumed to comprise many independent lengths. This implies that a thick component can be approximated as a set of stacked layers unconnected by through-thickness shear stresses.[67] Through-thickness residual stresses can be obtained by monitoring the change in the core length as the outer core depth is increased.[68] The deep hole drilling technique has most frequently been used on metal parts where residual stresses have been measured

in welds,[66,69–71] railway track[72] and rolls in steel mills.[73] In these investigations, EDM was used to make the cut around the central core since the cutting stresses introduced by this method are negligible.

The technique has also been applied to a laminated carbon-fibre composite.[67] In this case, EDM could not be used to remove the core around the hole and a diamond encrusted hole saw was used instead. In addition, the analysis technique to allow the change in hole shape to be related to the original residual stresses was extended to account for the use of orthotropic material.

The deep hole drilling technique relies on the assumption that the material at each depth can be treated as a continuum. When applied to a laminated composite, the measured residual stresses are simply averages of the stresses within the fibre and matrix. This means that the method cannot be directly applied to the measurement of micro-scale residual stresses because the heterogeneous structure of the composite is not accounted for. The method is only able to resolve meso-scale residual stresses, which in unloaded unidirectional laminates are non-existent.

Drilling a small diameter hole results in the cutting of fibres on the hole wall. Micro-scale residual stresses in the fibres are consequently released and the material near the ends of the fibres responds elastically. If it is possible to monitor this response, it becomes potentially possible to modify the DHD method to measure the longitudinal micro-scale residual stresses in unidirectional GFRP.

Attempting to modify the technique to achieve this objective presents a few intractable problems however:

- The first problem involves the method of creating the hole. As discussed in section 3.1.3, the elastic response to the release of fibre stress is extremely localized around the break in the fibre. If this response is to be monitored, it must be distinguishable from that caused by the release of cutting stresses generated while making the hole. Mechanical methods of creating the hole result in cutting stresses on the hole wall[x]. The breaks in the fibres occur also on the hole wall, meaning that the elastic responses from cutting stresses and that from the release of micro-scale residual stresses are coincident. The two effects cannot be distinguished from each other, preventing the use of mechanical methods for making the hole. EDM cannot be used either, because GFRP is not conductive.
- The second challenge revolves around the issue of measurement resolution. In

[x]This is a necessary side effect of exceeding the yield strength during material removal.

order to monitor the elastic response to the release of fibre stress, the modified technique must involve measurement of the profile of the hole wall at scales smaller than that of the diameter of the glass fibre. This is not easily achieved inside a hole.

- The last difficulty also involves the method of creating the hole. If the profile of the hole wall is to be monitored, material that tends to move radially inwards in response the fibre being cut cannot be removed in the process of making the hole. It is unclear how this requirement could be met.

It is clear therefore that the deep hole drilling technique cannot be used directly to measure the micro-scale residual stresses that exist in the fibre direction of unidirectional GFRP. Modification of the technique, to allow this measurement, presents problems that cannot be practically resolved.

3.1.6 Incremental slitting method

The incremental slitting method is often referred to as the "crack compliance", "compliance" or "slitting" method. In this approach a slot is incrementally cut into a component containing residual stress. The slot releases the residual stresses normal to the plane of the slot and the part deforms to restore force equilibrium. By measuring the deformations as the slot depth is increased, it is possible to determine the original residual stresses as a function of depth. Clearly, a single slot only allows the measurement of residual stresses perpendicular to its plane. If a biaxial stress field is to be measured, two orthogonal slots are used.[22, 74]

The analysis component of the method consists of two parts: the forward and inverse solutions. The forward solution, often known as the compliance calculation, involves determining the response of the part as the slot depth is increased for a range of known stress distributions. The inverse solution involves finding the residual stress distribution that best matches the experimentally measured response. The inverse solution is often performed using a series expansion incorporating a least squares approach. If this approach is used, the calculated solution does not need to match the measurements exactly[75] and is therefore tolerant of small measurement errors.

Various methods can be used to measure the elastic response to the introduction of the slot. These include moiré interferometry,[76, 77] the measurement of crack mouth opening displacement[78, 79] and digital image correlation (DIC) of high resolution micrographs of the surface adjacent to the crack mouth.[80–82] The use of strain

gauges is, however, by far the most commonly used technique. In this case, the gauges are placed perpendicular to the slot to maximize their response[xi]. Placing a strain gauge on the "back face", opposite the entrance of the slot, enables the measurement of residual stresses all the way through the thickness[xii]. In contrast, residual stresses immediately below the surface are best measured using a gauge placed on the "front face" in close proximity to the slot.[75] Since the response of the gauge on the front face saturates at some depth, a back face strain gauge is always required unless residual stresses near the surface only are needed.

A number of methods have been used to create the slot. These include electric discharge wire machining (EDWM),[74,76] saws[22,77,84] and focused ion beams.[80–82] EDWM is the preferred method of cutting the slot[75] because the use of a fine wire gives a narrow slot and the residual stresses introduced by the cutting process are very small. In addition, since the part is usually submerged beneath deionized water during the cutting process, it is easy to take all strain measurements at a constant temperature. The only significant disadvantage of EDWM is that it can only be used on conducting materials. Saws are not limited to conducting materials only, but their use is not ideal. Residual stresses are progressively introduced into the tip of the slot in the process of removing material. These cutting stresses can affect strain readings obtained from the gauge on the front-face.[75] If possible, saws should therefore be avoided if near surface stresses are required. The back face strain-gauge, however, is relatively insensitive to cutting stresses and so it is possible to obtain reasonable through-thickness results if the temperature is allowed to stabilize before measurements are taken.[75] The use of a focused ion beam allows the incremental slitting method to be applied to tiny components because extremely fine slots can be cut.[81] Its chief disadvantage is that it is limited to the creation of very small slots which prevents its application on larger components.

A key assumption of the incremental slitting method is that stresses are invariant in the direction of the slot width. Effectively this implies that the material removed by the slot can be treated as a homogeneous continuum. If the heterogeneous structure of a fibrous composite is treated as homogeneous,[22,84,85] the measured residual stresses are averages of the matrix and reinforcement stresses.[86] This means that

[xi] Gauges have been placed parallel to the slot to verify the plane-strain assumption in this direction.[74]

[xii] Until publication of a recent paper by Schajer and Prime[83] which uses equilibrium constraints to enable the stress field to be extrapolated through the entire thickness, the maximum depth was limited to approximately 90% - 95% of the thickness.

in the fibre direction, only residual stresses at the meso-scale can be found[xiii]. The incremental slitting method therefore requires adaptation to account for material heterogeneity if micro-scale residual stresses in the fibre direction are to be measured.

The adapted method must have sufficient resolution to monitor the elastic response to the release of residual stress from individual fibres if the heterogeneous nature of the material to be properly accounted for. Also, since the fibre stresses return to far-field conditions over a few fibre diameters, the measurement system must operate at a small scale. As discussed for the hole drilling method, section 3.1.3, optical techniques are probably most appropriate.

Mechanical methods of cutting the slot leave cutting stresses on the inner surfaces of the slit. This is exactly the region where the elastic response to the release of fibre residual stresses is greatest. The elastic response caused by cutting stresses and those caused by residual stresses in the fibres cannot be distinguished from each other and so mechanical methods cannot be used in this application. EDWM cannot be used on GFRP either since neither constituent is conducting. The only remaining method of cutting the slot is the use of a focused ion beam. This method has been used to cut slots measuring 10 μm long, 0.35 μm wide and 0.3 μm deep.[81] The width of this slot is, however, significantly smaller than the size of a typical glass fibre. In addition, it is reported[80] that problems exist in introducing narrow and deep slots using a focused ion beam. It consequently appears that this approach is not feasible even for cutting through a single glass fibre, never mind the surrounding matrix material.

It is possible, however, that the use of a focused ion beam could introduce a flaw of sufficient size in a glass fibre to cause it to fracture. This would essentially result in the micro-indentation approach discussed in section 3.1.3. In principle, an analytic method could be developed to enable the elastic response of the matrix material around the fibre break to be related to the residual stress in the fibre. Problems would still, however, hinder its implementation. The technique would require the heterogeneity of the material at small structural scales to be considered. Since the sub-surface structure is not directly known, but still influences the elastic response on the surface, the method would depend on information that is not readily available.

[xiii] In the transverse direction it is possible to measure micro-scale residual stress using the incremental slitting method. In the only reported case,[86, 87] the residual stresses transverse to tungsten fibres embedded in a Kanthal alloy were measured. Slitting of the matrix was performed parallel to the fibres and no fibres were cut. The material removed by the slot was homogeneous and so incremental slitting could be used.

Consequently, it can be seen that neither the incremental slitting method, nor adaptations of the method can be used to measure micro-scale longitudinal residual stresses unidirectional GFRP.

3.1.7 Contour method

The contour method is a powerful method of measuring residual stresses that vary in two dimensions.[88] The method involves cutting a planar surface through a part with residual stress. The residual stresses across the plane are released by the cut and the newly exposed surface responds by deforming out-of-plane.

By measuring the out-of-plane deformations, it is possible to determine the original residual stresses across the cut through the use of the finite element method. This is done by imposing displacement boundary conditions on the cut surface that are equal to the negative of the measured deflections. The method has been used to map complicated residual stress fields such as those found in railway track[89] and welds[90,91] as well as those caused by hypersonic impact.[92]

In principle, this method is ideal for measuring the longitudinal residual stresses that exist in unidirectional GFRP. The use of the finite element method easily allows the heterogeneous structure of GFRP to be modelled. If the out-of-plane displacement around the fibres can be measured accurately enough, possibly using laser probe scanning,[93] the residual stresses in the fibre can be readily determined.

The contour method requires that a very accurate planar section be cut through the stressed material. Mechanical methods of making the cut are not suitable because they have a tendency to introduce cutting stresses and to trim down out-of-plane deflections as they appear. For this reason, EDWM is typically used because it removes material only at the tip of the cut and introduces virtually no cutting stresses. Unfortunately, EDWM cannot be used for making the cut through GFRP material because neither constituent is conducting. The contour method therefore cannot be applied to the measurement of micro-scale residual stresses in the longitudinal direction of GFRP.

3.1.8 Sectioning method

The sectioning method involves removing sections of interest from a component containing residual stress. The sections are removed in such a way that it can be

reasonably assumed that the final stress state is zero. The total change in strain from the original state to the unstressed state corresponds to the negative of the strain in the component prior to testing.

One version of the method makes use of strain gauge rosettes. In this case, the section is parted from the rest of the component by cutting as close as feasible to the edges of the rosette to ensure that the final stress state is as low as possible. If the through-thickness stress variation is required, additional gauges can be attached to the newly exposed surfaces. Further cuts can then be made to part sub-sections, each with its own gauge. The approach has been described as the "slice-and-dice" method.

The sectioning method based on the use of strain gauges has been widely applied to metallic components. The residual stress variations across a welded steel H-section,[94] in cold-bent steel plate[95] and in welded seams[96] have all been measured using this approach. By employing the finite element method in a more sophisticated analysis, it is possible to estimate triaxial stresses at points different from those where strain gauges were positioned. This approach has been simulated in the residual stress analysis of a welded joint.[97, 98]

The sectioning technique employing strain gauges has also been used to measure the residual stresses in filament wound tubes.[99] When the stiffness of the removed section is low however, the use of strain gauges is inappropriate. In this case, moiré interferometry can be utilized to measure the released strains since the measurement system applies no loading to the removed section. Moiré interferometry has consequently been used to measure the residual stresses in individual plies of cross-ply laminates[100, 101] and thick-walled cross-ply cylinders.[101]

Irrespective of the measurement technique used, the sectioning method is not, however, suitable for measuring micro-scale residual stresses in unidirectional fibre reinforced plastic. The thickness of each removed section is far greater than the diameter of the reinforcement fibres and the method consequently lacks the resolution to discriminate between these stresses at the micro-scale. Since the fibre and matrix stresses are in mutual equilibrium, cutting sections from an unloaded unidirectional laminate will not elicit any response.

3.1.9 Radial cutting method

The radial cutting method is a variant of the sectioning method. This technique has been widely applied to the rapid measurement of residual stresses in fibre reinforced tubes[84, 102–107] and rings.[108, 109] The residual stresses in these structures are assumed to be invariant with axial and circumferential position. It is consequently possible to release them by means of a single axial cut. The variation in circumferential and radial residual stresses through the laminate thickness can be deduced by monitoring the extent to which the laminate opens up or closes in[xiv].

In all analyses except that of Kaddour *et al.*,[102] the axial residual stress is assumed to be zero. Measurement of the strains in this direction, however, allows improved estimates of the circumferential stresses to be obtained in addition to non-zero axial stresses.[102]

Current analytical methods of using this technique are limited to laminates which are balanced with respect to the cylindrical coordinate system. The residual shear stresses are consequently assumed to be zero. Kaddour *et al.*[102] have found that this assumption is not necessarily correct. Thin filament-wound laminates exhibit a change in axial displacement across the cut. This implies the existence of a built-in twist with corresponding residual shear stresses.

The radial cutting method relies on measurement of the elastic response of the laminate as a whole and also on the assumption of homogeneous materials. Both of these conditions prevent the resolution of residual stresses at the micro-scale.

3.1.10 Matrix removal methods

Matrix removal methods rely on the fact that residual stresses are in a state of mutual self-equilibrium. In unidirectional laminates, stresses within the fibres are opposed by stresses in the matrix. If the matrix material is removed, the stresses within the fibres are released. The consequent elastic response of the fibre allows the residual stresses to be determined.

Depending on the composite, the matrix can be removed using a variety of methods provided that the method does not damage the fibre. Metal matrices can be etched away by strong acids, polymer matrices surrounding carbon and aramid fibres can

[xiv] When the cut closes completely it is necessary to remove additional material by making a second cut parallel to the first.

be removed using acid digestion whilst polymer matrices surrounding glass fibres can be vaporized by high temperatures.[110]

One technique making use of matrix removal relies on microbuckling of the reinforcement fibres.[111] The fibre stress in metal matrix composites is usually compressive at room temperature. The fibres are prevented from buckling due to the support provided by the surrounding matrix. If the matrix is removed, however, the fibres are free to buckle. The technique requires that a small amount of metal matrix is etched from the surface of a composite plate until the underlying fibres are exposed. By measuring the lengths of both buckled and unbuckled fibres, estimates of the critical buckling length are made. In principal, the "clamped-clamped" Euler buckling stress corresponds to the residual fibre stress. Unfortunately, the method requires the introduction of a "knock-down factor" to account for initial fibre imperfection and misalignment. Uncertainty regarding this value[xv] appears to have limited further use of the method.

The "etching" or "dissolution" technique has been extensively used to measure the fibre stress in silicon-carbide reinforced titanium alloys. The method was first used by Cox *et al.*[112] who dissolved the matrix from the central part of long rectangular specimens and subsequently measured their change in length. The change in length was then related back to the average fibre strain resulting from the release of residual stresses.

The etching technique has been improved since it was first presented.[113–115] The most recent development of the method[115] is accurate and simple to implement. In addition, it completely releases the strains in every fibre thereby allowing the residual stress in individual fibres to be determined. The method requires that a flat face, perpendicular to the fibre direction, be prepared at the end of a composite specimen. This face acts as a reference surface. Two long narrow slits are then cut along the fibre direction from the reference surface. The matrix between the slits is etched away and the change in individual fibre length in this region is measured relative to the reference surface. The released strain is known once the exposed fibre lengths are also measured. The thermal residual stress in the fibres can then be determined using a concentric cylinder model.[115]

Some complications associated with bending of the fibres after matrix dissolution

[xv] A knock-down factor was "back-calculated" from published stresses in silicon-carbide/titanium composites. It was then assumed that the same value could be applied to graphite/aluminium and graphite/magnesium composites. It seems, however, doubtful that this value can be applied to situations where the elastic relationship between the fibres and matrix is different to that from which the original knock-down factor was extracted.

exist.[115] The extension of the fibre appears shorter than it actually is because some of the fibre length is inclined to the "length" direction. In addition, bending of the fibres changes their apparent position on the reference plane. Since it is not possible to align the reference plane perfectly normal to the measurement axis, the change in position alters the apparent change in length relative to the reference plane. Notwithstanding these issues, the method has subsequently been used in further investigations into the residual stresses within silicon-carbide reinforced titanium alloys.[76, 116]

The etching technique appears not to have been used on fibre reinforced plastics. This is probably because of the combination of two factors; the low elastic modulus of polymers and the small diameter of the fibres used with polymer matrices. Since the modulus of polymers is significantly lower than that of metals, the residual strain retained in the fibres is lower for polymer matrix composites than for metal matrix composites. In order to retain acceptable resolution in the displacement of the fibre ends, the matrix must be removed over a greater fibre length. This makes the exposed fibres susceptible to bending, the effect of which is greatly exacerbated by their small diameter in comparison to those used in the metal matrix composites studied previously.[76, 115, 116] Significant bending of the fibres reduces the accuracy of the measured change in fibre length, thereby limiting the usefulness of this technique with fibre reinforced plastics.

Even if the effect of bending was not significant in fibre reinforced plastics, an additional problem would limit the usefulness of the method with GFRP. Strong acids cannot be used to remove the matrix because the fibres are susceptible to corrosion and cracking.[117] It is, however, possible to use high temperatures to vaporize, or burn off, the polymer matrix.[110] Vaporization of the matrix between the slits would, almost certainly, expose the neighbouring material to high temperatures, thereby changing the residual stress state in the reference material. It therefore seems that to adapt the method for use with GFRP would require the simultaneous burning off of all the matrix within the specimen. By comparing the length of the glass fibres before and after removal of the matrix, it would, in principle, be possible to deduce the original residual stress. It would not be possible to measure the length of individual fibres prior to the burn-off process. Separate, parallel, reference surfaces would consequently be required at each end of the specimen so that the original lengths of all fibres could be assumed to be identical. The destruction of the reference surfaces during the burn-off process however means that the change in length of the fibres would be measured over their complete length rather than relative to a reference surface. This greatly complicates accurate measurement of

the fibre strain and, in conjunction with the difficulty in manufacturing the parallel reference surfaces to the required accuracy, limits the viability of the technique for use with GFRP.

It is apparent, therefore, that modifications to the etching process could, in principle, allow the measurement of the longitudinal fibre stresses within GFRP. Fibre bending and the need to vaporize rather than etch the matrix away, however, result in a loss of measurement accuracy. The practicality of the method is therefore questionable.

3.1.11 Micro-indentation methods

Micro-indentation techniques are one of several micro-mechanical methods used to test the interfacial characteristics of composites. Micro-indentation techniques, unlike other methods such as fibre pull-out and fragmentation tests, do not require the use of model composite systems[118] and are consequently worth considering further.

Micro-indentation testing has been extensively used in the mechanical characterization of composite interfaces.[119–123] Two variations of the test[118,120] exist. These are known as the single fibre push-in and single fibre push-out methods. Both consist of applying a compressive longitudinal load to the end of a single fibre using a small indenter. The end of the fibre is exposed by cutting the composite perpendicular to the direction of the fibres and then polishing the cut surface. Since the test inherently relies on the heterogeneous nature of a composite material it has the potential to allow measurement of micro-scale residual stresses.

In push-in tests, the reverse face of the specimen is completely supported by a backing plate. As the compressive load on the fibre increases, the interface stress between the fibre and matrix also increases. Eventually a stress is reached where the interface fails and debonding consequently occurs at the fibre end. As the load is further increased the debond extends progressively along the fibre. The overall fibre length is long however, and the debond length never extends beyond a small fraction of the embedded fibre length.[120]

In push-out tests, the thickness of the specimen is small. The debond length consequently can extend over the complete fibre length whereupon the fibre is pushed out the rear of the specimen. In this test, the backing support must clearly be designed to accommodate unimpeded protrusion of the fibre.

The initiation and propagation of the debond clearly depend on the mechanical

properties of the fibre and matrix, the strength and fracture toughness of the interface and the friction between fibre and matrix. In addition, residual stresses in the form of the radial clamping stress and longitudinal stress must also be considered. Characterization of the interface properties is typically achieved by fitting analytical predictions,[119–121, 123, 124] which depend on a number of unknown parameters, to the measured variation in applied load with fibre end displacement. The parameters corresponding to the best fit can then be used to completely characterize the interface including both longitudinal and clamping residual stresses.

The effect of longitudinal residual stresses on the measurements is easy to visualize. The release of longitudinal residual compression in the fibre with increasing debond length causes the fibre to extend. The extension is in the opposite sense to the applied compressive loading. Consequently, the displacement of the fibre end is less for a given applied load than if longitudinal residual stresses were not present.

The analysis methods developed for use with the single-fibre push-in and push-out methods allow them to be applied directly to the measurement of micro-scale residual stresses in the longitudinal direction. Problems exist though in their application to glass fibre. The majority of cases where these techniques have been applied have made use of large diameter (> 100 μm) fibres.[119, 121–123] The comparatively large size of the fibres facilitates positioning of the indenter. In addition, the loading forces and fibre end displacement are quite large which aids in their measurement.[120] As a consequence, test rigs to do these measurements can be constructed at a reasonable price.[125]

The small diameter of E-glass fibres, typically around 15 μm, however, presents some difficulties. At this size, the positioning and measurement requirements are a lot more demanding. Although work has been performed on fibres of comparable size to E-glass fibres,[118, 120, 124, 126] the testing systems used have positioning accuracy for the load applicator of at least $\pm$ 1 μm and measurement resolution of 1 mN and 0.1 μm for the load and end displacement respectively. Manufacture of a test rig to meet these requirements is not an easy task. The financial implications are therefore of concern.

Of even greater concern, however, is the accuracy in measurement of the longitudinal residual stress obtained at this size scale. It appears that the residual stresses in fibres of small diameter have only been reported once.[120] The scatter in these results is approximately 80% each side of measured value. This was partly ascribed to the complex distribution of residual stress along the fibre.[120] Measurement of the longitudinal residual stresses in larger diameter fibres does not, however, appear

to suffer from scatter to the same extent.[119, 121, 123] This implies that the scatter is more related to fibre size than to the distribution of longitudinal stress[xvi].

The scatter was also ascribed to the underlying analytical models making assumptions that might not represent reality.[120] This, unfortunately, is a potential worry irrespective of the fibre diameter. Residual stress in the fibres is not measured directly but rather inferred simultaneously with a number of other interfacial characteristics by least-squared methods. Due to the nature of the problem it is possible to obtain a reasonable fit to the measured data even if some of the interfacial characteristics are poorly determined.[120] It follows that inadequacies in the analysis technique can therefore result in flawed measurements of residual stress.

It is seen therefore that although the fibre push-in and push-out techniques are potentially able to allow the measurement of micro-scale residual stresses in GFRP there are a number of problems with these approaches. The measurement system is likely to be expensive and will quite possibly yield considerable measurement scatter. In addition, the residual stresses are not measured directly but are inferred with a number of other interfacial characteristics. This makes the technique vulnerable to inadequacies in the analysis technique used.

3.2 Methods that measure the apparent failure strength

The estimation of residual stresses through the measurement of the change in apparent failure strength can, in principle, be applied to any material with a well defined failure (or yield) strength. The method appears, however, only to have been applied to the measurement of transverse residual stresses in composite materials in the form of the "first ply failure method".

3.2.1 First ply failure method

Cracking of transversely loaded plies has been used to estimate the transverse residual stresses in cross-ply laminates.[19, 21, 128] This technique relies on measuring the difference between the apparent transverse tensile strength of unidirectional material and the stress required to initiate transverse cracking when the same material

[xvi] It has been found that the surface roughness of the fibre can significantly influence both the stress transfer across the interface and also the interfacial debonding behaviour.[127] For roughness of a given dimension, the effect is more significant for fibres of small diameter. This effect is perhaps the underlying cause of the increased scatter reported for small fibre dimensions.

is embedded in a cross-ply laminate. The assumption is made that the transverse strength remains constant and hence tensile residual stresses reduce the additional stress that can be applied before failure.

Although good results have been obtained using this approach,[21] it has been demonstrated that the transverse tensile strength is not an intrinsic ply property.[129] The transverse strain in plies orientated perpendicular to the applied load is constrained by neighbouring plies that are more aligned with the load. The apparent strength of the transversely loaded plies is consequently increased. The constraining effect is most significant when plies aligned with the load sandwich a single ply orientated perpendicular to the load. The strength has been documented to increase by a factor of 2.48 in a $(0_2/90)_s$ laminate.[129] To reduce the constraining effect of adjacent plies, residual stress measurements are consequently limited to the outer plies of the laminate.

The method relies entirely on the assumption that the transverse stresses in a unidirectional laminate are zero. This is valid at the meso-scale, but is incorrect at the micro-scale. At the micro-scale, the residual stress field in the plane perpendicular to the fibres is clearly very complicated. The method is consequently limited to the measurement of meso-scale residual stresses in the transverse direction.

In the longitudinal direction, the residual strain field of a unidirectional material is uniform at points remote from the fibre ends. There is the potential therefore that by loading the laminate in the fibre direction, the approach could be adapted to measure the micro-scale residual stresses aligned with the fibres. Since the strain to failure of glass fibres is greater than that of some thermoset resins, measurement of the strain required to initiate resin cracking could give an indication of the longitudinal residual stresses. This approach, however, requires knowledge of the strain required to initiate resin cracking when no longitudinal residual stresses are present. Since there is no way of knowing when the residual stresses in a laminate are zero, the information required to use the method cannot be obtained. The strain to failure of unreinforced resin cannot be used either since the triaxial stress state experienced within the laminate is different from the uniaxial stress state in a tensile test of pure resin.[130] The cracking stress of the resin in a laminate is consequently different from that of unreinforced resin and use of the method is consequently prevented.

3.3 Methods that rely on changes in the material structure

Methods that rely on changes in the material structure include X-ray diffraction[xvii], neutron diffraction[xviii], Raman spectroscopy, photoelasticity and the use of acoustic waves. Only the use of acoustic waves requires contact with the specimen and all methods are potentially completely non-destructive.

3.3.1 X-ray diffraction

The X-ray diffraction technique is widely used in residual stress measurement.[131] Although X-rays from synchrotron sources have greater penetration,[133] soft X-rays are most commonly used. These have small penetration depth, however, and only allow measurement of strains to a depth of about 50 μm.[134] Through-thickness stress variation can be measured, but this requires the successive removal of layers of material - rendering the technique destructive and hence negating the greatest benefit of the method.

X-ray diffraction measures the strains in the crystal lattice of polycrystalline materials by studying variations in the interplanar spacing. Apart from the requirements that the sampled material be macroscopically isotropic and homogeneous,[131] the material must be crystalline. This last requirement limits the direct applicability of the method to polymer composite materials.

The method can, however, be directly applied to metal matrix composites. Microscale residual stresses in silicon-carbide reinforced titanium alloys have accordingly been examined.[112,114,134]

X-ray diffraction has also been applied to fibre reinforced plastics.[135–137] Since the polymer matrix is non-crystalline however, small metallic particles of roughly the same size as the fibre diameter must be incorporated into the matrix. The stress in these particles is then measured using X-ray diffraction. It is necessary, however, to relate the measured stress in the particles to the residual stress in the surrounding matrix. Additional experiments are consequently required to develop a "stress transmission tensor".[138] All six components of the stress field can then be determined.[138]

[xvii] A detailed description of the method can be found in the review article of Lu.[131]

[xviii] Further details of this method can be found in the review article of Albertini.[132]

This investigation is, however, aimed at finding an experimental technique that can be used in an investigation into the effect of residual stresses on environmentally assisted cracking. Since the metal particles might affect the mechanism of environmentally assisted cracking, this is not a feasible approach.

3.3.2 Neutron diffraction

Neutron radiation has far greater penetration than X-rays.[132] As a consequence, the neutron diffraction technique can measure residual stresses to depths of about 50 mm in engineering materials.[75] The technique has limited resolution, however, and cannot measure residual stress variations over distances less than about 1 mm.[75]

Although the method has been used to measure residual stresses in silicon-carbide reinforced titanium alloys,[134] it cannot be used directly to measure the residual stresses in GFRP. This is because neither the fibre nor the matrix of this material are crystalline and, like the X-ray diffraction method, the neutron diffraction method can only measure residual stresses in crystalline materials.[75]

The incorporation of small metallic particles into a GFRP laminate might allow the residual stresses to be measured. This approach is not practical, however, for the same reasons preventing its use with the X-ray diffraction technique.

3.3.3 Raman spectroscopy

Raman spectroscopy is a technique based on the inelastic scattering of light. By illuminating a material with a suitable excitation source, a faint Raman spectra containing a number of characteristic luminescence peaks can be obtained. The frequency of the luminescence spectra depend the applied strain.[139] It is thus possible to deduce stress by measuring the shift in the frequency of particular luminescence peaks from the unstressed condition.[140]

The stress-induced change in frequency has been extensively used to study the deformation micromechanics of aramid, carbon and ceramic fibre-reinforced composites in polymer matrices.[141–144] These studies make use of a technique known as micro-Raman spectroscopy. In this technique, an area significantly smaller than the fibre diameter is illuminated. By progressively moving the illuminated area along the length of the fibre, it is possible to determine the variation in stress along the fibre length. This technique has also been used to directly measure the residual stresses

in ceramic fibres.[145]

However, micro-Raman spectroscopy is not ideal for measuring residual stresses in GFRP. Although intensity peaks in Raman spectra are well defined for crystalline materials, they are broadly spread for amorphous solids,[146] and since glass is amorphous, it does not have well-defined Raman spectra.[147] Additionally the band shifts of amorphous materials are very small.[148] Accurate measurement of the frequency shift is consequently prevented. Only a single study involving the measurement of stress in glass fibre is presented in the literature.[147] In this case, the fibres were coated with a specially synthesized coating so that well-defined Raman spectra could be obtained from the fibre-matrix interface. The use of this coating prevents the use of Raman spectroscopy in the current work. Modifications to the glass fibre are not desirable since they might interfere with the mechanisms involved in environmentally assisted cracking.

An alternative approach makes use of the fact that for amorphous polymers, the intensity of Raman scattering from polarized light is determined by the distribution of the molecular orientations.[148] In other words, the strain in the matrix can be determined by measuring the angular variation in the intensity of Raman scattering. The drawback to this approach is that it measures the strain in the matrix rather than the stress. The relationship between strain and intensity has been measured as linear even above the yield limit.[148] This is not a problem when the matrix is operating in the elastic range, but polymer matrices are viscoelastic.[149] During post-curing of the room temperature curing resins frequently used in corrosion applications, the polymer is heated to high temperatures. The thermal stresses caused by the mismatch in the thermal expansions of the fibre and resin can be expected to promote viscous flow in the resin. This means that "strains" are locked in even when the stress state is non-existent. The technique consequently cannot be applied with room temperature curing resins that are post-cured, or if any other non-linear resin behaviour is expected.

The use of conventional Raman spectroscopy for the purposes of this investigation is ruled out by the necessity of using a special coating on glass fibre. The alternative technique, where the intensity of Raman scattering from the resin system is measured, is also excluded because it cannot take account of non-linear behaviour in the resin system.

3.3.4 Photoelasticity

Stress alters the distribution of the molecular orientation within amorphous polymers. This effect changes the polarization of transmitted light.[148] Photoelasticity is a measurement technique which exploits this effect to determine the direction of, and the difference between, the principal stresses.[150] The technique yields results in the form of a fringe pattern over the area of study. It is possible to resolve this pattern over small regions using a microscope.

Photoelasticity has been widely applied to investigate the stress fields surrounding single fibres embedded in a polymer matrix.[151–155] Although most of these studies have been directed at the bonding between the fibre and matrix, residual stresses around single fibres have been quantified.[153, 155]

Residual stresses have also been investigated in typical unidirectional composite materials.[156, 157] Andersson *et al.*[156] investigated the transverse residual stresses in a cross section of GFRP containing thousands of fibres. Light was transmitted along the fibre direction through specimens of 200 μm to 300 μm thickness. Quantitative values of stress were not determined, but it is apparent that the stress state in a realistic laminate is extremely complex. A source of concern in this investigation is that the observed fringe pattern did not change with the application of external loading. It was deduced that the fringe pattern does not reflect the existing stresses, but rather the "stress history" of the matrix. This effectively means that the method does not accurately reflect the residual stresses in the laminate.

Nairn and Zoller[157] investigated the residual stresses in carbon fibre reinforced polysulfane and epoxy. To enable the measurement of in-plane stresses, they transmitted light through the thickness of the laminate. It was clear from their investigation that the principal residual stresses are aligned with and perpendicular to the fibre direction. The stress difference between the principal stresses in the matrix was also determined in both cases. It was not, however, possible to determine the principal stresses individually without making an assumption regarding one of these values. Although the thickness of the laminate is not stated, it was necessary to keep the fibre volume fraction fairly low so that regions of transparency could be found between fibres.

Although the studies of Andersson *et al.* and Nairn and Zoller demonstrate that micro-scale residual stresses in unidirectional composites can be investigated using the photoelastic technique, they also highlight some serious concerns:

- The photoelastic technique might not reflect the residual stress state in real laminates.

- The photoelastic technique requires that light be transmitted through the laminate under investigation[xix]. The experimental technique, however, is required to be applicable to laminates containing fibres bundles uniformly distributed throughout the thickness. It is extremely unlikely, therefore, that a path exists in such a laminate through which light can be transmitted without being blocked by a fibre[xx]. This problem can possibly be overcome by reducing the thickness of the laminate until a transparent region appears between the fibres. It would be necessary, however, to somehow avoid the introduction of residual stresses during this process.

- The technique allows the difference in principal stresses to be determined, but unless assumptions are made, it is not possible to measure these stresses individually. This problem can be resolved by using holographic interferometry in conjunction with conventional photoelasticity.[155] The technique is, however, more complex than the conventional approach and has not seen widespread use since being proposed in 1994.

Although not discussed in any of the references listed above, there is another problem with the use of the photoelastic technique for this work. The experimental method must be applicable to specimens cured at room temperature and then post-cured at elevated temperatures. Thermal stresses arise, however, when the material is heated. These stresses and the associated high temperatures can be expected to promote viscous flow since the matrix is viscoelastic and is not fully cross-linked at this stage. As a result of viscous flow during the post-cure process, there is no longer a direct correspondence between stress and the distribution of molecular orientation. The photoelastic technique is therefore not applicable.

[xix] Reflective material can be bonded to the surface of an opaque subject. By applying a layer of photoelastic material over the reflective coating it is possible to measure the change in stress, and hence strain, in the photoelastic material from the reflected light. Once the change in strain on the surface is known, the change in stress within the subject can be determined. The measured stress in this case is the equivalent change in stress applied to a homogeneous material. Micro-scale residual stresses within individual components of a heterogeneous material cannot be measured using reflective photoelasticity since these stresses are in self-equilibrium when the photoelastic material is applied.

[xx] Glass fibres are transparent and GFRP is consequently translucent. It might seem, therefore, that this issue can be avoided with GFRP. The measured difference in principal stress is, however, an average through the sample thickness.[157] Since the stress in the glass and its photoelastic sensitivity are different from those of the polymer matrix, useful measurements are prevented if light travels through a fibre.

3.3.5 Acoustic waves

Both the velocity and polarization of acoustic waves are altered by stress.[158] By measuring changes in these parameters, therefore, acoustic energy can be used to measure residual stresses.

Residual stress measurement using changes in wave velocity has been widely performed.[159, 160] The sensitivity of this technique is, however, limited because the wave velocity typically changes by less than 1%.[158] In addition, the wave speed is strongly influenced by temperature.[161]

Changes in polarization give rise to interference between waves that would, in the absence of stress, remain in phase. The resulting patterns of interference, which are not affected by temperature, allow the underlying stress patterns to be deduced.[158] This approach has been used by Ostertag and Drescher-Krasicka[158] to image the residual stresses in silicon-carbide reinforced alumina. In this case, interference between shear waves propagating through the thickness of a model composite allowed the stress patterns around the three internal fibres to be observed along their length[xxi].

The use of acoustic waves for residual stress measurement in heterogeneous materials is, however, problematic. The wave length must be long enough that it does not "see" the microstructural features within the laminate. This allows the propagation of the wave, but effectively means that the samples appear as homogeneous[158] with consequential limitations in resolution. The measured stress is effectively the average stress over the path that the wave travelled. No information regarding the stress in either the fibre or matrix individually is available.

Ostertag and Drescher-Krasicka[158] imaged residual stresses in model composites with large (140 μm diameter) fibres. Differences in stress magnitude were apparent between specimens with large and small radial residual stresses. These stresses were not quantified, however, because the average stress sampled by the wave as it travels through the laminate thickness cannot be related to a quantifiable stress component. In real laminates, with significantly smaller fibres packed throughout the laminate, the lack of resolution would prevent the stress pattern around individual fibres from being discerned.

[xxi] The high resolution required of such measurements required the use of a scanning acoustic microscope rather than more readily available ultrasonic equipment.

Rather than propagating waves in the plane perpendicular to the fibres, the longitudinal micro-scale residual stresses in GFRP could perhaps be measured by propagating longitudinal waves down their length and measuring stress related changes in the wave properties. Compatibility between the strains in the fibre and the surrounding matrix, however, ensures that the wave must propagate at the same speed in both constituents. The wave must accordingly disperse into the surrounding matrix, becoming equivalent to a longitudinal wave propagating through a "homogeneous composite" material. It would only be possible to extract information regarding the "average" stress in the composite material in this situation. Since this stress is zero irrespective of the micro-scale residual stress state, this approach is unworkable.

It is apparent therefore that the propagation of acoustic waves both in the plane perpendicular to the fibres and in the fibre direction is associated with a lack of resolution. The use of acoustic waves for quantifying the micro-scale residual stresses in GFRP is accordingly prevented.

3.4 Methods that measure the elastic response to temperature changes

3.4.1 Measurement of curvature

Measurement of the temperature-related change in curvature has been frequently used to measure the residual stresses within unsymmetric laminates.[19, 21, 162–166] The method is based on the phenomenon exploited in thermostats using bi-metallic strips. The curvature of an unsymmetric laminate varies with temperature if the coefficient of thermal expansion in a particular direction changes from ply to ply. This variation can be predicted using classical lamination theory, which typically predicts simultaneous curvature in the two reference directions. In reality, thin laminates are bi-stable, meaning that the laminate assumes a cylindrical shape, the axis of which can be swapped between two directions.[21] This occurs because curvature in one direction tends to restrain curvature in the other.[21] For this reason, curvature measurements are performed on thin strips aligned in the direction of interest. The short dimension across the strip minimizes the displacements, and the consequential restraining effects, resulting from the secondary curvature.[21]

The technique relies on finding the "stress-free" temperature. This is typically done by measuring the curvature at a number of temperatures and then extrapolating these measurements to find the temperature at which the laminate is flat. Once the

stress-free temperature is found, the meso-scale stresses at other temperatures can be found using classical lamination theory.[21] It is also possible to determine the micro-scale residual stresses within a ply if a mathematical model such as that of Nairn[167] is used. It is simply necessary to know the stress-free temperature and the temperature-dependent elastic properties of the constituent materials.

Symmetric laminates do not curve with changes in temperature. Symmetrical laminates have, however, been cured onto a thin steel sheet[165] which acts as a "dummy ply". This has the effect of creating an unsymmetric laminate, allowing the measurement of the stress-free temperature and hence the micro-scale residual stresses.

A dummy ply, therefore, allows the measurement of micro-scale residual stresses in unidirectional laminates. This is only true, however, if the laminate is cured onto the dummy ply. Under these circumstances, the laminate is flat when both the micro-scale and meso-scale residual stresses are zero. This approach cannot be used for this work, however, because the dummy ply must be removed from the GFRP specimens prior to their immersion in a corrosive medium so that the rate of environmentally assisted crack growth can be measured. This prevents measurement of the residual stresses in the specimens at the completion of the test. This is an important limitation, because moisture diffuses into the laminate while it is immersed in the corrosive medium and hence alters the residual stress state.

Another problem with the use of a dummy ply is alluded to by Gigliotti *et al.*.[163] Differences in thermal expansion cause shear stresses at the interface between a composite specimen and a tool surface. These stresses result in non-thermoelastic strain,[163] presumably as a result of viscous flow during the curing process. Since the dummy ply is equivalent to a tool in this situation, it can be expected that the non-thermoelastic strains artificially influence the measured stress-free temperature.

The use of a dummy ply cannot be used either with laminates that were fabricated for purposes other than for performing residual stress measurements. This prevents the residual stresses from being measured in, for instance, failure investigations[xxii]. Although this particular limitation is not necessarily important, the inability of the method to be applied in investigations into the rate of environmentally assisted cracking means that an alternative approach is required. If this method can also be used on existing laminates, this would be advantageous.

[xxii] Unless the dummy ply is applied during cure, the method cannot reveal the stress-free temperature, and hence the micro-scale residual stresses, in the laminate. Unidirectional laminates are symmetrical and are consequently always flat irrespective of the micro-scale residual stress magnitude. Adding the dummy ply at a later stage merely allows the stress-free temperature of the adhesive to be found. This has no relation to the stress-free temperature of the laminate.

3.4.2 Cure referencing method

The cure referencing method[168–170] is an elegant method of measuring the residual strains associated with the curing process of polymer composites. Attempts to measure these strains using embedding strain gauges[171,172] and fibre optic Bragg gratings[173] have been subject to criticism regarding whether they measure the residual stress in the laminate, or rather the effect of the sensors on the residual stress.[168]

The cure referencing method avoids these concerns by replicating a moiré diffraction grating onto the surface of a laminate prior to gelation of the resin in an autoclave. The grating is thus applied to the laminate in its stress-free state. After curing, the strains relative to this condition can be measured by means of moiré interferometry. The polymerization cure shrinkage can be isolated from the thermal strains by measuring the residual strain at the cure temperature.

The longitudinal residual stresses in a unidirectional laminate can clearly be found using this method. Since the fibres and matrix are bonded together they both have the same longitudinal strain as the laminate. If they were unstressed, however, they would strain to different degrees. The difference between the laminate strain and the unstressed strain of each constituent consequently defines its micro-scale residual strain. The micro-scale residual stresses can be found using a model such as that of Nairn.[167]

The cure referencing method is, however, unsuitable for use with room temperature cured laminates that are later post-cured. The post-curing process involves heating the resin system to promote further cross-linking. Cross-linking, therefore, does not take place at a constant temperature. Furthermore, since polymer matrices are viscoelastic,[149,174] the high temperatures combined with the associated thermal stresses can be expected to promote some viscous flow prior to full cross-linking of the resin. The temperature at which the moiré grating is undeformed, therefore, cannot be taken as corresponding to the temperature of the stress-free state.

Although it is not necessarily important, the cure referencing method has another disadvantage. The moiré grating must be applied during manufacture, and so the method can only be applied to laminates that are specifically fabricated for the purpose of measuring residual stress.

3.4.3 Local heating methods

The need to drill a hole, thereby damaging the subject of interest, is a major disadvantage of the hole drilling method. An alternative technique has been developed,[175–177] that makes use of localized heating to achieve the same result.

A small spot (2 mm diameter) on the surface of a steel subject is heated to around 200°C for a few seconds by means of an infra-red laser. The elevated temperature in this region results in the localized reduction of the yield strength. Plastic flow can thus occur, thereby releasing some of the residual stress. The resulting surface deformations in the surrounding material are measured using electronic speckle pattern interferometry when the subject has cooled to ambient conditions. The measured surface deformations are then processed to determine the strain relief and hence the residual stresses prior to heating.[177]

Although the method is conceptually simple, it is complicated by a number of factors. The method relies critically on the variation in yield stress, elastic modulus and coefficient of thermal expansion with temperature.[175] This information is incorporated into a finite element model to determine the degree of stress release. The model must incorporate the changing temperature through the thickness of the subject. In addition, since the degree of heating is deliberately kept low[xxiii], the stress release that occurs at low stress levels is limited.[176]

The method has only been applied on steel to date. The method could, however, be adapted to the measurement of residual stresses in unloaded unidirectional GFRP. In this case, viscous flow of the polymer matrix would make it far more sensitive to heating than the glass fibres. Upon cooling, the stress state of the matrix would be different to that prior to heating. Interferometric techniques could be used to measure the resulting elastic response in the material surrounding the heated zone.

As with the original method, the response would need to be calibrated against a finite element model. Required input parameters for the model would include the variation in yield stress, elastic modulus, coefficient of thermal expansion and heat transfer coefficients of the matrix as a function of temperature. The model would also need to incorporate the effects of directional fibre reinforcement.

Heating of the matrix can cause viscous flow to occur, particularly when the stresses

[xxiii] Non-linear processes other than the release of stress are not desired.[175] Thus the application of too much heat or the too rapid heating of the material must be avoided. In addition, localized compressive plastic flow from constrained thermal expansion must be avoided.

are high. It is consequently improbable that non-linear behaviour of the system could be avoided. The finite element model would therefore need to incorporate polymerization cure shrinkage and the viscous response of the matrix as a function of both temperature and stress. Maximum sensitivity would then be achieved by heating the matrix to above the glass transition temperature, T_g. In this scenario, the cool material around the area of localized heating would largely prevent its thermal expansion, giving rise to compressive stresses. The high temperatures combined with the stresses in the heated area would facilitate viscous flow, resulting in the release of both the compressive stress and the original residual stresses. Upon cooling, significant thermal stresses would develop in the matrix of the heated region. The change in these stresses as a result of the heating process could be deduced from the elastic response in the surrounding material. This would allow the original residual stress state to be determined.

This approach has the advantage over the original method in that large changes in the matrix stress within the heated zone would correspond to small residual stresses. It is complicated, however, by the need to build a detailed non-linear finite element model which would not be easy to calibrate. In addition, for typical fibre volume fractions, the low stiffness of the matrix in comparison to that of the fibres would limit the magnitude of the elastic response of the surrounding material in the direction of the fibre. This effect would reduce the overall sensitivity, and hence utility, of the method.

3.5 Proposed new method

Of all the experimental techniques that exist for measuring residual stress, only three can possibly be considered as meeting the specifications of the required measurement technique. None of them are ideal and all have serious problems associated with them:

- The micro-indentation method appears to require expensive equipment. Even using the appropriate equipment it seems that considerable scatter in the measured results should be expected. In addition, the method relies heavily on the assumptions inherent to the analysis technique used to interpret the results.
- The matrix etching technique has not been used with either small diameter fibres or polymer matrices. It appears that problems associated with removal of the polymer matrix and subsequent fibre bending will prevent its practical use with

GFRP.

- The local heating method would require the use of a sophisticated non-linear finite element model for calibration purposes if applied to a polymer composite. In addition, its sensitivity is expected to be poor.

Although neither method can practically be used on its own, both the matrix etching technique and the local heating method possess significant advantages. The matrix etching technique relies only on measurement of the change in fibre length and the matrix is not considered. Since the fibre can be assumed to be elastic, the analysis is simple even if the matrix exhibits significant non-linearity in material properties. The local heating method exploits changes in the matrix material properties without physically removing the material.

The two methods are thus complementary. The benefits of each compensate for the disadvantages of the other. If they could be combined in such a way so as to maintain their benefits without introducing additional complications, a very useful new technique would be obtained. This technique would be ideal for use on unloaded unidirectional GFRP.

One way in which these techniques can be combined is to heat the entire unidirectional laminate to temperatures above T_g. At these temperatures the elastic modulus of the resin system can be two orders of magnitude smaller than that at room temperature.[149] The elastic constraints on the fibre are thus minimized without physically removing the matrix material. The problems of the matrix etching technique are consequently no longer an issue. The matrix is not physically removed and the fibres are not free to bend. By heating the entire laminate rather than a localized region, elastic constraints on the heated region are minimized and the sensitivity of the method is improved in comparison to that of the local heating technique. Additionally, since this approach would not require the manufacture of laminates specific to its use, it would be applicable to unidirectional laminates that are manufactured for reasons other than residual stress measurement.

The residual stress state can be found by monitoring the apparent thermal expansion of the material as it is gradually heated. Even though the glass fibre and the matrix have different coefficients of thermal expansion, the strain in these constituents is identical because internal stresses develop to force compatibility. The internal stress state consequently varies with temperature. At temperatures above T_g, however, the elastic modulus of the matrix is very low in comparison to that at room temperature. The matrix is consequently unable to apply significant restraint to the fibres and

the composite expands at a rate equal to that of unstressed glass fibre. The linear thermal response of the fibres above T_g can be extrapolated back to temperatures less than T_g, thereby defining the locus of zero stress in the glass fibre. The difference between the measured thermal response of the composite (and hence the glass fibre) and the locus of zero fibre stress defines the mechanical strain in the fibres. Once the mechanical strain in the fibres is known, the residual stresses can be found either through the use of Hooke's Law or the model of Nairn.[167] The method and its theoretical basis are explained more fully in the following chapter.

4 Basis for proposed method

The rate of longitudinal thermal expansion in a unidirectional composite material does not typically correspond to that of either of its constituents. The compatibility condition requires that the overall strain of the fibres matches that of the matrix. Since the individual coefficients of thermal expansion of the constituents are different, stresses are set up between the fibres and matrix that allow compatibility to be satisfied. The effective coefficient of thermal expansion (CTE) of the composite material consequently falls between that of the fibres and that of the matrix, the actual position depending on the volume fractions and the relative moduli of the constituents.

The elastic modulus of a polymer matrix changes with temperature. For a thermoset resin the modulus drops off dramatically as the glass transition temperature, T_g, is approached.[149] This effect is illustrated in Figure 4.1 for Derakane 411-350 epoxy vinyl-ester resin[i]. It is apparent that the elastic modulus drops to approximately 2.5% of the room temperature value at the nominal glass transition temperature of 120℃. At higher temperatures, the elastic modulus drops still further to well below 1% of the value at ambient conditions.

It is necessary, therefore, to take account of the changes in resin modulus when attempting to model the thermal response of a composite material. In addition, allowance must be made for changes in the coefficient of thermal expansion of the resin which increases significantly at temperatures above the glass transition temperature.[179] It must also be recognized that polymer matrices are viscoelastic[149, 174] and their response to mechanical loading consequently has both elastic and viscous components. If the material exhibits linear viscoelasticity, this effect can be considered by using a complex modulus with real and imaginary components. The real

[i]These DMA (Dynamic Mechanical Analysis) data were collected by Mr. K. M. Midor using a TA Instruments DMA 2980 apparatus. The temperature was ramped at a rate of 3.0℃/min and the storage modulus was recorded at an oscillation frequency of 2.0 Hz. Data were recorded every two seconds. To correct errors introduced in DMA,[19] the presented data are scaled to match the room temperature elastic modulus of 3200 MPa as listed by the supplier.[178]

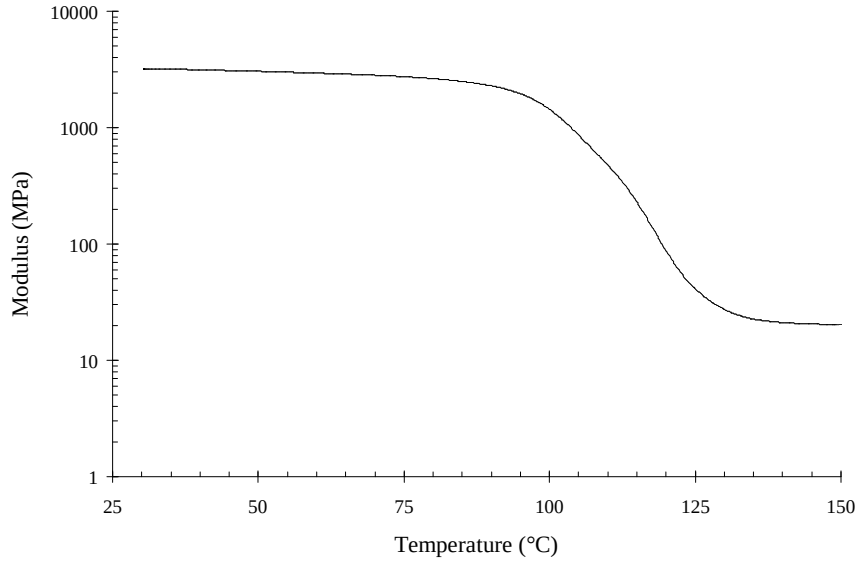


Figure 4.1: Temperature variation of modulus in Derakane 411-350

component, known as the storage modulus, relates stresses to elastic strains. The imaginary component, known as the loss modulus, relates stresses to viscous strain rates.

The measured relationship between the components of the complex modulus and the temperature depends on the time scale of testing. A consequence of the principle of time-temperature equivalence, however, is that the shape of a curve describing this relationship, such as that for the storage modulus illustrated in Figure 4.1, is constant and is merely shifted along the temperature axis to reflect changes in experimental time scale.[19] The slower the time scale, the more the curve is shifted to the left. This means that matrix properties such as T_g depend also on the experimental time scale.[180] A slow time scale results in the measurement of a lower T_g than a fast one, for instance. Since the storage modulus does not change significantly with temperature at either ambient conditions or temperatures well above T_g, it is not affected to any great extent by shifts along the temperature axis. The time-dependency of the storage modulus in these regions is thus low.

The reduction in storage modulus illustrated in Figure 4.1 arises from the uncoiling of macromolecular chains in the polymer at temperatures in the vicinity of T_g. Strains arising from macromolecular uncoiling are known as conformational strains. Since these strains cause the chains to slide over each other, they are responsible for the viscous response of polymers. The rates of conformational strains depend significantly on temperature.[181] At temperatures well above T_g, conformational strains are so fast as to be essentially instantaneous, whereas at temperatures well

below T_g the rate is very slow and so the strains appear "frozen in".[181] In both of these regions, therefore, the material behaves elastically and viscous effects are negligible.

Analysis methods based on elasticity can consequently be used in these temperature ranges without introducing significant error. It is only at intermediate temperatures that viscous stresses become important.[181] In cross-linked materials, viscous flow cannot continue indefinitely[182] however, and so if time is provided for their dissipation, the elastic response, which can be predicted using elastic techniques, still remains. A slow rate of heating consequently helps minimize viscous stresses, resulting in an approximately elastic response. An elastic solution can thus be used at these temperatures also. A slow rate of heating, however, causes thermal stresses to increase only gradually and so increases the experimental time scale. The variation in modulus with temperature illustrated in Figure 4.1 must consequently be shifted to the left to be relevant.

An elastic solution developed by Nairn[167] allows the thermal expansion of a unidirectional composite to be considered. This solution accommodates temperature-dependent matrix properties and Poisson's effects, but the necessary mathematical manipulations obscure the underlying mechanisms. A simpler method, having a form similar to that of the well-known equation of Schapery[183] is consequently developed in Appendix A. An approximation to the longitudinal thermal response, ϵ_{1-2}, of a composite material between temperatures T_1 and T_2 can be obtained from the following equation.

$$\epsilon_{1-2} = \frac{E_f V_f \alpha_f + E_{m_2} V_m \alpha_{m_{02}}}{E_f V_f + E_{m_2} V_m} (T_2 - T_0) - \frac{E_f V_f \alpha_f + E_{m_1} V_m \alpha_{m_{01}}}{E_f V_f + E_{m_1} V_m} (T_1 - T_0) \tag{4.1}$$

where E_f, α_f and V_f are the longitudinal elastic modulus, the coefficient of thermal expansion and the volume fraction of the fibre. E_{m_1} and E_{m_2} are the elastic moduli of the matrix at temperatures T_1 and T_2 respectively. $\alpha_{m_{01}}$ and $\alpha_{m_{02}}$ are the effective coefficients of thermal expansion of the matrix between the stress-free temperature, T_0, and T_1 and T_2 respectively. V_m is the volume fraction of the matrix.

The above equation also assumes elastic conditions but neglects Poisson's effects. It is clear that the thermal response between temperatures T_1 and T_2 depends on the stress-free temperature, T_0. Illustrative behaviour predicted for an EPON 828

epoxy/E-glass laminate[ii] of 40% fibre volume fraction is presented in Figure 4.2 for three different stress-free temperatures.

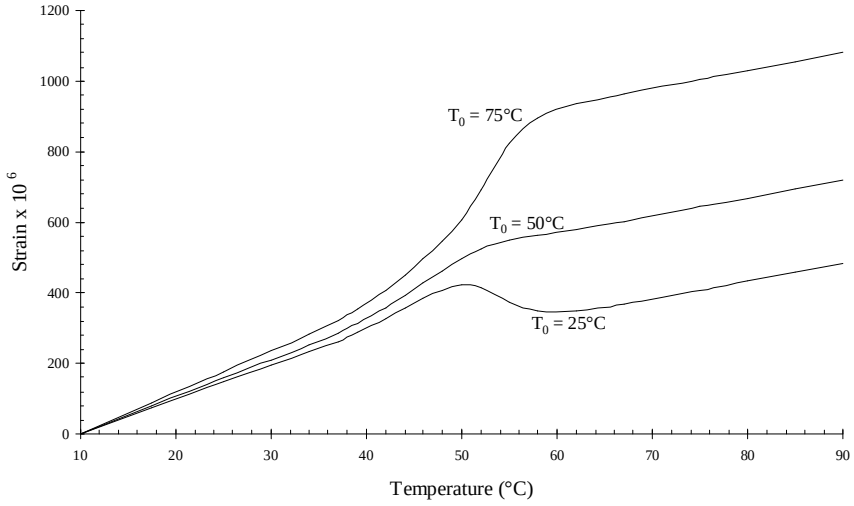


Figure 4.2: Illustrative longitudinal thermal response of EPON 828/E-glass laminate

It can be seen from Figure 4.2 that the thermal response depends significantly on the stress-free temperature. Differences in temperature relative to the stress-free temperature define the state of residual stress within the composite material. It is consequently apparent that the state of residual stress in a composite material determines its thermal response. In addition, two regions of linearity are evident in the longitudinal thermal response of a composite material. At low temperatures the modulus of the matrix varies only slowly and as a consequence the thermal response is fairly linear. At high temperatures the elastic modulus of the matrix drops to very low values. As a consequence, the matrix is unable to significantly influence the thermal response of the fibre. The measured thermal response of the composite above a certain temperature, referred to as the relaxation temperature, is thus hardly distinguishable from the linear response of the unstressed fibre. It is this phenomenon that provides a means of estimating the residual strains within a unidirectional GFRP laminate. The technique is discussed in the next section.

4.1 Finding the residual strain in the fibres

The simplest approach to finding the residual strain in the glass fibres of GFRP is to assume that the matrix modulus drops sufficiently low at high temperatures

[ii] Inputs for equation 4.1 were obtained from the work of Hsueh and Chen.[184] The appropriate calculations are shown in Appendix A.2.

that it is unable to influence the thermal response of the glass fibre. The thermal response of the composite thus coincides with that of unstressed glass fibre in this region. Since the coefficient of thermal expansion of glass fibres is uniform over the operational range of polymer composites, the thermal response of unstressed glass fibre is linear. The region of linear response at high temperatures can therefore be extrapolated to lower temperatures, thereby defining a locus of zero stress in the fibre. The locus of zero fibre stress is illustrated in Figure 4.3 for the data set in Figure 4.2 corresponding to $T_0 = 25$℃.

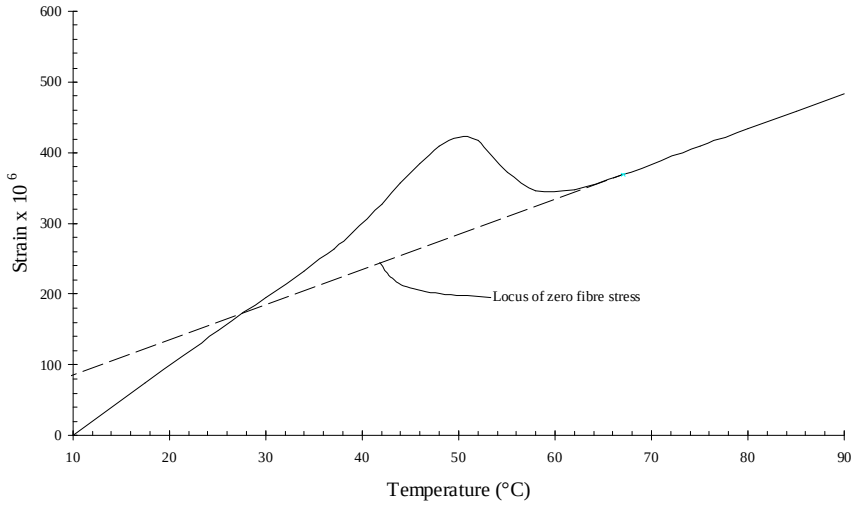


Figure 4.3: Extrapolation of the linear response at high temperatures defines the locus of zero fibre stress

The difference between the measured strain in the composite material and the locus of zero stress defines the longitudinal residual strain in the glass fibre. The residual strain obtained from the data presented in Figure 4.3 is plotted in Figure 4.4.

This approach is simple, and very convenient for it does not require knowledge of either the matrix or fibre properties. Since the matrix properties vary with temperature and environmental conditions this is an important advantage. Additionally, the method is unaffected by inelastic matrix strains, irrespective of their cause, since the matrix modulus always reduces to low values above the relaxation temperature. It can be seen, however, from Figure 4.4 that the temperature at which the residual fibre strains are zero does not correspond exactly with the stress-free temperature of 25℃ used to calculate the original curve in Figure 4.2. The discrepancy can be traced to the assumption that the thermal response of the composite coincides with that of unstressed glass fibre at high temperatures.

Although the elastic modulus of the matrix reduces to very low values, it never

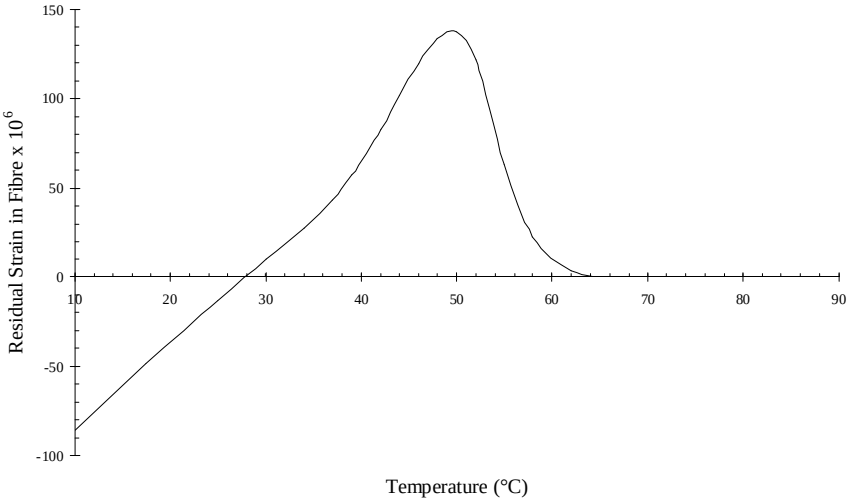


Figure 4.4: Variation in the residual strain in the fibre with temperature

reduces to zero. Since the coefficient of thermal expansion of the matrix is higher than that of the fibre, the actual thermal response of a composite in this region will always be slightly greater than that of unstressed fibre. In addition, its slope will not entirely match that of unstressed glass fibre. The magnitude of the discrepancy, $\Delta\epsilon$, can be found by comparing the thermal response of the composite material to that of unstressed glass fibre between the stress-free temperature, T_0, and a temperature, T_2, within the region where the matrix modulus has reduced to a low value.

$$\begin{aligned}
\Delta\epsilon &= \frac{E_f V_f \alpha_f + E_{m_2} V_m \alpha_{m_{02}}}{E_f V_f + E_{m_2} V_m} (T_2 - T_0) - \alpha_f (T_2 - T_0) \\
&= \left(\frac{E_f V_f \alpha_f + E_{m_2} V_m \alpha_{m_{02}}}{E_f V_f + E_{m_2} V_m} - \alpha_f \right) (T_2 - T_0) \\
&= \frac{E_{m_2} V_m}{E_f V_f + E_{m_2} V_m} (\alpha_{m_{02}} - \alpha_f) (T_2 - T_0) \\
&= \frac{\frac{E_{m_2}}{E_f} \frac{V_m}{V_f}}{1 + \frac{E_{m_2}}{E_f} \frac{V_m}{V_f}} (\alpha_{m_{02}} - \alpha_f) (T_2 - T_0) \qquad (4.2)
\end{aligned}$$

Since $\frac{E_{m_2}}{E_f} \frac{V_m}{V_f}$ is small (a requirement of the experimental technique) equation 4.2 can be written as follows:

$$\Delta\epsilon \approx \left(1 - \frac{E_{m_2}}{E_f} \frac{V_m}{V_f}\right) \left(\frac{E_{m_2}}{E_f} \frac{V_m}{V_f}\right) (\alpha_{m_{02}} - \alpha_f) (T_2 - T_0)$$

and if second order terms are neglected:

$$\Delta\epsilon \approx \left(\frac{E_{m_2}}{E_f}\frac{V_m}{V_f}\right)(\alpha_{m_{02}} - \alpha_f)(T_2 - T_0) \tag{4.3}$$

It is apparent that $\Delta\epsilon$ is equal to the ratio of matrix and fibre stiffnesses multiplied by the difference in their thermal strains. As a consequence, the lower the stress-free temperature, the greater the magnitude of the discrepancy between the thermal response of the composite at high temperature and that of unstressed glass fibre. The increase is not linear with temperature however, since neither E_{m_2} nor $\alpha_{m_{02}}$ are constant.

Provided that the variation in matrix modulus and coefficient of thermal expansion are known, it is possible to use equation 4.3 to calculate improved estimates of the residual strain in the glass fibre. The equation cannot be used directly, however, because the stress-free temperature, T_0, is unknown. The use of an iterative approach, therefore, eases solution of the problem.

As a first approximation, the error is assumed to be zero, and a line with slope equal to the known CTE of unstressed glass fibre is extrapolated back from the measured strain at T_2 to lower temperatures. The intersection between the measured thermal response of the composite and that of unstressed glass fibre defines the first estimate of the stress-free temperature, T_0. This value is substituted, along with the appropriate material properties, into equation 4.3 to find an estimate of the error. Once this value is known, the thermal response of the glass fibre is offset vertically by the corresponding quantity and a new estimate of T_0 is obtained. The value of the effective coefficient of thermal expansion, $\alpha_{m_{02}}$, is updated and a better estimate of the error is then found. This process is repeated until the calculated error converges to a constant value.

A process of this sort can be applied to the data presented in Figure 4.3. The results are presented in Figure 4.5. It can be seen that the locus of zero fibre stress is shifted downwards by approximately 11 $\mu\epsilon$. As a consequence, the intersection between the thermal response of the composite and that of unstressed glass now occurs at 25℃, as required.

The corresponding plot of the residual strain in the glass fibre is shown in Figure 4.6. Although the locus of zero residual stress was only shifted through approximately 11 $\mu\epsilon$, this is a material percentage of the measured residual strain. The use of a technique to better position the locus of zero stress can thus noticeably improve the measurement accuracy.

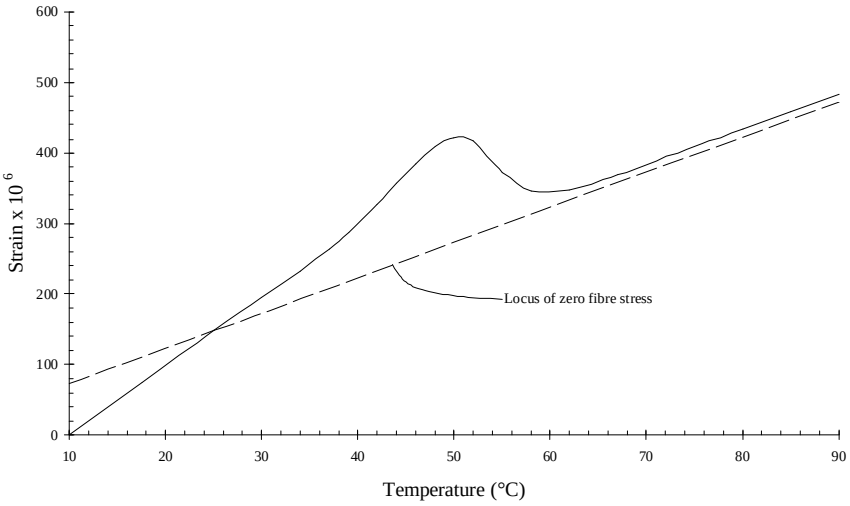


Figure 4.5: Corrected locus of zero fibre stress

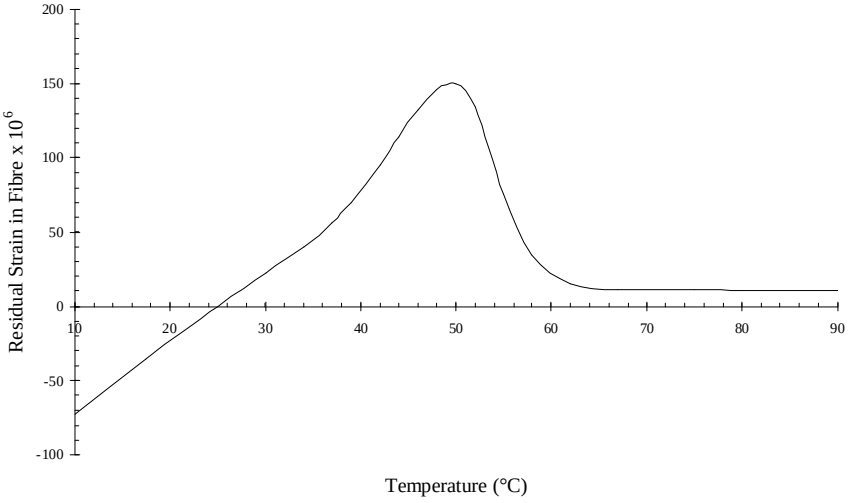


Figure 4.6: Corrected variation of residual fibre strain

Although equation 4.3 accommodates variations in matrix modulus and CTE with temperature, it is based on an analysis that ignores the effect of Poisson's strains. It is tempting to use a more comprehensive theory, such as that of Nairn,[167] to include Poisson's effects and so obtain an improved estimate of $\Delta\epsilon$. The usefulness of such an approach is questionable, however, because the improved estimate of $\Delta\epsilon$ is unlikely to be significantly different from that calculated using equation 4.3. Since $\Delta\epsilon$ calculated in the illustrated example is fairly small, inclusion of Poisson's effects is unlikely to change its value by more than a few micro-strains at most, well within the scatter bound of any likely measurement technique. The limited gains in accuracy are obtained at the expense of significantly greater complexity.

It must be acknowledged that viscous relaxation and polymerization shrinkage can occur as the composite is heated. Neither of these processes are elastic. It is therefore, at this stage, necessary to consider the effects of inelastic matrix behaviour on the accuracy of the calculated strains. The effects of viscous flow and polymerization shrinkage are considered individually.

Equation 4.1 is based on the assumption of linear viscoelastic matrix behaviour and that heating occurs sufficiently slowly that viscous stresses can dissipate. The assumption that viscous stresses dissipate is valid at temperatures where the resin modulus reduces to low values since conformational changes occur so fast in this region as to be nearly instantaneous.[181] It is not necessarily true that the matrix exhibits linear viscoelasticity, however. Stresses during a test can become sufficiently high that non-linear creep occurs and inelastic strains develop in the matrix. These strains are not considered in equation 4.1 and so this equation cannot be used under these conditions.

Equation 4.1 assumes that thermal stresses develop relative to a stress-free temperature. It does not consider the effect of additional stresses which develop from polymerization shrinkage when the composite is heated to temperatures greater than any previously experienced. If the polymerization shrinkage of the resin during heating is known as a function of temperature, it is possible to incorporate the effects of resin shrinkage into equation 4.3. This is done using the approach of Stone *et al.*[12] who recognized that cure shrinkage is analogous to thermal expansion. The component of equation 4.3 corresponding to the difference between the thermal expansion of the matrix and fibre is simply modified to incorporate the cure shrinkage, s_{0-2}, between T_0 and T_2.

$$\Delta\epsilon \approx \left(\frac{E_{m_2}}{E_f}\frac{V_m}{V_f}\right)\Big((\alpha_{m_{02}} - \alpha_f)\,(T_2 - T_0) - s_{0-2}\Big) \tag{4.4}$$

Equation 4.4 requires that the thermal history of the composite is known. The s_{0-2} term is the resin shrinkage that occurs during testing, rather than the total shrinkage between T_0 and T_2. Since the composite may already have been heated to a temperature higher than T_0, some shrinkage might already have occurred. The shrinkage that occurs during testing, therefore, is possibly smaller than the total shrinkage between T_0 and T_2.

Since equation 4.4 incorporates the effects of both viscous flow and cure shrinkage, it is the most accurate method of positioning the locus of zero fibre stress. Its use is limited to linear viscoelastic situations only, however, and requires that both the properties and thermal history of the matrix are known. If either non-linear creep develops during testing or the thermal history of the composite is not known, it is not possible to obtain a better estimate of $\Delta\epsilon$. It is probably preferable to abandon the use of $\Delta\epsilon$, and acknowledge the limitations of the subsequent strain measurements, rather than to introduce unknown errors.

4.2 Calculation of residual stress

Once the longitudinal residual strain in the fibre is known, the longitudinal residual stress can be estimated. The simplest approach is through the use of Hooke's Law. Since the modulus of glass fibre is constant over the operational range of polymer composites, an approximation to the longitudinal residual stress in the fibre can be found:

$$\sigma_f = E_f \epsilon_f \tag{4.5}$$

where σ_f and ϵ_f are the longitudinal residual stress and strain in the fibre at a given temperature.

The longitudinal residual stress in the matrix can then be found from equilibrium considerations:

$$\sigma_m = -\sigma_f \frac{V_f}{V_m} \tag{4.6}$$

The use of Hooke's Law neglects the effects of Poisson's strains caused by radial

and circumferential stresses. The magnitude of the errors caused by this omission is, however, limited by two effects:

- The radial and circumferential residual stresses in unidirectional GFRP are usually only a fraction of the longitudinal stress[iii].
- The Poisson's ratio of the glass fibre is low (0.22[185]), and so the effect of the transverse stresses is reduced.

It is important to emphasize that although the use of Hooke's Law limits the accuracy of the measured longitudinal residual stresses, it relies solely on the elastic properties of the fibres and does not require knowledge of any of the matrix properties. Since these depend on the resin system, the state of cure, the temperature, the moisture content, and potentially also on time and prior loading, this is a very important advantage. Furthermore, as will be discussed in the remainder of this section, it is in many situations impossible or impractical to improve on the accuracy of this approach.

More accurate estimation of the longitudinal residual stress requires knowledge of the transverse stresses so that Poisson's strains can be accounted for. Unfortunately these stresses are not easily measured. The same factors that plague almost all experimental methods when measuring the longitudinal residual stresses prevent their use in the measurement of the transverse stresses. The only way in which these stresses might be measured in GFRP is through the use of the incremental slitting method. This has been done for tungsten fibres embedded in a Kanthal matrix.[86, 87] The fibres were significantly larger, however, and spaced further apart than is typical in GFRP. In addition, the metallic matrix allowed the use of EDM which is prevented in this case. The smaller scales, coupled with the probable introduction of cutting stresses while creating the slit mechanically, render the practicality of this approach doubtful.

The only feasible approach to estimate the transverse stresses would thus appear to be the use of analytical methods. Both Ramamurty *et al.*[115] and Nairn[167] have presented methods that accommodate the effects of transverse thermal stresses in elastic systems. The method of Nairn is more general, however, and is therefore preferable. This method can also be adapted to calculate the elastic stresses arising from cure shrinkage and the release of preload strains in the fibre. Although the

[iii] The stresses are low in the transverse directions because the matrix strain is unrestricted by the fibres except in their immediate vicinity. In contrast, the matrix strain in the longitudinal direction is restricted by the fibres over the complete specimen volume.

polymer matrix behaves viscoelastically at temperatures near the T_g, it is possible to make use of an elastic solution to provide estimates of the stress state in this region if the matrix is heated only slowly so that viscous stresses have time to dissipate. Detailed discussion of the analysis methods and their implementation is presented in Appendix B.

Unfortunately, problems arise when combined loading is considered. Although Nairn's method can be applied to the calculation of elastic stresses arising from thermal effects, cure shrinkage and fibre preload, care has to be taken where these stresses are jointly present. In this situation, an infinite number of loading combinations can result in the same longitudinal fibre strain. The ratio of the transverse stresses to the longitudinal stresses is different for each loading case and so the Poisson's effects differ from load case to load case. The longitudinal stress can consequently only be calculated if the strain contributions from each load case can be determined. This is not possible in the general case where the loading history of the material is unknown, since only the combined strain can be established. As a consequence, the use of more sophisticated analytical methods is prevented and there is thus no point in attempting to obtain stress estimates more accurate than those obtained through the use of Hooke's Law. This issue is discussed in more detail in Appendix B.1.4.

In situations where the loading and thermal history of the laminate is known, it is possible to estimate the contributions to the longitudinal strain arising from thermal loading, cure shrinkage and preloading. In this situation, the use of Nairn's method can be used to obtain the elastic stresses acting on the fibre. Provided that linear viscoelasticity applies throughout the loading history, the use of an elastic solution provides a reasonable estimate of the elastic stresses.

At higher stresses and temperatures it is possible for relaxation to occur through non-linear creep. Linear viscoelasticity is no longer applicable and so the relationship between transverse and longitudinal stresses can no longer be reliably estimated using Nairn's method. Analysis of non-linear creep in the triaxial stress field around the fibres is not easily performed. In addition, the necessary temperature-dependent rheological information to properly model the matrix is not readily obtained. It is consequently not feasible to estimate the stress state under these conditions.

In summary, it is not possible to improve on the accuracy of Hooke's Law unless the loading and thermal history of the laminate is known. If this information is available, it is possible to obtain estimates of the elastic stresses provided that linear viscoelasticity applies throughout the loading history. If non-liner creep occurs,

however, it is only possible to obtain reasonable estimates of the stresses through the use of a sophisticated model that requires extensive knowledge of the matrix rheology. It is consequently impractical to find the stress state in this situation.

5 Experimental Technique

Although the conceptual approach required for measuring the residual stress in a unidirectional GFRP is easily understood, it is not entirely obvious as to how to go about performing these tests. As such, the experimental method evolved in response to specific problems that were encountered during each new attempt to perform the tests.

This section covers the entire evolution of the experimental technique from the first attempts through to the measurement of final results.

5.1 Basic equipment

As a practical method of measuring the residual stress in unidirectional GFRP was sought, it was found that the experimental approach was constantly evolving. As each approach was modified, some of the relevant equipment was no longer needed. In turn, however, this usually necessitated that new equipment had to be selected and applied in the modified approach.

Some equipment, however, was used throughout the development process. The details of this equipment are supplied in this section.

Equipment that was used for only part of the development process is described in the section where it was first specified.

5.1.1 Oven

The oven used for this work has internal dimensions of approximately 220 mm by 240 mm by 580 mm in the width, depth and height directions respectively. The oven is designed to fit within the uprights of J.J. Lloyd bench top tensile testing

machines. All surfaces, exterior and interior, are manufactured from stainless steel. Two holes of diameter 26 mm, at the centres of the top and bottom surfaces, allow access to the interior of the oven. Instrumentation wiring was run through the upper port, the lower port was blanked off.

The oven is equipped with a fan to ensure that the internal temperature distribution is uniform. Regulation of the internal temperature is achieved by means of a JUMO dTRON 04.1 programmable temperature controller with ramping function. The temperature signal for this controller is provided by a Pt100 resistance temperature sensor.

5.1.2 Temperature sensor

Temperature within the oven was measured by means of an LM35D integrated-circuit temperature sensor with a maximum operating temperature of 150℃. This chip was supplied with a 10.0 V DC power supply. The output signal of this sensor is directly proportional to temperature, 10 mV/℃, with a typical accuracy of ±0.9℃.[186]

Silicone rubber insulation for the power supply and output wires of this sensor were selected so that the insulation did not break down after an extended period at high temperature.

5.1.3 Data logger

Data were recorded by means of an ADC-100 data logger from Pico Technology Limited. This data logger performs analogue to digital conversion which is then communicated to a computer for storage via a serial cable.

The first of the two available channels recorded the output signal from the temperature sensor, the second recorded data that, after processing, yielded thermal strain readings.

5.1.4 Computer

A computer running PicoLog for Windows - Release 5.10.3 through Microsoft XP was used to control the data logger and store the resulting data. Since each test was

expected to last many hours, the computer was powered through an uninterruptable power supply (UPS).

5.1.5 Power supply

A DC power supply was used to provide power to the temperature sensor.

5.1.6 GFRP specimens

Two GFRP laminates with differing longitudinal residual stresses were manufactured using a custom-built precision winder to accurately position Owens-Corning T111A E-glass rovings with a linear mass of 400 tex around a steel frame. The frame comprised two drum sections held a distance of 1750 mm apart by removable steel plates. Winding the glass fibre onto the frame, created two "sheets" of unidirectional fibre, separated by the diameter of the drums, which increasingly grew in strand density and hence thickness. Once sufficient fibre had been wound onto the frame, it was removed from the winder and located into a loading rig. Each sheet of unidirectional fibre was then placed between two ground steel plates which were separated from each other by steel spacers of 3.00 mm thickness.

The plates separating the drums of the winding frame were then removed and hydraulic jacks were used to increase the distance between the drum centres. This tensioned the glass fibres within the steel plates. The fibres of one laminate, designated "Unloaded", were tensioned just enough to prevent displacement of the fibres during infusion of Derakane 411-350 epoxy vinyl-ester resin using vacuum assistance. The fibres of the other laminate were pre-tensioned prior to resin infusion.

The laminates were cured at a temperature of 60℃ and a pressure of 6 bar. They were then post-cured overnight at a temperature of 92℃ after which they were cooled before the preload tension was released and they were removed from the mould. The use of a high curing pressure ensured laminates of nearly zero void content. The cured laminates had an average fibre volume fraction of 40%, a uniform thickness of 2.95 mm and good fibre alignment.

Specimen sets were then cut from each of the plates using a rotary diamond cutter. The specimens had a length of 250 mm aligned with the fibres and a width of

20 mm[i]. The specimens from the pretensioned laminate were then divided into two sets. One set was designated "Preloaded" and the other set, designated "Annealed", was placed into an oven at 80℃ for a period of 100 hours to promote relaxation of residual stresses.

5.2 Measurements using strain gauges

By far the most convenient method of measuring the strain in the specimens as a function of temperature would be through the use of strain gauges. The necessary equipment is low in cost and the required skills are readily available within most industrial organizations. If this equipment could be used it would dramatically increase the potential use of the method in practical situations.

It was also recognized from the start, however, that strain gauges are not really appropriate for application where the elastic modulus of the specimen is low. This could preclude the use of strain gauges in this application.

The potential benefits associated with low cost and ease of use however, made it worthwhile to investigate the possibility of performing tests in this manner. This section describes the method that was followed and presents results obtained using this approach.

5.2.1 Introduction

The method used for determining the strain response to changes in temperature was based on that described by Jeronimidis and Parkyn.[21] Two active strain gauges and two strain gauges mounted on a reference material with known thermal response, in this case AISI 4340 steel, were used to complete a full bridge. The temperature of the bridge was ramped at a rate of 6℃ per hour. Strain was measured relative to the known expansion of the steel reference material. The overall strain of the specimens was then found by simply adding the measured strain to the known strain response of the reference material.

[i]The dimensions of the specimens were determined by the needs of the overarching investigation into EAC which loads the specimens in 4-point bending. A long specimen ensures a low compliance in bending, allowing the stress intensity to be accurately adjusted using displacement control. A length of 500 mm is intended for the EAC investigation. Since this specimen will be cracked at its midpoint, the specimens used in the current investigation are taken each side of the crack and so are only half as long.

5.2.2 Additional equipment

5.2.2.1 Strain gauges

Kyowa foil gauges of type KFG-5-120-C1-11 were used. Details of the gauges are listed below:

Nominal gauge length : 5 mm
Nominal resistance : 120 Ω
Gauge factor : 2.11 ± 1 % (24℃, 50% RH)
Transverse sensitivity : 0.40 % (24℃, 50% RH)
Temperature coefficient of the gauge factor : 0.8 ± 0.5 %/100℃
Maximum rated temperature : 150℃

5.2.2.2 Specimens

Two different types of specimen were used; pure cast resin and resin reinforced with unidirectional glass. Two specimens of each type were manufactured.

The specimens of cast resin (Derakane 411-350) were manufactured by cutting two blocks measuring approximately 20 mm by 20 mm from a plate of approximately 5.5 mm thickness. This plate had been left to cure at room temperature for 24 hours. It was then subjected to a post-cure schedule whereby the temperature was ramped from 50℃ to 90℃ at a rate of 10℃ per hour. Thereafter, the plate was left overnight at a temperature of 90℃. To prevent unsymmetric bending, the plate was held between two heavy steel plates during the post-cure schedule.

After appropriate surface preparation, two strain gauges were bonded to opposite faces of each specimen. The adhesive used for the first specimen was Kyowa CC-33A , a fast-curing cyanoacrylate adhesive with a maximum rated temperature of 120℃. The adhesive used for the second specimen was HBM X280. This is a two part, room-temperature curing adhesive with a maximum operating temperature of 280℃.

The glass reinforced specimens comprised a single specimen each of the unloaded and preloaded specimen types. Each specimen was prepared by lightly sanding one its faces and then cutting the strip in half. The two halves were then “folded” onto each other and bonded (using Derakane 411-350 - the resin system used for the

matrix) such that the sanded faces were mating. This technique ensured that the specimens were symmetric and hence prevented spurious measurements resulting from temperature dependent curvature.

A length of approximately 20 mm was then cut from each of the two bonded specimens. These specimens had a thickness of approximately 5.9 mm and a width of 20 mm. After the correct surface preparation, a strain gauge was bonded to each of the two edge faces aligned in the fibre direction. Care was taken to ensure that each gauge was centrally located over, and aligned with, the mid-plane of the specimen. The adhesive used for the glass reinforced specimens was HBM X280.

5.2.2.3 Wheatstone Bridge

Four strain gauges were used in a full-bridge configured to eliminate a bending response. Two active gauges were bonded to opposite sides of each test specimen, the remaining two gauges were bonded to opposite sides of an AISI 4340 steel plate using HBM X280 adhesive.

To eliminate any potential problems caused by changes in lead resistance, the strain gauges were all soldered directly to a "Veroboard" strip. The electrical resistance of the channels on this strip was reduced as far as possible by minimizing the length of each channel (approximately 25 mm) and by applying a thick bead of solder along each channel. The layout of the bridge is shown diagrammatically in Figure 5.1.

The entire bridge was heated as a unit. Since the rate of heating was low, it could be assumed that all gauges were at the same temperature. Consequently, the output signal from the bridge depended only on the differential thermal expansion between the AISI 4340 steel plate and the test specimens.

5.2.2.4 Strain amplifier

Amplification of the output signal from the Wheatstone bridge was performed using a Q2 amplifier manufactured by I.E.M. (Instruments for Engineering Measurement) of Germiston, South Africa. This amplifier uses a 188 Hz AC carrier frequency to reduce the effects of electrical noise, and so increase its sensitivity. The amplifier is designed to be used with I.E.M. strain gauges with a gauge factor of 2.05. When using an I.E.M. gauge in a quarter bridge configuration, the internal amplification has three pre-calibrated settings such that the maximum output of ± 10.00 V DC

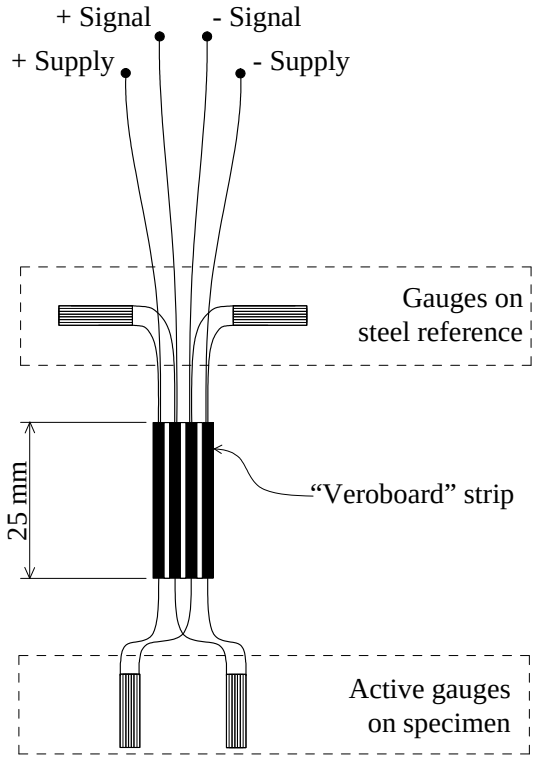


Figure 5.1: Schematic layout of Wheatstone bridge connections

corresponds to either $\pm 100\ \mu\epsilon$, $\pm 1\ 000\ \mu\epsilon$ or $\pm 10\ 000\ \mu\epsilon$. When using strain gauges with gauge factors other than 2.05, the measured strain can be obtained by taking the ratio of the two gauge factors and multiplying that value against the nominal measurement.

5.2.3 Experimental method

The gauges of each specimen were soldered directly to the "Veroboard" strip used in the Wheatstone bridge.

The supply and signal wiring of the Wheatstone bridge was threaded through the port at the top of the oven and connected to the strain amplifier. The bridge was then suspended in the centre of the oven. The temperature sensor was threaded through the same port until it hung next to the specimen. The door of the oven was then closed.

The output terminals from the strain amplifier and temperature sensor were connected to the data logger using shielded cable with BNC connectors at each end.

The data logging software was started and a new file opened. The software was set up to record data every minute. The values of the two logged parameters (temperature and strain) were averaged over this time interval.

The output from the amplifier was zeroed.

The logging software was started and left for approximately 30 minutes. This ensured that the software was working properly, and that the bridge was at the same temperature as the inside of the oven.

The data logging process was stopped and then restarted. This process overwrote the initial data recorded.

The oven was turned on and set so that its internal temperature increased at a rate of 6℃ per hour up to a maximum of 150℃. (A maximum temperature of 120℃ was used for the resin sample bonded with Kyowa CC-33A adhesive.)

When the maximum temperature of 150℃ was reached, the oven was turned off and logging of data was stopped.

5.2.3.1 Precautions

The amplifier and data logging equipment should be left on between tests to ensure that they are fully warmed up at the start of a new test.

5.2.4 Results

The results, as measured, reflect twice the difference in thermal strain between the specimen and the AISI 4340 steel plate because the bridge uses two active gauges. In order to obtain the actual thermal strain of the specimens, the measured strain must be halved and then added to the strain of the steel plate. This strain can be obtained by suitable manipulation of the data contained in literature such as the "Metals Handbook".[187] The process by which the thermal strains in the specimens is calculated is presented in Appendix C.

The method presented in Appendix C considers the effects of temperature on the output of the gauge but does not take into account errors introduced by transverse sensitivity of the gauge. These errors depend on the Poisson's ratios of both the AISI 4340 steel plate and the specimens.[188] The Poisson's ratio for the steel plate

is easily determined, but that of the specimens is more problematical. Depending on the temperature of the specimens, the elastic properties of the resin system change. Consequently, the Poisson's ratio for the specimens is a function of temperature. In principle, it is possible to determine the nature of this relationship and hence take account of the errors introduced by transverse sensitivity. Given the effort required and the limited gains in accuracy to be attained (the transverse sensitivity of the gauges is small - 0.40%) it was felt that the effort was not justified at this stage of the investigation.

5.2.4.1 Cast resin

Strain data for pure cast resin as measured on Specimen 1 using strain gauges affixed with Kyowa CC-33A cyanoacrylate adhesive are presented in Figure 5.2. Similar results as measured on Specimen 2 using strain gauges affixed with HBM X280 adhesive are superimposed on those of Specimen 1 in Figure 5.3. Data are offset to reflect zero strain at a room temperature of 25℃. Measured coefficients of thermal expansion for temperatures of 50℃ and less are presented in Table 5.1.

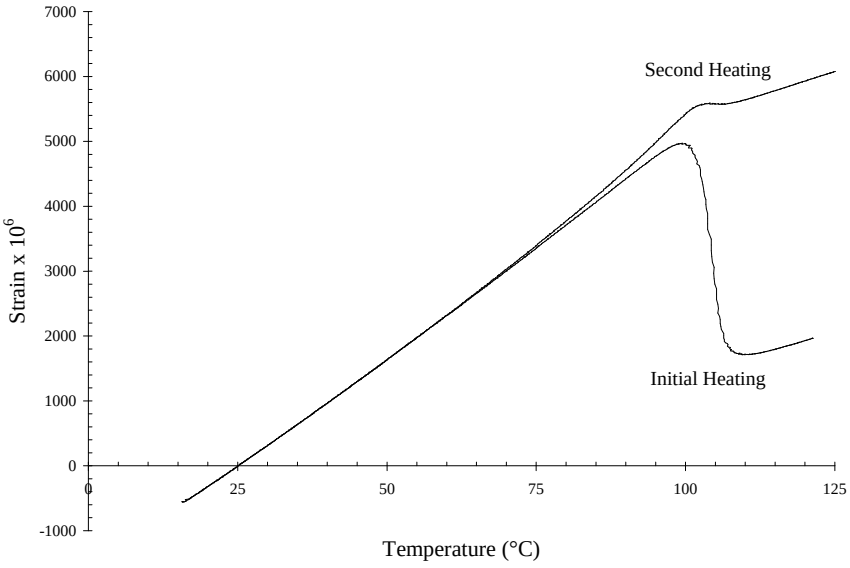


Figure 5.2: Apparent strain in cast resin - Gauges affixed with cyanoacrylate

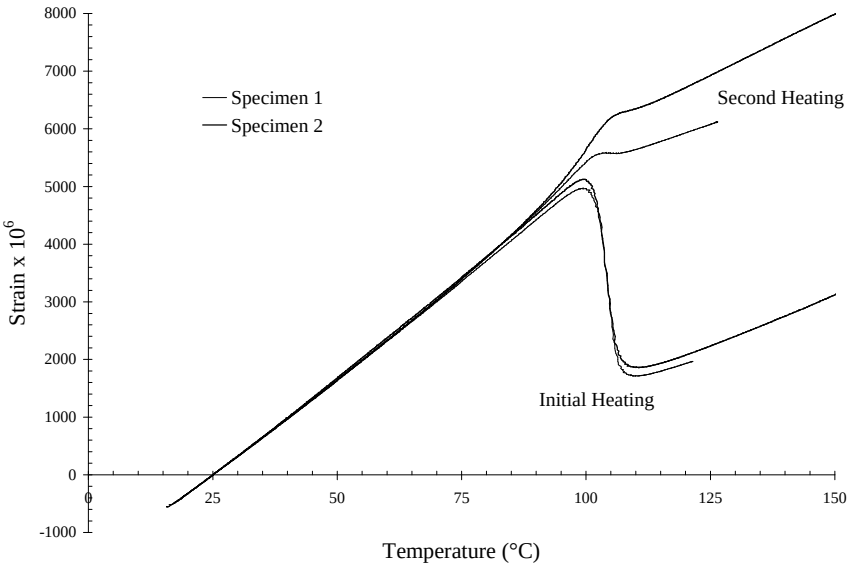


Figure 5.3: Comparison between apparent strains obtained from specimens with different strain-gauge adhesives

Table 5.1: Coefficients of thermal expansion of pure resin

	Temperatures ⩽50℃	
	Initial heating	Second heating
	($\mu\epsilon$/℃)	($\mu\epsilon$/℃)
Specimen 1	64.7	64.5
Specimen 2	66.5	65.6

5.2.4.2 Reinforced specimens

The strain data for the specimens reinforced with unidirectional glass fibre are presented in Figure 5.4. Again, data are offset to reflect zero strain at a room temperature of 25℃. Measured coefficients of thermal expansion for temperatures of 50℃ and less and also for temperatures of 120℃ and more are presented in Table 5.2.

Table 5.2: Apparent coefficients of thermal expansion of reinforced resin

	Temperatures ⩽50℃	Temperatures ⩾120℃
	($\mu\epsilon$/℃)	($\mu\epsilon$/℃)
Unloaded specimen	10.3	9.4
Preloaded specimen	9.6	8.7

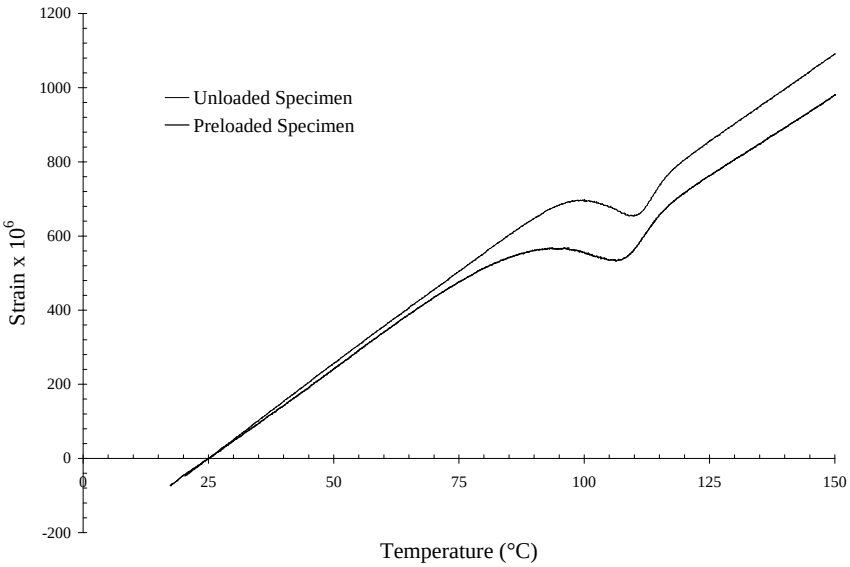


Figure 5.4: Apparent strain in glass fibre reinforced specimens

5.2.5 Discussion

5.2.5.1 Pure resin

5.2.5.1.1 Specimen 1

The first specimen to be tested made use of the Kyowa CC-33A cyanoacrylate adhesive for bonding the strain gauges. The results for the initial heating process of this specimen are shown in Figure 5.2. A linear increase in measured strain with temperature is visible up to approximately 100℃ as a consequence of thermal expansion. The measured slope at temperatures less than 50℃, prior to any significant drop in resin modulus, is 64.7 $\mu\epsilon$/℃. This value is in excellent agreement with the manufacturer's data-sheet[189] which lists an average value for the coefficient of thermal expansion of 64.8 $\mu\epsilon$/℃ between 24℃ and 49℃.

At a temperature of approximately 100℃, an abrupt change in behaviour is visible. Between this temperature and approximately 110℃, the strain data show an apparent contraction of approximately 3300 $\mu\epsilon$. This behaviour is expected as a result of additional polymerization reactions which occur at temperatures higher than those used in previous post-cure treatments. These reactions caused shrinkage which was significantly larger than the thermal expansion, thus dominating the measured strain in this temperature regime.

At still higher temperatures, from 110℃ up to 120℃, the maximum rated temperature for the adhesive affixing the strain gauges, the contraction of the specimen is no longer apparent and thermal expansion is again indicated. Once again, the measured behaviour of the specimen conforms to that expected. As the temperature of the resin increased, additional polymerization occurred until all available reaction sites within the polymer were exploited. No further polymerization could take place and further increases in temperature simply resulted in additional thermal expansion.

In broad outline then, the results from the first test making use of strain gauges appeared to be somewhat promising.

The same specimen was then tested again. It was expected that no further polymerization shrinkage would occur and that the measured response would correspond to thermal expansion only. The results for the second heating are overlaid on those of the initial heating process in Figure 5.2. The data before and after the initial test are essentially identical up to a temperature of approximately 65℃. This behaviour is expected since no cure reactions would have occurred so far below the post-cure temperature of approximately 92℃ in the first test, let alone the second test.

The data sets progressively diverge at a greater rate between 65℃ and 100℃. The data from the second test reveal a gradual increase in slope between 65℃ and 100℃, whereas the data from the first test are linear in this region. The measured data in the second test conform with typical experimental results for polymers[179] which indicate that the thermal expansion coefficient of polymers at temperatures well above than the glass transition temperature are greater than those below the glass transition temperature. A gradual increase in the rate of thermal expansion as the temperature approaches the glass transition temperature of approximately 120℃ is therefore expected. The linear behaviour between 65℃ and 100℃ in the first test reveals that shrinkage had started to develop at these temperatures, but it was not readily apparent. Since no curing reactions are expected below the post-cure temperature, the slow onset of shrinkage well below the post-cure temperature can probably be ascribed to hygrothermal shrinkage resulting from expulsion of moisture.

Between temperatures of approximately 100℃ and 110℃ almost no change in thermal strain is apparent in the results of the second heating. At temperatures greater than 110℃, the apparent coefficient of thermal expansion is very similar to that observed in the results of the initial heating process. The measured coefficient of thermal expansion at high temperatures is thus lower than that at low temperatures. This is contrary to typical measurements,[179] as well as the trends observed at lower temperatures, and indicates that strain gauges do not reflect the true strain of the

specimen above 100℃.

The discrepancy between actual strain and measured strain could arise for two reasons. Either the low modulus of the resin at higher temperatures prevents the application of sufficient load to overcome the elastic response of the gauge, or the adhesive between the specimen and the gauges shears as a consequence of the high temperatures. It was to distinguish between these two possibilities that the tests were repeated making use of a different adhesive.

5.2.5.1.2 Specimen 2

In this case, the adhesive used for affixing the gauges was HBM X280, a cold curing epoxy adhesive with a maximum operating temperature of 280℃. The maximum test temperature of 150℃ is well within the operating limits of the adhesive and hence shearing of the adhesive layer would not occur. If similar measurement errors as occurred in the results of the first specimen were found to recur, these could then be ascribed to the loss of resin modulus at high temperature.

The results from the tests on the second specimen are shown overlaid on those of the original tests in Figure 5.3. It is seen that the response of the second set of tests is almost identical to that of the first tests. The only significant discrepancy occurs at temperatures above 100℃ when the specimens are reheated.

The identical response for the initial heating of the specimens indicates that the incorrect slope of the thermal expansion curve at high temperatures is not caused by problems with the adhesive. Rather, the erroneous response must presumably be a consequence of the low resin modulus at high temperatures. This hypothesis is supported by noting that the onset of the erroneous response occurs in the 99℃ to 104℃ temperature range quoted by the resin manufacturer[189] as the heat distortion temperature (HDT). Under these circumstances, the resin is unable to apply sufficient load to overcome the inherent stiffness of the strain gauge. The result of this is that the coefficient of thermal expansion at high temperatures is underestimated.

The hypothesis is additionally supported by the discrepancy between the two sets of data above 100℃ during the reheating tests. The major difference between the testing procedures used for the two specimens is that the second specimen was initially heated to 150℃ instead of 120℃ as for the first specimen. Since the second specimen was heated well above the nominal glass transition temperature, all viscous stresses could dissipate whereas some were still present in the first specimen at 120℃. On cooling the second specimen to 120℃ the tensile stress in the gauges of

this specimen was consequently less than that in the gauges of the first specimen. Cooling the resin system to room temperature would have eventually placed the gauges into compression, the compressive strain in the gauges of the second specimen being greater than that in the gauges of the first specimen. When the specimens were reheated, the resin would again have applied tensile load to the strain gauges. The tensile stress in the gauges of the second specimen would, however, have been lower than that in those of the first specimen. Consequently, the second specimen could be heated to a higher temperature before the resin could no longer support the tensile stress in the gauge and erroneous results developed. This is exactly the type of behaviour demonstrated by the experimental results.

One of the consequences of this scenario is that the apparent cure shrinkage is overestimated. This is because the cure shrinkage occurs in the same temperature range as the drop in resin modulus. As a result, the tensile stress in the strain gauges prior to the onset of cure shrinkage is relieved when the resin softens. While the strain gauges contract under their own elasticity they are also exposed to simultaneous cure shrinkage. The consequence of this is that the apparent cure shrinkage is made up of both strain relief due to resin softening as well as cure shrinkage. The measured shrinkage therefore merely defines an upper bound to the cure shrinkage.

Although the experimental observations tie up with predictions made using the above hypothesis, it is, in fact, irrelevant whether or not the hypothesis is correct. The experimental observations clearly show that the use of strain gauges for measuring thermal expansion in the Derakane 411-350 resin system above a temperature of approximately 100℃ is invalid. The coefficient of thermal expansion at temperatures greater than this is incorrectly measured. In addition, it seems that the measured post-cure shrinkage is overpredicted.

In view of this conclusion, it was improbable that acceptable results would be obtained using reinforced specimens. In this situation, however, the strain gauges would be bonded, at least partly, to the glass fibres. This bond would not have been affected by the temperatures experienced during the test and it was therefore possible that the fibres might apply sufficient restraint to compensate for the resin. If this was the case, accurate results could possibly be obtained. It was therefore decided to investigate this possibility by testing a single specimen manufactured from each of the unloaded and preloaded specimens, reflecting the presumed minimum and maximum states of residual stress.

5.2.5.2 Reinforced specimens

The strain gauges of the reinforced specimens were affixed with of HBM X280 adhesive which has an operating range up to 280℃. Measurement errors arising from degradation in adhesive performance were therefore eliminated over the entire range of temperature measurement.

It is observed from Figure 5.4 that the thermal expansion of the two specimens is linear at low temperatures. Linear regressions taken through the two sets of data at temperatures of 50℃ and less, prior to significant non-linearity, indicate coefficients of thermal expansion of 10.3 $\mu\epsilon$/℃ and 9.6 $\mu\epsilon$/℃ for the unloaded and preloaded specimens respectively. The difference in these two values can probably be ascribed both to differences in fibre volume fractions between the two specimens and also to differences in internal stress state as evidenced in Figure 4.2.

The response of the unloaded specimen remains linear to high temperatures. The first hint of curvature occurs in the region of 90℃ which is very similar to the post-cure temperature of 92℃. Since no loads were deliberately applied to this specimen during post-cure, the internal stresses in this specimen are presumably low at this temperature. As a consequence, non-linearity arising from the release of internal stresses is delayed to higher temperatures where the modulus of the resin is significantly reduced.

Increasingly non-linear behaviour in the preloaded specimen is apparent as the temperature increases. The departure from linearity appears to begin at a temperature of approximately 65℃ and becomes increasingly apparent as the temperature increases.

Between a temperature of approximately 100℃ and temperatures of 107℃ and 110℃ for the preloaded and unloaded specimens respectively, the apparent strain in Figure 5.4 progressively reduces. Based on the results of the tests conducted on pure resin, it would be expected that contraction associated with polymerization shrinkage would become evident in this temperature range. The apparent reduction in strain can therefore be explained as a combination of progressive release of internal stress and post-cure shrinkage.

The strain results obtained for pure resin indicate that the available reaction sites for polymerization are fully utilized beyond temperatures around 110℃. Shrinkage associated with additional polymerization should therefore cease and thermal expansion should become evident as the temperature increases. Since the modulus of the resin

is dropping significantly at these temperatures, as seen from Figure 4.1, it would be expected that the coefficient of thermal expansion of the specimens would tend to monotonically approach that of E-glass fibre on its own. Instead, the apparent strain in the specimens rises sharply between temperatures of approximately 110℃ and 120℃ before falling back to a constant value similar to that at low temperatures.

Unfortunately, it is this behaviour that indicates the presence of erroneous readings and hence prevents the use of strain gauges in this application. The lack of correlation between the apparent coefficients of thermal expansion at high temperature and that of pure E-glass runs counter to the theoretical basis of the technique. Instead of a coefficient of thermal expansion of around 5.0 $\mu\epsilon$/℃ as given by literature for E-glass,[185, 190, 191] the measured coefficients of thermal expansion are 8.7 $\mu\epsilon$/℃ and 9.4 $\mu\epsilon$/℃ for the two specimens. These are far closer to the values measured at temperatures less than 50℃ than to the expected value at high temperatures.

In addition, the rapid rise in apparent strain between 110℃ and 120℃ is difficult to explain if the readings are correct. Trends in the data at lower temperatures indicate that the release of internal stresses tends to cause a reduction in apparent thermal strain. This is particularly true for the preloaded specimen. Further, polymerization of the resin system is expected to cause shrinkage rather than expansion. The most plausible explanation for this sharp rise in the apparent strain of both specimens is the release of compressive strain in the gauges. Such behaviour was able to occur when the modulus of the resin system reduced sufficiently that the specimens were unable to constrain the inherent stiffness of the strain gauges.

For this hypothesis to have any validity, the strain gauges must be loaded in compression at high temperatures. This can be checked by considering the apparent coefficients of thermal expansion shown in Figure 5.4 at temperatures greater than 120℃. The resin is unable to constrain the gauges properly in this region and as a consequence the gauges respond somewhat independently of the specimen. Since the coefficients of thermal expansion are over-predicted, it implies that the strain gauges are straining more rapidly than if they were properly constrained by the specimens. The coefficient of thermal expansion of the gauges must consequently be greater than that of the specimens and the gauges must therefore be loaded in compression, strengthening the case of the hypothesis outlined in the previous paragraph.

A consequence of this hypothesis is that the reduction in apparent thermal strain measured in the reinforced specimens between the temperatures of 100℃ and 110℃ is probably underestimated. The tests on pure resin indicate that strain gauges yield incorrect results at temperatures above about 100℃. In the tests on the reinforced

specimens, the bonding of the gauges to the glass fibres probably helped constrain the gauges and reduce this effect. It would appear reasonable to assume, however, that the apparent reduction in strain in this temperature region resulted from post-cure shrinkage effects and contractions arising from stress relaxation within the specimen combined with an apparent expansion arising from unconstrained strain gauge elasticity. Depending on the magnitude of this last effect, the reduction in apparent thermal strain was underestimated to a greater or lesser extent.

Whether or not the hypothesis is correct, is once again irrelevant. As was expected before the tests on reinforced specimens were started, the results are erroneous. It is clear that some other method of measuring the thermal response of the specimens is required.

Prior to developing a new experimental method, it is worth at this stage considering the effects of the "folding" procedure used during the manufacture of the specimens. Although every care was taken in the production of the original specimens, it was not possible to ensure that the specimens were completely symmetrical. By "folding" the specimens in half and bonding the two halves together, it is possible to manufacture specimens that are very nearly symmetrical. In addition, doubling the thickness of the specimens also increases the bending stiffness by a factor of eight. Any potential measurement errors introduced by a bending response during heating are thus minimized by this approach. It is possible, however, that additional errors are introduced by the addition of a layer of adhesive between the two halves of the specimen. This effect needs to be considered.

The faces of the original specimens were very smooth and flat. When the two faces were clamped together, the resulting layer of adhesive on the centre-plane was extremely thin. Since the same resin system used in the original manufacture of the specimens was used as an adhesive, the overall effect of the bonding process was that the fibre volume fraction of the specimen decreased by a tiny amount. It is thus expected that the measured coefficient of thermal expansion of the specimen over-predicts the actual value. It should be stressed, however, that this effect is negligible in comparison with the variation introduced by differences in fibre volume fraction from specimen to specimen and in comparison with the improvement in measuring accuracy obtained by minimizing the bending response.

5.2.6 Conclusions

Strain gauges do not correctly measure the strain in a GFRP specimen once the temperature is sufficiently high that the modulus of the resin drops significantly.

Strain gauge methods cannot be applied for this work.

Errors introduced by the "folding" technique used during manufacture of the specimens are negligible.

5.3 Initial approach using a dilatometer

5.3.1 Introduction

The results of the initial investigation showed that strain gauges are unsuitable for this work because the inherent stiffness of the gauges prevents them from straining in unison with the underlying specimen once the elastic modulus of the resin system drops appreciably. It should be pointed out that even if special low-stiffness gauges were available, their use would merely postpone measurement errors to a higher temperature rather than prevent them altogether.

Since it is not feasible to measure the strain directly with strain gauges, some other measurement technique is required. It was decided to investigate the use of instruments that measure changes in length with temperature and hence allow the apparent thermal strain to be deduced. These instruments include dilatometers, thermomechanical analysers and dynamic-mechanical analysers. Dilatometers are the simplest of these instruments and measure thermal strains without mechanically loading the sample. Thermomechanical analysis (TMA) measures the thermal strain while applying a defined load to the specimen. If this load is set to be very small, TMA measurements correspond with those of dilatometry. Dynamic-mechanical analysis (DMA) is the most sophisticated technique. In this approach an oscillating force is applied to the sample. This allows the temperature-dependent viscoelastic properties to be determined. To an extent, DMA and TMA equipment overlaps. Some TMA instruments can perform rudimentary DMA work and some DMA machines can perform TMA measurements.

Since the experimental approach inherently requires that the specimen is unloaded, the use of dilatometers was considered first. Most dilatometers are intended for

use with metals and ceramics and are unsuitable for use in this investigation. Specialized dilatometers are, however, available for use with polymers[ii]. No suitable dilatometer was available, however, and so the use of TMA and DMA equipment was investigated.

TMA and DMA machines can all accommodate polymer specimens. Due to their greater sophistication and hence cost, however, it was not possible to gain access to such machines for the length of time required in this investigation. Since neither a suitable dilatometer, nor TMA/DMA equipment was available, it became necessary to design and build a device to obtain the necessary measurements. Since the application of a controlled load is not desired, it was decided to base the design on a dilatometer.

Although it was not realized at the time, the decision to design and build a test rig based specifically on the needs of the investigation had significant benefits. Freedom existed to make design changes as the investigation unfolded. It is not necessarily possible to make the same changes to commercially available equipment. As will be discussed in section 5.3.6, unforeseen deformation of the specimen end faces prevented the use of unmodified dilatometry and TMA/DMA equipment. The design changes needed to solve this issue could be relatively easily incorporated into the design. It is by no means certain that these changes could have been effected in commercially available equipment.

Ideally, measurement of the change in specimen length takes place without any contact between the specimen and measurement system whatsoever. Unfortunately, this is impractical and some form of restraint is necessary. It clearly therefore becomes necessary to design the measurement system to minimize errors arising from the restraint.

One way of reducing these errors is to increase the free length of the specimen. A longer specimen has a greater proportion that is unaffected by the local effects of restraint. This tends to reduce the relative magnitude of the measurement errors. This approach has the additional advantage that changes in specimen length are increased and so the sensitivity of strain measurement is enhanced. The scheme is easy to implement but has limitations in terms of available material and oven dimensions.

[ii] An example of such a machine is the L75/120LT dilatometer available from Linseis Messgeräte GmbH. This machine has a maximum operating temperature of 160°C which corresponds well with the required temperature range. It also accommodates specimens with rectangular cross-sections which makes its use practical with composite laminates.

Thermal expansion measurements of polymers are typically performed in the vertical direction to minimize the effects of friction and asymmetrical gravitational loading. The specimen is supported on a platform and changes in length are monitored by the vertical displacement of the upper end. The specimen is thus loaded in compression by its own weight. Since relatively long specimens are desirable, and since the experimental approach requires the modulus of the resin system to drop significantly at high temperatures, the potential exists for the specimen to buckle. This is clearly undesirable and it was consequently elected to suspend the specimens vertically, thereby loading them in tension.

A consequence of suspending a specimen from its upper end is that mechanical clamping becomes necessary. The design of the clamps must clearly be approached with caution to avoid the introduction of spurious strain measurements. This issue is especially important at high temperatures when the modulus of the resin system reduces to very low values. One way of reducing clamping errors is to limit these loads as far as possible. A minimum load is required to achieve restraint of the specimen, but increasing the load further serves only to increase clamping strains and thereby measurement errors. It must be remembered also that the magnitude of the clamping force changes as a function of temperature, depending on the relative thermal expansions of the clamping mechanism and the specimen.

If the clamping mechanism obtains grip by pressing directly against the glass fibres of the specimen it is not necessary for the grips to penetrate into the resin. Resin flow at high temperatures can hence be minimized, reducing measurement errors at the grips. Design of a clamping mechanism must take all of the above factors into consideration. In addition, it must ensure that further measurement errors are not introduced through rotation of the specimen about the grips or through bending of the specimen. Both of these effects tend to decrease the apparent length of the specimen relative to a fixed sensor.

Measurement of the displacement at the end of the specimen can be achieved by a number of different sensors. Most of these, however, have fairly limited maximum temperature limits. If they are selected, it becomes necessary to isolate the sensor from the interior of the oven. This introduces complications in terms of how the measurements are performed.[iii]

[iii] These problems are not intractable, commercially available dilatometers and TMA/DMA machines usually rely on a displacement sensor mounted outside the oven. Motion at the specimen end is mechanically transferred to the sensor by means of probe of low thermal expansion. Errors in measured displacements arising from thermal expansion of the probe can be calibrated.

If the maximum test temperature is within the operating limits of the sensor, however, measurement of the displacement at the end of the specimens is significantly eased. Measurement can be directly performed and it becomes unnecessary to use a mechanism to transfer the displacement through the walls of the oven. The maximum test temperature planned for these tests was limited to 150℃ by the LM-35D integrated circuit temperature sensor. It was decided that a minimum requirement for the sensor was operating limits that included the temperature range from room temperature up to 150℃. It was thereby possible to measure displacement directly within the oven.

In addition to meeting the temperature requirements, the ideal sensor does not make contact with the specimen. This prevents errors being introduced by contact stresses at high temperatures and also facilitates mounting of the specimen in relation to the sensor. Additionally, a high sensitivity over a limited operating range is advantageous due to the small displacement of the specimen end.

A range of non-contact sensors was considered in respect of the requirements listed above. These included laser interferometers, capacitance sensors and eddy current sensors. Although they failed to satisfy the non-contact requirements specified above, a variety of linear variable differential transformers was also considered. The temperature requirements imposed by the decision to measure displacement directly within the oven precluded the use of most available sensors.

An eddy current sensor from Kaman Measuring Systems, however, stood out as being essentially ideal. It was consequently selected as the displacement sensor. A test fixture was designed to accommodate this sensor and the restraint requirements described above.

5.3.2 Additional equipment

5.3.2.1 Specimens

Five specimens each were prepared from the “Unloaded”, “Preloaded” and “Annealed” specimen groups in the same manner as described in section 5.2.2.2. The specimens were prepared by lightly sanding one of the faces of the original specimen strips and then cutting this specimen in half. The two halves were then folded onto each other and bonded (using Derakane 411-350 - the resin system used for the matrix) such that the sanded faces were mating. This technique resulted in symmetric specimens measuring 124 mm by 20 mm by 5.9 mm.

An additional specimen was manufactured from cast resin with dimensions nominally identical to those of the GFRP specimens. This specimen was to be used in a test that would check whether, as planned, the new test fixture avoided the type of measurement errors previously experienced and described in section 5.2.5.1.

5.3.2.2 Displacement transducer

The Kaman Measuring Systems 1UEP non-contact displacement sensor coupled with a KD2300 oscillator/demodulator from the same manufacturer was selected for this work. The sensor contains of a coil which is subjected to high frequency excitation. Eddy currents are consequently induced in a conductive target. The electrical impedance resulting from these currents depends on the distance between the sensor and the target. This principle allows the displacement of the target relative to the sensor to be measured.

The spatial relationship between the sensor and the target is illustrated in Figure 5.5. A minimum clearance of 0.13 mm between sensor and target is specified.

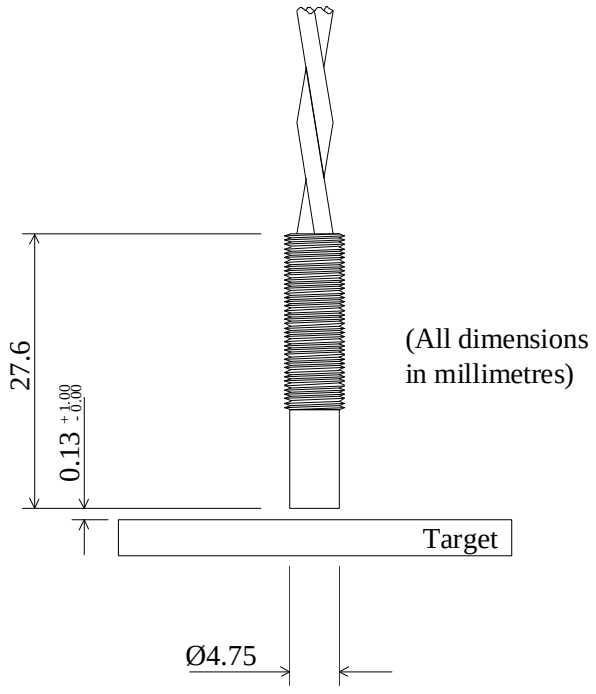


Figure 5.5: Position of displacement sensor relative to target

Specifications of the sensor at room temperature are listed below:[192]

Measurement range : 1.0 mm
Sensitivity : 1.000 V/mm (using an aluminium target)
Static Resolution : 0.1 μm
Linearity : $\pm$0.005 mm
Operating temperature range : -269℃ - 204℃
Oscillator frequency : 1.00 MHz

The sensor was placed within the heated interior of the oven and thus the specimen displacement could be measured directly. The sensor output signal passed from the oven to ambient conditions where it was amplified. The sensitivity of the sensor varies as a function of temperature. It was thus necessary to calibrate the measured displacement against both signal voltage and temperature. Details of the calibration process are described in section 5.3.4.

5.3.2.3 Target

The GFRP specimens are non-conductive and consequently require that conductive targets be affixed to their ends to allow the measurement of displacement.

Due to a radial spread of the electric field lines, as illustrated in Figure 5.6, the eddy currents within the target extend beyond the edges of the sensor. The currents decay rapidly with distance from the edges of the sensor and are negligible beyond three sensor radii. The minimum target diameter is consequently three sensor diameters, or 14.25 mm. Depending on the conductivity of the target and the frequency of the electric field emitted by the sensor, the eddy currents penetrate a short distance beneath the surface of the target. For a low resistance target and the selected sensor, the minimum target thickness is 0.30 mm.[193]

Since the width of the specimens was 20 mm, it was decided to increase the target diameter to match. Aluminium was selected for the target material due to its low density which would reduce the mass of the target. In addition, the sensor had been originally calibrated by the manufacturer using this material. Circular target discs were thus manufactured using aluminium sheet of 0.5 mm thickness. It was, however, discovered that the targets were so thin that they bent very easily and it was not possible to manufacture the discs perfectly flat.

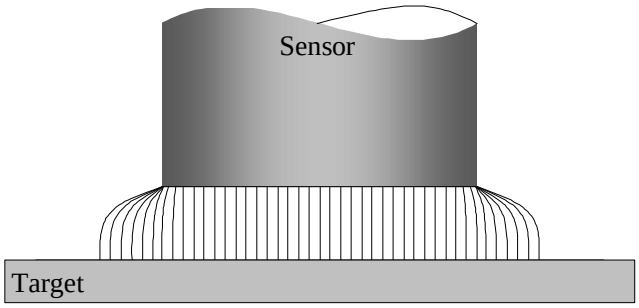


Figure 5.6: Spread of electric field lines

The thickness of the targets was thus increased to 2.0 mm. The thicker targets did not bend easily and could be more easily handled. The surfaces of both sides were lapped to ensure planar surfaces. The positioning of the target relative to the specimen and the sensor is illustrated in Figure 5.7.

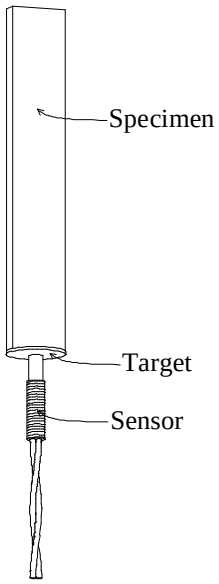


Figure 5.7: Configuration of specimen and measurement system

5.3.2.4 Test rig

The test rig was designed to enable accurate measurements of specimen displacement over the complete range of testing temperatures. It consisted of a steel frame supporting the displacement sensor at one end and grips for the specimen at the other end. The specimen was mounted in the grips such that it extended towards the sensor. The arrangement of the test rig and specimen is shown in Figure 5.8. Both the specimen and frame varied in length depending on the oven temperature.

The gap between the sensor and the specimen varied accordingly. After calibration, the variation in the gap spacing enabled the thermal strain of the specimen to be determined.

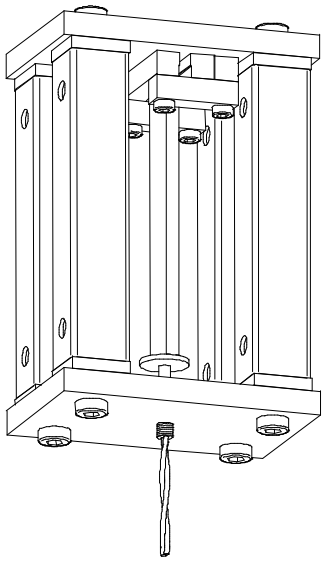


Figure 5.8: Test rig including specimen

5.3.2.4.1 Frame

Maximum sensitivity in the measurement of specimen displacement requires that the distance between the grips and the sensor be held as constant as possible. The frame was consequently manufactured from steel because it has a high elastic modulus and a coefficient of thermal expansion that reasonably matches that of unidirectional GFRP.

The basic construction, shown in Figure 5.9, consisted of two rectangular plates offset from each other by four equi-length spacing legs positioned at the corners. In the centre of one of the plates a threaded hole was cut so that the displacement sensor (not shown) could be screwed into position facing towards the second plate. Threaded holes were cut into the second plate to facilitate mounting of the grips. The entire construction was then securely bolted together at the ends of the spacing legs.

The thermal expansion in the frame, in a direction aligned with the specimen, occurred primarily in the spacing legs as a consequence of their length. The legs were therefore manufactured from hollow tubing to reduce their thermal inertia. Holes were drilled through the tube walls to allow internal airflow, improving heat transfer and thereby improving the thermal expansion response still further.

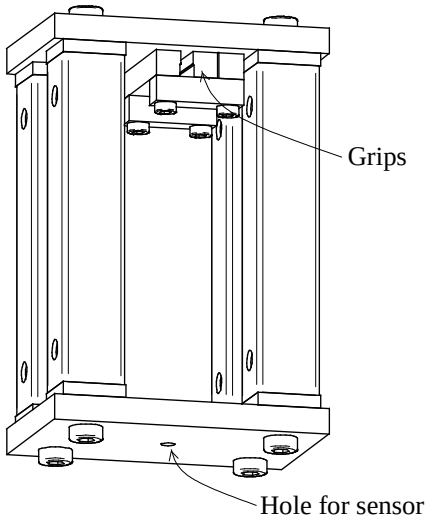


Figure 5.9: Configuration of test frame

5.3.2.4.2 Restraints

The specimens required two forms of restraint. Longitudinal restraint was required to fix one end of the specimen within the frame. Steel grips mounted on the end-plate opposite the sensor were used for this purpose. Rotational restraint was also necessary to prevent rotation about the grips and potential bending of the specimen. This was achieved by bonding the specimen to fine strands of carbon fibre stretched between the spacing legs of the frame.

Longitudinal Restraint

Measurement of thermal strain requires that the free-length of the specimen is clearly defined. In addition, the possibility of slippage caused by differential thermal expansion between the grips and the specimen must be eliminated. This is most easily achieved by using grips that make contact with the specimen for only a short distance in the longitudinal direction. A secondary advantage of this approach is that the contact area between the grips and specimen is minimized. This limits the extent of the material affected by contact stresses. It was thus decided to make use of blunt "knife-edge" grips to provide longitudinal restraint. The contacting surface had a width of 0.5 mm. This width was chosen to limit contact stresses and hence prevent breaking of the glass fibres at the specimen surface. Each of the two jaws of the grips was cut from a 10 mm square bar of key-steel. The basic cross section is shown in Figure 5.10.

The jaw faces adjacent to the contacting surfaces were recessed by 0.5 mm to prevent

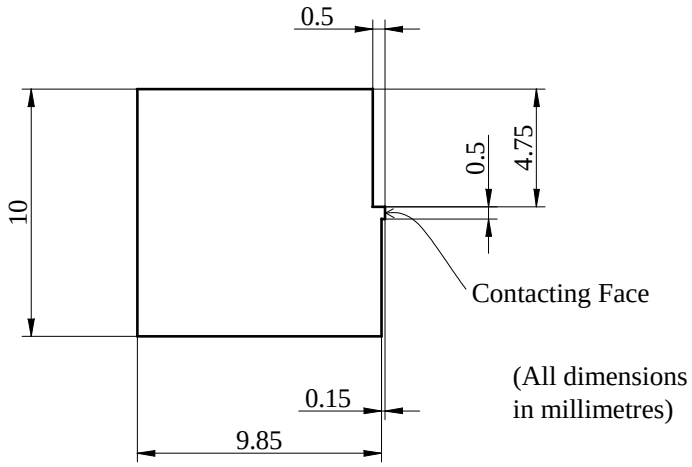


Figure 5.10: Cross-section through a jaw of the "knife-edge" grips

contact with the specimen. Such contact could apply unwanted restraint to the free length of the specimen. The steel on the reverse side of the contacting surfaces was recessed by 0.15 mm. The intention was that the limited space between the specimen and the jaws would restrict specimen rotation about the axis of the knife-edge. The configuration of the grips when holding a specimen is shown in Figure 5.11.

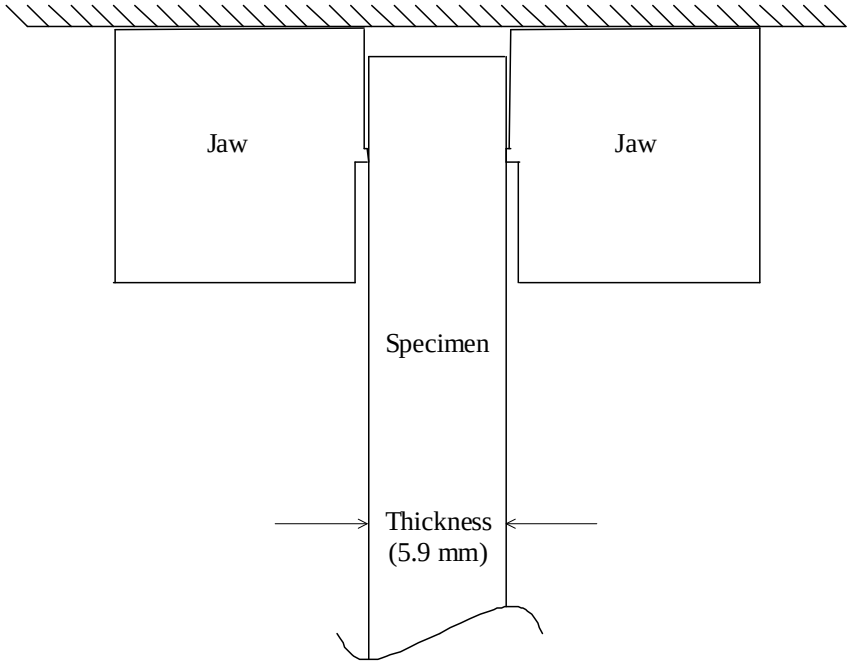


Figure 5.11: Specimen positioned within clamping jaws

Tightening of the grips was achieved by means of a M4 cap screw pressing into a conical recess on the reverse of the sliding jaw. The entire grip assembly was constrained in the longitudinal direction by the two clamping bars extending over

the jaws and bolted into the underlying steel plate. The overall grip assembly is shown in Figure 5.12.

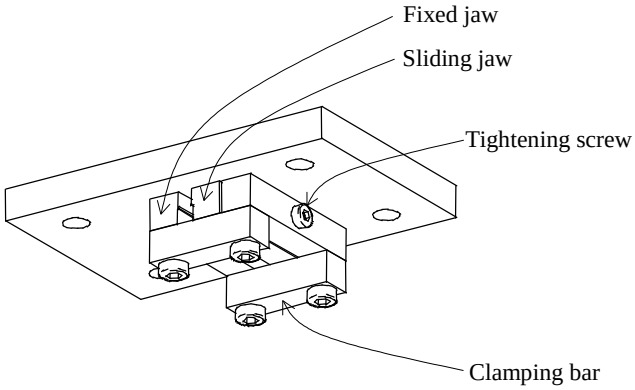


Figure 5.12: Configuration of grip assembly on backing plate

Rotational restraint

Rotation of the specimen about the grips and bending of the specimen both tend to make the specimen appear shorter when viewed from the sensor. This clearly results in measurement errors which must be reduced as far as possible. Some form of rotational restraint is therefore required.

The contact surfaces of the "knife-edge" grips were narrow and they were thus unable to provide proper rotational restraint. A limited degree of rotational restraint was provided by the 0.15 mm recess behind the contacting surfaces but this was inadequate to prevent rotational motion altogether. Some other method of applying rotational restraint was therefore required.

It was, however, imperative that the application of rotational restraint did not result in the addition of longitudinal restraint to the free-length of the specimen. It was decided to exploit the low transverse stiffness of a stretched fibre in this regard. The specimen was supported laterally by the midpoints of carbon fibre strands stretched taut between the spacing legs of the frame. Motion in the direction of the fibre lengths was prevented but small movement in the remaining directions was still allowed. Bending of the specimen was prevented by applying the restraints at several points along the length of the specimen. To ensure symmetry, the specimen was fastened to the carbon fibres along both edges. The concept employed is illustrated in Figure 5.13.

It was clearly important that the method of attaching the specimen to the carbon

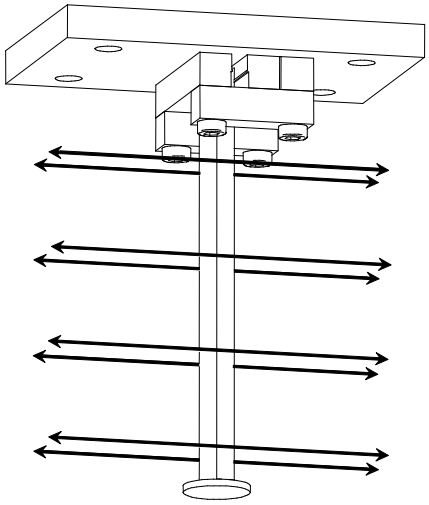


Figure 5.13: Tensioned carbon threads attached to specimen - Spacing legs are not shown in the interests of clarity

fibre strands minimized measurement errors. Mechanical fastening would have introduced localized contact stresses, and corresponding strains, resulting in errors in measured displacement. It was consequently decided to employ an adhesive joint. A bonding paste based on Derakane 470-300 epoxy vinyl-ester resin was selected as the adhesive. This system cures at room temperature in approximately 30 minutes but has a heat distortion temperature (HDT) of approximately 145°C.[178] This is well above that of the resin system used in the specimens.[189] Loads in the adhesive caused by thermal effects in the specimens consequently diminished to negligible values prior to the deterioration in adhesive performance. To limit interference effects, the bond area and thickness of the adhesive was kept as small as possible. The carbon fibres were bonded to the spacing legs using the same adhesive.

5.3.3 Experimental method

Specimens of several different types were tested. Initially calibration specimens were tested. Subsequent to this, the single specimen of cast resin was tested and then retested to check whether the test fixture could correctly measure the thermal strain of unreinforced resin at high temperatures. Following from this check, the specimens of GFRP were tested. This section describes how a test was set up irrespective of the actual specimen used.

5.3.3.1 Attachment of target

It was necessary to affix the target to the specimen without introducing sources of experimental error. It was consequently decided to bond the target directly to the end of the specimen so that stress concentration effects associated with mechanical joining could be avoided. The bond-line thickness was minimized to reduce its thermal expansion. This was achieved by flattening the bonding face of the specimen to match that of the target disc.

The ends of the specimens were flattened using sand paper. Each specimen was clamped square to a steel block such that approximately 0.5 mm of the specimen end protruded beyond the block. The end of the specimen was then removed by moving the steel block over progressively finer sand paper mounted on a surface table. The end of the specimen contacted the sand paper with comparatively high pressure and was preferentially removed. The final sheet of sand paper used in this process had a roughness of 1200 grit.

The bonding faces of the target and specimen were then cleaned using acetone and lint-free cloth and bonded together using a small amount of silicone rubber sealant. The sealant was then allowed to cure at ambient temperatures for a period of approximately one week.[iv]

5.3.3.2 Mounting of the specimen in the test rig

The test rig was positioned vertically with the grips at the top and the sensor at the bottom facing upwards.

The clamping bars over the grips were loosened and the grips opened.

[iv] Initial tests using steel specimens and cyanoacrylate adhesive clearly showed non-linearity at a temperature of approximately 80°C. Since this effect was not present when the specimens were heated again, it was ascribed to deformations caused by post-cure shrinkage in the adhesive. These deformations would be indistinguishable from those caused by stress relaxation in the test specimens, and so it was imperative that they be eliminated by changing the adhesive. It was also recognized that the unconstrained thermal expansions of the two adherents were dissimilar. Due to the low bond-line thickness, significant shear strains would develop in the adhesive. The adhesive stresses, and consequent deformations in the target and specimen, would be minimized by using a very compliant adhesive. Silicone rubber sealant was attempted in this role. After attaching the target to the specimen it was left to cure at ambient conditions for about a week. Subsequent tests using steel specimens showed no evidence of localized non-linearity over the complete range of temperature measurements. Silicone rubber sealant was consequently used as the adhesive in all subsequent tests.

A polymer sheet of 0.4 mm thickness was positioned on the measurement face of the sensor. This sheet acted as a spacer to ensure a constant distance between the target and the sensor.

The specimen was rotated into a vertical orientation with the target at the bottom. The upper end of the specimen was positioned within the grips and the target was then placed on the polymer sheet covering the sensor. The position of the specimen was adjusted until it was centrally located within the grips and axially aligned. Since the width of the specimen corresponded to the gap between the legs of the frame, accurate placement of the specimen was enabled by visually ensuring the edges of the specimen were parallel with the legs and that the specimen was centrally positioned between the legs.

The grips were tightened until the specimen was secure. Care was taken to ensure that the grips were not over tightened which would have increased errors associated with contact strains around the grips.

The clamping bars over the grips were tightened to lock the entire assembly into place.

The polymer spacing sheet between the target and sensor was removed. Support for the specimen was consequently transferred to the grips. By hanging the specimen from the grips in this way, lateral translations caused by gravity could be eliminated.

At this point, the correct rotational position of the specimen was not assured. It was discovered that the output of the sensor depended on the angle between the target and the axis of the sensor. The output was maximized when the target was perpendicular to the sensor. The specimen was thus rotated slightly about the knife edge grips until the sensor output was maximized. This process required a small amount of slippage between the specimen and the grips which affected the sensor output. Errors were thereby introduced which were only discovered at a later stage and are discussed in section 5.3.6.

When the rotation of the specimen was correctly aligned with the sensor, the carbon fibre threads used for rotational restraint of the specimen were bonded in place.

5.3.3.3 Test procedure

When the specimen was properly mounted, the rig was transferred onto a small stand in the oven. The sensor wiring was threaded through the port at the top of

the oven and connected to the KD2300 oscillator/demodulator. The temperature sensor was threaded through the same port until it hung next to the specimen. The door of the oven was then closed.

The output terminals from the KD2300 oscillator/demodulator and temperature sensor were connected to the data logger using shielded cable with BNC connectors at each end.

The data logging software was started and a new file opened. The software was set up to record data every minute. The values of the two logged parameters (temperature and strain) were averaged over this time interval.

The logging software was started and left for approximately 30 minutes. This ensured that the software was working properly, and that the specimen and test-rig were at the same temperature as the inside of the oven.

The data logging process was stopped and then restarted. This process overwrote the data initially recorded while the temperatures within the oven settled.

The oven temperature was then ramped at a rate of 6℃ per hour up to a maximum of 150℃.

When the maximum temperature of 150℃ was reached, the oven was turned off and logging of data was stopped.

5.3.3.4 Precautions

The amplifier and data logging equipment should be left on between tests to ensure that they are fully warmed up at the start of a new test.

5.3.4 Calibration

The output of the displacement measuring system was calibrated by the manufacturer prior to delivery. The output varies with sensor temperature[192] and the calibration was therefore only valid at room temperature. Since the temperature of the sensor varied continuously throughout a test, it was necessary to calibrate the sensor as a function of temperature and displacement over the complete range of test temperatures.

Calibrating the sensor alone, however, could not provide an accurate measure of the specimen extension. This is because the sensor measures the gap width between itself and the target. This width varies not only as a consequence of the thermal expansion of the specimen, but also because of the thermal expansion of the steel test rig, the sensor, the aluminium target and even the adhesive between the target and the specimen. The sensor cannot therefore be calibrated individually but must be considered as part of an overall system. This prevents the use of a series of ceramic calibration spacers, as is typical for this system.[194]

It was decided to calibrate the system in its entirety by making use of known thermal expansion data. Aluminium, copper, steel and graphite together span thermal expansion rates significantly greater than that expected during testing of the GFRP specimens. Accurate thermal expansion data for commercially pure copper and aluminium as well as AISI 4340 steel are known.[187, 195] Thermal expansion data for a readily available graphite, Ellor +20, were measured using strain gauges. Calibration specimens from each of these materials were manufactured geometrically identical to the GFRP specimens to be used in testing. These specimens served as reference specimens which were each tested exactly as described for the actual test specimens in section 5.3.3.2. The data obtained from these tests were then used to calibrate the test fixture.

The change in thermal strain from the reference temperature of 25℃, to every measured temperature was known for each of the reference materials. The measured change in thermal strain for each of the reference materials was then assumed to be related to the measured temperature and displacement sensor output voltage by means of the following equation:

$$\Delta\epsilon_{cal} = C_1(\Delta V_{cal}) + C_2(\Delta T_{cal}) + C_3(\Delta V_{cal})(\Delta T_{cal}) + C_4(\Delta V_{cal})^2 + C_5(\Delta T_{cal})^2 \tag{5.1}$$

where $\Delta\epsilon_{cal}$ corresponds to the measured change in thermal strain (in $\mu\epsilon$) relative to the strain at the reference temperature of 25℃, ΔT_{cal} corresponds to the change in temperature (in ℃) relative to the reference temperature and ΔV_{cal} corresponds to the change in displacement sensor output voltage (in mV) relative to that at the reference temperature. The coefficients C_1 to C_5 correspond to calibration constants.

The unknown values of the calibration coefficients were then adjusted to obtain the best fit to the known thermal expansion data. For an assumed set of coefficients C_1

to C_5, the error between the reference strain and the calculated strain was computed for each datum point. These errors were then squared and summed together. By adjusting the values of the coefficients, the value of the sum varied. The best fit was assumed to correspond to the minimum value of the sum. Details of the calculations involved can be found in Appendix D.

A comparison between known thermal expansion and measured thermal expansion using the best-fit calibration is illustrated in Figure 5.14. Data measured at temperatures near room temperature are not presented. Problems were experienced in maintaining accurate control of the oven temperature in this temperature range. Affected data were consequently not used in the calibration. It can be seen that the correlation is extremely good, with the measured data and reference data being almost indistinguishable from each other. The coefficient of determination, R^2, of the fit is 0.999967. The standard deviation between measured strains and reference strains is 4.5 $\mu\epsilon$.

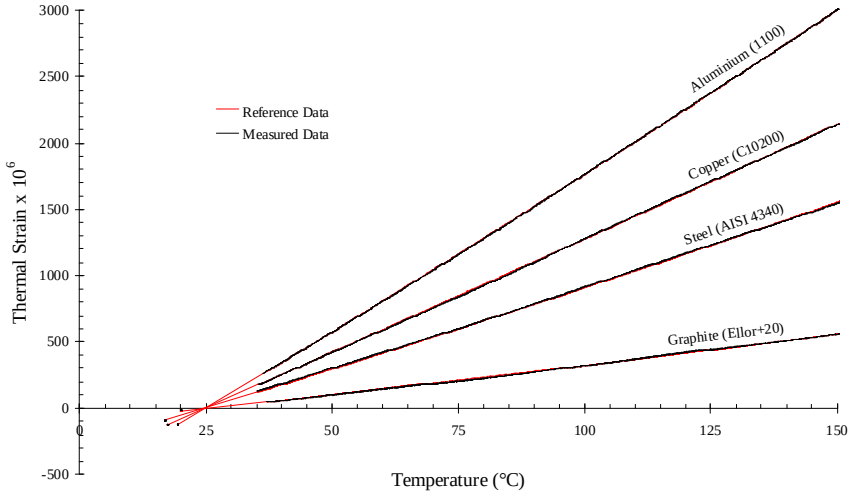


Figure 5.14: Comparison between reference thermal strains and calibrated measurements

5.3.5 Results

The raw data measured during each test were processed using equation 5.1 and the calibration coefficients listed in Table D.5 to determine the variation in specimen strain with temperature. The results for the specimen of cast resin are shown in Figure 5.15. Data for both the initial test and the subsequent test where the specimen was reheated are presented. The results for the reinforced specimens are given in Figures 5.16 though 5.18. Discontinuous lines are used in these figures to

represent missing data at temperatures near ambient conditions. These data were discarded because problems were experienced in maintaining accurate control of the temperature within the oven in this temperature range. The discontinuous lines linearly connect data measured prior to turning the oven on and data measured when accurate temperature control was re-established at higher temperatures.

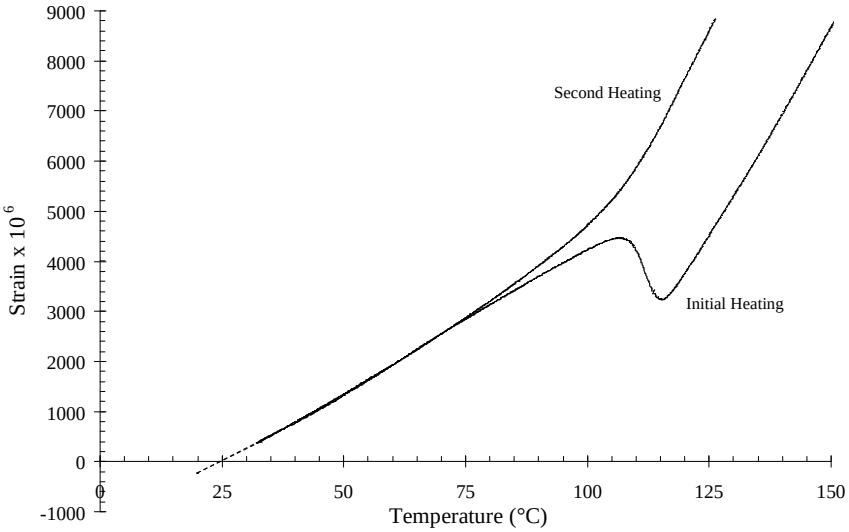


Figure 5.15: Measured strain in cast resin as a function of temperature

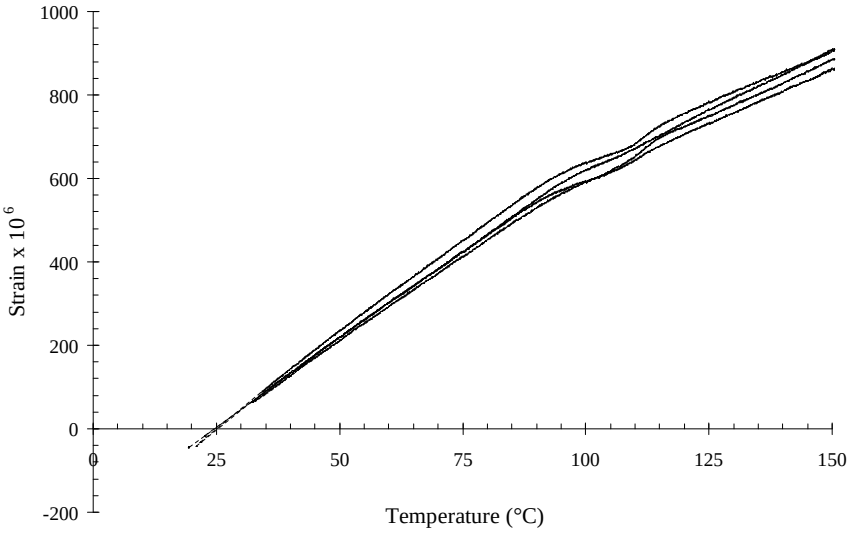


Figure 5.16: Measured strain in unloaded specimens as a function of temperature

Linear coefficients of thermal expansion determined in each test are presented in Tables 5.3 and 5.4. The values were determined using linear regression analyses at temperatures of 50℃ and lower and at 120℃ and higher respectively. The minimum coefficients of determination, R^2, for within each set of data are 0.9982 and 0.9904 respectively.

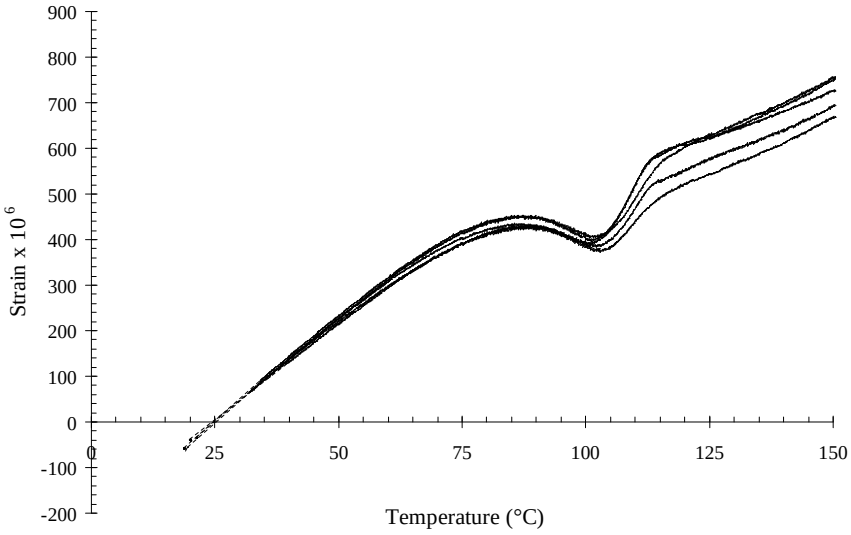


Figure 5.17: Measured strain in preloaded specimens as a function of temperature

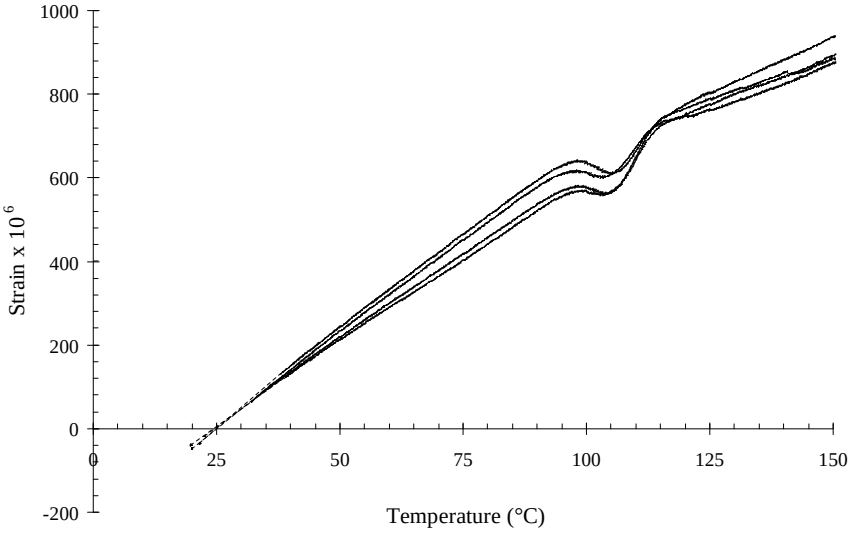


Figure 5.18: Measured strain in annealed specimens as a function of temperature

Table 5.3: Coefficients of thermal expansion at temperatures ⩽50℃

	Unloaded specimens ($\mu\epsilon$/℃)	Preloaded specimens ($\mu\epsilon$/℃)	Annealed specimens ($\mu\epsilon$/℃)
	8.6	9.2	9.4
	8.8	9.2	9.3
	9.3	9.5	8.9
	8.7	8.3	8.5
	—	8.6	—
Average	**8.9**	**8.9**	**9.0**
Std deviation	0.3	0.5	0.4

Table 5.4: Coefficients of thermal expansion at temperatures ⩾120℃

	Unloaded specimens ($\mu\epsilon$/℃)	Preloaded specimens ($\mu\epsilon$/℃)	Annealed specimens ($\mu\epsilon$/℃)
	5.2	5.0	4.0
	5.2	4.5	5.4
	4.9	3.7	4.4
	5.8	4.5	4.1
	—	4.8	—
Average	**5.3**	**4.5**	**4.5**
Std deviation	0.3	0.5	0.7

The locus of zero stress in the glass fibres was determined using a linear regression analysis of the strain data presented in Figures 5.16 through 5.18 at temperatures of 120℃ and higher. For illustrative purposes, the locus of zero fibre stress is shown for a single unloaded specimen in Figure 5.19. The residual strain in the fibres was determined by taking the difference in strain, at any temperature, between that of the specimen and that of the locus of zero stress. The results are plotted in Figures 5.20 through 5.22.

5.3.6 Discussion

5.3.6.1 Pure resin

Figure 5.15 indicates that the measured strain response in the initial test of pure resin is linear with temperature. The calculated coefficient of thermal expansion at

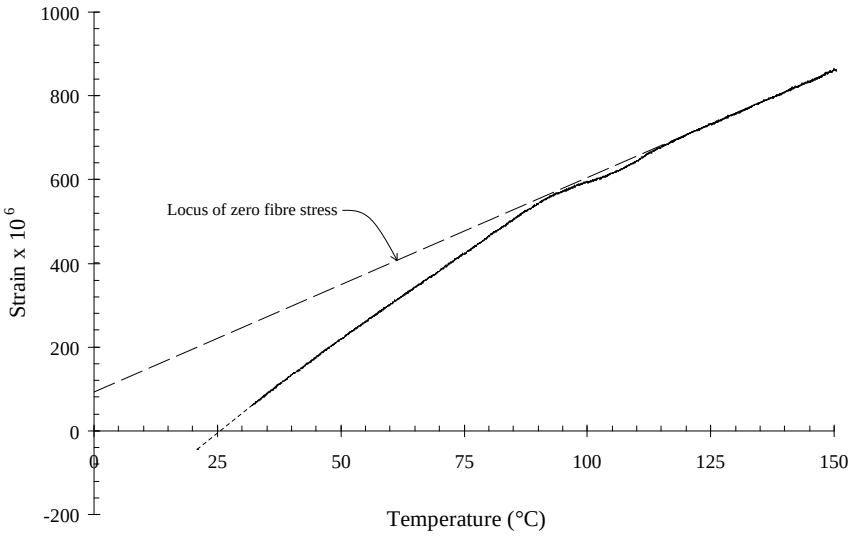


Figure 5.19: Locus of zero stress in glass fibres

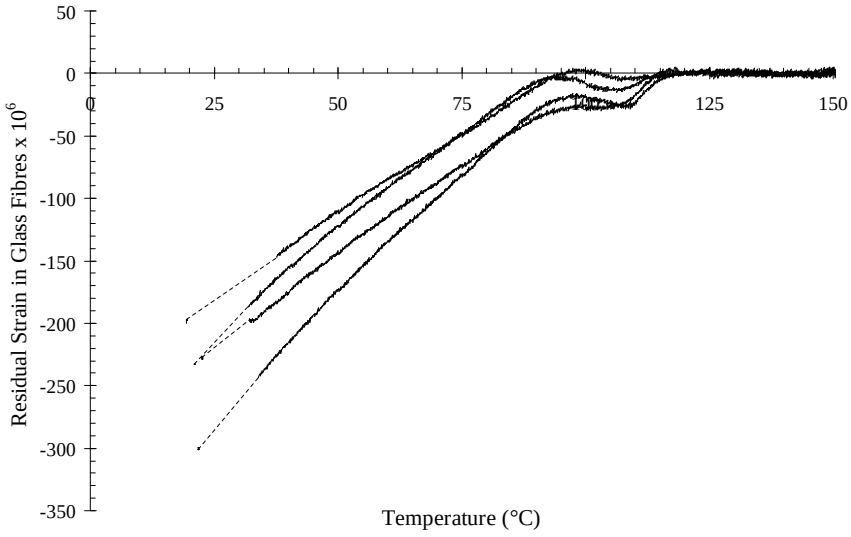


Figure 5.20: Residual strain in glass fibres of unloaded specimens

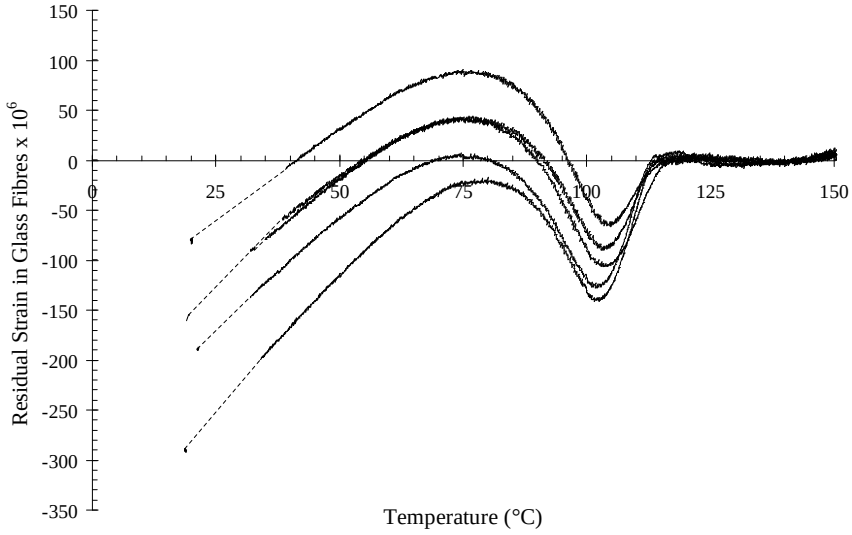


Figure 5.21: Residual strain in glass fibres of preloaded specimens

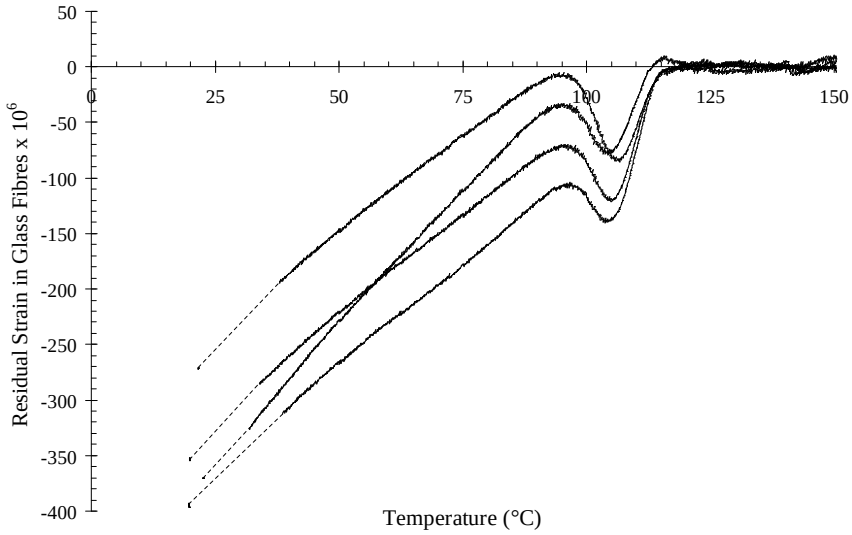


Figure 5.22: Residual strain in glass fibres of annealed specimens

temperatures up to 100℃ is 58.4 $\mu\epsilon$/℃ which is in reasonable agreement with the value of 64.8 $\mu\epsilon$/℃ listed by the manufacturer[189] even though the test rig was not calibrated to such high values of CTE.

At temperatures between approximately 105℃ and 115℃ the measured strain is seen to drop by approximately 1250 $\mu\epsilon$. This is expected and is associated with additional polymerization shrinkage at temperatures greater than the initial post-cure temperature. In section 5.2.5.1 an apparent polymerization shrinkage of approximately 3300 $\mu\epsilon$ was noted in this temperature region. It was explained in this section, however, that errors associated with the use of strain gauges caused this shrinkage to be overstated. The current measurements, indicating a smaller shrinkage, are therefore in agreement with earlier conclusions.

At temperatures higher than 115℃, when all available reaction sites for chemical bonding have been utilized, the measured strain is seen to increase rapidly. The CTE calculated for this specimen in the linear region at temperatures above 125℃ is found to be about 166 $\mu\epsilon$/℃. This large increase in CTE behaviour at temperatures above T_g is typical of polymer materials.[179]

The behaviour of the specimen when retested is almost identical to that during the initial test except that no additional polymerization shrinkage is evident. This confirms that the shrinkage apparent in the initial test was a result of polymerization shrinkage and not some artefact of the testing process. The CTE changes smoothly from a value of approximately 54 $\mu\epsilon$/℃ at low temperatures to a value of 190 $\mu\epsilon$/℃ at temperatures well above T_g. This behaviour is typical of a polymer[179] and the test-rig thus yielded the type of results that are expected. This is in marked contrast to the results presented in Figure 5.3.

The type of measurement errors associated with the use of strain gauges are not apparent in these results. The measured response of the specimen is in agreement with that expected from polymers and no other problems with the results are obvious. It therefore appears that the test rig was able to measure the thermal strain of pure resin over the entire range of testing temperatures.

5.3.6.2 Reinforced specimens

Figures 5.16 to 5.18 show that the thermal response of every GFRP specimen exhibits two clear regions of linearity. The first occurs at temperatures lower than about 50℃ and the second occurs at temperatures higher than about 120℃.

The slopes of the linear regions correspond to the apparent coefficients of thermal expansion. At temperatures less than 50℃ these values range between 8.3 $\mu\epsilon$/℃ and 9.5 $\mu\epsilon$/℃ which is in reasonable agreement with the values 9.6 $\mu\epsilon$/℃ and 10.3 $\mu\epsilon$/℃ measured using strain gauges in section 5.2.5.2. At temperatures greater than 120℃, the measured coefficients of thermal expansion range between 3.7 $\mu\epsilon$/℃ and 5.8 $\mu\epsilon$/℃ which encompass the values for E-glass fibre which vary between 4.7 $\mu\epsilon$/℃ and 5.4 $\mu\epsilon$/℃.[185, 190, 191] The apparent coefficients of thermal expansion at both low and high temperatures therefore agree with expected values, confirming the basis of the experimental technique.

Although the apparent coefficients of thermal expansion at both low and high temperatures show reasonable agreement with expected values, it had been expected that the correlation would be better. The discrepancy can be traced to the method of mounting the specimens in the grips. As mentioned in section 5.3.3.2, the output of the sensor depended on the angle between the target and the sensor. The output was maximized when the target was perpendicular to the sensor. The specimen was therefore rotated slightly within the grips in order to maximize the output of the sensor. Slippage between the grips and the specimen therefore occurred, causing the longitudinal position of the specimen to change slightly. This, in turn, affected the output of the displacement sensor, making it difficult to determine the exact position where the specimen was aligned perpendicular to the sensor. As a consequence, the response of the sensor varied from test to test. Errors were thus introduced during both the calibration and the measurement stages. Clearly, some method of automatically ensuring that the specimens were mounted perpendicular to the sensor was required. In addition, the method of tightening the grips needed modification to ensure that rotation of the specimen would not occur during the tightening process. These requirements were considered during the design of the next iteration of the test rig.

Between the regions of linearity described above, the behaviour of the different specimen types differs markedly. These differences result from differences in residual stress. The unloaded specimens, Figure 5.16, display linear behaviour up to approximately the post-cure temperature of 92℃. This behaviour is expected because the specimens were post-cured with very little fibre tension and so the internal stresses are low at this temperature. Consequently, the loss of significant resin modulus at temperatures slightly higher than 92℃, as seen in Figure 4.1, does not result in a dramatic strain response and only a slight kink is seen.

In contrast, the preloaded specimens were post-cured with high fibre tension. The residual stresses are therefore predicted to be large at high temperatures. The highly

non-linear behaviour of the preloaded specimens in Figure 5.17 is therefore expected, because it results from the release of significant residual stress.

The annealed specimens show linear behaviour in Figure 5.18 up to a temperature of approximately 95℃, whereupon a sudden change in slope becomes apparent. The linear behaviour at temperatures less than 95℃ is similar to that of the unloaded specimens, but the significantly greater response of the annealed specimens above 95℃ shows that more residual stress was retained in the annealed specimens at this temperature than was present in the unloaded specimens.

Between temperatures of approximately 102℃ and 115℃, all specimen types display a sudden increase in apparent strain before settling down to the expected linear behaviour at still higher temperatures. Due to the lower CTE of the glass fibres in comparison to that of the resin, relief of thermal residual stress would tend to cause a reduction in strain, as would polymerization shrinkage. It was not immediately evident what could be causing this apparent increase in strain. The experimental results were consequently further processed to reveal the apparent residual strain in the glass fibres as is shown in Figures 5.20 through 5.22.

These figures reveal a disturbing feature most evident in Figure 5.21. The apparent residual strain in the glass fibres of the preloaded specimens changes from a compressive stress at low temperatures to a low tensile stress around 75℃. Any further increase in temperature would tend to increase the thermal mismatch between the resin and the glass fibre and would hence increase the tensile residual stress in the glass. At the same time, an increase in temperature would reduce the resin modulus. Depending on the rate at which the resin stiffness dropped, it is possible that the slightly tensile residual stress in the glass fibre might increase still further, but it would eventually dissipate to a state of zero stress as the resin stiffness reduced to a negligible value. No conceivable process can account for the residual stress becoming rapidly compressive.

The apparent state of compressive residual stress in the glass fibres cannot be real, and appears to be an artefact of the sudden unexplained increase in apparent strain described above. The effect of this increase is to offset the whole residual stress curve by some unknown strain value, thereby invalidating the entire set of calculated strains.

It is observed from Figures 5.20 through 5.22 that the increase in strain is largest for the preloaded specimens and smallest for the unloaded specimens. This observation

hints that the problem may have had something to do with the degree of residual stress in the specimens. After considerable investigation it was found that the problem could be traced back to the bonded interface between the GFRP specimen and the aluminium target disc. As a consequence of the release of internal stresses, the end face of the specimen became dimpled. This caused movement of the target disc to become decoupled from that of the fibre ends. Typical profile measurements of the surface of a preloaded specimen prior to and after heating are presented in Fig. 5.23. It can be seen from this figure that the profile amplitude changed through approximately an order of magnitude after heating. Because the profile of the end face of the specimen changed during the heating process, movement of the target did not correspond to the displacement of the fibre ends and so spurious measurements resulted.

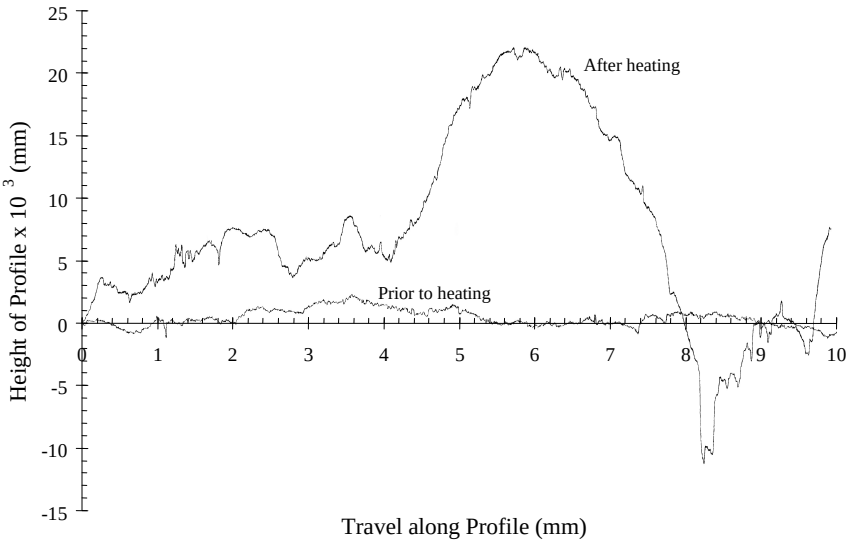


Figure 5.23: Surface roughness profile on the end face of preloaded specimens

The dimpling of the end surface can be explained through considering the interface loads between the fibres and the resin. Over the majority of the specimen length the resin is constrained to translate with the glass fibres and so plane sections remain plane. The loads required for such constraint develop at the ends of the specimen, where the loads are transferred between the resin and the fibres in the form of shear. During the heating process, residual stresses in the resin are relieved through a combination of longitudinal strain over most of the specimen length and shear strain near the ends. As a consequence of the shear strains in the resin near the ends of the specimen, the end surface is no longer constrained to remain flat and the fibres pull away from the end face giving it a dimpled appearance. The larger the residual stress at high temperature, the larger the dimpling and consequently the larger the erroneous movement of the target disc - exactly the effect observed in

these tests.

The method of measuring the change in specimen length must therefore be unaffected by the dimpling of the end faces. Essentially, this requires measurement of the change in length of the inner part of the specimen, whilst ignoring that over the outer portions. This clearly means that bonding the target to the end of a specimen is inappropriate. It also means that unmodified dilatometers and TMA/DMA equipment are unsuitable for this work. This equipment typically makes use of probes to measure the end displacement of the specimen and is consequently susceptible to errors introduced by the dimpling of the specimen ends[v].

Apart from this problem though, it appeared that the new system was a significant improvement on the use of strain gauges. The test-rig was able to measure the strain response of pure resin over the complete range of test temperatures. This was possible because the unreinforced resin was not stressed and consequently no dimpling of the end face took place. Problems associated with dimpling of the end face only occurred in reinforced specimens because of the stresses resulting from the mismatch in thermal expansion between the fibres and the resin. These problems, however, were not considered insurmountable and simply required a different method of supporting the target.

5.3.7 Conclusions

The measurements obtained with the new test rig were a substantial improvement over those obtained using strain gauges. Further development work was, however, still required.

- The grips required modification so that they could be tightened without causing rotation of the specimen. In addition, it was necessary to mount the specimens in such a way that the target was automatically positioned perpendicular to the sensor.
- The method of supporting the target required alteration to eliminate measurement errors caused by dimpling of the end faces of the reinforced specimens.

[v] Some DMA equipment, such as the PerkinElmer DMA 8000 system, can perform CTE measurements in a tension mode. These systems employ mechanical clamping on the specimen sides. Although, in principle, such systems avoid the problems associated with dimpling of the end faces, an application note[196] makes it clear that these tests are limited to temperatures within the glassy region of the polymer. Since there is a need in this investigation to operate well beyond T_g, this equipment is also unsuitable.

5.4 Final design

5.4.1 Introduction

It was apparent from the initial results obtained using the Kaman non-contact displacement sensor that the basic experimental method was valid. It was also apparent, however, that the test rig required further development work to iron out errors caused both by poor alignment of the target with the sensor and by dimpling of the specimen end face.

- In order to improve the alignment of the target relative to the sensor it was decided to make use of spacing blocks between the target and the test rig. By correctly locating the extremities of the target relative to the test rig, far greater control over the alignment of the target could be achieved. The spacing film between the target and sensor that was initially used could not provide good alignment due to the small diameter, 4.75 mm, of the sensor face.
- Even if the specimen was initially aligned correctly, tightening of the jaws could potentially cause misalignment. It was therefore necessary to consider the manner in which the jaws were tightened and to make the necessary changes to components of the jaws and the tightening technique.
- The method of attaching the target to the specimen required modification. It was elected to make use of "knife-edge" grips similar to those used to support the specimen in the test rig. This approach would ensure that dimpling of the end face did not cause spurious motion of the target.

In addition to the necessary alterations mentioned above, it was also found that the use of carbon fibre threads to prevent rotation of the specimen was inconvenient. It was decided to develop a more convenient method of restraint.

Each of the modifications is described in detail in the following sections. The basic configuration of the final design, however, is presented in Figure 5.24.

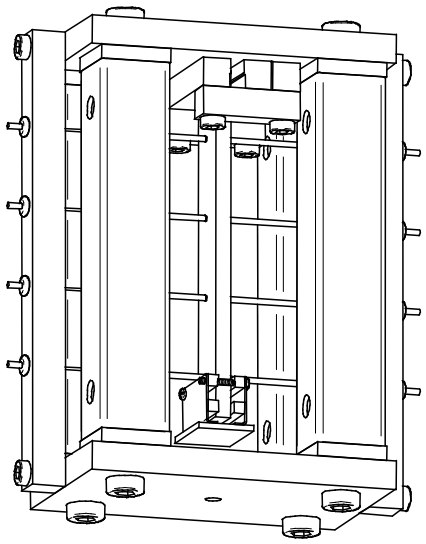


Figure 5.24: Final configuration of test frame

5.4.2 Modifications to equipment

5.4.2.1 Spacing blocks

Spacing blocks were used to position the face of the target perpendicular to the axis of the displacement sensor and at a constant distance from its measuring face. Due to the small diameter of the sensor face, it was elected to locate the target relative to the steel plate which held the sensor in the test rig. To ensure the best positioning of the target face, the overall size of the blocks needed to be larger than the extremities of the target.

The spacing blocks were manufactured from steel gauge plate of 12 mm thickness. Although the surfaces had been surface ground prior to delivery, they were lightly sanded on a surface table using 1200 grit water-paper to improve the surface finish. After appropriately setting the screw depth of the sensor into its mounting plate, the spacing blocks ensured that the face of the target was always perpendicular to the axis of the sensor and (depending on ambient temperature) at a distance of very nearly 0.5 mm from its measuring face.

Although a single spacing block covering the whole of the target face would have been the simplest approach, it was necessary to use two blocks so that they could be removed after the specimen was tightened in its grips. Each block had a semi-circular groove running up the face that mated with the other block in order to accommodate the sensor. The method of fitting the blocks around the sensor is

illustrated in Figure 5.25.

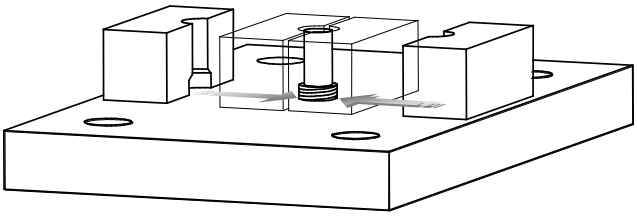


Figure 5.25: Fitment of spacer blocks around sensor

5.4.2.2 Grips

The tightening technique used in the initial tests unintentionally caused the specimens to rotate as the jaws tightened. The technique therefore required modification, a consequence of which was that the design of the grips needed small alterations.

Before discussing the changes to either the tightening technique or the grips, it is worth describing the initial tightening technique and its problems. To help clarify the description, the configuration of the grip assembly is presented again in Figure 5.26.

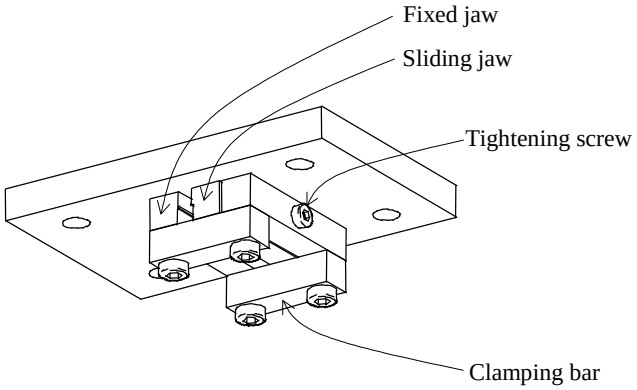


Figure 5.26: Configuration of grip assembly

In order to fit the specimen between the jaws of the grip assembly, the cap screws securing the clamping bars to the backing plate were loosened. This allowed the jaws to be opened so that the specimen could be fitted. Once the specimen was located in the correct position, the tightening screw was turned, causing the sliding jaw to press into the specimen and thus clamp it in place. The screws securing the clamping bars were then tightened, clamping the jaws in place.

Although this mechanism worked well to secure the specimens in place, it did not prevent rotation of the specimen during the clamping process. This is because the

position of neither the fixed jaw nor the sliding jaw was controlled in the direction aligned with the axis of the specimen whilst the clamping bars were loose. The jaws were thus free to move axially when they were closed. When the clamping bars were tightened, the jaws were forced back into their position flush with the backing plate and thus moved in the longitudinal direction. Small differences in the longitudinal motion of the two jaws resulted in rotation of the specimen.

In trying to rectify this situation, it was initially attempted to loosen all the cap screws of the clamping bars by the same amount. The intention was that the two jaws would move the same amount during the tightening process and therefore the specimen would not rotate. Unfortunately it was not possible to achieve repeatable results using this method.

It was eventually concluded that the only way to achieve consistent results was to leave the clamping bars securely in position. This would prevent any movement of the fixed jaw. The thickness of the sliding jaw was trimmed just enough that it could slide between the clamping bars and the backing plate to enable tightening of the grips, but could not move in the longitudinal direction. To aid sliding of the jaw between the backing plate and the clamping bars, the contact faces of both the clamping bars and the backing plate were lightly sanded on a surface table using 1200 grit water paper. Both contacting faces of the sliding jaw were then sanded down using the same process until the jaw was just able to move freely[vi]. Lubricants were not used to reduce friction out of fear that they would spread at high temperature and hence reduce the level of grip between the jaws and the specimen.

Although the sliding jaw could be freely slid back and forth using fingers it did not apply a uniform clamping load across the specimen width. The tightening screw on the rear of the sliding jaw was centrally located relative to the width of the specimen and so it was expected, based on equilibrium considerations, that the clamping load would have a fairly uniform distribution across the specimen width. It was eventually discovered that the jaw was jamming within its track and that some of the clamping load was being transferred into the backing plate and clamping bars. The reason for this was that the conical recess on the back of the sliding jaw was not located perfectly at the mid-thickness position. As a consequence, the tightening screw was not centred within the conical recess and it consequently applied a load to the jaw aligned in the longitudinal direction of the specimen. This load caused the friction between the jaw and the support assembly to increase and jamming consequently

[vi] Clearly this process took some time to get correct. It was discovered that a single stroke of the jaw over 1200 grit waterpaper made the difference between it being clamped in place and moving freely.

occurred. The problem was resolved by placing a small steel bearing ball into the conical recess. The tightening screw was unable to apply a sufficiently large axial load through the ball to enable jamming to occur and no further problems with the grips were experienced. The location of the ball relative to the sliding jaw and tightening screw is illustrated in Figure 5.27.

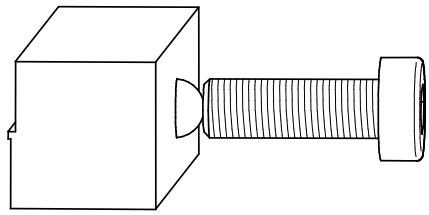


Figure 5.27: Steel ball positioned between tightening screw and sliding jaw

5.4.2.3 Target

Before designing a new method of attaching the target, it was worth considering the distance over which the loads required to force compatibility between fibres and matrix are transferred. This could be estimated using the shear-lag analysis of Nairn.[54] An investigation, as detailed in Appendix E, revealed that at room temperature, 99% of the load was transferred in a distance of less than approximately 0.63 mm. By assuming that the heating rate was sufficiently slow that constraint loads transferred by viscous effects could be neglected, and hence that elastic effects were dominant, it was possible to reanalyse the situation at high temperatures. When the resin modulus dropped to less than 1% of its original value, the load transfer distance remained essentially unchanged.[vii]

The grips clamping the specimen to the test rig made contact approximately 4 mm from the specimen end, well outside the shear lag region. Since they appeared to both work well and avoid the shear-lag region they were chosen as the model for attaching the target. It was thus elected to use a set of "knife-edge" grips to support the target on the specimen. In order to reduce weight as far as possible the grips were fabricated from 4 mm square key steel rather than the 10 mm square key steel used on the original grips where weight is not an issue. The dimensions of the contacting faces and also of the recesses adjacent to these surfaces were left unchanged. The

[vii] This seems counterintuitive, but Nairn shows that an "iso-stress" fibre volume fraction exists at which the load transfer rate is unaffected by the ratio of fibre and matrix moduli. He calculates this point to occur at a fibre volume fraction of 42% which is in the vicinity of the fibre volume fraction of the specimens. It is therefore expected that the load transfer distance is not significantly affected by the drop in resin modulus at high temperatures.

grips were tightened with M2 stainless steel machine screws located each side of the specimen and aligned through the centreline of the gripping surfaces.

To facilitate the interface between the grips and the target, the shape of the target was changed to rectangular. The length matched the required grip length, 27 mm, and the width was left the same as the original diameter of the circular target, 20 mm. The larger size of the new target aided in its alignment using the spacer blocks. The structures joining the target to the gripping surfaces were manufactured from 0.4 mm sheet steel. Sheet was selected because it is stiff in the plane, but flexible out of plane. In this case, flexibility out of plane was advantageous to prevent the transfer of significant clamping loads through the target. Such a situation would have caused bending of the target, with associated loss of measurement accuracy. Although the minimum required target thickness is only 0.3 mm, as discussed in section 5.3.2.3, its thickness was selected as 2.0 mm to ensure that it would not bend as a result of handling or clamping loads. Copper was selected as the target material to enable soldering to be used to join all the components of the target assembly.[viii] After all the components were soldered together, the surface of the target facing the sensor was polished on a surface table with 1200 grit water paper to ensure a smooth, flat surface against which the sensor could measure. The basic configuration of the target assembly is presented in Figure 5.28.

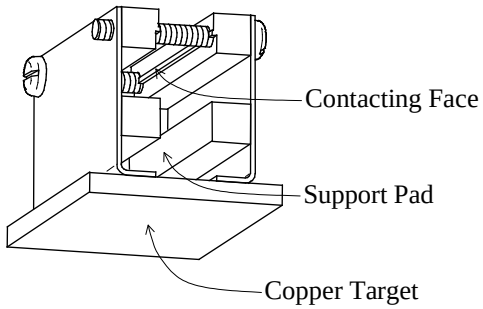


Figure 5.28: Configuration of target support

[viii] In order to reduce weight, it was attempted to make use of an aluminium target plate, riveted to the rest of the assembly with aluminium rivets. Unfortunately, this approach was not successful. During the heating process, small discontinuities in the apparent thermal response of the specimens were observed. In addition it was found that the slope of the first set of measurements after affixing the grip to a steel specimen differed from that observed on subsequent heatings of the same specimen. It seems that the discontinuities and change in measured slope are associated with movement between the target and the rest of the assembly. Two different configurations of aluminium target were tested, both with the same problems. It was then decided to attempt the use of continuous fastening rather than rivets. Since aluminium is incompatible with steel when making use of thermal joining techniques, copper was selected instead. Although possessing a high density, copper has good electrical conductivity and can be joined to steel using solder.

In order to limit rotation of the target assembly around the "knife-edge" grips, support pads were positioned so that they would make light contact near the ends of the specimens. These pads were manufactured from 4 mm square key-steel. The arrangement of the target assembly when located on the specimen is illustrated in Figure 5.29.

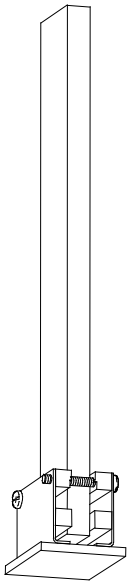


Figure 5.29: Target assembly mounted on specimen

5.4.2.4 Rotational restraints

Although no measurement problems were experienced with the use of carbon fibre thread to prevent rotation of the specimens, it was found that this approach was inconvenient. The adhesive used to attach the threads had to be mixed and then it took approximately 30 minutes to cure. At the end of each test, the adhesive had to be chipped off the test fixture before the next specimen could be installed.

It was decided to make use of a more convenient mechanical system to prevent rotation of the specimens. Cantilever beams have low bending stiffness, but high axial stiffness. This concept was exploited in the form of threaded rods of narrow diameter and fine thread pitch (modified bicycle spokes). The rods could be easily screwed into position to prevent rotation of the specimen, but had low bending stiffness so that longitudinal displacement of the specimens was not inhibited. The form of the rods is shown in Figure 5.30. The necked area was obtained by carefully grinding the surface of the spoke away on a bench grinder.

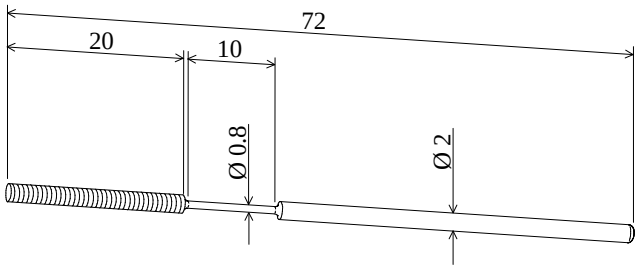


Figure 5.30: Rods used to provide rotational restraint

Four rods were equispaced along the centreline on each side of the specimen, preventing bending as well as rotation. The rods were screwed through bicycle spoke nipples mounted in support beams of 10 mm square key steel. The fine thread pitch allowed for easy positioning of the rods so that they just touched the specimen without applying a significant contact load. The arrangement of the rods within the test fixture is illustrated in Figure 5.31.

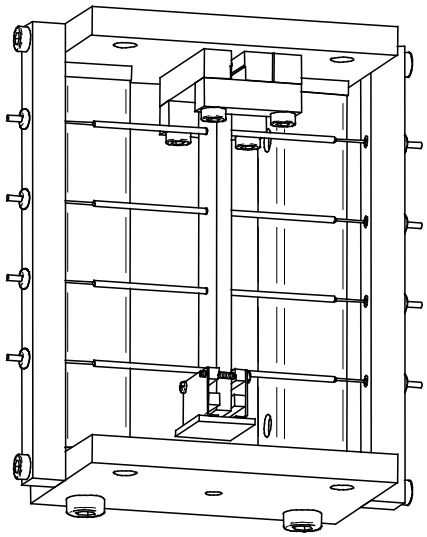


Figure 5.31: Arrangement of rods providing rotational restraint - Front spacing legs are omitted for clarity

5.4.3 Experimental method

5.4.3.1 Mounting of target

One end of the specimen was lightly sanded on both faces until its thickness matched that of the gap between the jaws and the support pads of the target assembly. The assembly was then slid into position over the end of the specimen. A small space

between the end face of the specimen and the rear of the target plate was left to prevent the specimen contacting the target as a result of thermal expansion. The target assembly was squared relative to the axis of the specimen by means of a steel set-square. The stainless steel fastening screws in the jaws of the target assembly were then tightened using a screwdriver. The screws were tightened until the jaws were firmly positioned, but not overtightened.

The configuration of the target assembly mounted on the specimen is illustrated in Figure 5.29.

5.4.3.2 Mounting of the specimen in the test rig

The test rig was positioned vertically with the sensor at the bottom and the grips at the top.

The tightening screw of the grips was loosened and the jaws were opened. The threaded rods used to prevent rotation of the specimen were loosened thereby making room for fitting the specimen into the test rig.

The free end of the specimen was positioned within the grips and raised until it made contact with the backing plate of the grip assembly. The spacing blocks were then slid into position around the sensor and the specimen assembly was lowered until the target plate rested on the spacing blocks.

The spacing blocks could be moved slightly as a unit because of the small clearance between the sensor and the blocks. The specimen assembly was supported on the blocks and its position could therefore be adjusted. The specimen face to be gripped by the stationary jaw was aligned parallel with this jaw and just making contact with it. In addition, the target was centrally located over the sensor.

The sliding jaw was then manually moved forward until it almost touched the other face of the specimen across its complete width. The tightening screw of the grip assembly was then tightened so that the sliding jaw moved forward and gripped the specimen. The jaws were tightened until the specimen was securely gripped but not overtightened.

The threaded rods used to prevent rotation of the specimen about the “knife-edge” grips were then tightened until the end of each rod just made contact with the specimen. Bending and rotation of the specimen was thereby prevented.

The spacing blocks were carefully slid out from under the target plate. The specimen was now completely supported by the test rig and was ready for testing.

5.4.3.3 Cooling of oven

Considerable effort was put into developing the method of supporting the target on the specimen. Unless the experimental equipment could yield repeatable results using a steel specimen, there was little hope of obtaining worthwhile results on GFRP specimens. As a result, a steel specimen was tested on multiple occasions as different configurations of target assembly were tested. Eventually the more obvious problems (such as discontinuities in measurement and changes in slope from initial test to subsequent tests) had been ironed out. At this stage, a problem with the measured linearity in the results was observed. All tests were highly repeatable at temperatures less than 90℃ and at temperatures greater than 140℃. Between these temperatures, however, some sets of measurements were fairly linear whilst others were less so. Initially no correlation between the linearity and test parameters could be found. It was eventually determined that rapid cooling of the oven after a test (by opening the door and circulating cooling air with the internal fan) resulted in non-linearity in the subsequent set of measurements. Leaving the interior of the oven to cool gradually and only opening the door of the oven when its interior had cooled to room temperature resulted in measurements of greater linearity in the subsequent test. This effect is illustrated in Figure 5.32. This figure shows the results for eight completely separate tests. In each test the steel specimen was removed from the target assembly and supporting grips before being refitted. The most linear set of test results resulted from the slowest rate of cooling in the preceding test, whereas the most non-linear results resulted from the fastest cooling.

Initially it was thought that the cooling-rate dependency could be caused by creep in the solder holding the copper target to the steel of the rest of the target assembly. Copper and steel have different coefficients of thermal expansion and would thus expand by different amounts as the specimen was heated. The solder joining the two materials would thus be required to transfer compatibility loads. The elevated temperatures experienced during the testing process could cause creep in the solder with resultant relaxation of these loads. On cooling, the copper and steel constituents of the target assembly would again set up compatibility loads. Depending on the rate of cooling, the time available for load relaxation in the solder would vary and differing amounts of relaxation could potentially occur. This effect might result in differing amounts of non-linearity in the measurements.

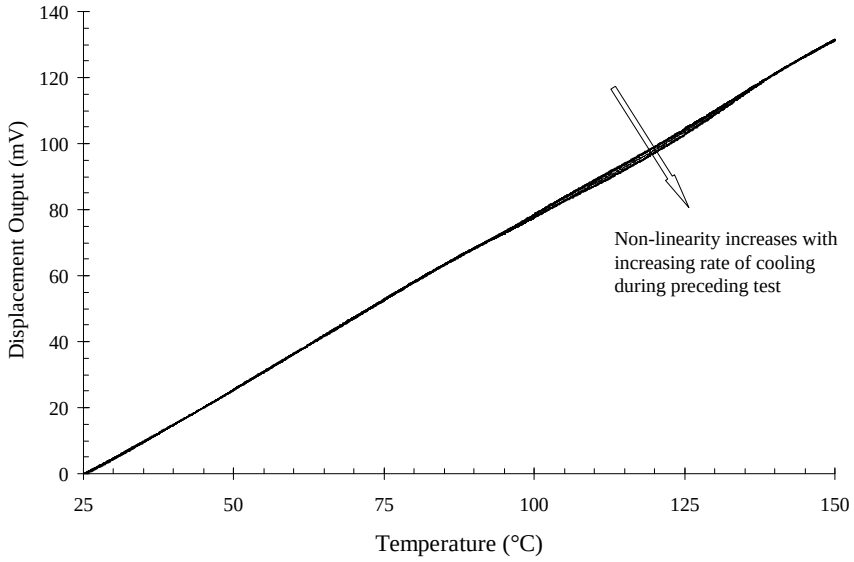


Figure 5.32: Effect of rate of oven cooling on measurement linearity

To check this hypothesis, a new target assembly was manufactured. This assembly was identical to the first one, but was joined using silver solder. Both the strength and melting point of silver solder are significantly higher than that of ordinary plumbing solder. This material is therefore far less likely to allow relaxation of the compatibility loads during heating of the specimen. The measured response using the new target assembly was, however, absolutely identical to that of the original assembly. Creep in the solder was therefore ruled out as the cause of the non-linear response.

It appears that the lack of linearity can be attributed to the sensor itself. The sensor consists of a coil embedded in a polymer matrix. The properties of the polymer are unknown, but it appears conceivable that such non-linear response could be a result of the relaxation of internal thermal loads during rapid cooling of the sensor. Irrespective of the cause of the non-linearity however, it appeared that the only way to ensure the most linear response of the measurement system was to allow the oven to cool naturally to a low temperature (taken as 30°C) before opening its door. This approach was followed for all future work.

5.4.3.4 Test procedure

When the specimen was properly mounted, the rig was transferred onto a small stand in the oven. The sensor wiring was threaded through the port at the top of the oven and connected to the KD2300 oscillator/demodulator. The temperature

sensor was threaded through the same port until it hung next to the specimen. The door of the oven was then closed.

The output terminals from the KD2300 oscillator/demodulator and temperature sensor were connected to the data logger using shielded cable with BNC connectors at each end.

The data logging software was started and a new file opened. The software was set up to record data every minute. The values of temperature and strain were averaged over this time interval.

The logging software was started and left for approximately 30 minutes. This ensured that the software was working properly, and that the specimen and test-rig were at the same temperature as the inside of the oven.

The data logging process was stopped and then restarted. This process overwrote the data initially recorded while the temperatures within the oven settled.

The oven temperature was then ramped at a rate of 6℃ per hour[ix] up to a maximum of 140℃[x].

When the maximum temperature of 140℃ was reached, the oven was turned off and logging of data was stopped. The specimen was only removed when the internal temperature of the oven had reduced to less than 30℃. This ensured the most linear response from the displacement transducer during the subsequent test.

[ix] The slow heating rate was selected to accommodate two processes that can affect the accuracy of the measured results. The first process is thermal lag, which can result in temperature variations within both the specimen and the test rig. The second process is viscous flow. A slow heat up rate provides sufficient time for viscous flow and also minimizes temperature variations. By interrupting the rate of temperature increase and holding the temperature constant it was possible to check whether the selected heating rate was suitable. The measured strains did not vary significantly at either low or high temperatures and it was thus determined that the selected heating rate was sufficiently low.

[x] The initial design of the rig was heated to a maximum temperature of 150℃. The duration of testing thus lasted for five hours after the region of linear thermal expansion was established at around 120℃. In order to speed up the testing process it was decided to limit the maximum test temperature to 140℃ for this set of tests. This saved nearly two hours of testing time while still providing a clearly defined region of linearity.

5.4.3.5 Precautions

The amplifier and data logging equipment should be left on between tests to ensure that they are fully warmed up at the start of a new test.

The oven must be left for a considerable period to cool down before starting a new test. Even when the interior is cool to the touch, it is possible for residual heat to be stored within the fan ducts. If this heat remains when a new test is started, it is found that the air temperature climbs far more rapidly than desired at the start of the test.

5.4.4 Calibration

The calibration of the final test rig was performed in essentially the same way as that of the initial test rig. The measured change in thermal strain was assumed to be related to the measured temperature and displacement sensor output voltage by means of equation 5.1, repeated below for clarity:

$$\Delta\epsilon_{cal} = C_1(\Delta V_{cal}) + C_2(\Delta T_{cal}) + C_3(\Delta V_{cal})(\Delta T_{cal}) + C_4(\Delta V_{cal})^2 + C_5(\Delta T_{cal})^2$$

where $\Delta\epsilon_{cal}$ corresponds to the measured change in thermal strain (in $\mu\epsilon$) relative to the strain at the reference temperature of 25℃, ΔT_{cal} corresponds to the change in temperature (in ℃) relative to the reference temperature and ΔV_{cal} corresponds to the change in displacement sensor output voltage (in mV) relative to that at the reference temperature. The coefficients C_1 to C_5 correspond to calibration constants.

Four different reference materials were used to provide the calibration data. These materials comprised aluminium, copper, steel and graphite which were selected because they span thermal expansion rates significantly greater than those expected during testing of the GFRP specimens. Each reference material was tested three times and was completely removed from the test rig and target assembly between tests and remounted according to the method specified for the actual test specimens in section 5.4.3.1 and section 5.4.3.2.

The calibration coefficients C_1 to C_5 were adjusted to minimize the error between the strain predicted using equation 5.1 and the known thermal strain of the reference materials at every test temperature. Details of the calculations involved can be found in Appendix D.

A comparison between known thermal expansion and measured thermal expansion using the best-fit calibration is illustrated in Figure 5.14. It is apparent from this figure that that a close fit between reference and measured data exists. The coefficient of determination, R^2, of the fit is 0.999845. The standard deviation between measured strains and reference strains is 9.0 $\mu\epsilon$.

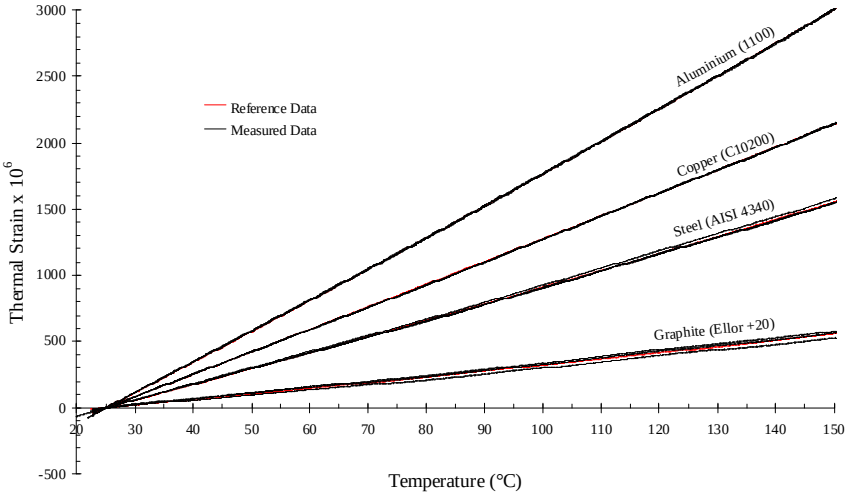


Figure 5.33: Comparison between reference thermal strains and calibrated measurements

6 Results

The results are presented in four sections. The measured strain response is presented first. This information is used in the subsequent two sections to calculate the residual fibre strain and then the residual stress in both fibre and matrix. Finally, experimental strains are juxtaposed on theoretical predictions.

6.1 Response to thermal loading

The raw data measured during each test were processed using equation 5.1 and the calibration coefficients listed in Table D.6 to determine the variation in specimen strain with temperature.

6.1.1 Cast resin

The results for the specimen of cast resin are shown in Figure 6.1. Data for both the initial test and the subsequent test where the specimen was reheated are presented.

For comparison purposes, the data presented in Figure 6.1 are shown again in Figure 6.2 alongside data, originally presented in Figure 5.3, obtained using strain gauges affixed with HBM X280 adhesive.

6.1.2 Reinforced specimens

The variations in specimen strain with temperature for the three different types of glass reinforced specimens are given in Figures 6.3 though 6.5. For comparison purposes, these results are also presented on the same set of axes in Figure 6.6.

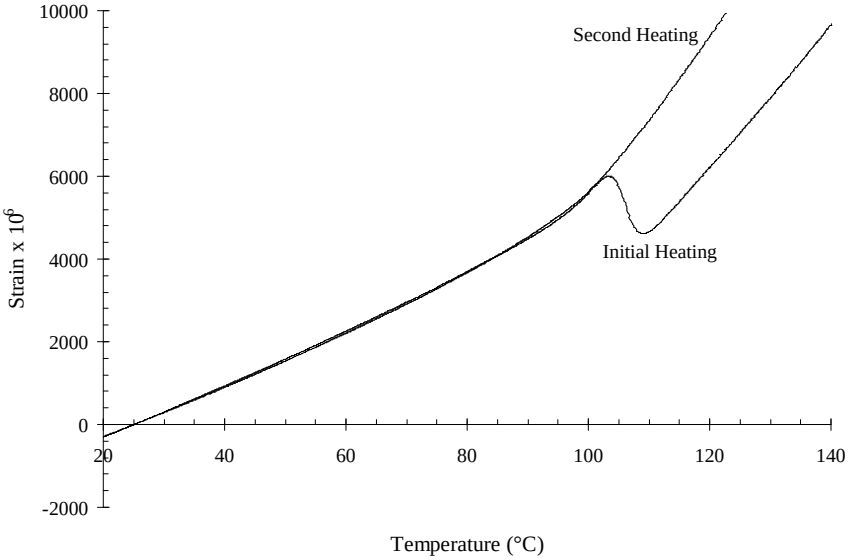


Figure 6.1: Measured strain in cast resin as a function of temperature

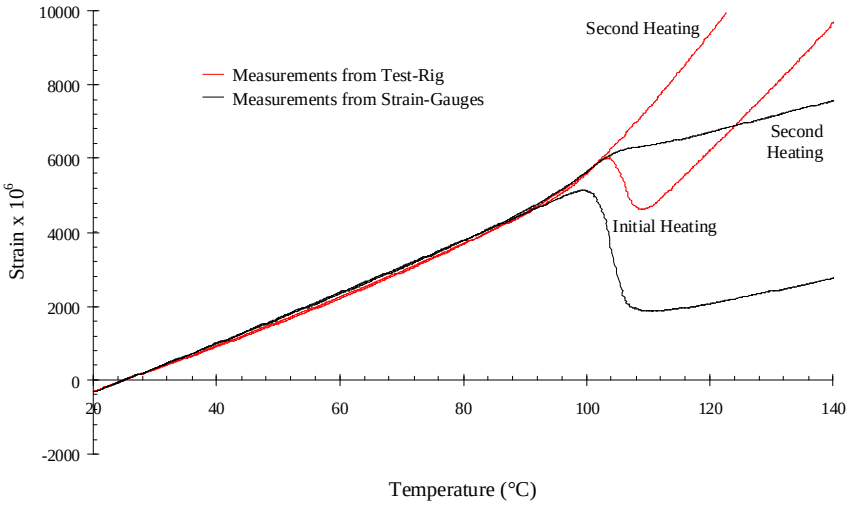


Figure 6.2: Comparison of the measured thermal strain of cast resin obtained using the final test rig and strain gauges

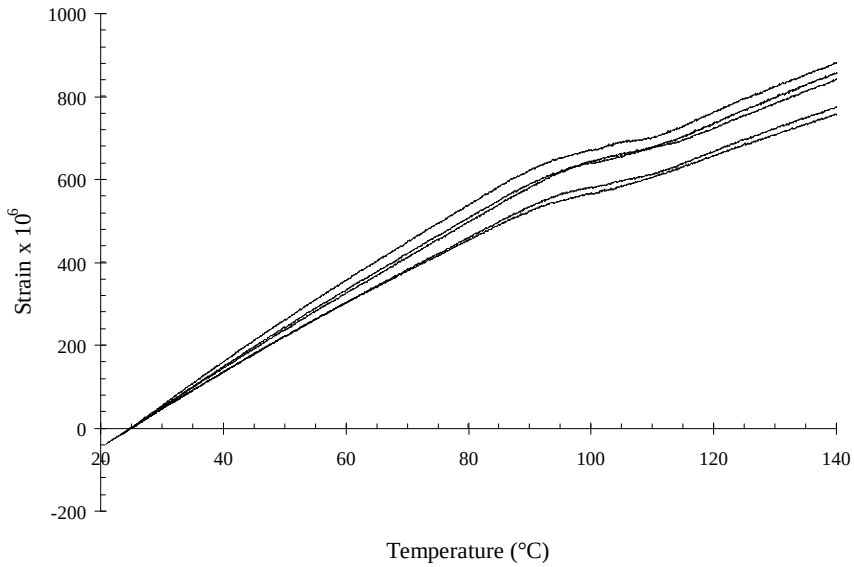


Figure 6.3: Measured strain in unloaded specimens

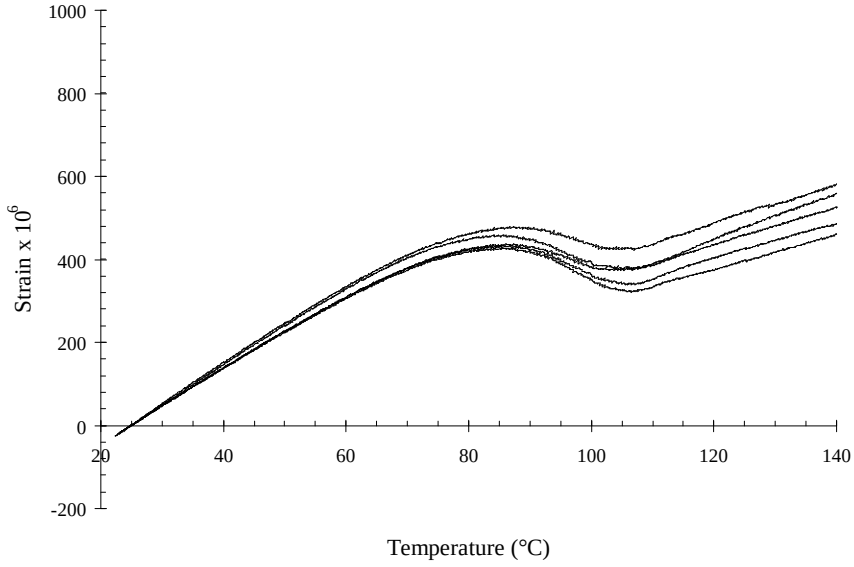


Figure 6.4: Measured strain in preloaded specimens

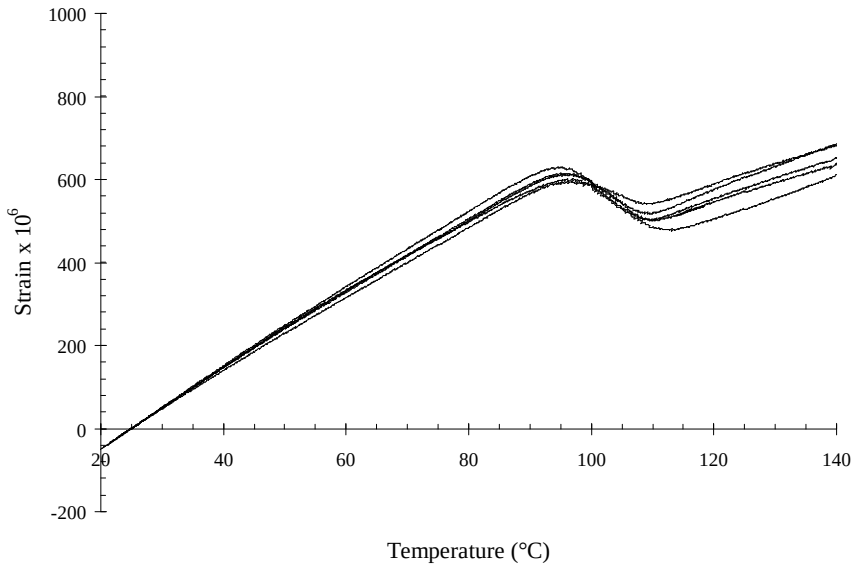


Figure 6.5: Measured strain in annealed specimens

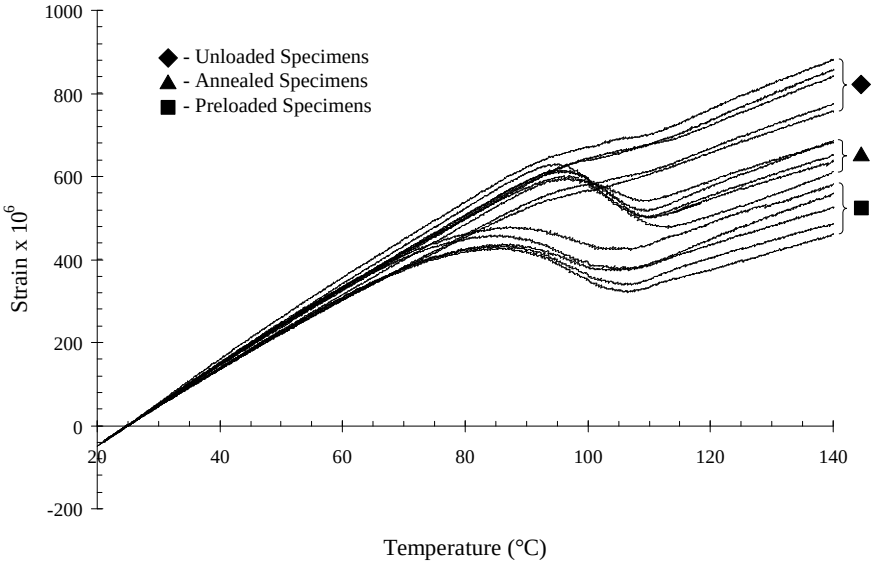


Figure 6.6: Comparison between measured strains in different specimen types

Linear coefficients of thermal expansion determined for the glass reinforced specimens are presented in Tables 6.1 and 6.2. The values are determined using linear regression analyses from 25℃ to 50℃ and from 115℃ to 140℃ respectively. The smallest coefficient of determination, R^2, extracted from each set of data is 0.9996 and 0.9942 respectively.

Table 6.1: Coefficients of thermal expansion from 25℃ to 50℃

	Unloaded specimens ($\mu\epsilon$/°C)	Preloaded specimens ($\mu\epsilon$/°C)	Annealed specimens ($\mu\epsilon$/°C)
	10.5	9.8	9.6
	9.5	9.7	9.2
	9.7	9.1	9.7
	8.8	9.0	10.0
	8.9	9.0	9.8
Average	**9.5**	**9.3**	**9.6**
Std deviation	0.7	0.4	0.3

Table 6.2: Coefficients of thermal expansion from 115℃ to 140℃

	Unloaded specimens ($\mu\epsilon$/°C)	Preloaded specimens ($\mu\epsilon$/°C)	Annealed specimens ($\mu\epsilon$/°C)
	6.0	4.6	5.6
	6.2	5.6	4.8
	5.9	4.2	4.9
	5.4	4.2	4.7
	5.1	4.5	5.1
Average	**5.7**	**4.6**	**5.0**
Std deviation	0.5	0.6	0.4

6.2 Residual strains

6.2.1 Residual strains obtained without knowledge of matrix properties

A linear regression analysis of the strain data presented in Figures 6.3 through 6.5 at temperatures of 115℃ and higher defines the locus of zero stress in the glass fibres. This line can be extended back to lower temperatures as illustrated for a

single preloaded specimen in Figure 6.7. The residual strain in the fibre at any temperature is determined by taking the difference in strain between that of the specimen and that of the locus of zero stress. The residual strain in the glass fibre of the three different specimen types is plotted in Figures 6.8 through 6.10. For comparison, these results are also presented on the same set of axes in Figure 6.11.

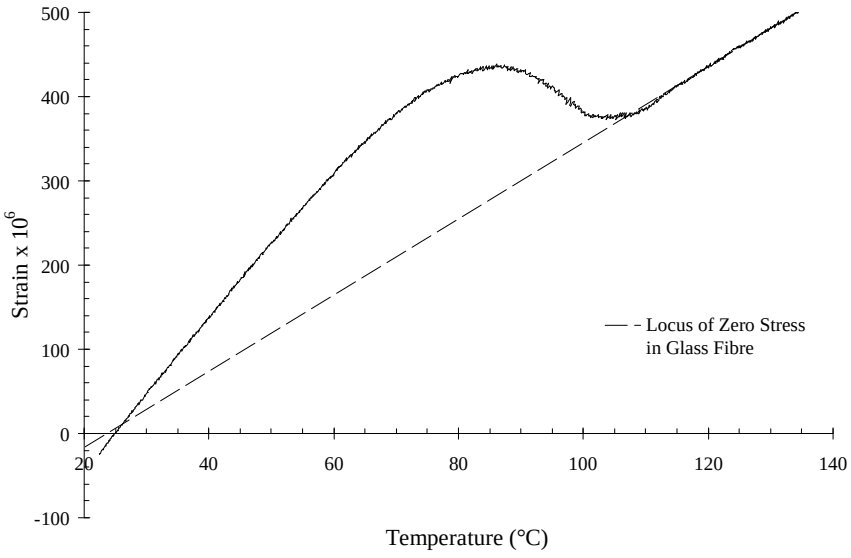


Figure 6.7: Locus of zero stress in glass fibre

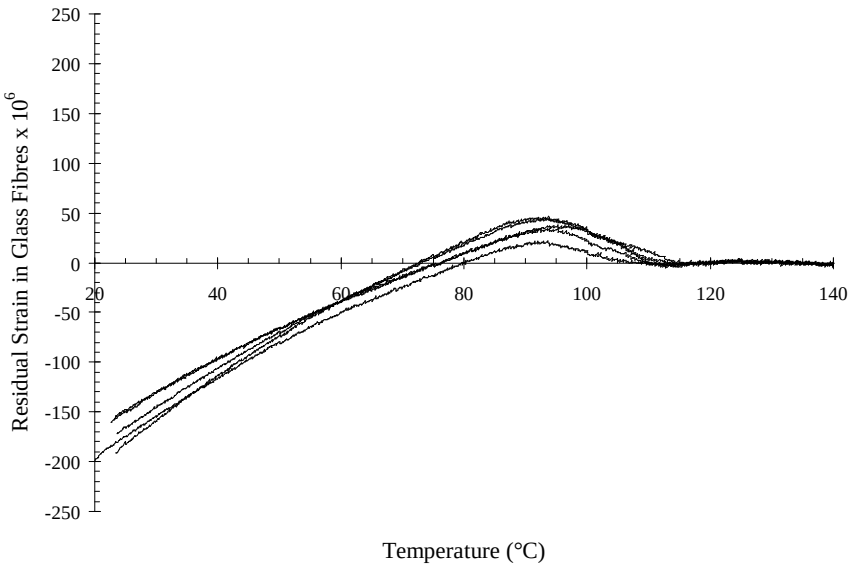


Figure 6.8: Residual strain in glass fibres of unloaded specimens

The coefficient of thermal expansion for the glass reinforced specimens is expected to correspond to that of pure glass at temperatures above the relaxation temperature. As a consequence, the residual strain in the glass fibre can also be determined by replacing the experimentally measured data in this region by data obtained from

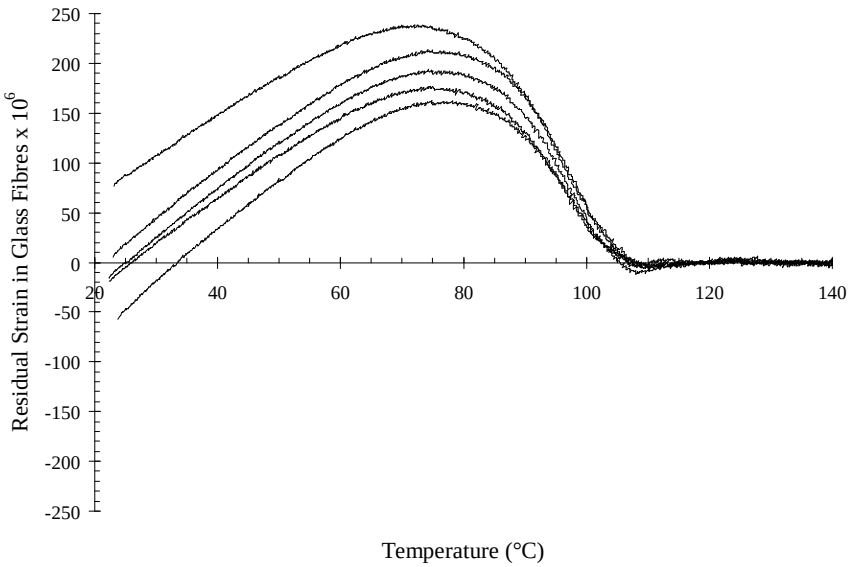


Figure 6.9: Residual strain in glass fibres of preloaded specimens

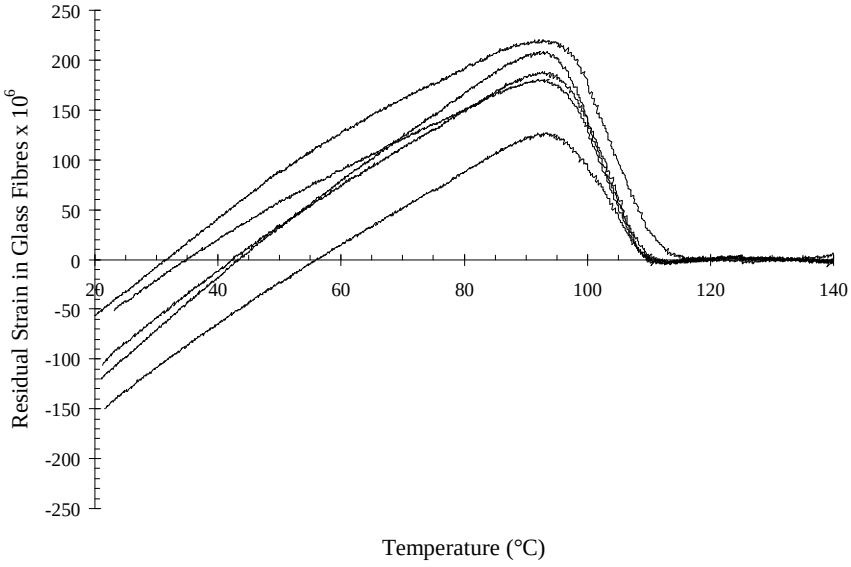


Figure 6.10: Residual strain in glass fibres of annealed specimens

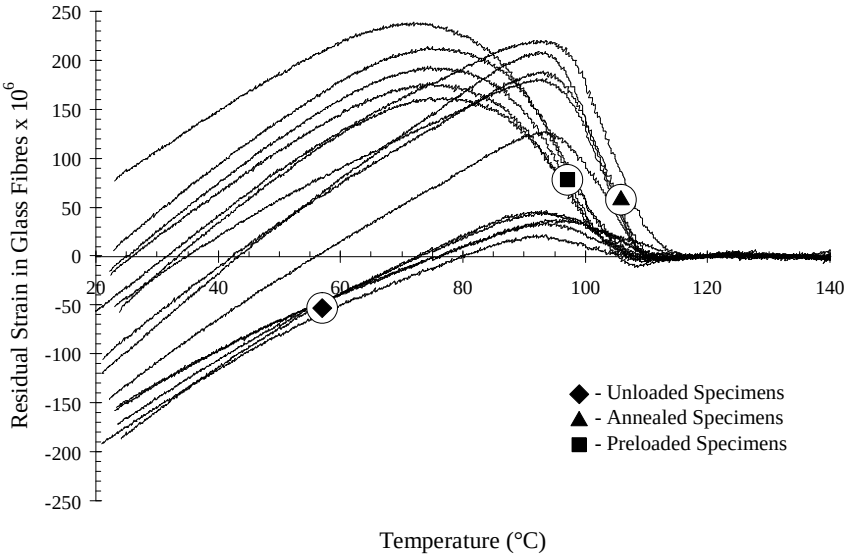


Figure 6.11: Comparison between residual strains in glass fibres of different specimen types

the literature. The coefficient of thermal expansion of glass fibre is listed from 4.7 $\mu\epsilon/°\text{C}$ to 5.4 $\mu\epsilon/°\text{C}$.[185, 190, 191]

Data corresponding to the approximate mid-range of published values, 5.0 $\mu\epsilon/°\text{C}$,[185] are consequently fitted tangential to each data set, thereby defining the locus of zero stress in the glass fibres. For illustrative purposes, a typical fit to the experimental data is shown in Figure 6.12 for a single preloaded specimen. Experimental data at temperatures above the point of tangency are assumed to lie on the fitted curve and are consequently discarded. The residual strain in the fibres of the different specimen sets is then calculated and plotted in Figures 6.13 through 6.15. For comparison purposes, these results are also presented on the same set of axes in Figure 6.16.

Numerical estimates for the residual strains in the glass fibre at the reference temperature of 25°C are determined by performing a linear regression analysis using the data from Figures 6.13 through 6.15 between temperatures of 23°C and 27°C. The results are presented in Table 6.3.

6.2.2 Residual strains obtained by considering matrix properties

The results presented in section 6.2.1 are based on the assumption that the modulus of the matrix decays to negligible values in the region of linear response at high

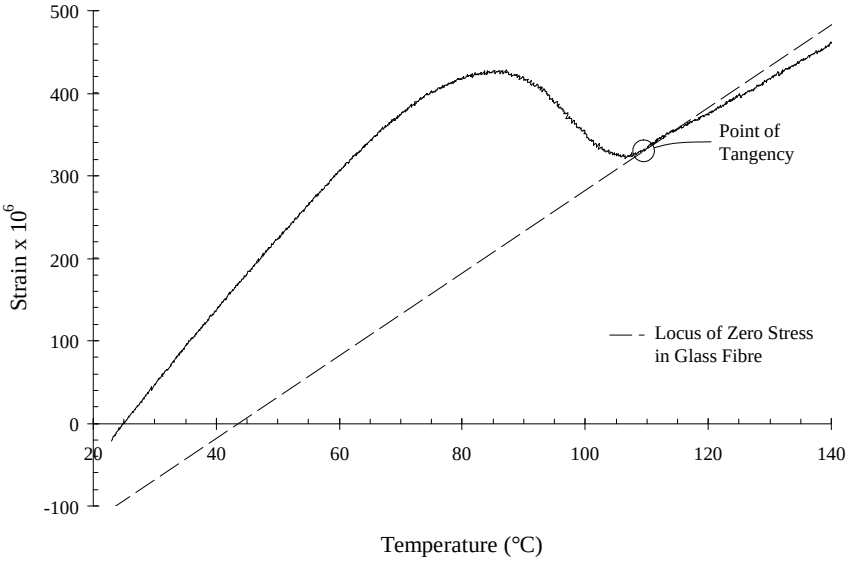


Figure 6.12: Improved method of finding the locus of zero stress in the glass fibre

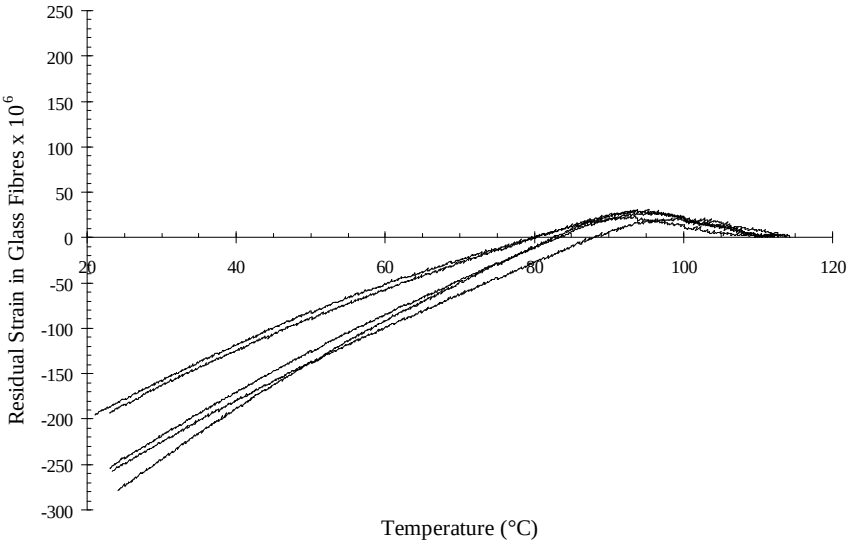


Figure 6.13: Residual strain in glass fibres of unloaded specimens

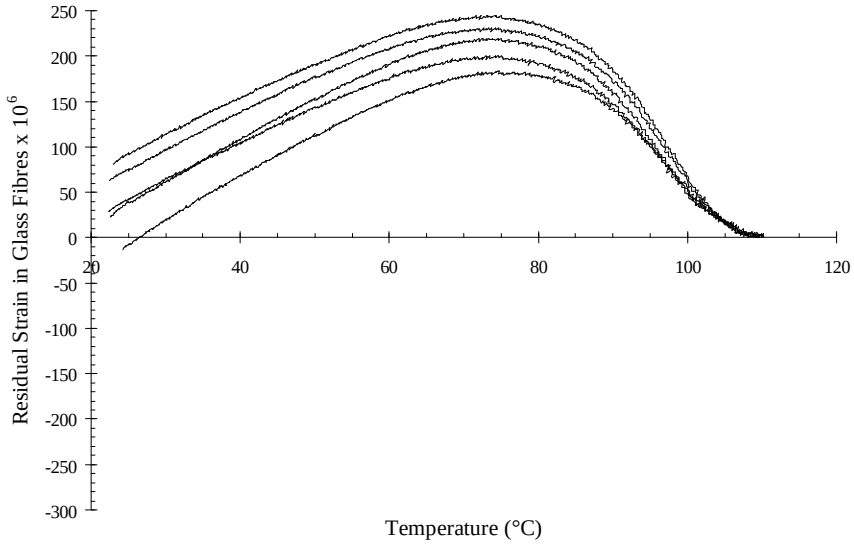


Figure 6.14: Residual strain in glass fibres of preloaded specimens

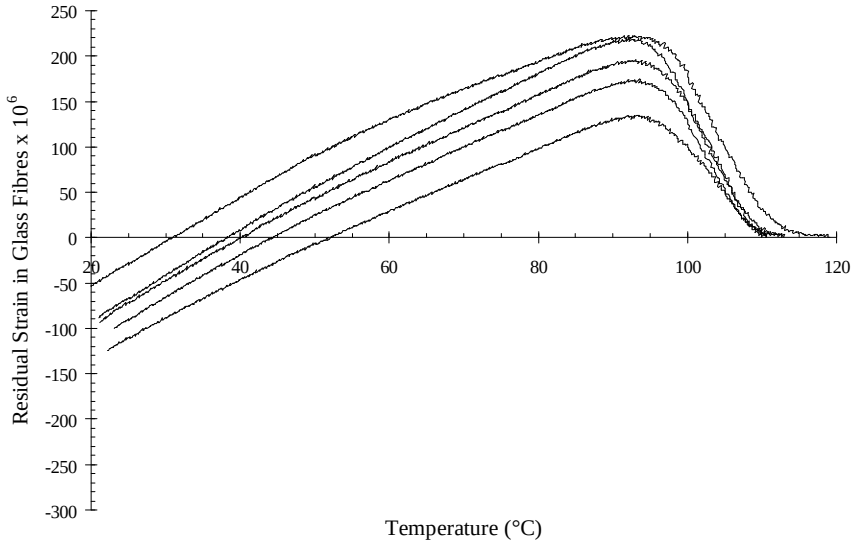


Figure 6.15: Residual strain in glass fibres of annealed specimens

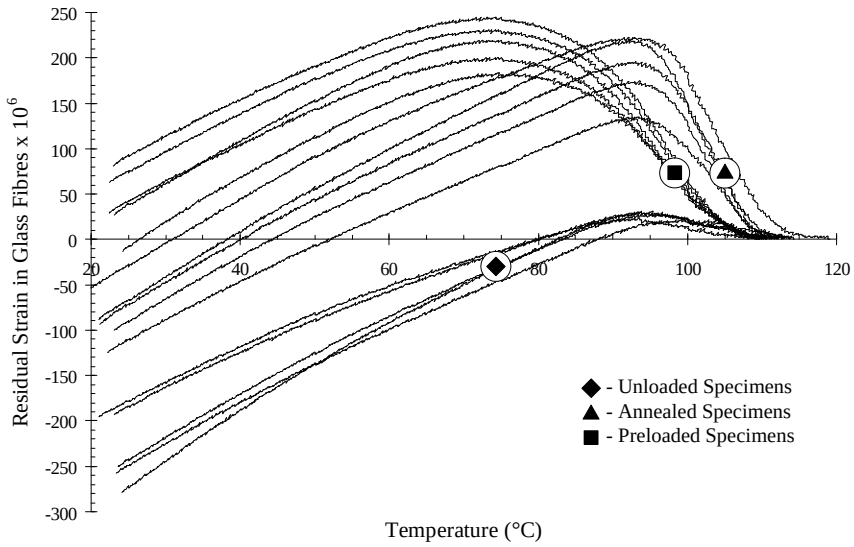


Figure 6.16: Comparison between residual strains in glass fibres of different specimen types

Table 6.3: Residual strain in glass fibres at 25°C

	Unloaded specimens ($\mu\epsilon$)	Preloaded specimens ($\mu\epsilon$)	Annealed specimens ($\mu\epsilon$)
	-274	-9	-90
	-249	38	-111
	-243	75	-72
	-185	92	-67
	-178	42	-29
Average	**−226**	**47**	**−85**
Std deviation	42	39	20

temperatures. The accuracy of these results can be improved if the actual matrix properties are considered. Necessary information includes the variation in matrix modulus with temperature and the strain response, including polymerization shrinkage, of the matrix as it is heated from the stress-free state into the region of linear response at high temperatures.

The effect of considering non-zero matrix properties is that the measured strain response of the composite is shifted upwards relative to the locus of zero fibre stress. The residual strains in the fibre are consequently increased by an amount corresponding to the offset strain, $\Delta\epsilon$, calculated using equation 4.4. The detailed calculations to determine the offset strain are presented in Appendix F.

The calculated strain free temperature, T_0, and strain offset, $\Delta\epsilon$ for each specimen are presented in Table 6.4. The data within specific locations in this table correspond to data in the same locations of Table 6.3.

Table 6.4: T_0 and $\Delta\epsilon$

	Unloaded		Preloaded		Annealed	
	T_0 (℃)	$\Delta\epsilon$ ($\mu\epsilon$)	T_0 (℃)	$\Delta\epsilon$ ($\mu\epsilon$)	T_0 (℃)	$\Delta\epsilon$ ($\mu\epsilon$)
	82.2	1.4	24.8	9.4	43.1	4.8
	87.6	0.9	15.5	11.1	51.1	3.5
	82.8	1.3	7.0	12.5	38.6	7.2
	79.5	1.6	4.1	13.3	37.4	4.2
	79.3	1.6	13.7	10.3	30.1	3.4
Average	**82.3**	**1.3**	**13.0**	**11.3**	**40.1**	**4.6**
Std deviation	3.0	0.3	7.2	1.4	6.9	1.4

Figures 6.13 through 6.16 are adjusted to reflect the strain offset appropriate to each specimen and are represented as Figures 6.17 through 6.20.

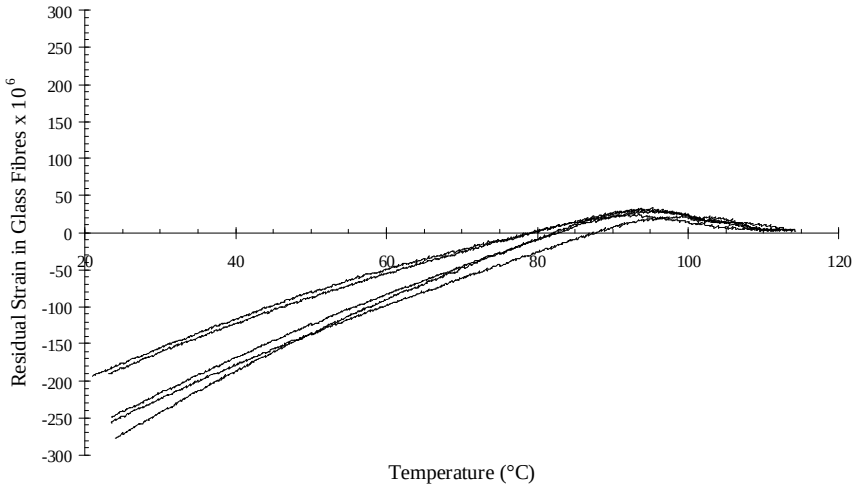


Figure 6.17: Residual strain in glass fibres of unloaded specimens

Updated estimates of the residual strains in the glass fibre at the reference temperature of 25℃ are presented in Table 6.5. The difference between the strain data presented in Table 6.5 and that presented in Table 6.3 corresponds to the calculated strain offset for each specimen.

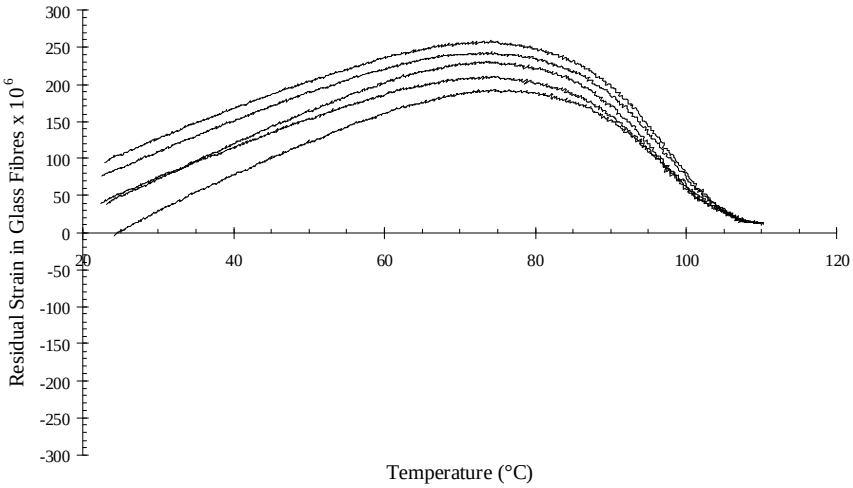


Figure 6.18: Residual strain in glass fibres of preloaded specimens

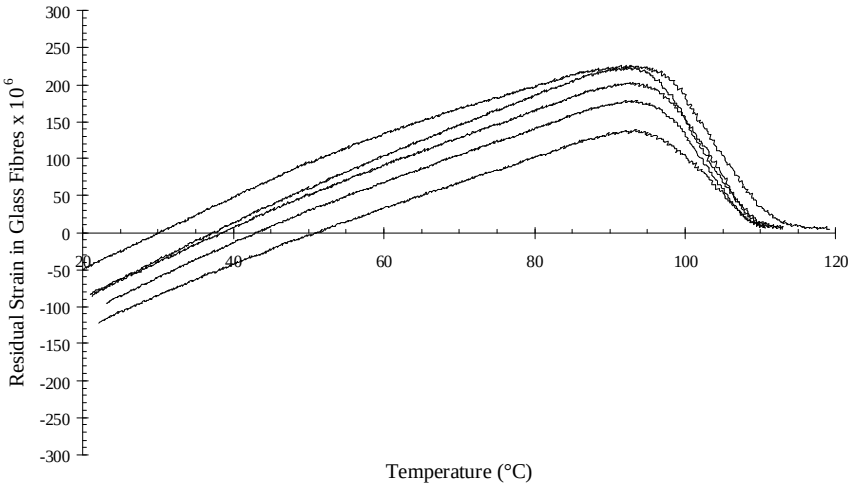


Figure 6.19: Residual strain in glass fibres of annealed specimens

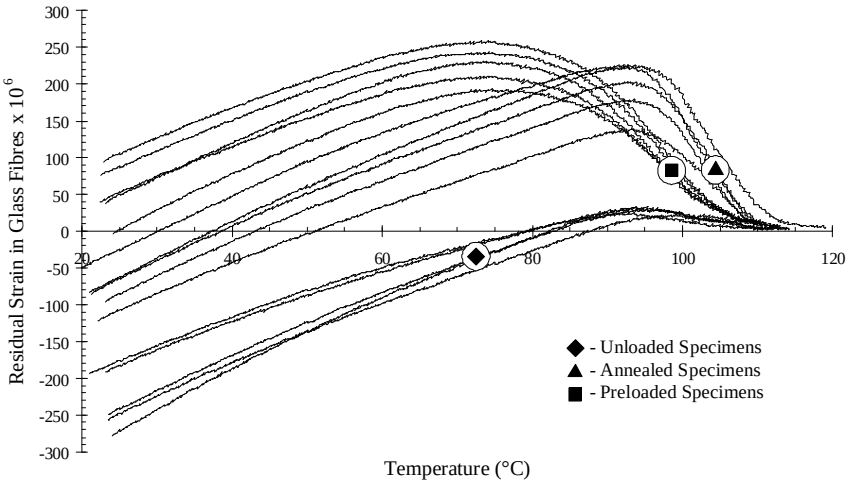


Figure 6.20: Comparison between residual strains in glass fibres of different specimen types

Table 6.5: Residual strain in glass fibres at 25°C

	Unloaded specimens ($\mu\epsilon$)	Preloaded specimens ($\mu\epsilon$)	Annealed specimens ($\mu\epsilon$)
	-272	0	-86
	-248	49	-108
	-242	87	-65
	-183	105	-63
	-176	52	-25
Average	**−224**	**59**	**−69**
Std deviation	42	40	31

6.3 Residual stresses

6.3.1 Residual stresses obtained without knowledge of matrix properties

The longitudinal strain results presented in Table 6.3 are used to determine the longitudinal residual stresses within all specimen sets at the reference temperature of 25°C. These results are presented in Table 6.6. The average residual strains in the glass fibre are converted to stresses using Hooke's law with the elastic modulus of the glass fibre taken as 72 GPa.[185] The stresses in the matrix are then determined using equilibrium considerations:

$$\sigma_m = -\sigma_f \cdot \frac{V_f}{V_m} \tag{6.1}$$

where σ_f, V_f and V_m are the average fibre stress, and the volume fractions of the fibre and matrix respectively. The matrix stresses are determined using the nominal fibre volume fraction of 40%. The strains in the matrix are determined using Hooke's law with the elastic modulus of the matrix taken as 3200 MPa as shown in Figure 4.1.

Table 6.6: Residual strains and stresses at 25℃ in longitudinal direction

		Unloaded specimens	Preloaded specimens	Annealed specimens
Fibre strain	($\mu\epsilon$)	-226	47	-85
Fibre stress	(MPa)	-16.3	3.4	-6.1
Matrix stress	(MPa)	10.8	-2.3	4.1
Matrix strain	($\mu\epsilon$)	3390	-705	1275

6.3.2 Residual stresses obtained by considering matrix properties

More accurate stress results than those presented in Table 6.6 can be obtained if the effects of Poisson's strains are known. The detailed calculations to determine this information are presented in Appendix G. It is shown that improved estimates of the residual stresses in the unloaded and preloaded specimens can be determined, but this is not possible for the annealed specimens. The annealed specimens were created by heating the preloaded specimens to 80℃ and allowing stresses to dissipate for 100 hours. Stresses relaxed as a consequence of non-linear creep and so the final stress state cannot be estimated with the elastic analysis technique used in this work.

The method of better determining the residual stresses in the unloaded and preloaded specimen sets makes use of a modified form of an equation presented by Nairn.[167] The original equation was intended to consider thermal effects only[i]. Stresses in these specimens arise also from cure shrinkage of the resin system and from fibre preload. It is possible, however, to adapt Nairn's equation to account for these

[i]The equation presented in the original publication[167] is actually incorrect for the case where the material properties are temperature dependent. The original equation integrates stresses over the temperature range of interest. Stresses cannot be summed in this way if matrix modulus changes with temperature. Rather, the stress driving term, in this case the mismatch in thermal strains between fibre and matrix, must be integrated and the stresses determined using the material properties applicable at the temperature of the end of the integration interval. This issue is discussed in more depth in Appendix B.1.1.2 where the corrected form of the equation is presented.

additional loads[ii].

Estimation of the residual stresses clearly requires knowledge of the change in temperature from the stress-free state, the cure shrinkage of the resin and the fibre preload. Temperature dependent material properties are required between the temperature of interest and the temperature at which the residual stresses dissipate to zero as defined by the point of tangency illustrated in Figure 6.12. The properties of the glass fibre can be assumed constant over the temperature range considered in this work, but those of the matrix vary dramatically.

The matrix properties that need to be considered include the elastic modulus, the Poisson's ratio and the strain response to changes in temperature.

The elastic modulus has been measured using DMA equipment. These data are presented in Figure 4.1 but cannot be used directly because they were measured at an oscillation frequency of 2.0 Hz. They consequently have a time-scale quite different to that used in this experimental work. The principle of time-temperature equivalence can, however, be used to resolve this problem. Although the exact value of the temperature shift is not precisely known, it is estimated in Appendix F.2 that the DMA data are applicable to the current work if the measured data are used at temperatures approximately 9℃ lower than that at which they were measured.

The Poisson's ratio of the matrix is not measured directly. It is assumed similar to that of epoxy resin at room temperature and so a value of 0.36[191] is used. As the matrix tends towards the rubbery state at high temperatures it is expected that its Poisson's ratio tends towards 0.50.[174] In principle, the analysis should incorporate changes to the Poisson's ratio with temperature, but it has been found that the Poisson's ratio has little effect on the development of residual stress.[174] This is confirmed by considering parts b. of both Figures G.3 and G.5 where it is apparent that significant changes to the Poisson's ratio of the matrix do not materially affect the residual strain.

The strain response to changes in temperature is only required to investigate the development of thermal stresses. The response was measured earlier in this investigation and is presented in Figure 6.1.

Analysis of the stress calculations reveals that the ratio of the transverse stresses to the longitudinal stress depends on whether the stresses arise as a result of thermal

[ii] More details regarding the method of making the necessary changes are presented in Appendices B.1.2 and B.1.3.

stresses, cure stresses or preload stresses. Interestingly, this ratio does not vary significantly with temperature. For thermal and cure stresses the ratio varies between 0.2698 and 0.2794 only. The ratio is essentially constant at 0.036 for loading arising from fibre preload.

This information considerably simplifies calculation of the residual stresses. It also means that the potential errors associated with not precisely knowing the temperature shift associated with time-temperature equivalence do not have a significant effect on the calculated residual stress.

The stress calculations for the unloaded specimens are based on the strain data presented in Table 6.5. The corresponding calculations for the preloaded specimens are not based on this table but rather those of Table 6.3. This is because there is reason to believe, as will be explained in Chapter 7, that the use of this data is more appropriate.

The result of the stress calculations is presented in Table 6.7. The spread in the range of presented stress values arises because the ratio of the transverse stresses to the longitudinal stress for thermal and cure stresses is not entirely constant. Stress values are consequently calculated at the limits of this ratio. The data are presented in such a way that data at the start and end of a range are consistent. The transverse stresses are constant and identical throughout the fibre. The transverse stresses in the matrix are identical to those of the fibre at the fibre/matrix interface but vary logarithmically in opposite directions with increasing radius.[167]

Table 6.7: Residual strains and stresses at 25℃

		Unloaded specimens	Preloaded specimens
Longitudinal fibre strain	($\mu\epsilon$)	-224	47
Longitudinal fibre stress	(MPa)	-18.54 to -18.64	1.18 to 1.28
Longitudinal matrix stress	(MPa)	12.36 to 12.43	-0.79 to -0.85
Longitudinal matrix strain	($\mu\epsilon$)	3318	-1363
Transverse stresses	(MPa)	-5.50 to -5.72	-5.01 to -4.79

6.4 Comparison between experiment and theory

The theoretical method used to predict the residual stresses presented in Table 6.7 can also be used to predict the response of the residual fibre strain to changes in temperature. Once this information is known, it becomes possible to predict the

strain response of the entire composite laminate. These calculations are presented in detail in Appendix G. The predicted strain response is compared with the strain response measured in Figures 6.17 through 6.20 because these measurements rely on the same material data as the predicted results. If there is any error associated with this data, the residual strains at temperatures higher than the relaxation temperature are similarly affected in both sets of data.

The preloaded specimens are identical to the unloaded specimens except that an additional fibre preload is applied. It is therefore logical to first predict the behaviour of the unloaded specimens and then add the effect of the additional preloading to find the behaviour of the preloaded specimens.

The prediction of the strain response of the unloaded specimens requires individual assessment of the response to changes in temperature, the response to cure shrinkage and the response to an initial fibre preload. The fibre preload is known and so the corresponding strain response is easily calculated. The response to thermal loading is readily calculated if the stresses at the post-cure temperature are assumed negligible. Unfortunately, insufficient material data are available to allow the calculation of the response to cure shrinkage. An *a priori* prediction of the behaviour of the unloaded specimens is thereby prevented.

It is still possible to obtain useful predictions, however, if a single point of measured strain is incorporated into the analysis. The mathematical form of the equations used to predict the thermal response is identical to that of the equations used to predict the response to cure shrinkage. It is thus possible to use a single equation to predict the combined response of both thermal loading and cure shrinkage. When cure shrinkage stresses are added to thermal stresses, the effect is identical to changing the zero-stress temperature in a purely thermal analysis. The zero-stress temperature in the thermal analysis is consequently adjusted until the predicted strain at the post-cure temperature matches the average measured strain, thereby accounting for the effects of cure shrinkage. Once this is done, the rest of the strain response is directly calculated.

The predicted residual strain in the fibres of the unloaded specimens is presented in Figure 6.21. Data are presented for the nominal fibre volume fraction of 40%, corresponding almost exactly to the average fibre volume fraction, and for the maximum and minimum fibre volume fractions measured across this specimen group. For comparison purposes, the predicted residual strain response is overlaid on measured strain results, as presented in Figure 6.17.

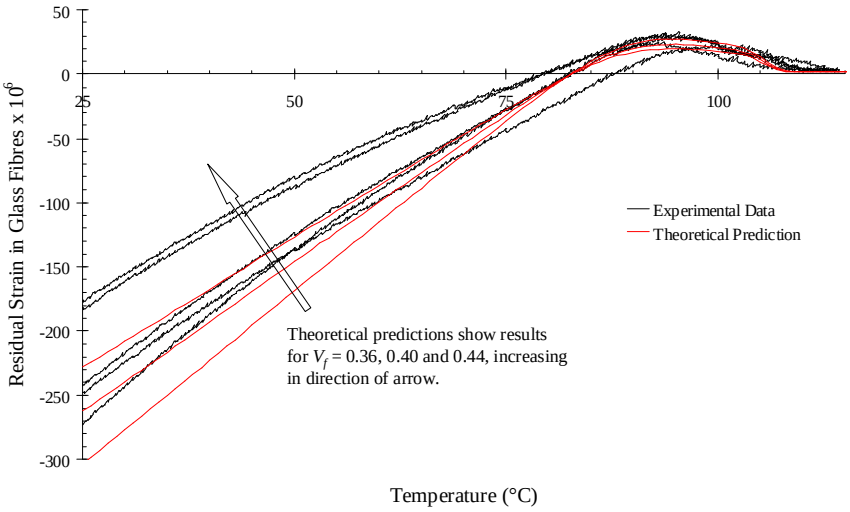


Figure 6.21: Comparison between predicted residual strain variation and experimental data - Unloaded specimens

The predicted strain response of the unloaded specimens is obtained by adding changes in the residual strain data presented in Figure 6.21 to the strain response of unstressed glass fibre. Figure 6.22 presents the resulting curves overlaid on the corresponding experimental measurements originally presented in Figure 6.3.

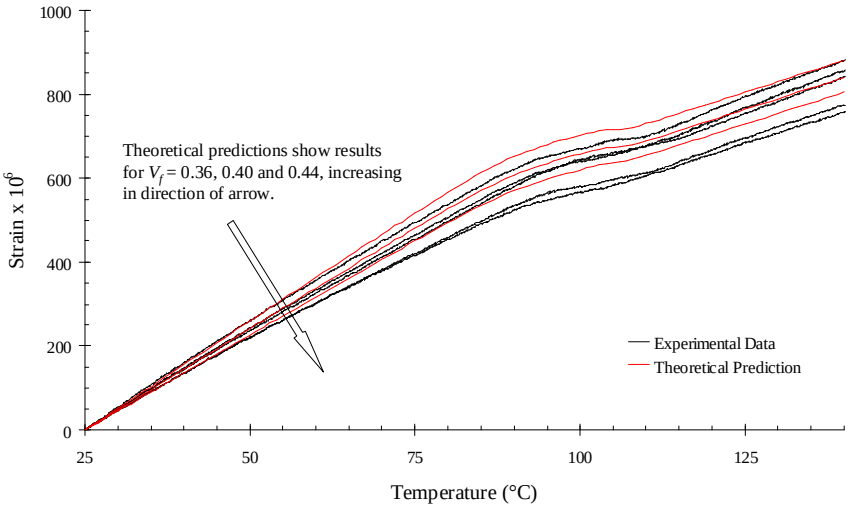


Figure 6.22: Comparison between predicted strain variation and experimental data - Unloaded specimens

The strain response of the preloaded specimens is obtained by adding the effect of the additional fibre preload to the strain response of the unloaded specimens. The preload could not be measured directly on the bare fibres and so attempts were made to infer its value by measuring the compressive strain of the laminate on its release. The measured contraction is not reliable, however, and so it is necessary to

calculate the additional preload strain in the fibres.

The additional fibre preload is calculated so that the predicted residual strain of the unloaded specimens at 25℃ moves to the average measurement of the preloaded specimens at the same temperature. Calculations are based on the nominal fibre volume fraction of 40%. The same preload is used to determine the response for fibre volume fractions of 36% and 44% also. The predicted residual strain in the fibres of the preloaded specimens is presented in Figure 6.23. The predicted results are overlaid on the corresponding experimental data presented in Figure 6.18.

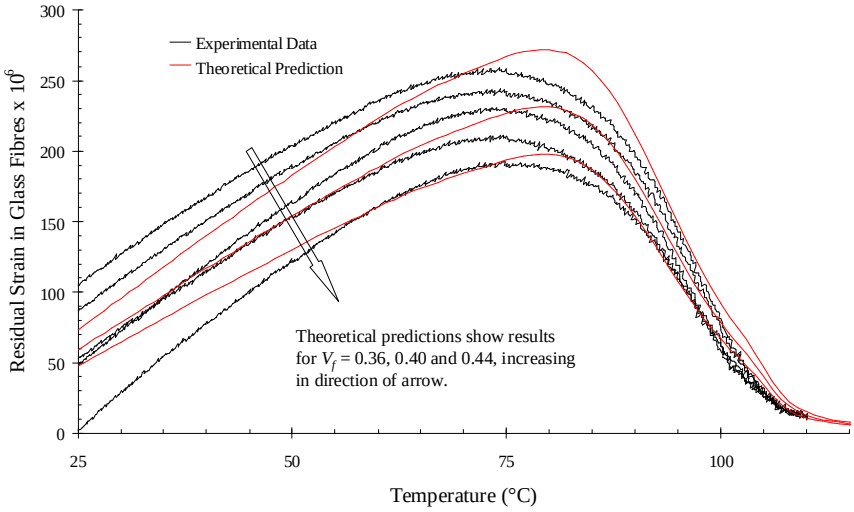


Figure 6.23: Comparison between predicted residual strain variation and experimental data - Preloaded specimens

The corresponding variation in the overall strain of the preloaded specimens is presented in Figure 6.24.

The theory used to predict the variation in the residual fibre strains of the unloaded and preloaded specimens is not applicable to the annealed specimens. The annealed specimens were prepared by heating preloaded specimens to 80℃ and allowing residual stresses to dissipate through non-linear creep for 100 hours. Although the elastic stress state in the preloaded specimens at the start of the annealing process can be estimated, it is not possible to use the same theory to find the stresses in the annealed specimens at its end.

This theory can be used to find the stresses in the annealed specimens at other temperatures, however, if the stress state at the completion of the annealing process is established by some other means. It is found, however, that it is not necessary to know the stress state at the end of the annealing process to determine the strain

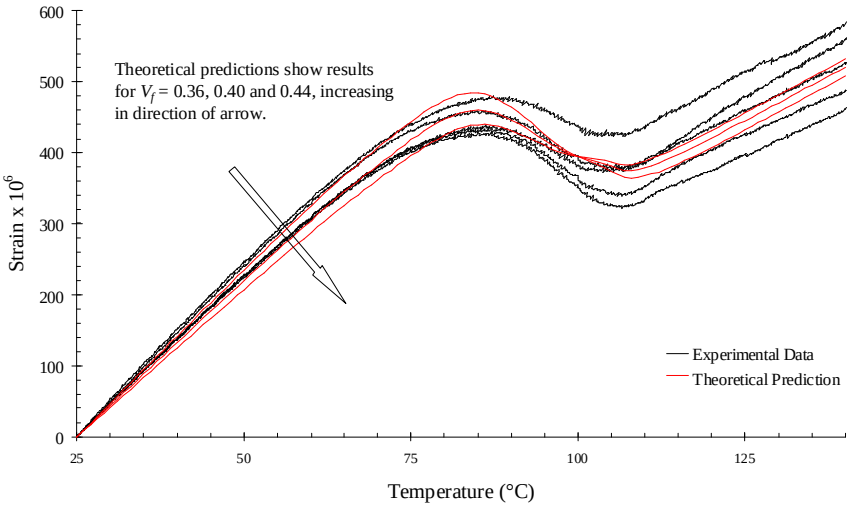


Figure 6.24: Comparison between predicted strain variation and experimental data - Preloaded specimens

response. The strain response is independent of the stress state provided that the predicted strain response curves all pass through a single common point. Matching the strain response to pass through any experimental datum point, therefore, results in the same predicted strain response irrespective of the stress state. It is consequently possible to plot the predicted strain response of the annealed specimens without any knowledge of the internal stresses.

The predicted residual fibre strain in the annealed specimens is selected to pass through the average measured strain at 80°C. The resulting curves are presented in Figure 6.25. The corresponding variation in overall specimen strain is given in Figure 6.26.

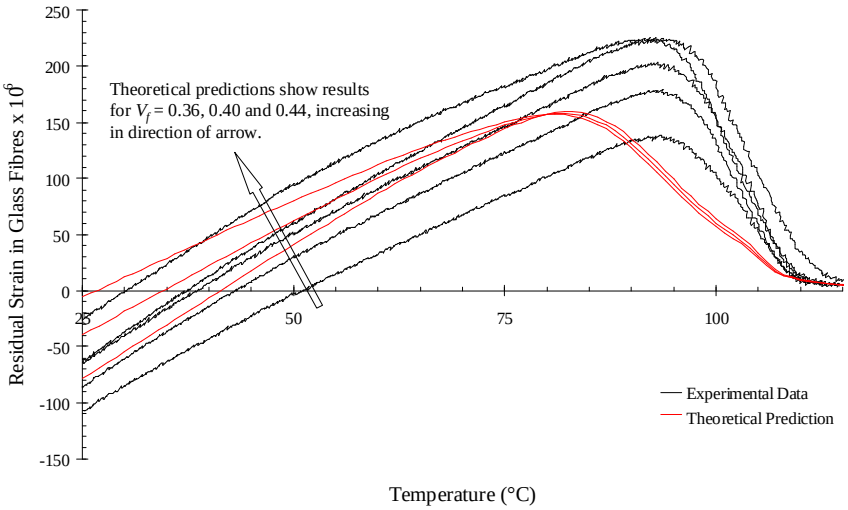


Figure 6.25: Comparison between predicted residual strain variation and experimental data - Annealed specimens

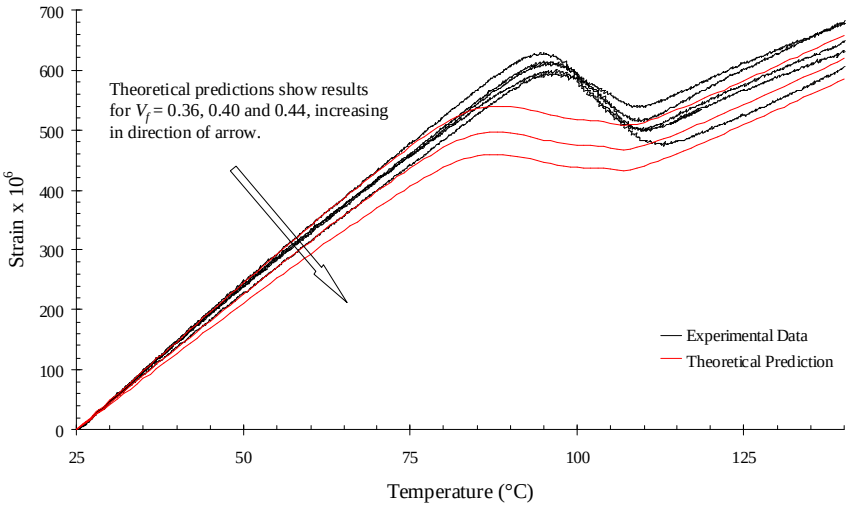


Figure 6.26: Comparison between predicted strain variation and experimental data - Annealed specimens

7 Discussion

Before any worthwhile discussion of the measured residual strains and associated stresses can be made, it is imperative to verify the accuracy of the strains from which these data are extracted. Discussion of the results is consequently broken into three parts. In the first section, the accuracy of the measured strain data is verified. The measured residual strains are then discussed. The section concludes with an assessment of the residual stresses at ambient conditions.

7.1 Accuracy of measured strains

The accuracy of the measured strains is assessed in three parts. The measured strain response of pure resin is first assessed. The general form of the strain response in the reinforced specimens is then checked against expectations. Once it is established that there is no reason to doubt the accuracy of the measured strains, the experimental data are then compared to numerical predictions.

7.1.1 Pure resin

Prior to testing reinforced specimens, tests were conducted on pure resin. The primary purpose of conducting these tests is to verify that the test rig yields valid measurements when testing specimens with an elastic modulus that varies considerably over the range of testing temperatures. If the test rig yields valid results with these specimens, it is probable that it also yields valid results with reinforced specimens since their modulus varies to a smaller extent due to the effect of the glass fibres.

The thermal response of pure Derakane 411-350 resin to being heated for the first and second times is shown in Figure 6.1. Both sets of data are essentially identical

up to a temperature of approximately 100℃. This temperature falls in the range 99℃ to 104℃, listed by the manufacturer[189] as the heat distortion temperature. It is therefore convenient for discussion purposes to choose 100℃ as the boundary above which the loss of resin modulus becomes significant.

Assessment of the measured results at temperatures less than 100℃ is considered first. The manufacturer[189] lists the same value of thermal expansion, 64.8 $\mu\epsilon$/℃, in the ranges from 23.9℃ to 48.9℃ and from 25℃ to 100℃. Linear behaviour up to 100℃ is therefore implied. There is, however, a gradual increase in slope in the measured response in this temperature range. The measured coefficients of thermal expansion in the listed ranges are 63.0 $\mu\epsilon$/℃ and 71.2 $\mu\epsilon$/℃ respectively. The first value is in fairly good agreement with the manufacturer's data while the second is approximately 10% higher.

The measured results in this temperature range can also be compared against data from strain gauges. When the strain gauge results are overlaid on those obtained using the test rig, as presented in Figure 6.2, it is seen that a good correlation exists up to 100℃. It is also apparent that both sets of results obtained using the test rig correlate better with the strain gauge results for the second heating of the specimen than with those for the initial heating. The strain gauge results for the second heating, however, are expected to be more reliable than those for the first heating. This is because favourable residual stresses in the gauges reduce the load transfer to the resin system at temperatures approaching 100℃, as discussed in section 5.2.5.1.2.

The two sets of data obtained from strain gauges diverge at temperatures above 90℃, with the results from the first heating being more linear. It is not known how the coefficient of thermal expansion was measured by the manufacturer. It is possible, however, that strain gauges were used and that only the values obtained during the first heating are presented. This would account for the constant coefficient of thermal expansion over the two temperature ranges listed in the manufacturer's data. The strain gauge results from the first heating of the resin system are, however, expected to be less reliable than those from the second heating. Since the manufacture's data are possibly based on comparatively unreliable data, the 10% discrepancy between the measured coefficient of thermal expansion in the range 25℃ to 100℃ and that listed by the manufacturer is probably not significant. The correlation with the more reliable of the strain gauge results provides good evidence that the test rig is performing appropriately.

If the results obtained using the test rig and the results obtained using strain gauges are considered further, it is apparent that the latter are more linear at temperatures

less than 100℃. This discrepancy can probably be explained by considering that the coefficient of thermal expansion of the resin system is well outside the range considered during the calibration of the test rig. Since the calibration function, given by equation 5.1, for the test rig contains quadratic terms, it is not surprising that some evidence of non-linear behaviour is evident in the measured data. This hypothesis is supported by the linear response observed for the different reference specimens during calibration as presented in Figure 5.33.

Overall, the results measured with the test rig agree well with strain gauge data at temperatures less than 100℃. Agreement with manufacturer's data is not as good, but this information is not truly reliable and so the discrepancy in coefficients of thermal expansion is probably not critical. Some evidence of non-linear response is evident in the measured data, but this is believed to be a result of operating outside the range of coefficients of thermal expansion that the rig was calibrated against.

When temperatures above 100℃ are considered, it is not possible to make use of strain gauge data for comparison purposes due to the loss in resin modulus at higher temperatures, as discussed in section 5.2.5.1.2. Manufacturer's data are also not available. Assessment of the results must therefore be done on a qualitative basis. Internal inconsistencies in the data require that the results be rejected as invalid. The results at temperatures greater than 100℃ are now considered with this in mind.

The response to the initial heating of the specimen, as shown in Figure 6.1 is considered first. A contraction of roughly 1400 $\mu\epsilon$ is evident between temperatures of approximately 100℃ and 110℃. This effect is expected as a result of polymerization shrinkage at temperatures above the post-cure temperature. The measured shrinkage is consistent with the similar value of 1250 $\mu\epsilon$ observed in section 5.3.6.1 during the testing of the initial rig. In addition, although it is not possible to confirm the accuracy of the measured shrinkage, the fact that it is smaller than the upper bound of approximately 3300 $\mu\epsilon$ determined using strain gauges[i] conforms with expectations.

At temperatures greater than 110℃, shrinkage is no longer evident and expansion with temperature is once again observed. This behaviour is expected because polymerization ceases once all available reaction sites are used up. Shrinkage associated with polymerization therefore no longer occurs and the effects of thermal expansion

[i] As discussed in section 5.2.5.1.2, the shrinkage value measured using strain gauges comprises apparent strains arising from both resin shrinkage and the release of tensile residual stresses in the strain gauges. Since the apparent strains resulting from the release of stresses in the gauge are non-negligible, the measured strain cannot be taken as an accurate representation of the cure shrinkage and merely defines an upper limit to this value.

once again become visible. The measured coefficient of thermal expansion in the linear region at temperatures greater than 115℃ is 173.1 $\mu\epsilon$/℃, a value significantly greater than those measured at lower temperatures. The large increase in the coefficient of thermal expansion at elevated temperatures is consistent with the behaviour typical of polymer materials.[179]

If the response to the second heating of the specimen, as presented in Figure 6.1 is now considered, it is apparent that the rate of thermal expansion increases smoothly with temperature. The coefficient of thermal expansion at temperatures far above T_g is expected[179] to be considerably larger than that far below T_g. The increasing slope of the measured data is thus consistent with the behaviour typical of a polymer material.

No abrupt change in behaviour occurs as the temperature increases beyond 100℃ during the second heating of the specimen. Such behaviour would be indicative of a measurement error. The lack of such a change in behaviour is encouraging, and indicates that the shrinkage between 100℃ and 110℃ observed during the initial heating of the specimen reflects polymerization shrinkage rather than an artefact of the testing process. It consequently appears that the loss in resin modulus at temperatures above 100℃ does not affect the measured results.

At temperatures less than 100℃, the test rig yields results that are in good agreement with reliable strain gauge results. At temperatures greater than 100℃, the behaviour of the measured results is consistent with that typical of a polymer material. In addition, it would appear that the test rig is unaffected by the loss in resin modulus at high temperatures. Although this type of assessment is unable to prove that the test rig is yielding valid results at temperatures greater than 100℃, no data suggest otherwise.

7.1.2 Reinforced specimens

The tests conducted on pure resin indicate that the test rig yields valid results across the entire range of testing temperatures from ambient conditions up to 140℃. It is, however, necessary to verify that this is also true when tests are conducted on glass fibre reinforced specimens. This discussion is focused on checking the general form of the measured strain response of these specimens against expectations. A comparison against numerical predictions is performed in the next section.

The manner in which the reinforced specimens are expected to respond to increasing

temperature is described in Chapter 4. At ambient conditions the modulus and coefficient of thermal expansion of the polymer matrix are relatively constant. The thermal strain is consequently expected to be linear with temperature. At higher temperatures, the matrix modulus and coefficient of thermal expansion start to change. Polymerization shrinkage can also potentially occur. These effects all result in non-linear thermal expansion. When the temperature is high enough however, the modulus of the matrix drops sufficiently low that it is unable to exert much influence on the expansion of the glass fibre reinforcement. Under these conditions the specimen strains at the same rate as pure E-glass fibre and a second region of linear thermal expansion becomes evident.

The thermal response of the unloaded specimens is shown in Figure 6.3. Two distinct regions of linear behaviour are apparent in a strain response that generally increases with temperature. The first region exists at temperatures less than approximately 90℃ while the second occurs at temperatures greater than about 115℃. Between these two regions, a non-linear response evolves smoothly from one region of linearity to the next.

Figure 6.4 presents the response of the preloaded specimens. A region of linearity exists at low temperatures, but the limits of this region are not well defined because the response becomes increasingly non-linear as the temperature is raised. The non-linearity eventually becomes so pronounced that the initially positive slope becomes negative. Above a temperature of about 100℃ the non-linear behaviour dissipates. At 105℃ the measured slope is once again positive and at about 110℃ the response is clearly linear.

The response of the annealed specimens is illustrated in Figure 6.5. Two distinct regions of linear behaviour are evident. One region occurs at temperatures less than approximately 90℃. The second appears at temperatures greater than about 115℃. Between these two regions a highly non-linear response is evident which develops fairly rapidly into a range with negative slope.

The measured strains of each specimen type are overlaid in Figure 6.6 to enable comparison. It is seen that the thermal responses at ambient conditions are similar. The response of all specimens is linear at temperatures less than 50℃, with the lowest coefficient of determination, R^2, being 0.9996. The measured slopes, which correspond to the coefficients of thermal expansion, are presented in Table 6.1 and vary between 8.8 $\mu\epsilon$/℃ and 10.5 $\mu\epsilon$/℃. The measured coefficients of thermal expansion fall within the range of those considered during calibration and are thus believed to be accurate. As a check, however, they were compared against strain

gauge measurements[ii] on seven additional specimens. The coefficients of thermal expansion obtained from strain gauge measurements fall in the range 9.3 $\mu\epsilon$/℃ to 10.3 $\mu\epsilon$/℃ and are thus in agreement with the data from the test rig. The accuracy of the rig at temperatures less than 50℃ is therefore confirmed.

The standard deviation in the measured coefficients of thermal expansion, presented in Table 6.1, is greater for the unloaded specimens than for those of the preloaded and annealed specimen types. This discrepancy probably arises from differences in the manufacturing process of the three specimen types. Both the preloaded and annealed specimen types were cured with significant fibre tension. The fibres of the unloaded specimens were not tensioned to nearly the same extent. A small tensile load was applied to prevent large-scale fibre movement during resin infusion but some movement presumably still occurred. Increased variation in the fibre volume fraction of the unloaded specimens thereby resulted, with a consequential increase in the variation in the measured coefficients of thermal expansion.

The thermal response of the different specimens in Figure 6.6 is similar at temperatures greater than 115℃. All specimens exhibit a linear thermal response with the lowest coefficient of determination, R^2, being 0.9942. The measured coefficients of thermal expansion, presented in Table 6.2 vary between 4.2 $\mu\epsilon$/℃ and 6.2 $\mu\epsilon$/℃. They thus span the range 4.7 $\mu\epsilon$/℃ to 5.4 $\mu\epsilon$/℃, presented in the literature[185, 190, 191] as the coefficient of thermal expansion of E-glass, and confirm the underlying basis of the technique.

It is not easy to assess the strain response between the regions of linear behaviour without making use of detailed calculations. The strain response in this region can, however, be examined by considering the relaxation behaviour of the specimens. Relaxation of residual strains occurs when the matrix modulus reduces sufficiently that internal stresses can no longer be supported. Since the modulus of the resin system used as the matrix in this work both departs the region of high modulus asymptotically and approaches the region of low modulus asymptotically, as is visible in Figure 4.1, the measured non-linear strain response should connect asymptotically to the two regions of linear response. Additionally, since the matrix modulus decreases continually in this region, an equation describing this behaviour possesses only a single point of inflection. The strain measurements in the non-linear region should, therefore, mimic this behaviour and connect to the linear regions monotonically. Examination of the non-linear data presented in Figures 6.3 through 6.5 reveals that these requirements are indeed satisfied.

[ii] These complementary tests were performed using the method and equipment presented in section 5.2.

At this stage it therefore appears that the measured strain response of the specimens agrees with the behaviour predicted in Chapter 4. All specimens exhibit two regions of linear behaviour, one at temperatures less than 50℃, the other at temperatures higher than about 115℃. These two regions are connected by a region of non-linearity, as expected. The slopes of the linear data at temperatures less than 50℃ are in good agreement with results obtained using strain gauges. The slopes of the linear data at temperatures greater than 115℃ correlate well with the thermal expansion coefficient of E-glass. The behaviour of the strain response in the non-linear region conforms to expectations. The test-rig therefore appears to be yielding results which are worth comparing to theoretical predictions.

7.1.3 Comparison with theory

Theoretical predictions of the strain behaviour of the different specimen types are obtained by modifying the method of Nairn.[167] This theory assumes an elastic stress state and is not truly applicable to the situation under discussion since the polymer matrix of the specimens behaves viscoelastically. If the viscous stresses are assumed to be negligible however, then an elastic solution can be applied. At temperatures much above T_g, conformational strains rates are high,[181] viscous stresses consequently dissipate rapidly and the assumption of pure elasticity is good. At temperatures well below T_g, conformational strains are "frozen in" and the assumption of pure elasticity is again reasonable.[181] The rate of temperature change in this work is selected to be slow, however, so that viscous stresses have time to dissipate, leaving only elastic stress. Depending on the extent to which the viscous stresses relax, the analysis technique used in this work can also provide reasonable predictions in this temperature region.

Prior to assessing the measured results of individual specimen types, it is worth considering the data as a whole. It is apparent that a fair degree of experimental scatter is present. It is evident from Figure 4.2 that theory predicts the slope of the measured strain at ambient conditions to increase with increasing strain-free temperature. The unloaded specimens are therefore predicted to have the highest slope and the preloaded specimens the lowest. Scatter within the measured results prevents this effect from being observed, however. Differences in slope within a single specimen set are larger than those between sets and the average measured slopes of the different specimen types appear very similar.

The predicted strain response of the unloaded specimens is compared to experimental data in Figure 6.22. If an allowance is made for the experimental scatter, very

good agreement between the experimental data and the theoretical predictions is evident. It must be remembered, however, that an *a priori* prediction of the strain response is impossible due to a lack of material data required to predict the cure shrinkage. As a result, a single strain measurement is incorporated into the predicted response to compensate for this lack of information. The inclusion of this measurement has the effect of calibrating the predicted response to match the measured data. The change in predicted strain between 92℃ and the start of the upper region of linearity is, in effect, matched to the average measured results. Close correlation here is thus meaningless, but correlation in the two sets of results is nonetheless excellent over the remaining temperature range.

The predicted response of the preloaded specimens is overlaid on experimental measurements in Figure 6.24. Once again, very good correlation is evident between experimental and predicted strains after an allowance for scatter is made. Caution in interpreting these results, is again required however. The predicted strain response of the preloaded specimens is obtained by adding the response of the additional fibre preload to the predicted strain response of the unloaded specimens. The preload strain could not be successfully measured, and so the magnitude of the residual strain used in the prediction is selected to match experimental data at 25℃. This has the effect of forcing the predicted strain at the onset of the upper region of linearity to match the average experimental measurements. Although good correlation here is insignificant, the theoretical predictions and experimental measurements are clearly in excellent agreement over the remaining data.

Contrary to the unloaded and preloaded specimens, the strain response of the annealed specimens cannot be assembled by considering the individual effects of thermal loading, cure shrinkage and fibre preload. These specimens were manufactured by heating the preloaded specimens to 80℃ for 100 hours and allowing residual stresses to relax through non-linear creep. This process cannot be modelled using the purely elastic analysis technique used in this work. The stress state at the end of the annealing process cannot, consequently, be determined. If the response is forced to match an experimental measurement after annealing is completed, however, the theory allows the response at other temperatures to be predicted. Although this approach can be used to find the strain response, it must be remembered that the material data used for the other specimen types do not necessarily apply in this case. Inelastic strains in the matrix might affect the variation in its elastic modulus with temperature.

The predicted strain response of the annealed specimens is presented with experimental data in Figure 6.26. The predicted strain response is forced to pass through

the average measured strain at 80℃ and so correlation between the two sets of data at this temperature is required. It is apparent that the measured strain response is significantly different to that predicted between approximately 80℃ and 110℃. This issue could be construed as symptomatic of a problem with the measured results. Considering there is no indication that the test rig provides erroneous results and that the correlation between the theoretical and measured strain responses of the other specimen types is excellent, however, this is unlikely. The test procedure used for these specimens is identical to that used for the other specimen types and so the accuracy of the measured results should be similar. Since non-linear creep relaxation of the matrix stresses occurred in these specimens, it is far more likely that the discrepancies in strains arise from limitations in the predicted results than from problems with the measured results. This issue is discussed in more detail in section 7.2.3.

Earlier in this discussion the general form of the measured results is considered in sections 7.1.1 and 7.1.2. All measured results conform to expected behaviour and consequently it appears that there is no reason to doubt their accuracy.

This assessment still remains true after the measured results are evaluated against theoretical predictions. For the unloaded and preloaded specimens, where the theory and material data are believed valid, excellent agreement is found. Although the agreement is to some extent artificial, due to the incorporation of experimental data into the predictions, it is nonetheless very good in regions where it is not forced to be so. The correlation between theory and experiment is not very satisfactory for the annealed specimens, but in this case the discrepancies can probably be explained by limitations in the predicted results. It is consequently believed that the measured results are accurate and so further analysis of the data is justified.

7.2 Residual strains

Discussion of the residual strain variation with temperature is broken down into three parts. Residual strain measurements obtained without any knowledge of the matrix properties are considered first. The measurements obtained by including the effects of matrix stiffness at high temperatures are then discussed before a comparison of these results with theoretical predictions is presented.

7.2.1 Residual strains obtained without any knowledge of the matrix properties

It is possible to obtain residual strain measurements without any knowledge of either the matrix properties or the fibre properties. Such measurements are presented in Figures 6.8 through 6.10. The variation in the residual strain of each specimen type with temperature is considered in turn.

The residual strains in the glass fibre of the unloaded specimens are presented in Figure 6.8. Under ambient conditions the residual strain is negative. As the temperature increases, the residual strain becomes less negative. This behaviour is expected because the coefficient of thermal expansion of the resin system is greater than that of the glass fibres. As a consequence, an increase in temperature causes the resin to expand at a greater rate than the glass fibre, placing an additional tensile load onto the fibres, thereby reducing their compressive strain. The variation in residual strain is fairly linear up to a temperature of approximately of 90℃ where a state of low tensile residual strain exists.

At temperatures greater than about 90℃, relaxation of the residual strains in the glass fibre starts to occur. The residual strains reduce to negligible values at temperatures greater than about 108℃ to 115℃, depending on the specimen. This behaviour is expected as the modulus of the resin diminishes and equilibrium of the internal stresses allows relaxation of the residual strains.

The residual strains in the glass fibre of the preloaded specimens are shown in Figure 6.9. The residual strains at room temperature conditions are low. As expected, a temperature increase results in the residual strain becoming increasingly tensile. Initially the response is fairly linear but above a temperature of about 60℃ the behaviour of the specimens becomes increasingly non-linear. The residual strain reaches a peak at temperatures around 75℃ and thereupon begins to reduce rapidly until negligible strains are indicated at temperatures greater than about 108℃.

The residual strains in the glass fibre of the annealed specimens are illustrated in Figure 6.10. Under ambient conditions, the strains are slightly negative. The strain increases fairly linearly with temperature until the maximum tensile strain is reached at about 92℃, whereupon relaxation of the residual strain begins. The residual strain then decreases rapidly and negligible strains are measured at around 110℃.

Since Figures 6.8 through 6.10 can be obtained without any knowledge of fibre or matrix properties, they are useful in a qualitative assessment of the measured relaxation of the residual strain. It is clear that the measured data asymptote monotonically towards zero. Rapid changes in the apparent residual strain immediately prior to full relaxation, of the type presented in Figures 5.20 through 5.22, are not evident. This agreement with theoretical predictions provides further evidence of the validity of the measured strain results[iii].

For comparison purposes, the data sets of all three specimen types are presented in Figure 6.11. It is apparent that the residual fibre strains at ambient conditions are, on average, compressive in the unloaded specimens and tensile in the preloaded specimens. The residual strains in the annealed specimens fall almost midway between those of the other specimen sets. Compressive strain at room temperature is expected in the fibres of the unloaded specimens because they were only lightly tensioned at the post-cure temperature of 92℃. At lower temperatures, therefore, the resin increasingly loads the fibres into compression due to its comparatively high coefficient of thermal expansion. The fibres of the preloaded specimens, however, were heavily tensioned prior to curing and consequently the measured strain in these specimens is more tensile than those of the unloaded specimens. The increment in tensile strain in the annealed specimens is smaller than that of the preloaded specimens because some of the preload strain was relieved during the annealing process. The measured residual strains of the annealed specimen set consequently fall between those of the other two sets.

It is also apparent from Figure 6.11 that the rate at which the residual strain varies with temperature at ambient conditions is significantly different from specimen to specimen. It is known, however, that the slopes of the specimens in this figure should all be similar, because the thermal response of the specimens, as shown in Figure 6.6, is similar in this temperature range. The discrepancy can be traced to variations in the linear behaviour of individual specimens at temperatures greater than 115℃.

The linear region at temperatures greater than 115℃ is used to determine the locus of zero stress in the glass fibre of the specimens. The residual strains plotted in Figure 6.11 are found by taking the difference between the thermal response of each specimen and the locus of zero stress in its glass fibres, as illustrated in Figure 6.7. An error in the measurement of the slope at temperatures above 115℃ will therefore be propagated as an error in the slope of the residual strain plotted against

[iii] The new method of supporting the target plate therefore appears to have resolved the problems encountered with the initial test rig.

temperature.

Accurate measurement of the residual strains is therefore entirely dependent on precise measurement of the strain response at temperatures above 115℃. This is exactly where the modulus of the resin is low and consequently measurements are most difficult to accomplish. It has been established that the range of slopes measured in this temperature range are in fair agreement with published values[185,190,191] of the coefficient of thermal expansion of E-glass, as theory requires. The underlying basis for the technique is thus valid, but it is almost certain that some degree of error exists in the absolute value measured for each individual specimen. It is not appropriate, therefore, to rely too heavily on the measured slope of an individual specimen to determine its residual strain. Rather, the same slope should be used for all specimens since the coefficient of thermal expansion of glass fibre is invariant from specimen to specimen. By adopting this approach, differences in the slope of the residual strain variation with temperature correspond then with differences in the coefficients of thermal expansion in Figure 6.6, as demanded by theory. It is proposed that a modified technique, using a value of 5.0 $\mu\epsilon$/℃, corresponding to a value[185] in the midrange of published data[185,190,191] for the coefficient of thermal expansion of E-glass, be used as the slope of the locus of zero fibre stress.

The modified technique defines the slope of the locus of zero fibre stress, but its position is still undefined. In order to satisfy the requirements of the underlying technique, it is necessary that the residual strain in the glass fibres asymptotes towards negligible values as the residual strain relaxes. This requirement provides the necessary means of fixing the locus of zero stress, and it is fitted tangent to the measured data near the onset of the linear region which exists above 115℃.

It is easy to position the locus so that it is tangent to the measured data where the slope of the linear region above 115℃ is greater than that of the locus of zero fibre stress. In principle, though, it is impossible to position the locus for data sets where the linear region at temperatures above 115℃ has a slope less than that of the locus of zero fibre stress. In turns out, however, that if the locus of zero fibre stress is taken to have a value of 5.0 $\mu\epsilon$/℃ it is possible to position the locus of zero fibre stress quite acceptably. In these instances, the data immediately prior to the linear region curve to a slope slightly greater than 5.0 $\mu\epsilon$/℃ before settling back to a lower value. It is therefore possible to determine a point of tangency within these data. This point then defines the position of the locus of zero fibre stress. This situation is illustrated in Figure 6.12 using data from a preloaded specimen. For analysis purposes, all data at temperatures higher than that at the point of tangency are assumed to lie on the locus of zero stress and can consequently be discarded.

Since only data at temperatures lower than that at the point of tangency are utilized using the modified technique, it is worth discussing whether the use of a dilatometer type test rig is still necessary with this approach. It is clear that it is necessary to reliably identify the point of tangency, but it is not necessary to reliably measure strains at higher temperatures. The point of tangency however defines, in the modified technique, the temperature at which the strains are fully relaxed. Any technique that relies on load transfer cannot be used to reliably determine this point because these loads dissipate as the matrix modulus reduces. The accuracy of the measured results consequently drops progressively as the temperature at the point of tangency is approached. Techniques such as the use of strain gauges cannot be used therefore, and dilatometer type instrumentation is still necessary.

Residual strain results, obtained through the use of the modified technique, are presented in Figures 6.13 through 6.15. When these figures are compared against Figures 6.8 through 6.10 respectively, it is seen that the modified approach does not change the fundamental appearance of the data in any significant way. Descriptions of the residual strain behaviour exhibited by each specimen type in Figures 6.8 through 6.10 apply equally well to the behaviour exhibited when these results are determined using the modified technique. Improvements in the internal consistency of the results are, however, visible.

When considered at large scales, it is apparent that the unmodified residual strain results, presented in Figures 6.8 through 6.10, asymptote towards a negligible residual strain as the internal stresses relax. This behaviour is in accordance with theory. When these results are considered at finer scales, however, it is apparent that the measured results of some specimens overshoot the horizontal axis by a small amount[iv], thereby introducing offset errors. These errors are not significant, but removal of the offset enables the measured results to better satisfy the demands of theory. The modified technique eliminates the overshoot and hence improves the consistency of the measured residual strain results.

Another improvement in the measured results is evident when the results obtained through the use of the modified technique are overlaid on each other, as plotted in Figure 6.16. The slopes of the data in this figure are far more uniform at temperatures less than 50°C than those presented in Figure 6.11. The differences in slope correspond now with differences in the slope of the data presented in Figure 6.6. This effect is demanded by the theory and thus provides a considerable improvement in the consistency of the measured results. Discussion of differences in the overall behaviour of the three specimen sets is therefore enabled.

[iv] The overshoot is in one case 13 $\mu\epsilon$ and in all other cases considerably less than 10 $\mu\epsilon$.

If the unloaded and annealed specimens sets are considered first, it is apparent that the general form of the results presented in Figure 6.16 conforms entirely with that predicted in Chapter 4. The response of both specimen sets is very similar at temperatures less than 90℃, except that the annealed specimens are shifted vertically by approximately 140 $\mu\epsilon$. The residual strain measured in the glass fibres of both specimen types increases with temperature in this range. Since the thermoset matrix has a higher coefficient of thermal expansion than the glass fibres it applies a tensile load to the glass fibres that increases with increasing temperature. At a temperature of approximately 90℃, the response of both sets of specimens starts to exhibit increasingly non-linear behaviour. As the temperature is increased further, the residual strain starts to reduce, decaying to zero at temperatures around 110℃ to 115℃. The rate of relaxation in the annealed specimens is necessarily higher than that of the unloaded specimens because the residual strain is higher for these specimens at the start of the relaxation process.

It is also apparent from Figure 6.16 that the response of the preloaded specimens is far less linear than that of the other specimen sets. Increasingly non-linear behaviour is evident at around 60℃. The maximum strain is reached at approximately 75℃, whereupon the strain begins relaxing, diminishing to zero at approximately 110℃. As the strain in these specimens relaxes, the measured response cuts across the still increasing strain of the annealed specimens. This type of intersection cannot be readily explained if the strain response of both specimen sets is the linear combination of strain responses arising from thermal effects, cure shrinkage and preload. This issue requires more detailed examination, which is left until section 7.2.3 where predicted results provide the necessary illumination.

The results presented in Figures 6.13 through 6.15 are as accurate as is possible to obtain without any knowledge of the matrix properties. It is possible, however, to improve on the accuracy of these results if the variation in matrix properties is known with temperature. Under these circumstances it is possible to account for the non-zero matrix modulus at the relaxation temperature. The results obtained through the use of this technique are discussed in the next section.

7.2.2 Residual strains obtained with knowledge of the matrix properties

The accuracy of the measured strains can be improved through the use of equation 4.4. This equation enables the measured strain to be offset by a small amount

to compensate for the non-zero matrix modulus at high temperatures. Its use, however, requires knowledge of the variation in matrix modulus, coefficient of thermal expansion and cure shrinkage with temperature. Since this information is available for the resin system used in this investigation, the strain offset for each specimen can be calculated. The data presented in Figures 6.13 through 6.15 are updated and plotted in Figures 6.17 through 6.19.

It is apparent that the changes to the residual strain results are not large. Table 6.4 reveals that the average offsets for the unloaded, annealed and preloaded specimens are only 1.3 $\mu\epsilon$, 4.6 $\mu\epsilon$ and 11.3 $\mu\epsilon$ respectively. Offsets of this magnitude do not change the form of the residual strain results, and descriptions of the residual strain behaviour presented in Figures 6.13 through 6.15 apply also to the updated data presented in Figures 6.17 through 6.19.

The calculated strain offset is smallest for the unloaded specimens and largest for the preloaded specimens. This is because the strain offset is proportional to the difference in the free expansions of the matrix and fibre at the relaxation temperature. Since the unloaded specimens have the highest strain-free temperature, the difference between this temperature and the relaxation temperature is smallest in these specimens. The mismatch in matrix and fibre strains is consequently the lowest and so they have the least offset strain. The strain-free temperature of the preloaded specimens is the lowest and so they have the greatest offset strain. Additionally, the relaxation temperature of the preloaded specimens is marginally lower than that of the other specimens. The resin modulus is consequently slightly higher at relaxation and this further increases the offset strain of the preloaded specimens.

The residual strain results presented in Figures 6.17 through 6.19 incorporate the effects on non-zero matrix modulus at high temperatures. The same matrix properties used to determine the offset strain are used as input parameters to determine the theoretically predicted response. The theoretical predictions are consequently compared against this set of measured data in the following section.

7.2.3 Comparison with theory

Theoretical predictions of the residual strain response of the different specimen types are presented in Figures 6.21, 6.23 and 6.25. For comparison purposes, these figures also include the corresponding strain measurements presented in Figures 6.17 through 6.19.

It is apparent that some scatter exists in all the experimental results. Some of the scatter can be accounted for by variations in fibre volume fraction. Although the average fibre volume fraction of the unloaded specimens is almost exactly 40%, the volume fraction in these specimens varies between approximately 36% and 44%. The difference between the maximum and minimum measured slopes of these specimens visually corresponds well with the difference in slopes predicted for this range of fibre volume fraction. This implies that most of the scatter in the measured data of these specimens can be accounted for by variations in fibre volume fraction.

The variation in the fibre volume fraction of the preloaded and annealed specimens is less than that of the unloaded specimens. The variation in the measured slopes of these specimens is consequently also smaller. Scatter in the preloaded and annealed specimens most significantly takes the form of differences in offset from the horizontal axis prior to relaxation. The source of this scatter is presumably variations in the tension applied to the glass roving when it was wound onto the preloading frame.

Figure 6.21 shows a comparison between the predicted and measured residual strain responses of the unloaded specimens. Allowing for the scatter in the measured data, it is apparent that the general form of the predicted response closely matches that of the experimental measurements. Caution is necessary when interpreting this correlation however. The predicted strain is forced to match the average measured strain at 92℃ to compensate for a lack of data regarding the cure shrinkage of the matrix. Correlation at this temperature is thus meaningless. No other control was applied to the predicted response, however, and still the correlation in the general shape of the two sets of data is very good, implying that the measured results have validity. The strain at room temperature is negative in both cases, increasing approximately linearly to zero at a temperature of around 83℃. The data overshoot the horizontal axis by a small amount, reaching its maximum value at around 95℃, before decaying to small values around 110℃. The most striking difference in the two sets of data is that the predicted strain is lower than the experimental strain at ambient conditions. This arises because the measured slope between 25℃ and 80℃ slowly decreases with increasing temperature whereas the predicted slope is nearly constant. Although the average measured slope is very similar to the predicted value at ambient conditions, the reduced slope at higher temperatures results in the experimental strain at 25℃ being nearly 15% higher than predicted. A possible reason for the reduction in measured slope with increasing temperature is discussed in greater depth later in this section.

The general form of both the predicted and the measured residual strain responses of the preloaded specimens, shown in Figure 6.23, is clearly different from that of the

unloaded specimens. Both theory and measured data are in agreement regarding the overall shape of the response which is far less linear than the unloaded specimens. Although the predicted strain is matched to the average measurement at room temperature, the general behaviour of this data is not manipulated any further. The correlation at other temperatures is, however, still reasonable and supports the validity of the experimental measurements. The strain becomes increasingly tensile as the temperature is raised above ambient conditions. A maximum value of between 190 $\mu\epsilon$ and 270 $\mu\epsilon$ is reached between temperatures of 73°C and 80°C, depending on the specimen and volume fraction, before the strain relaxes rapidly to low strains at around 110°C. The most obvious differences between the two sets of data are that the average measured slope is approximately 12% higher than the predicted slope at ambient conditions, and that the temperature at which the maximum strain is reached is approximately 7°C lower for the measured data than for the predicted data. These two factors oppose each other and so the maximum strains in both cases are similar.

One possible reason for the experimental measurements reaching a maximum value at lower temperatures than predicted is viscous relaxation of the matrix to an elastic state. The predicted results are based on the assumption that viscous stresses have dissipated and so relaxation is complete. The heating rate used in these tests is kept low to allow time for viscous flow, but some viscous stresses are present at lower temperatures where conformational motions are not very rapid. When these stresses begin to relax, the residual fibre strain no longer increases at the same rate. This effect reduces the slope of the measured strain response and so the maximum measured strain occurs at a lower temperature than is predicted.

Unfortunately, non-linear creep is an alternative explanation for the difference in temperatures at which the maximum residual strain is reached. The annealed specimens were manufactured by heating the preloaded specimens to 80°C for 100 hours and allowing residual stresses to dissipate. It appears that relaxation of the stresses took place through non-linear creep since Figure 6.20 indicates that the average measured residual strain in the annealed specimens is approximately 59 $\mu\epsilon$ lower than that in the preloaded specimens at 80°C. This difference cannot be explained using linear viscoelasticity and is discussed in greater depth in Appendix G.5. It is not unreasonable to expect then that some degree of non-linear creep occurred when the preloaded specimens were heated to near 80°C in these tests. If this is the case, then it can be expected that further non-linear creep occurred at higher temperatures still. The effects of these strains are similar to the effects of linear viscoelastic

relaxation. A reduction in the temperature at which the maximum strain is measured is therefore expected. Non-linear creep, however, also affects the calculation of the strain offset given by equation 4.4. This equation assumes linear viscoelastic conditions and does not consider non-linear creep. The strain offset of 11.3 $\mu\epsilon$ used to obtain Figure 6.19 is consequently artificially high by an unknown amount. Use of this figure to represent the residual strain measurements in the preloaded specimens is thus probably inappropriate. It might be better to use Figure 6.14 and acknowledge that errors are present which arise from not calculating the offset.

A comparison between the predicted and measured residual strain response of the annealed specimens is presented in Figure 6.25. As is expected, based on earlier discussion of Figure 6.24, the correlation between experiment and theory is poor. The residual strain is predicted to decrease rapidly above 80℃ whereas the measured strains continue to increase beyond 90℃ at more or less the same slope as below 80℃. The poor correlation evident in this figure serves, however, to illustrate how comparatively good the correlation between theory and experiment is for both the unloaded and preloaded specimens.

In section 7.2.1 it is mentioned that the intersection between the measured strain responses of the preloaded and annealed specimens in Figure 6.19 is difficult to explain if the responses arise from the linear combination of thermal loads, cure shrinkage and fibre preload. At first glance it appears that the measured response of the preloaded specimens is in error since it has a form so different to that of the other specimen types. Once the measured data are compared to experimental data, however, it is clear that the measured results of the unloaded and preloaded specimens conform with expectations and that it is the measured response of the annealed specimens that needs explanation.

Since the annealed specimens were tested in an identical manner to the other specimens there is no fundamental reason why the measured results should be incorrect. It consequently reasonable to suspect that the changed form of the residual strain measurements of the annealed specimens is related to the difference in their method of manufacture. Two possibilities seem apparent; non-linear creep alters the relationship between the different stress components in the laminate and so changes the form of the residual strain curves, or the material properties of the matrix are modified by prolonged exposure to high temperatures and/or non-linear creep. These possibilities are now examined.

It appears unlikely that an altered stress state can affect the form of the residual strain plot to the extent evident in Figure 6.23. As is demonstrated in Appendix G.5.1, the predicted strain response of the annealed specimens is independent of stress state once a single point is defined on the curve. Since the predicted response of Figure 6.23 is defined by matching it to the average measured residual strain at 80℃, it does not change irrespective of the internal stress state in the annealed specimens.

The most likely explanation for the different strain response of the annealed specimens is a change in material properties. One way in which the measured response can be explained is through a change in matrix modulus. Increased cure of the matrix can cause the glassy plateau with high modulus, evident in Figure 4.1, to extend to higher temperatures.[197–199] The region of nearly linear strain response consequently also increases. Since the matrix was post-cured at 92℃, heating it to 80℃, even for an extended period, is not likely to result in significantly increased cross-linking, however. In addition, if further cross-linking did occur, the curve describing the region of rapid modulus reduction in Figure 4.1 is expected to shift to the right.[197–200] The relaxation temperature is consequently expected to rise with increased cure. Although the relaxation temperature of one specimen does seem to have shifted by about 6℃, it is clear from Figure 6.20 that the relaxation temperature of most of the annealed specimens is comparable to that of the other specimen types. The possibility of the matrix properties changing significantly as a result of increased cure can consequently be dismissed.

It seems then that the matrix properties change as a consequence of non-linear creep. This effect can perhaps be explained by considering the effect of conformational strains during this process.

Linear viscoelasticity predicts that a cross-linked polymer can relax only until conformational strains, which arise from molecular uncoiling, are exhausted,[182] and so it is expected that the matrix relaxes to the elastic state. During the annealing process, the longitudinal stress relaxed beyond the elastic state as a consequence of non-linear creep of the matrix. This additional relaxation presumably involved the breaking of some of the cross-links in the polymer to allow the translation of molecules, thereby freeing up further conformational strains in the matrix which were locked in place by the plastic flow.

When the annealed specimens were subsequently heated during these tests to temperatures greater than that of the annealing process, the conformational strains that would ordinarily have developed had already taken place. The compliance of

the matrix could not increase as a result of molecular uncoiling and so the storage modulus of the material remained on the glassy plateau. This state of affairs could not persist indefinitely, however, and eventually the thermal energy of the matrix was sufficient that additional conformational strains became possible and the modulus dropped rapidly. Since no further cross-linking occurred during the annealing process however, the relaxation temperature remained unchanged.

The changed form in the variation in storage modulus that could have resulted from such a hypothesis is illustrated in Figure 7.1. It is exactly this type of variation that is required to explain the changed form of the residual strain response of the annealed specimens.

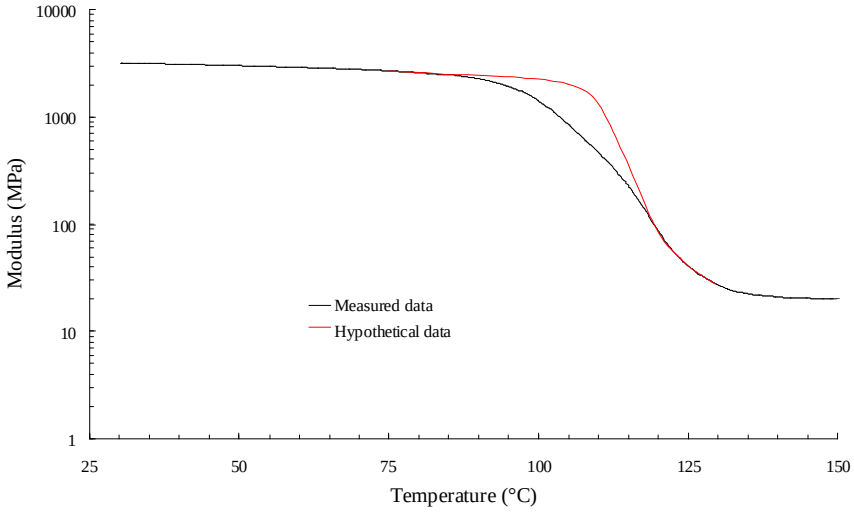


Figure 7.1: Hypothetical changes to matrix modulus

The measured residual strain response of the annealed specimens can therefore probably be explained by changes in the matrix modulus brought about by the annealing process. Furthermore, the measured responses of both the unloaded and preloaded specimens agree well with predicted results. It is consequently fair to conclude that all the measured residual strain results are valid. Two small differences in the predicted and measured residual strain responses are still apparent, however, and need to be investigated.

The first difference relates to the linearity of the measured results. The predicted residual strain response of the unloaded specimens is almost linear between 25°C and 80°C. The measured response in this region has a slowly decreasing slope however. This effect is also apparent in the annealed specimens and might be present in the preloaded specimens but the generally non-linear behaviour of these specimens prevents it from being observed. It is not entirely clear how this non-linear effect

arises. It is possible that it arises from the non-linear terms in the calibration equation used to obtain the overall strain measurements of the laminates. Replacing the calibration equation with one having only linear terms, however, has only a small effect on the measured strains and any changes to the slow reduction in measured slope are not easily discernible. It appears, therefore, that the effect is not an artefact of the calibration equation. If the effect is caused by relaxation of viscous stresses in the matrix it is expected that the curvature of the residual strain measurements of the annealed specimens has opposite sign on each side of the horizontal axis. Since this effect is not apparent, this possibility, too, must be rejected.

It seems therefore that the effect might be caused by slight differences in the actual matrix properties compared with those used to calculate the predicted strains. It is, for instance, possible that incorrect thermal expansion data have been used to obtain the predicted results. The thermal expansion data used in this analysis were obtained during testing of the specimens made of pure resin. During discussion of these results, it is commented that comparable strain gauge data are linear whereas data from the test rig are slightly non-linear, most probably because the rig was used outside its calibration range. It is perhaps not appropriate, therefore, to use the measured data in regions where alternative information exists. This hypothesis is tested by replacing the measured thermal expansion data with manufacturer's data[189] at temperatures lower than 90°C[v]. The results of such an exercise, presented in Figure 7.2, for a fibre volume fraction of 40% make it apparent that this argument has some merit. The predicted strain response of the unloaded specimens now clearly has a non-linear component which corresponds more closely with the measured results. The measured results are thereby further validated. The slow reduction in measured slope can now be ascribed to the gradual reduction in matrix modulus with temperature.

The second difference the measured and predicted results that requires investigation relates to the slope of the measured results at ambient conditions. It has been explained that the slope of the preloaded specimens is predicted to be lower than that of the unloaded specimens. This result is not visible in the measured results since experimental scatter causes differences in slope within a specimen set to be larger than those between sets and the slopes of all specimen sets appear similar. The measured slope of the unloaded specimens at ambient conditions is very similar to the predicted slope whereas that of the preloaded specimens is approximately 12% higher. This implies that the "average" measured slope is about 6% higher than than

[v]The manufacturer's data-sheet implies linear thermal expansion below 100°C. Strain gauge data are in agreement but only for temperatures below 90°C.

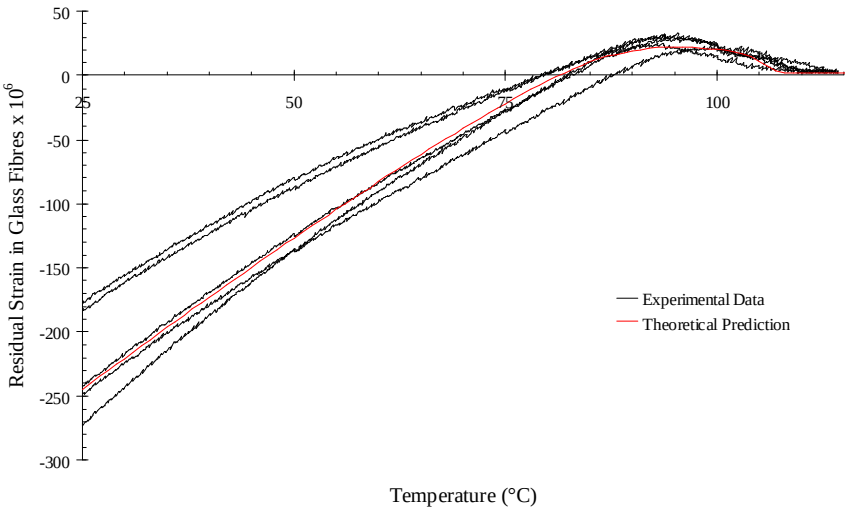


Figure 7.2: Predicted response of unloaded specimens when using manufacturer's data for CTE

predicted. This difference might be accounted for by the use of inaccurate matrix properties to obtain the predicted results. Input data for the modulus are based on manufacturer's[189] data and are probably not accurate to this level of resolution.

At this stage, it is probably worth discussing the merits of incorporating material data into the processing of the strain results. In principle, the more this is done, the greater the measurement accuracy. It is possible to obtain residual strain measurements without any knowledge of the properties of either fibre or matrix. It has been shown, however, that residual strain measurements that are more consistent with theory are obtained if known thermal expansion data of the fibre are incorporated. If the properties of the matrix are additionally included into the residual strain calculations, the non-zero matrix modulus at high temperatures can be accounted for. Whether this is worth doing, however, is open to debate.

The matrix properties are included into the residual strain calculations in the form of an offset through which the measured data should be shifted vertically. The offsets calculated in this work are, however, all a lot smaller than the range of scatter in the room temperature residual strain measurements. Additionally, the offset magnitudes are, at most, comparable to the standard deviation between measured and reference strains, 9.0 $\mu\epsilon$, calculated during calibration of the test rig. The use of these offsets can consequently be questioned. Further issues arise, however, when the offsets of the preloaded and annealed specimen sets are considered individually.

The average offset calculated for the preloaded specimens is 11.3 $\mu\epsilon$. This value is slightly larger than the standard deviation in the measured results and so the

extra effort required to calculate its value might be defended. It seems probable, however, that these specimens experienced non-linear creep during the tests. Since the associated strains cannot be determined using linear viscoelasticity, the offset cannot be properly calculated and so the quoted value is incorrect. There seems little point in spending the time and effort required to calculate the offset.

It seems that the matrix properties of the annealed specimens changed as a consequence of the annealing process. The input data used to find the offset of these specimens are accordingly incorrect. Unless further testing is performed to find the modified material properties, the correct offset cannot be determined.

It seems then that, in the current work, the calculated offset values are either small and their effects inconsequential or are incorrect. As a result, the effort required to obtain better estimates of the residual strain is probably not justified. This is not necessarily always the case, however, and the offset value should be calculated if at all feasible. A decision on whether to incorporate it into improved estimates of the residual fibre strain can then be made.

In this work, the correct offset has been calculated for the unloaded specimens. Although it is very small, 1.3 $\mu\epsilon$, there is no harm in using it and so the data presented in Figure 6.17 consequently provide the best estimate of the residual strains in these specimens. The offsets calculated for both the preloaded and annealed specimens are incorrect, however, and so should not be used to find the best estimate of the residual strains in these specimens. It is preferable to recognize that an error in the residual strain measurements is present as a result not incorporating an accurate estimate of the offset value into their calculation, than to include an estimate of the offset that is known to be incorrect. The best estimate of the residual strains in the preloaded and annealed specimens is consequently obtained from Figures 6.14 and 6.15.

It might seem that the comparison between predicted and measured residual strains in the preloaded and annealed specimens should be updated to reflect the change in the best estimate of their measured results. This is not necessary, however, since the form of the measured residual strains is not significantly affected by neglecting the effect of the offset strain. All aspects of the discussion to this point are consequently still valid. In addition, calculation of the theoretical residual strain and the offset strain is based on the same assumptions. The comparisons presented so far are based, therefore, on data that embody the same set of assumptions. If these assumptions are violated and the offset strain is incorrectly calculated, the theoretical predictions are similarly affected. Updating the comparison is pointless because it requires analysis

of data based on different assumptions.

Now that the best estimate of the residual strains has been determined for each of the specimen types it is worthwhile considering the residual stresses at ambient conditions. These are discussed in the following section.

7.3 Residual stresses at 25°C

Residual stresses are easily estimated if the matrix properties are not considered. Fibre stresses are found using Hooke's Law and the matrix stresses are found using equilibrium considerations. This approach is very convenient since the matrix properties are not considered and so the stresses can be calculated irrespective of non-linear effects in the matrix. In this work, for instance, the stresses in the annealed specimens arise from inelastic processes but can still be determined as easily as those of the other specimen types. The strains of the different specimen types at 25°C are taken from Table 6.3 and used to determine the stresses presented in Table 6.6.

The longitudinal fibre stresses are compressive in the unloaded specimens, as expected, since the fibre preloading is small in these specimens and thermal effects are dominant. The fibre stress in the preloaded specimens is indicated as slightly tensile. Since the fibres were prestrained in these specimens, it is expected that the stress is more tensile than in the unloaded specimens. The residual stress in the fibres of the annealed specimens lies between that of the other two specimen types. Again, this is expected since the annealing process allows some of the tensile stress in the preloaded fibres at 80°C to dissipate and hence reduce the stresses relative to the preloaded specimens. It is not expected that the stresses at this temperature relax to zero, however, and so the stresses do not relax as low as those of the unloaded specimens which have a very low residual strain at 80°C.

In many cases it is simply not feasible to obtain stresses more accurate than those obtained from the use of Hooke's Law. Improved estimates require that Poisson's stresses are considered. Since these cannot be measured, it becomes necessary to make use of analysis techniques to estimate them. Temperature dependent matrix properties are consequently required alongside knowledge of the manufacturing process and thermal history. Even if this information is available it might not be useful if the specimen does not conform to the assumptions embedded within the analysis. For instance, in the current work, the necessary information is available to calculate

the residual stresses in all the specimen types. The annealed specimens experienced non-linear creep during the annealing process, however, and so the analysis technique used in this work, which considers only elastic stresses, is not applicable to these specimens. As a consequence, the residual stresses presented in Table 6.6 are the best estimates that can be obtained for the annealed specimens.

The predicted strain response of the unloaded specimens corresponds well with the measured responses. There is therefore no reason to believe that the analysis technique used in the current work cannot be applied to these specimens. The measured offset strain at the relaxation temperature is consequently calculated and used to obtain the most accurate strain measurements possible. Analysis also allows the Poisson's stresses associated with thermal loading, cure shrinkage and fibre prestrain to be estimated. The measured strain data at room temperature are used to estimate the relative contributions of each of the contributing loads, thereby defining the complete stress state. The resulting stress state is presented in Table 6.7. The presented stresses occupy a small range which arises because the ratio of transverse stresses to longitudinal stresses arising from both thermal loading and cure shrinkage is not exactly defined. The presented results correspond to limits in this ratio.

The preloaded specimens are identical to the unloaded specimens apart from the use of a fibre prestrain. Since this strain tends to reduce the stresses within the laminate, there is no cause to suspect that the limits of linear viscoelasticity are exceeded. The current analysis technique can therefore be used to estimate the longitudinal and transverse stresses in these specimens. It appears, however, that non-linear creep occurs during the testing of these specimens. This has the effect of preventing the accurate calculation of the offset strain. Rather than use a value that is known to be incorrect, it is elected to dispense with the use of the offset strain altogether. The measured strain data of Figure 6.18 are therefore not used to estimate the residual stress. The data of Figure 6.14 are used instead. This reduces the accuracy of the measurement somewhat, but does not artificially introduce unknown errors. The resulting stresses are presented in Table 6.7.

The data presented in Tables 6.6 and Table 6.7 are worth comparing. It is clear that the residual fibre strains of the unloaded specimens are very similar in the two tables. Since the difference in the two values is small, the stresses can be readily compared. The magnitude of the calculated longitudinal stresses is about 12% smaller when the properties of the matrix are ignored than when they are considered. This effect arises because it is clear from Table 6.7 that the transverse fibre stresses have the same sense as the longitudinal fibre stress. The transverse stresses cause the longitudinal strain to be reduced as a consequence of Poisson's

effects. If the effect of the transverse stresses is not accounted for, the reduction in longitudinal strain makes the longitudinal stress appear smaller than it is in reality.

When the preloaded specimen set is considered, it is seen that the relative magnitude of the longitudinal fibre stress is significantly larger when Hooke's Law is used than when Poisson's effects are considered. Since these stresses are both small, such a comparison is misleading, however. The absolute difference in these stresses is almost the same as that of the unloaded specimens. The reason for this is that the preloaded specimens are identical to the unloaded specimens apart from the application of a preload. The Poisson's stresses caused by a fibre prestrain are very small, however, and consequently are similar to the nonexistent stresses of Hooke's Law. The change in longitudinal stress caused by fibre preload is therefore almost the same whether or not Poisson's effects are considered.

A secondary effect of the low Poisson's stresses associated with fibre preload is that the transverse stresses of the preloaded specimens are similar to those of the unloaded specimens. Since the longitudinal stresses in the preloaded specimens are considerably smaller than those of the unloaded specimens however, this means that the transverse stresses of the preloaded specimens are several times larger than the longitudinal stresses. Ignoring their effect through the use of Hooke's Law consequently leads to the relatively large error in the longitudinal stress. Since the longitudinal stress is small though, the absolute error caused by this approach remains comparatively small.

The residual stresses presented in Tables 6.6 and Table 6.7 do not appear significant. It is instructive, however, to consider the residual strains in the resin. It is clear that the relatively low stiffness of the resin ensures that the elastic strain in the resin is significantly higher than that of the fibres. As an example, the elastic strain in the resin of the unloaded specimens is approximately 3300 $\mu\epsilon$. The maximum strain permitted by a frequently used design code, BS4994,[10] for pressure vessels, however, is only 2000 $\mu\epsilon$. The calculated strain in the unloaded specimens thus exceeds this value by 65% without the application of any mechanical loading. It is conceded that the fibres of these specimens are in compression, and are thus not susceptable to environmentally assisted cracking, but it is clear that the actual strains in a laminate can be seriously misrepresented if micro-scale residual stresses are not considered.

8 Conclusions

The work presented in the preceding chapters allows the following conclusions to be drawn:

- No current experimental method can be applied to finding the longitudinal residual stresses and strains in a pre-existing unidirectional GFRP laminate.
- The theoretical basis of a method to address this deficiency has been presented. The method exploits the significant reduction in the matrix modulus at temperatures near its T_g. The residual stresses are determined by measuring the apparent longitudinal thermal strain of a laminate as it is gradually heated to temperatures above the T_g of its polymer matrix.
- Strain gauges cannot be used to obtain the necessary strain measurements. At high temperatures, the modulus of the polymer matrix reduces to such an extent that the stiffness of the strain gauges affects the local strain of the laminate. The measured strain consequently does not reflect the free expansion of the laminate.
- Conventional dilatometry also cannot be used. Load transfer between the glass fibres and polymer matrix causes significant shear strains to develop in the polymer matrix at the laminate ends when the modulus of the polymer matrix reduces to low values. These strains cause the end faces of the laminate to dimple, thereby preventing the accurate measurement of their displacement.
- A practical method of performing the required measurements has been developed. The method used in this work uses a test rig designed and built in-house to measure the change in length of a specimen, not between its end faces, but between points a few millimetres away from the ends.
- The test rig was used to measure the apparent thermal strains of three sets of specimens that differ in their longitudinal residual stress. Two sets of specimens were manufactured with significant fibre preloading. The stresses in one of these

sets were subsequently annealed. The fibres of the third set of specimens were unloaded during manufacture.

- The measured longitudinal strain results validate the theoretical basis of the technique.
- Good correlation exists between the predicted and measured longitudinal strains of the unloaded and preloaded specimen types.
- The measured longitudinal strain results of the annealed specimens differ significantly from predicted results. The discrepancy can be explained by changes in the material properties which are not accounted for when calculating the predicted results.
- Experimental scatter is evident in the results. This scatter is attributed to variations in fibre volume fraction and fibre prestrain.
- Longitudinal residual strains in the fibres can be found without knowledge of either fibre or matrix properties. The accuracy and consistency of these strains can, however, be improved upon if material data are incorporated when the measured strain data are processed.
- Use of known fibre CTE data clearly improves the consistency of the measured longitudinal residual fibre strains.
- Incorporation of matrix data into the calculation of the residual fibre strains does not significantly change the measured results. The effort required to obtain the appropriate data and the potential for the calculations to be invalidated by nonlinear creep in the matrix before or during the test might mean that this technique is not justified.
- Longitudinal residual stresses are readily determined if Poisson's stresses are ignored. In this case Hooke's Law can be directly applied.
- The accuracy of the stress measurements obtained using Hooke's Law cannot be improved upon unless Poisson's stresses transverse to the fibre length are considered. Calculation of these stresses requires that the manufacturing method, the thermal history and the temperature-dependent matrix properties are known. Additionally, the stress state is required to remain within the limits of linear viscoelasticity throughout the specimen history so that the current analysis technique is applicable. In many cases, the lack of such information or the impracticality of obtaining it mean that the use of Hooke's Law is the only realistic method of estimating the residual stresses.

- In the current work, it is only possible to improve on the use of Hooke's Law for the unloaded and preloaded specimen types.
- The longitudinal stresses measured in these specimens when Poisson's effects are considered are not significantly different to those when these effects are ignored.
- The measured residual stresses are small. The matrix strains of the unloaded specimens are, however, significant even without the application of mechanical loads. The measurements indicate, therefore, that the strains in a laminate can be seriously misrepresented if micro-scale residual stresses are not considered.

9 Recommendations

The experimental method developed in this work is intended to be used in an investigation into the effects of micro-scale residual stresses on the rates of environmentally assisted cracking in GFRP. Since these stresses can be determined using the technique described in this work, an investigation of this sort is recommended.

The residual fibre strains measured in the annealed specimens indicate that non-linear creep strains can dramatically change the temperature dependent modulus of a polymer matrix at temperatures approaching T_g. No investigation into this effect could be unearthed during the course of this work, and one is consequently recommended.

REFERENCES

[1] A.K. Kaw. *Mechanics of Composite Materials*. CRC Press, Boca Raton, FL, 2nd edition, 2006.

[2] Tony Roberts. Rapid growth forecast for carbon fibre market. *Reinforced Plastics*, 51(2):10–13, February 2007.

[3] PolicyOne Research Inc. and RTI International. Maine comprehensive research and development evaluation 2006. Technical report, Maine Office of Innovation, February 2007.

[4] Vicki P. McConnell. Resurgence in corrosion-resistant composites. *Reinforced Plastics*, 49(10):20–25, November 2005.

[5] Amanda Jacob. Vinyl esters lead the corrosion challenge. *Reinforced Plastics*, 47(6):32–35, June 2003.

[6] George Marsh. Manipulating matrices. *Reinforced Plastics*, 47(7):22–24, July 2003.

[7] P.J. Hogg. Model for stress corrosion crack growth in glass reinforced plastics. *Composites Science and Technology*, 38(1):23–42, 1990.

[8] J.N. Price and D. Hull. Effect of matrix toughness on crack propagation during stress corrosion of glass reinforced composites. *Composites Science and Technology*, 28(3):193–210, 1987.

[9] B.D. Caddock, K.E. Evans, and D. Hull. Role of diffusion in the micromechanisms of stress corrosion cracking of E-glass/polyester composites. In *I Mech E Conference Publications (Institution of Mechanical Engineers)*, pages 55–62, Liverpool, England, 1986.

[10] British Standards Institution. *BS4994:1987, British standard specification for design and construction of vessels and tanks in reinforced composite materials*. British Standards Institution, London, 1987.

[11] American Society of Mechanical Engineers. *RTP-1c-1992, Reinforced thermoset plastic corrosion resistant equipment.* American Society of Mechanical Engineers, New York, 1992.

[12] M.A. Stone, I.F. Schwartz, and H.D. Chandler. Residual stresses associated with post-cure shrinkage in GRP tubes. *Composites Science and Technology*, 57(1):47–54, 1997.

[13] M. Kumosa, D. Hull, and J.N. Price. Acoustic emission from stress corrosion cracks in aligned GRP. *Journal of Materials Science*, 22(1):331 – 336, 1987.

[14] F.R. Jones. The role of moisture diffusion and matrix plasticisation on the environmental stress corrosion of GRP. *Journal of Strain Analysis for Engineering Design*, 24(4):223 – 233, 1989.

[15] H. Kawada and V.K. Srivastava. The effect of an acidic stress environment on the stress-intensity factor for GRP laminates. *Composites Science and Technology*, 61(8):1109 – 1114, 2001.

[16] S. Tarafder, M. Tarafder, and V.R. Ranganath. Compliance crack length relations for the four-point bend specimen. *Engineering Fracture Mechanics*, 47(6):901 –907, 1994.

[17] D.P. Rooke and D.J. Cartwright. *Compendium of Stress Intensity Factors - Volume 1.* Her Majesty's Stationary Office, London, 1976.

[18] R.G. Treuting and Jr. W.T. Read. A mechanical determination of biaxial residual stress in sheet materials. *Journal of Applied Physics*, 22(2):130–134, 1951.

[19] K.D. Cowley and P.W.R. Beaumont. The measurement and prediction of residual stresses in carbon-fibre/polymer composites. *Composites Science and Technology*, 57(11):1445–55, 1997.

[20] M.P.I.M. Eijpe and P.C. Powell. Residual stress evaluation in composites using a modified layer removal method. *Composite Structures*, 37(3-4):335–42, 1997.

[21] G. Jeronimidis and A.T. Parkyn. Residual stresses in carbon fibre-thermoplastic matrix laminates. *Journal of Composite Materials*, 22(5):401–15, 1988.

[22] N. Ersoy and Ö. Vardar. Measurement of residual stresses in layered composites by compliance method. *Journal of Composite Materials*, 34(7):575–598, 2000.

[23] J.-A.E. Månson and J.C. Seferis. Process simulated laminate (PSL). a methodology to internal stress characterization in advanced composite materials. *Journal of Composite Materials*, 26(3):405–431, 1992.

[24] T.J. Chapman, J.W. Gillespie Jr., R.B. Pipes, J.-A.E. Månson, and J.C. Seferis. Prediction of process-induced residual stresses in thermoplastic composites. *Journal of Composite Materials*, 24(6):616–43, 1990.

[25] G. Sachs. Der nachweiss innerer spannungen in stangen und rohren. *Zeitschrift für Metallkunde*, 19:352–357, 1927.

[26] M. Kovac, Y. Miyano, and T.C. Woo. Residual-stress measurement in SS304 seamless tube. *Experimental Mechanics*, 29(2):209–213, 1989.

[27] A. Stacey and G. A. Webster. Determination of residual stress distributions in autofrettaged tubing. *International Journal of Pressure Vessels and Piping*, 31(3):205–220, 1988.

[28] A.A. Garcia-Granada, V.D. Lacarac, D.J. Smith, and M.J. Pavier. A new procedure based on sachs' boring for measuring non-axisymmetric residual stresses: Experimental application. *International Journal of Mechanical Sciences*, 43(12):2753–2768, 2001.

[29] A.A. Garcia-Granada, V.D. Lacarac, D.J. Smith, and M.J. Pavier. A new procedure based on Sachs' boring for measuring non-axisymmetric residual stresses: Experimental application. *International Journal of Mechanical Sciences*, 43(12):2753–2768, 2001.

[30] T. Kuboki, M. Akiyama, Y. Neishi, and K. Kuroda. Effect of final drawing with light reduction on the levelling of residual stress distribution in cold bar drawing. *Proceedings of the Institution of Mechanical Engineers, Part C: Journal of Mechanical Engineering Science*, 214(11):1389–1400, 2000.

[31] B.K. Jones and J.W. Martin. Residual stress distribution in nitrided En41B steel as function of case depth. *Metals Technology*, 4(pt 11):520–523, 1977.

[32] A.T. Özdemir and L. Edwards. Measurement of the three-dimensional residual stress distribution around split-sleeve cold-expanded holes. *Journal of Strain Analysis for Engineering Design*, 31(6):413–421, 1996.

[33] V. Lacarac, D.J. Smith, and M.J. Pavier. Residual stress creep relaxation around cold expanded holes in an aluminum alloy. *AIAA Journal*, 42(7):1444–1449, 2004.

[34] D.J. Smith, C.G.C. Poussard, and M.J. Pavier. Assessment of the sachs method for measuring residual stresses in cold worked fastener holes. *Journal of Strain Analysis for Engineering Design*, 33(4):263–274, 1998.

[35] H. Waki, K. Ogura, I. Nishikawa, and Y. Kashihara. Residual stress measurement of plasma-sprayed coatings. *JSME International Journal, Series A: Solid Mechanics and Material Engineering*, 46(4):590–597, 2003.

[36] T. Yamada, K. Yokoi, and A. Kohno. Effect of residual stress on the strength of alumina-steel joint with al-si interlayer. *Journal of Materials Science*, 25(4):2188–2192, 1990.

[37] N.P. Hung. Use of an automatic data-acquisition system for the sachs' residual stress measurement method. *Experimental Techniques*, 13(4):24–26, 1989.

[38] J. Rasty, X. Le, M. Baydogan, and J. F. Càrdenas-Garcìa. Measurement of residual stresses in nuclear-grade Zircaloy-4(R) tubes Effect of heat treatment. *Experimental Mechanics*, 47(2):185–199, 2007.

[39] W.A. Olson and C.W. Bert. Analysis of residual stresses in bars and tubes of cylindrically orthotropic materialss. *Experimental Mechanics*, 6(9):451–457, 1966.

[40] G.Z. Voyiadjis, P.D. Kiousis, and C.S. Hartley. Analysis of residual stresses in cylindrically anisotropic materials. *Experimental Mechanics*, 25(2):145–147, 1985.

[41] G.Z. Voyiadjis and C.S. Hartley. Residual stress determination of concentric layers of cylindrically orthotropic materials. *Experimental Mechanics*, 27(3):290–297, 1987.

[42] American Society for Testing and Materials. *ASTM Standard E-837-92, "Measurement of Residual Stresses by the Hole-Drilling Strain-Gage Method"*. American Society for Testing and Materials.

[43] J. Mathar. Determination of initial stress by measuring the deformations around drilled holes. *Transactions of the A.S.M.E.*, 56:249–254, 1934.

[44] C.W. Bert and G.L. Thompson. A method for measuring planar residual stresses in rectangularly orthotropic materials. *Journal of Composite Materials*, 2(2):244–253, 1968.

[45] G.S. Schajer and L. Yang. Residual-stress measurement in orthotropic materials using the hole-drilling method. *Experimental Mechanics*, 34(4):324–333, 1994.

[46] O. Sicot, X.L. Gong, A. Cherouat, and J. Lu. Determination of residual stress in composite laminates using the incremental hole-drilling method. *Journal of Composite Materials*, 37(9):831–44, 2003.

[47] O. Sicot, X.L. Gong, A. Cherouat, and J. Lu. Influence of experimental parameters on determination of residual stress using the incremental hole-drilling method. *Composites Science and Technology*, 64(2):171–80, 2004.

[48] P. Pagliaro and B. Zuccarello. Residual stress analysis of orthotropic materials by the through-hole drilling method. *Experimental Mechanics*, 47(2):217–236, 2007.

[49] J. McKelvie. Moiré strain analysis: an introduction, review and critique, including related techniques and future potential. *Journal of Strain Analysis for Engineering Design*, 33(2):137–151, 1998.

[50] J.N. Petzing and J.R. Tyrer. Recent developments and applications in electronic speckle pattern interferometry. *Journal of Strain Analysis for Engineering Design*, 33(2):153–169, 1998.

[51] Y.Y. Hung and H.P. Ho. Shearography: An optical measurement technique and applications. *Materials Science and Engineering R: Reports*, 49(3):61–87, 2005.

[52] J.F. Càrdenas-Garcìa, S. Ekwaro-Osire, J.M. Berg, and W.H. Wilson. Nonlinear least-squares solution to the moiré hole method problem in orthotropic materials. Part I:Residual stresses. *Experimental Mechanics*, 45(4):301–313, 2005.

[53] Y.Y. Hung. Applications of digital shearography for testing of composite structures. *Composites: Part B*, 30(7):765–773, 1999.

[54] J.A. Nairn. On the use of shear-lag methods for analysis of stress transfer in unidirectional composites. *Mechanics of Materials*, 26(2):63–80, 1997.

[55] Owens Corning. *Pultrusion of Glass Fibre Composite - A Technical Manual, Publication No.5-PL-58644*. June 2003.

[56] Y.-J. Rao. Recent progress in in-fibre Bragg grating sensors: Applications. *Proceedings of SPIE - The International Society for Optical Engineering*, 3555:429–441, 1998.

[57] J.A. Guemes and J.M. Menéndez. Response of Bragg grating fiber-optic sensors when embedded in composite laminates. *Composites Science and Technology*, 62(7-8):959–966, 2002.

[58] S. Keil. Experimental determination of residual stresses with the ring-core method and an on-line measuring system. *Experimental Techniques*, 16(5):17–25, 1992.

[59] H. Wern, R. Cavelius, and D. Schlaefer. New method to determine triaxial non-uniform residual stresses from measurements using the hole drilling method. *Strain*, 33(2):39–45, 1997.

[60] H. Wern. New approach to triaxial residual stress evaluation by the hole drilling method. *Strain*, 33(4):121–125, 1997.

[61] F. Witt, F. Lee, and W. Rider. Comparison of residual-stress measurements using blind-hole, abrasive-jet and trepan-ring methods. *Experimental Techniques*, 7(2):41–44, 1983.

[62] A.K. Roy, A. Venkatesh, S. Dronavalli, V. Marthandam, D. Wells, F. Selim, and R. Rogge. Residual stress measurements in welded and plastically deformed target structural materials. *Journal of ASTM International*, 2(6):67–79, 2005.

[63] J. Schröder, J.M. Keuter, and H.G. Priesmeyer. Residual stress investigations on a hot-rolled plane sandwich-type composite X5 Cr Ni 18 9-C45-X5 Cr Ni 18 9 by means of neutron diffraction. *Journal of Strain Analysis for Engineering Design*, 30(1):15–20, 1995.

[64] W. Ren and K. Li. Application of miniature ring-core and interferometric strain/slope rosette to determine residual stress distribution with depth - Part II: Experiments. *Journal of Applied Mechanics, Transactions ASME*, 74(2):307–314, 2007.

[65] K. Li, B. Xiao, and Z. Feng. Interferometric strain rosette and incremental ring-core cutting applied to residual stress measurement on a spot weld. In *Proceedings of the SEM Annual Conference and Exposition on Experimental and Applied Mechanics 2007*, volume 3, pages 2021–2031, Springfield, MA, United States, 2007.

[66] A. Mirzaee-Sisan, A.J. Fookes, C.E. Truman, D.J. Smith, T.B. Brown, and T.A. Dauda. Residual stress measurement in a repair welded header in the as-welded condition and after advanced post weld treatment. *International Journal of Pressure Vessels and Piping*, 84(5):265–273, 2007.

[67] M.G. Bateman, O.H. Miller, T.J. Palmer, C.E.P. Breen, E.J. Kingston, D.J.

Smith, and M.J. Pavier. Measurement of residual stress in thick section composite laminates using the deep-hole method. *International Journal of Mechanical Sciences*, 47(11):1718–1739, 2005.

[68] E. Procter and E. M. Beaney. Trepan or ring-core method, centre-hole method, Sach's method, blind hole methods, deep hole technique. In *Advances in Surface Treatment: Technology - Application - Effects, Vol 4: Residual Stresses*, pages 165–198. Pergamon Press, New York, 1987.

[69] P.J. Bouchard, D. George, J.R. Santisteban, G. Bruno, M. Dutta, L. Edwards, E. Kingston, and D.J. Smith. Measurement of the residual stresses in a stainless steel pipe girth weld containing long and short repairs. *International Journal of Pressure Vessels and Piping*, 82(4):299–310, 2005.

[70] T.B. Brown, T.A. Dauda, C.E. Truman, D.J. Smith, D. Memhard, and W. Pfeiffer. Predictions and measurements of residual stress in repair welds in plates. *International Journal of Pressure Vessels and Piping*, 83(11-12):809–818, 2006.

[71] D. George and D.J. Smith. Through thickness measurement of residual stresses in a stainless steel cylinder containing shallow and deep weld repairs. *International Journal of Pressure Vessels and Piping*, 82(4):279–287, 2005.

[72] D. Stefanescu, P. Browne, C.E. Truman, and D.J. Smith. Residual stress measurement within a European UIC60 rail using integrated drilling techniques. *Materials Science Forum*, 440-441:85–92, 2003.

[73] E. Kingston and D.J. Smith. Residual stress measurements in rolling mill rolls using deep hole drilling technique. *Ironmaking and Steelmaking*, 32(5):379–380, 2005.

[74] M.B. Prime and M.R. Hill. Residual stress, stress relief, and inhomogeneity in aluminum plate. *Scripta Materialia*, 46(1):77–82, 2002.

[75] M.B. Prime. Residual stress measurement by successive extension of a slot: The crack compliance method. *Applied Mechanics Reviews*, 52(2):75–96, 1999.

[76] S. Güngör. Residual stress measurements in fibre reinforced titanium alloy composites. *Acta Materialia*, 50(8):2053–73, 2002.

[77] A. Neubrand, T.-J. Chung, J. Rodel, E.D. Steffler, and T. Fett. Residual stresses in functionally graded plates. *Journal of Materials Research*, 17(11):2912–2920, 2002.

[78] W.-K. Lim, J.-H. Song, and B.V. Sankar. Effect of ring indentation on fatigue crack growth in an aluminum plate. *International Journal of Fatigue*, 25(9-11):1271–1277, 2003.

[79] M.B. Prime. Measuring residual stress and the resulting stress intensity factor in compact tension specimens. *Fatigue and Fracture of Engineering Materials and Structures*, 22(3):195–204, 1999.

[80] K.-J. Kang, S. Darzens, and G.-S. Choi. Effect of geometry and materials on residual stress measurement in thin films by using the focused ion beam. *Journal of Engineering Materials and Technology, Transactions of the ASME*, 126(4):457–464, 2004.

[81] N. Sabaté, D. Vogel, A. Gollhardt, J. Keller, C. Cané, I. Gràcia, J.R. Morante, and B. Michel. Measurement of residual stress by slot milling with focused ion-beam equipment. *Journal of Micromechanics and Microengineering*, 16(2):254–259, 2006.

[82] N. Sabaté, D. Vogel, A. Gollhardt, J. Keller, B. Michel, C. Cané, I. Gràcia, and J.R. Morante. Measurement of residual stresses in micromachined structures in a microregion. *Applied Physics Letters*, 88(7):071910, 2006.

[83] G.S. Schajer and M.B. Prime. Residual stress solution extrapolation for the slitting method using equilibrium constraints. *Journal of Engineering Materials and Technology*, 129(2):227–232, 2007.

[84] J.M. Ganley, A.K. Maji, and S. Huybrechts. Explaining spring-in in filament wound carbon fiber/epoxy composites. *Journal of Composite Materials*, 34(14):1216–1239, 2000.

[85] B.-S. Kim, N. Bernet, P. Sunderland, and J.-A. E. Månson. Numerical analysis of the dimensional stability of thermoplastic composites using a thermoviscoelastic approach. *Journal of Composite Materials*, 36(20):2389–2403, 2002.

[86] M.B. Prime and M.R. Hill. Measurement of fiber-scale residual stress variation in a metal-matrix composite. *Journal of Composite Materials*, 38(23):2079–2095, 2004.

[87] M.B. Prime, P. Rangaswamy, and M.A.M. Bourke. Measuring spatial variation of residual stresses in a MMC using crack compliance. In D. Hui, editor, *Proceedings of the Seventh International Conference on Composites Engineering*, pages 711–712, Denver, CO, July 2000.

[88] M.B. Prime. Cross-sectional mapping of residual stresses by measuring the surface contour after a cut. *Journal of Engineering Materials and Technology, Transactions of the ASME*, 123(2):162–168, 2001.

[89] J. Kelleher, M.B. Prime, D. Buttle, P.M. Mummery, P.J. Webster, J. Shackleton, and P.M. Withers. The measurement of residual stress in railway rails by diffraction and other methods. *The Journal of Neutron Research*, 11(4):187–193, 2003.

[90] Y. Zhang, S. Ganguly, V. Stelmukh, M.E. Fitzpatrick, and L. Edwards. Validation of the contour method of residual stress measurement in a MIG 2024 weld by neutron and synchrotron X-ray diffraction. *The Journal of Neutron Research*, 11:181–185(5), 2003.

[91] M.B. Prime, T. Gnäupel-Herold, J.A. Baumann, R.J. Lederich, D.M. Bowden, and R.J. Sebring. Residual stress measurements in a thick, dissimilar aluminum alloy friction stir weld. *Acta Materialia*, 54(15):4013–4021, 2006.

[92] R.L. Martineau, M.B. Prime, and T. Duffey. Penetration of HSLA-100 steel with tungsten carbide spheres at striking velocities between 0.8 and 2.5 km/s. *International Journal of Impact Engineering*, 30(5):505–520, 2004.

[93] M.B. Prime, R.J. Sebring, J.M. Edwards, D.J. Hughes, and P.J. Webster. Laser surface-contouring and spline data-smoothing for residual stress measurement. *Experimental Mechanics*, 44(2):176–184, 2004.

[94] N. Tebedge, G. Alpsten, and L. Tall. Residual-stress measurement by the sectioning method. *Experimental Mechanics*, 13(2):88–96, 1973.

[95] C.C. Weng and R.N. White. Residual stresses in cold-bent thick steel plates. *Journal of Structural Engineering*, 116(1):24–39, 1990.

[96] M. Kovač. Method for residual stress measurement in welded seams. *Journal of Materials Processing Technology*, 52(2-4):503–514, 1995.

[97] M.R. Hill and D.V. Nelson. Inherent strain method for residual stress determination and its application to a long welded joint. In *Proceedings of the 1995 Joint ASME/JSME Pressure Vessels and Piping Conference*, pages 343–352, Honolulu, USA, 1995.

[98] M.R. Hill and D.V. Nelson. Determining residual stress through the thickness of a welded plate. In *Proceedings of the 1996 ASME Pressure Vessels and Piping Conference*, pages 29–36, Montreal, Canada, 1996.

[99] P. Casari, F. Jacquemin, and P. Davies. Characterization of residual stresses in wound composite tubes. *Composites Part A: Applied Science and Manufacturing*, 37(2):337–343, 2006.

[100] D. Joh, K.Y. Byun, and J. Ha. Thermal residual stresses in thick graphite/epoxy composite laminates - uniaxial approach. *Experimental Mechanics*, 33(1):70–76, 1993.

[101] H.E. Gascoigne. Residual surface stresses in laminated cross-ply fiber-epoxy composite materials. *Experimental Mechanics*, 34(1):27–36, 1994.

[102] A.S. Kaddour, S.T.S. Al-Hassani, and M.J. Hinton. Residual stress assessment in thin angle ply tubes. *Applied Composite Materials*, 10(3):169–188, 2003.

[103] M.A. Seif and S.R. Short. Determination of residual stresses in thin-walled composite cylinders. *Experimental Techniques*, 26(2):43–46, 2002.

[104] M.A. Seif, U.A. Khashaba, and R. Rojas-oviedo. Residual stress measurements in cfre and gfre composite missile shells. *Composite Structures*, 79(2):261–269, 2007.

[105] J.W. Kim, J.H. Lee, H.G. Kim, H.S. Kim, and D.G. Lee. Reduction of residual stresses in thick-walled composite cylinders by smart cure cycle with cooling and reheating. *Composite Structures*, 75(1-4):261–266, 2006.

[106] J.W. Kim and D.G. Lee. Measurement of residual stresses in thick composite cylinders by the radial-cut-cylinder-bending method. *Composite Structures*, 77(4):444–456, 2007.

[107] D. Cohen. Influence of filament winding parameters on composite vessel quality and strength. *Composites - Part A: Applied Science and Manufacturing*, 28(12):1035–1047, 1997.

[108] A.K. Roy. Response of thick laminated composite rings to thermal stresses. *Composite Structures*, 18(2):125–138, 1991.

[109] C. Aleong and M. Munro. Evaluation of the radial-cut method for determining residual strains in fiber composite rings. *Experimental Techniques*, 15(1):55–58, 1991.

[110] American Society for Testing and Materials. *ASTM Standard D-3171-06, "Standard Test Methods for Constituent Content of Composite Materials"*. American Society for Testing and Materials, 2002.

[111] G. Zong and H.L. Marcus. A microbuckling method for determination of the residual stress in metal matrix composites. *Scripta Metallurgica et Materialia*, 25(2):277–282, 1991.

[112] B.N. Cox, M.R. James, D.B. Marshall, and R.C. Jr. Addison. Determination of residual stresses in thin sheet titanium aluminide composites. *Metallurgical Transactions A (Physical Metallurgy and Materials Science)*, 21A(10):2701–2707, 1990.

[113] S.M. Pickard, D.B. Miracle, B.S. Majumdar, K.L. Kendig, L. Rothenflue, and D. Coker. Experimental study of residual fiber strains in Ti-15-3 continuous fiber composites. *Acta Metallurgica et Materialia*, 43(8):3105–3112, 1995.

[114] K.L. Kendig, W.O. Soboyejo, and D.B. Miracle. Measurement of residual stresses in Ti-15-3 SCS-9 continuously reinforced composites using X-ray diffraction and a matrix etching technique. *Scripta Metallurgica et Materialia*, 32(5):669–674, 1995.

[115] U. Ramamurty, F.-C. Dary, and F.W. Zok. Method for measuring residual strains in fiber-reinforced titanium matrix composites. *Acta Materialia*, 44(8):3397–3406, 1996.

[116] Q. Fang, P.S. Sidky, and G.M. Hocking. Residual stresses in titanium matrix composites (TMC) in thermomechanical cycling using matrix etching. *Materials Science and Engineering A: Structural Materials: Properties, Microstructure and Processing*, 288(2):293–297, 2000.

[117] R.L. Jones and H.D. Chandler. Strength loss in E-glass fibres after exposure to hydrochloric, hydrobromic and hydriodic acids. *Journal of Materials Science*, 20(9):3320–3324, 1985.

[118] T. Ramanathan, A. Bismarck, E. Schulz, and K. Subramanian. Investigationn of the influence of surface-activated carbon fibres on debonding energy and frictional stress in polymer-matrix composites by the micro-indentation technique. *Composites Science and Technology*, 61(16):2511–2518, 2001.

[119] T.A. Parthasarathy, P.D. Jero, and R.J. Kerans. Extraction of interface properties from a fiber push-out test. *Scripta Metallurgica et Materialia*, 25(11):2457–2462, 1991.

[120] E. Lara-Curzio and M.K. Ferber. Methodology for the determination of the interfacial properties of brittle matrix composites. *Journal of Materials Science*, 29(23):6152–6158, 1994.

[121] Chao M. Huang, D. Zhu, Y. Xu, T. Mackin, and W.M. Kriven. Interfacial properties of SiC monofilament reinforced β'-SiAlON composites. *Materials Science & Engineering A: Structural Materials: Properties, Microstructure and Processing*, A201(1-2):159–168, 1995.

[122] A.F. Kalton, S.J. Howard, J. Janczak-Rusch, and T.W. Clyne. Measurement of interfacial fracture energy by single fibre push-out testing and its application to the titanium-silicon carbide system. *Acta Materialia*, 46(9):3175–3189, 1998.

[123] J.D. Belnap and Dinesh K. Shetty. Interfacial properties of sapphire/epoxy composites: Comparison of fluorescence spectroscopy and fiber push-in techniques. *Composites Science and Technology*, 65(11-12):1851–1860, 2005.

[124] X.-F. Zhou, H.D. Wagner, and S.R. Nutt. Interfacial properties of polymer composites measured by push-out and fragmentation tests. *Composites - Part A: Applied Science and Manufacturing*, 32(11):1543–1551, 2001.

[125] J.I. Elridge. Desktop Fibre Push-Out Apparatus, NASA-TM-105341, 1991.

[126] G. Kalinka, A. Leistner, and A. Hampe. Characterization of the fibre/matrix interface in reinforced polymers by the push-in technique. *Composites Science and Technology*, 57(8):845–851, 1997.

[127] Y.S. Chai and Y.-W. Mai. New analysis on the fiber push-out problem with interface roughness and thermal residual stresses. *Journal of Materials Science*, 36(8):2095–2104, 2001.

[128] R.Y. Kim and H.T. Hahn. Effect of curing stresses on the first ply-failure in composite laminates. *Journal of Composite Materials*, 13(1):2–16, 1979.

[129] D.L. Flaggs and M.H. Kural. Experimental determination of the in situ transverse lamina strength in graphite/epoxy laminates. *Journal of Composite Materials*, 16(2):103–116, 1982.

[130] S.M. Lee and R.D. Schile. Investigation of material variables of epoxy resins controlling transverse cracking in composites. *Journal of Materials Science*, 17(7):2095–2106, 1982.

[131] J. Lu and D. Retraint. Review of recent developments and applications in the field of X-ray diffraction for residual stress studies. *Journal of Strain Analysis for Engineering Design*, 33(2):127–136, 1998.

[132] Gianni Albertini, Giovanni Bruno, Adele Carrado, Fabrizio Fiori, Massimo Rogante, and Franco Rustichelli. Determination of residual stresses in materials and industrial components by neutron diffraction. *Measurement Science & Technology*, 10(3):R56–R73, 1999.

[133] F. Fiori, G. Albertini, E. Girardin, A. Giuliani, A. Manescu, and F. Rustichelli. Neutron and synchrotron radiation non-destructive methods for the characterisation of materials for different applications. *Journal of Alloys and Compounds*, 382(1-2):39–45, 2004.

[134] P. Rangaswamy, M.B. Prime, M. Daymond, M.A.M. Bourke, B. Clausen, H. Choo, and N. Jayaraman. Comparison of residual strains measured by X-ray and neutron diffraction in a titanium (Ti-6Al-4V) matrix composite. *Materials Science & Engineering A: Structural Materials: Properties, Microstructure and Processing*, A259(2):209–219, 1999.

[135] P. Predecki and C.S. Barrett. Stress measurement in graphite/epoxy composites by X-ray diffraction from fillers. *Journal of Composite Materials*, 13(1):61–71, 1979.

[136] R.H. Fenn, A.M. Jones, and G.M. Wells. X-ray diffraction investigation of triaxial residual stresses in composite materials. *Journal of Composite Materials*, 27(14):1338–1351, 1993.

[137] R. Meske and E. Schnack. Particular adaptation of X-ray diffraction to fiber reinforced composites. *Mechanics of Materials*, 35(1-2):19–34, 2003.

[138] R. Meske and E. Schnack. A micromechanical model for X-ray stress analysis of fiber reinforced composites. *Journal of Composite Materials*, 35(11):972–998, 2001.

[139] D.R. Clarke and D.J. Gardiner. Recent advances in piezospectroscopy. *International Journal of Materials Research*, 98(8):756–762, 2007.

[140] C. Galiotis. Interfacial studies on model composites by laser raman spectroscopy. *Composites Science and Technology*, 42(1-3):125–150, 1991.

[141] D.J. Bannister, M.C. Andrews, A.J. Cervenka, and R.J. Young. Analysis of the single-fibre pull-out test by means of Raman spectroscopy: Part II. Micromechanics of deformation for an aramid/epoxy system. *Composites Science and Technology*, 53(4):411–421, 1995.

[142] J.S. Thomsen and R. Pyrz. Creep of carbon/polypropylene model composites-a Raman spectroscopic investigation. *Composites Science and Technology*, 59(9):1375–85, 1999.

[143] S. Goutianos, T. Peijs, and C. Galiotis. Comparative assessment of stress transfer efficiency in tension and compression. *Composites Part A: Applied Science and Manufacturing*, 33(10):1303–1309, 2002.

[144] R.B. Yallee and R.J. Young. Micromechanics of fibre fragmentation in model epoxy composites reinforced with α-alumina fibres. *Composites - Part A: Applied Science and Manufacturing*, 29(11):1353–1362, 1998.

[145] X. Yang and R.J. Young. Model ceramic fibre-reinforced glass composites: residual thermal stresses. *Composites*, 25(7):488–493, 1994.

[146] Y. Ward, R.J. Young, and R.A. Shatwell. Application of raman microscopy to the analysis of silicon carbide monofilaments. *Journal of Materials Science*, 39(22):6781–6790, 2004.

[147] R.J. Young, C. Thongpin, J.L. Stanford, and P.A. Lovell. Fragmentation analysis of glass fibres in model composites through the use of Raman spectroscopy. *Composites - Part A: Applied Science and Manufacturing*, 32(2):253–269, 2001.

[148] A.S. Nielsen and R. Pyrz. A novel approach to measure local strains in polymer matrix systems using polarised Raman microscopy. *Composites Science and Technology*, 62(16):2219–2227, 2002.

[149] V. Kominar. Thermo-mechanical regulation of residual stresses in polymers and polymer composites. *Journal of Composite Materials*, 30(3):406–415, 1996.

[150] A.W. Hendry. *Photoelastic analysis*. Pergamon Press, Oxford, 1st edition, 1966.

[151] A. Sjögren, R. Joffe, L. Berglund, and E. Mäder. Effects of fibre coating (size) on properties of glass fibre/vinyl ester composites. *Composites - Part A: Applied Science and Manufacturing*, 30(8):1009–1015, 1999.

[152] B.W. Kim and J.A. Nairn. Experimental verification of the effects of friction and residual stress on the analysis of interfacial debonding and toughness in single fiber composites. *Journal of Materials Science*, 37(18):3965–3972, 2002.

[153] Z.R. Xu and K.H.G. Ashbee. Photoelastic study of the durability of interfacial bonding of carbon fibre-epoxy resin composites. *Journal of Materials Science*, 29(2):394–403, 1994.

[154] F. Zhao, S.A. Hayes, E.A. Patterson, R.J. Young, and F.R. Jones. Measurement of micro stress fields in epoxy matrix around a fibre using phase-stepping automated photoelasticity. *Composites Science and Technology*, 63(12):1783–1787, 2003.

[155] X. Yan and T. Ohsawa. Measurement of the internal local stress distribution of composite materials by means of laser imaging methods. *Composites*, 25(6):443–450, 1994.

[156] B. Andersson, A. Sjögren, and L. Berglund. Micro- and meso-level residual stresses in glass-fiber/vinyl-ester composites. *Composites Science and Technology*, 60(10):2011–2028, 2000.

[157] J.A. Nairn and P. Zoller. Matrix solidification and the resulting residual thermal stresses in composites. *Journal of Materials Science*, 20(1):355–367, 1985.

[158] C.P. Ostertag and E. Drescher-Krasicka. Novel residual stress measurement techniques to measure residual stresses in fiber reinforced composites. *Journal of Materials Science*, 34(3):557–563, 1999.

[159] Y.-C. Lee, J.O. Kim, and J.D. Achenbach. Measurement of stresses by line-focus acoustic microscopy. *Ultrasonics*, 32(5):359–365, 1994.

[160] M. Duquennoy, M. Ouaftouh, and M. Ourak. Ultrasonic evaluation of stresses in orthotropic materials using Rayleigh waves. *NDT and E International*, 32(4):189–199, 1999.

[161] H. Zhang, Q. He, and Y. Yan. A new nondestructive technique for measuring pressure in vessels by surface waves. *Applied Acoustics*, 69(10):891–900, 2008.

[162] J.A. Nairn and P. Zoller. Residual thermal stresses in semicrystalline thermoplastic matrix composites. In *5th International Conference on Composite Materials*, San Diego, USA, 1985.

[163] M. Gigliotti, M.R. Wisnom, and K.D. Potter. Development of curvature during the cure of AS4/8552 [0/90] unsymmetric composite plates. *Composites Science and Technology*, 63(2):187–197, 2003.

[164] M.R. Wisnom, M. Gigliotti, N. Ersoy, M. Campbell, and K.D. Potter. Mechanisms generating residual stresses and distortion during manufacture of polymer-matrix composite structures. *Composites Part A: Applied Science and Manufacturing*, 37(4):522–529, 2006.

[165] J.W. Kim, J.H. Lee, H.G. Kim, H.S. Kim, and D.G. Lee. Reduction of residual stresses in thick-walled composite cylinders by smart cure cycle with cooling and reheating. *Composite Structures*, 75(1-4):261–266, 2006.

[166] W.J. Unger and J.S. Hansen. Effect of cooling rate and annealing on residual stress development in graphite fibre reinforced peek laminates. *Journal of Composite Materials*, 27(2):108–137, 1993.

[167] J.A. Nairn. Thermoelastic analysis of residual stresses in unidirectional, high-performance composites. *Polymer Composites*, 6(2):123–130, 1985.

[168] P.G. Ifju, B.C. Kilday, X. Niu, and S.-C. Liu. A novel method to measure residual stresses in laminated composites. *Journal of Composite Materials*, 33(16):1511–1524, 1999.

[169] P.G. Ifju, X. Niu, B.C. Kilday, S.-C. Liu, and S.M. Ettinger. Residual strain measurement in composites using the cure-referencing method. *Experimental Mechanics*, 40(1):22–30, 2000.

[170] W.A. Schulz, D.G. Myers, T.N. Singer, P.G. Ifju, and R.T. Haftka. Determination of residual stress and thermal history for IM7/977-2 composite laminates. *Composites Science and Technology*, 65(13):2014–2024, 2005.

[171] W.J. Unger and J.S. Hansen. Effect of thermal processing on residual strain development in unidirectional graphite fibre reinforced peek. *Journal of Composite Materials*, 27(1):59–82, 1993.

[172] A.S. Crasto, R.Y. Kim, and J.D. Russell. In situ monitoring of residual strain development during composite cure. *Polymer Composites*, 23(3):454–463, 2002.

[173] J.R. Dunphy, G. Meltz, F.P. Lamm, and W.W. Morey. Multifunction, distributed optical fiber sensor for composite cure and response monitoring. *Proceedings of SPIE - The International Society for Optical Engineering*, 1370:116–118, 1990.

[174] E. Ruiz and F. Trochu. Numerical analysis of cure temperature and internal stresses in thin and thick RTM parts. *Composites Part A: Applied Science and Manufacturing*, 36(6):806–826, 2005.

[175] C.S. Vikram, M.J. Pechersky, C. Feng, and D. Engelhaupt. Residual-stress analysis by local laser heating and speckle-correlation interferometry. *Experimental Techniques*, 20(6):27–30, 1996.

[176] M.J. Pechersky, E.G. Estochen, and C.S. Vikram. Improved measurement of low residual stresses by speckle correlation interferometry and local heat treating. In *SEM IX International Congress on Experimental Mechanics*, Orlando, FL, USA, June 2000.

[177] M.J. Pechersky. Determination of residual stresses by thermal relaxation and speckle correlation interferometry. *Strain*, 38(4):141–149, 2002.

[178] The Dow Chemical Company. *Provisional Product Information - Derakane Momentum 470-300, Form No. 125-00928-999X SMG.* September 1999.

[179] R.G.C. Arridge. *Mechanics of Polymers.* Oxford University Press, 1975.

[180] D.J. Williams. *Polymer Science and Engineering.* Prentice-Hall, Englewood Cliffs, New Jersey, 1971.

[181] D. Roylance. *Mechanics of Materials.* Wiley, New York, 1996.

[182] S.L. Rosen. *Fundamental Principles of Polymeric Materials.* Wiley, New York, 2nd edition, 1993.

[183] R.A. Schapery. Thermal expansion coefficients of composite materials based on energy principles. *Journal of Composite Materials*, 2(3):380–404, 1968.

[184] H.-B. Hsueh and C.-Y. Chen. Preparation and properties of LDHs/epoxy nanocomposites. *Polymer*, 44(18):5275–5283, 2003.

[185] ASM International. *Engineered Materials Handbook - Desk Edition.* Materials Park, Ohio, 1995.

[186] National Semiconductor. *LM35/LM35A/LM35C/LM35CA/LM35D Precision Centigrade Temperature Sensors.* September 1997.

[187] American Society for Metals. *Metals Handbook, Volume 1 - Properties and Selection: Irons and Steels.* Metals Park, Ohio, 9th edition, 1979.

[188] R.L. Pendleton and M.E. Tuttle, editors. *Manual on Experimental Methods for Mechanical Testing of Composites.* Society for Experimental Mechanics, Inc, Bethel, Connecticut, 1989.

[189] The Dow Chemical Company. *Derakane Epoxy Vinyl Ester Resins - Chemical Resistance and Engineering Guide, Form No.125-00043-1095X SMG.* 1995.

[190] K.K. Chawla. *Composite Materials - Science and Engineering.* Springer-Verlag, New York, 2nd edition, 1998.

[191] C.T. Herakovich. *Mechanics of Fibrous Composites.* John Wiley & Sons, Inc., 1998.

[192] Kaman Corporation. *Publication 860105-000, Rev. B.* 2000.

[193] Kaman Corporation. *KD-2300 Instruction Manual, Rev. F.* 2000.

[194] Kaman Corporation. *Publication 860103-000, Rev. C.* 2000.

[195] American Society for Metals. *Metals Handbook, Volume 2 - Properties and Selection: Nonferrous Alloys and Pure Metals*. Metals Park, Ohio, 9th edition, 1979.

[196] PerkinElmer Inc. *Expansion Coefficient of Polymeric Materials using DMA 8000, Application Note 007771A_02G*. 2007.

[197] S.R. White, P.T. Mather, and M.J. Smith. Characterization of the cure-state of DGEBA-DDS epoxy using ultrasonic, dynamic mechanical, and thermal probes. *Polymer Engineering and Science*, 42(1):51 – 67, 2002.

[198] E. Crawford and A.J. Lesser. Effect of network architecture on the thermal and mechanical behavior of epoxy resins. *Journal of Polymer Science, Part B: Polymer Physics*, 36(8):1371 – 1382, 1998.

[199] A.J. Lesser and E. Crawford. Role of network architecture on the glass transition temperature of epoxy resins. *Journal of Applied Polymer Science*, 66(2):387 – 395, 1997.

[200] H.-T. Chiu, R.-E. Jeng, and J.-S. Chung. Thermal cure behavior of unsaturated polyester/phenol blends. *Journal of Applied Polymer Science*, 91(2):1041 – 1058, 2004.

[201] R.D. Maksimov, E.Z. Plume, and J.O. Jansons. Comparative studies on the mechanical properties of a thermoset polymer in tension and compression. *Mechanics of Composite Materials*, 41(5):425–436, 2005.

[202] Carbone of America. *Data Sheet - Ellor +20*. Saint Marys, Pennsylvania, August 1997.

[203] G.S. Whitfield. Investigation into the fabrication and post-cure strains and spring back in glass fibre reinforced pipe flanges. Master's thesis, University of the Witwatersrand, Johannesburg, 2003.

[204] M.F. Ashby and D.R.H. Jones. *Engineering Materials 1 - An Introduction to their Properties and Applications*. Pergamon Press, Oxford, 1986.

APPENDIX A Prediction of the longitudinal thermal expansion of unidirectional GFRP

A.1 Theoretical derivation

The most frequently used method to predict the longitudinal coefficient of thermal expansion, α_{c_L}, of a unidirectional laminate is that of Schapery:[183]

$$\alpha_{c_L} = \frac{E_f V_f \alpha_f + E_m V_m \alpha_m}{E_f V_f + E_m V_m} \tag{A.1}$$

where E_f, V_f, α_f and E_m, V_m, α_m are the Young's modulus, the volume fraction and the coefficient of thermal expansion of the fibre and matrix respectively. Although this equation is convenient, it assumes that both the fibre and the matrix are isotropic and that the Poisson's ratios of both constituents are identical. The Poisson's ratios of E-glass and typical polymer matrices are different, however, and so equation A.1 is not truly applicable to GFRP.

The method of Nairn[167] considers anisotropic fibres and consequently takes proper account of Poisson's ratios. When simplified for isotropic materials so that it can be directly applied to GFRP, the equations of Nairn reduce to:

$$\alpha_{c_L} = \frac{A_3 - 2\nu_m A_1}{E_m} + \alpha_m \tag{A.2}$$

where ν_m is the Poisson's ratio of the matrix and A_1 and A_3 are found from:

$$\begin{bmatrix} A_1 \\ A_3 \end{bmatrix} = (\alpha_m - \alpha_f)\,[A]^{-1} \begin{bmatrix} 1 \\ 1 \end{bmatrix} \tag{A.3}$$

where

$$[A] = \begin{bmatrix} 2\left(\frac{\nu_m}{E_m} + \frac{\nu_f}{E_f}\frac{V_m}{V_f}\right) & -\left(\frac{1}{E_f}\frac{V_m}{V_f} + \frac{1}{E_m}\right) \\ -\left(\frac{1-\nu_f}{E_f}\frac{V_m}{V_f} + \frac{1-\nu_m}{E_m} + \frac{1+\nu_m}{E_m V_f}\right) & \left(\frac{\nu_m}{E_m} + \frac{\nu_f}{E_f}\frac{V_m}{V_f}\right) \end{bmatrix}$$

and where ν_f is the Poisson's ratio of the fibre.

To assess the difference between these two approaches, it is worth plotting, as a function of fibre volume fraction, the predicted coefficient of thermal expansion for unidirectional GFRP using the two methods. Assuming the use of Derakane 411-350 epoxy vinyl-ester resin, frequently used in industrial corrosion applications, the following elastic constants are used for the purposes of the comparison:

Table A.1: Elastic constants used in calculation of CTE

	E (MPa)	α ($\mu\epsilon$/°C)	ν
E-glass	72000[185]	5.0[185]	0.22[191]
Epoxy vinyl-ester	3200[178]	64.8[189]	0.36[a]

[a] Value based on epoxy.[191]

The resulting variation in coefficient of thermal expansion is plotted in Figure A.1 for each of the methods.

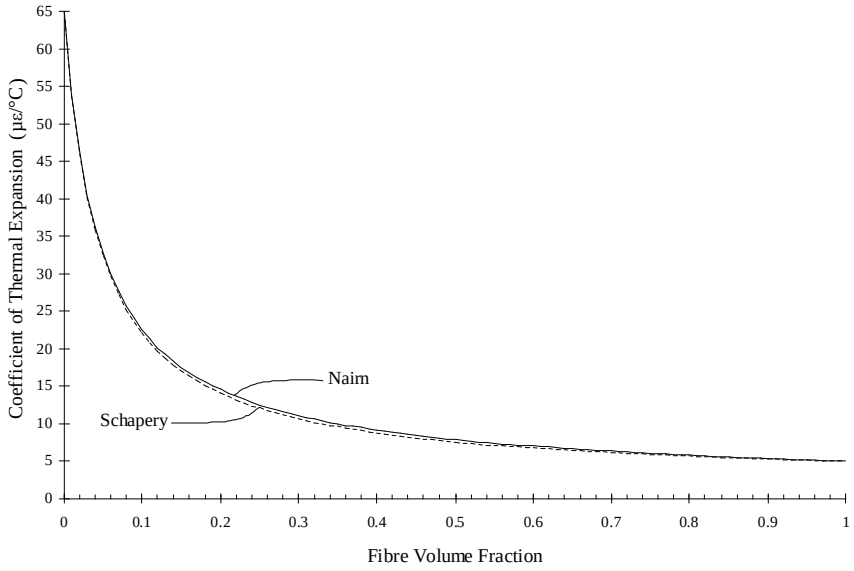


Figure A.1: Predicted longitudinal CTE for unidirectional GFRP

It can be seen that the two methods are in good agreement even though the method

of Schapery does not take into account the difference in Poisson's ratios between the glass fibre and vinyl-ester matrix. The maximum discrepancy between the two methods barely exceeds 4% at its maximum. For the purposes therefore of determining the general form of the thermal response of a GFRP laminate, there seems to be little benefit to be gained from using the more complicated approach of Nairn.

In reality, neither equation A.1 nor equation A.2 can be used because the elastic modulus and coefficient of thermal expansion of the matrix vary with temperature. Nairn,[167] however, presents information that allows the thermal expansion to be calculated in this situation[i]. The method relies on integrating the difference in the unconstrained thermal expansion of the fibre and matrix between the stress-free temperature and the temperature of interest. The matrix properties at this temperature are then used to calculate the longitudinal, radial and circumferential stresses acting on the fibres. Once all three stress components are known, the longitudinal fibre strain can be calculated. Unfortunately, this method relies on inverting the matrix $[A]$ used in equation A.3. Since matrix $[A]$ varies with temperature, it is not possible to present this method in a way that allows for ready understanding of the underlying physics.

It seems more appropriate to modify the simple, but still reasonably accurate, equation of Schapery so that it can take account of temperature dependent matrix properties. Although this equation was determined using energy methods, the identical equation can also be developed by simply considering equilibrium and compatibility in the longitudinal direction. For the purposes of developing a method that allows the general form of the thermal response of a GFRP laminate to be determined, this approach is selected. The development of this method follows:

The fibres and matrix material, illustrated in Figure A.2, are initially stress free at temperature T_0. If no constraints were present, the fibres and matrix material would each expand with an increase in temperature to T_1, and would consequently strain through $\epsilon_{f_{thermal}}$ and $\epsilon_{m_{thermal}}$ respectively. The compatibility requirement, however, forces the overall strain, ϵ_{0-1}, of the two components to be the same. Mechanical loads are thus developed at temperature T_1, causing additional strains $\epsilon_{f_{mech}}$ and $\epsilon_{m_{mech}}$ in the fibres and matrix material respectively.

The compatibility condition at temperature T_1 can be written as follows:

[i]The equation presented by Nairn for this situation is incorrect. The correct form of his equations is presented in Appendix B.

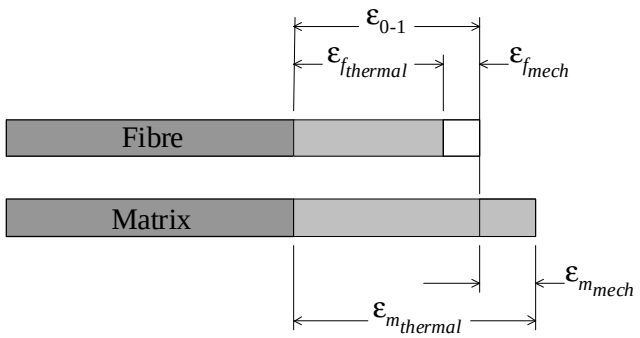


Figure A.2: Development of thermal strains in GFRP

$$\begin{aligned} \epsilon_{m_{thermal}} + \epsilon_{m_{mech}} &= \epsilon_{f_{thermal}} + \epsilon_{f_{mech}} \\ \epsilon_{f_{mech}} - \epsilon_{m_{mech}} &= \epsilon_{m_{thermal}} - \epsilon_{f_{thermal}} \end{aligned} \tag{A.4}$$

At this stage it becomes necessary to determine the unconstrained thermal expansion of the fibres and matrix. The coefficient of thermal expansion of the fibre, α_f, is constant, and hence its unconstrained thermal expansion is:

$$\epsilon_{f_{thermal}} = \alpha_f \left(T_1 - T_0\right) \tag{A.5}$$

The coefficient of thermal expansion of the thermoset matrix material is not constant and increases dramatically in the vicinity of the glass transition temperature, T_g.[179] The unconstrained thermal expansion of the matrix material must, therefore, be calculated using a different approach.

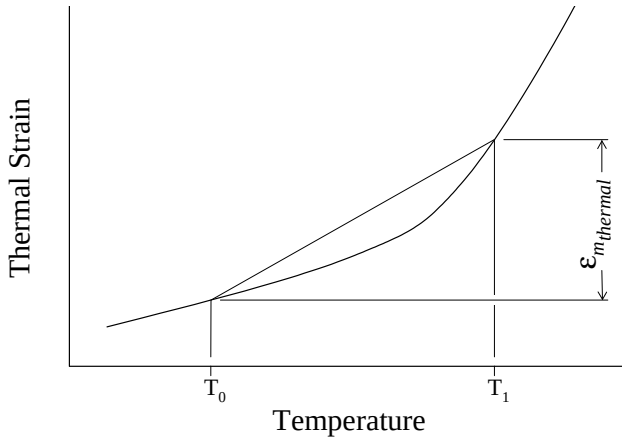


Figure A.3: Illustrative thermal strains in polymer matrix

If Figure A.3 is considered, it is apparent that the thermal expansion of of the matrix,

$\epsilon_{m_{thermal}}$, can be found by the use of integral techniques between temperatures T_0 and T_1, or by defining a coefficient of thermal expansion such that:

$$\epsilon_{m_{thermal}} = \alpha_{m_{01}}(T_1 - T_0) \tag{A.6}$$

$\alpha_{m_{01}}$ is thus the effective coefficient of thermal expansion of the matrix between temperatures T_0 and T_1.

By substituting equations A.5 and A.6 into equation A.4 the compatibility condition can be rewritten as:

$$\epsilon_{f_{mech}} - \epsilon_{m_{mech}} = (\alpha_{m_{01}} - \alpha_f)(T_1 - T_0) \tag{A.7}$$

The stresses in the polymer matrix consist of an elastic component and a viscous component. If the heating rate is sufficiently low, the viscous stresses are able to dissipate and hence it can be assumed that the matrix stresses at temperature T_1 are entirely elastic. Since Poisson's effects are neglected, the strains in the fibre and matrix can thus be found using Hooke's law. The elastic modulus of the matrix varies with temperature however, and so the modulus at T_1, E_{m_1}, must be used in these calculations. The equilibrium conditions require that the stresses in the fibres and matrix balance each other and hence the following holds:

$$E_{m_1} V_m \epsilon_{m_{mech}} = -E_f V_f \epsilon_{f_{mech}}$$

The above equation can be reformulated to give:

$$\epsilon_{m_{mech}} = -\frac{E_f}{E_{m_1}} \frac{V_f}{V_m} \epsilon_{f_{mech}} \tag{A.8}$$

By substituting equation A.8 into equation A.7, both the equilibrium and compatibility conditions can be satisfied simultaneously, yielding:

$$\epsilon_{f_{mech}} \left(1 + \frac{E_f}{E_{m_1}} \frac{V_f}{V_m}\right) = (\alpha_{m_{01}} - \alpha_f)(T_1 - T_0)$$

and so

$$\epsilon_{f_{mech}} = \frac{E_{m_1}V_m}{E_fV_f + E_{m_1}V_m}\left(\alpha_{m_{01}} - \alpha_f\right)\left(T_1 - T_0\right) \tag{A.9}$$

The overall state of strain, ϵ_{0-1}, of the combined glass fibre and polymer matrix composite can now be found by reconsidering Figure A.2 and making use of equations A.5 and A.9.

$$\begin{aligned}
\epsilon_{0-1} &= \epsilon_{f_{thermal}} + \epsilon_{f_{mech}} \\
&= \alpha_f\left(T_1 - T_0\right) + \frac{E_{m_1}V_m}{E_fV_f + E_{m_1}V_m}\left(\alpha_{m_{01}} - \alpha_f\right)\left(T_1 - T_0\right) \\
&= \left(\frac{E_fV_f\alpha_f + E_{m_1}V_m\alpha_f + E_{m_1}V_m\alpha_{m_{01}} - E_{m_1}V_m\alpha_f}{E_fV_f + E_{m_1}V_m}\right)\left(T_1 - T_0\right) \\
&= \left(\frac{E_fV_f\alpha_f + E_{m_1}V_m\alpha_{m_{01}}}{E_fV_f + E_{m_1}V_m}\right)\left(T_1 - T_0\right)
\end{aligned} \tag{A.10}$$

The effective coefficient of longitudinal thermal expansion of the composite between temperatures T_0 and T_1 is consequently found as:

$$\alpha_{c_{L_{01}}} = \frac{E_fV_f\alpha_f + E_{m_1}V_m\alpha_{m_{01}}}{E_fV_f + E_{m_1}V_m} \tag{A.11}$$

The format of this equation is identical to that of Schapery.[183] The current equation however, considers matrix properties that vary with temperature.

The thermal strain of the composite between two arbitrary temperatures, T_1 and T_2, is simply the difference between the thermal strains from the stress-free temperature to each of the respective temperatures:

$$\begin{aligned}
\epsilon_{1-2} &= \epsilon_{0-2} - \epsilon_{0-1} \\
&= \frac{E_fV_f\alpha_f + E_{m_2}V_m\alpha_{m_{02}}}{E_fV_f + E_{m_2}V_m}\left(T_2 - T_0\right) - \frac{E_fV_f\alpha_f + E_{m_1}V_m\alpha_{m_{01}}}{E_fV_f + E_{m_1}V_m}\left(T_1 - T_0\right)
\end{aligned} \tag{A.12}$$

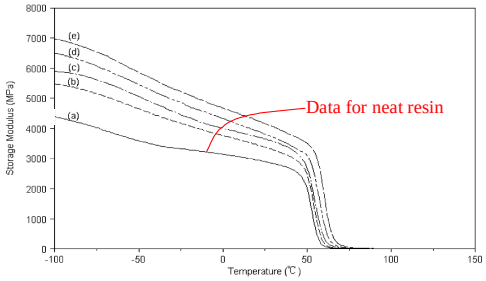
In the general case, the above equation cannot be simplified when calculating the effective coefficient of thermal expansion, $\alpha_{c_{L_{12}}}$, between temperatures T_1 and T_2.

Both the elastic modulus and the coefficient of thermal expansion of the matrix vary with temperature, preventing the stress-free temperature, T_0, from being eliminated. The apparent coefficient of longitudinal thermal expansion of the composite between temperatures T_1 and T_2 therefore varies as a function of the stress-free temperature:

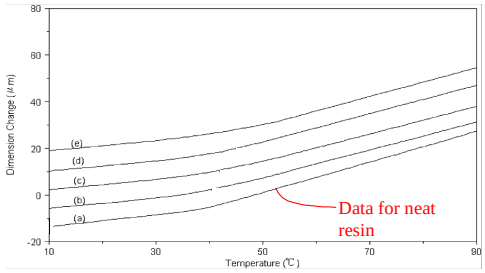
$$\alpha_{c_{L_{12}}} = \frac{\frac{E_f V_f \alpha_f + E_{m_2} V_m \alpha_{m_{02}}}{E_f V_f + E_{m_2} V_m} (T_2 - T_0) - \frac{E_f V_f \alpha_f + E_{m_1} V_m \alpha_{m_{01}}}{E_f V_f + E_{m_1} V_m} (T_1 - T_0)}{T_2 - T_1} \tag{A.13}$$

A.2 Application to published data

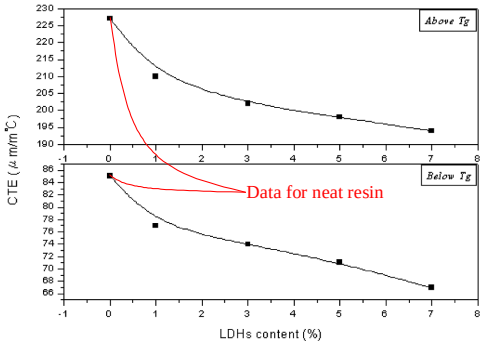
Hsueh and Chen[184] have published data for EPON 828 epoxy that can be used in equation A.12. Their study investigated the effects of adding layered double hydroxides (LDHs) into this resin. For comparison purposes, they also presented data for the neat resin. It is these data that are used in the following analysis. The relevant data from Figures 9, 10 and 11 of their work are extracted and are shown respectively as parts a., b. and c. of Figure A.4.



a. Variation in elastic modulus



b. Thermal expansion



c. Variation in CTE with LDH content

Figure A.4: Properties of EPON 828 cured with Jeffamine D400

Since the thermal expansion data presented in part b. of Figure A.4 are only supplied between 10℃ and 90℃ the analysis is limited to this range. By scaling from part c. of Figure A.4 it is found that the coefficient of thermal expansion at temperatures less than T_g is approximately 85.2 $\mu\epsilon$/℃. At temperatures greater than T_g, the coefficient of thermal expansion is approximately 227.2 $\mu\epsilon$/℃. At temperatures near T_g, the coefficient of thermal expansion gradually changes between these two values. The thermal expansion between 34℃ and 44℃ is thus assumed to vary parabolically between the two linear regions.

The storage modulus of the neat resin is scaled from part a. of Figure A.4 by overlaying a smoothed curve on a magnified view of this data. Approximate X-Y coordinates of the curve are thus extracted and are presented in TableA.2.

Table A.2: Storage modulus vs. temperature

Temperature (℃)	Storage Modulus (MPa)
10.0	3062
17.5	2988
25.0	2906
30.0	2842
34.0	2788
37.0	2740
39.0	2705
42.0	2628
44.0	2565
46.0	2463
48.0	2326
50.0	2068
52.0	1612
55.0	717
58.0	239
62.0	51
67.0	19
75.0	13
80.0	10
85.0	9
90.0	8

The effective coefficient of thermal expansion for the resin can be calculated between any two temperatures once the variation in thermal strain is known. Changes in the

thermal strain of the resin relative to 10℃ are therefore calculated, allowing the effective coefficients of thermal expansion relative to three stress-free temperatures (T_0 = 25℃, T_0 = 50℃ and T_0 = 75℃) to be determined using equation A.6. The resulting data are presented in Table A.3.

Table A.3: Variations in thermal strain and effective thermal expansion

Temperature, T_2	Thermal Strain	Effective CTE of resin, α_{02}		
		T_0 = 25℃	T_0 = 50℃	T_0 = 75℃
(℃)	($\mu\epsilon$)	($\mu\epsilon$/℃)	($\mu\epsilon$/℃)	($\mu\epsilon$/℃)
10.0	0	85.2	124.3	163.8
17.5	639	85.2	133.3	174.1
25.0	1278	85.2	147.7	187.4
30.0	1704	85.2	163.3	198.8
34.0	2045	85.2	182.8	209.9
37.0	2364	90.5	200.4	218.0
39.0	2648	97.9	211.1	222.3
42.0	3181	111.9	223.7	226.3
44.0	3607	122.6	227.2	227.2
46.0	4061	132.5	227.2	227.2
48.0	4516	140.8	227.2	227.2
50.0	4970	147.7	227.2	227.2
52.0	5424	153.6	227.2	227.2
55.0	6106	160.9	227.2	227.2
58.0	6788	167.0	227.2	227.2
62.0	7696	173.5	227.2	227.2
67.0	8832	179.9	227.2	227.2
75.0	10650	187.4	227.2	227.2
80.0	11786	191.1	227.2	227.2
85.0	12922	194.1	227.2	227.2
90.0	14058	196.6	227.2	227.2

With the necessary matrix properties calculated, it is possible to use equation A.12 to determine the thermal strain of a composite relative to some reference temperature. The reference temperature, T_1, is taken as 10℃ in this example. The data in Tables A.2 and A.3 are substituted into equation A.12 for a range of temperatures, T_2, and the three stress-free temperatures, T_0, listed in Table A.3. The fibre volume fraction, V_f, is assumed equal to 40%, and the required fibre properties are taken from Table A.1. The resulting thermal strain at temperature T_2 relative to 10℃ is presented in Figure A.5.

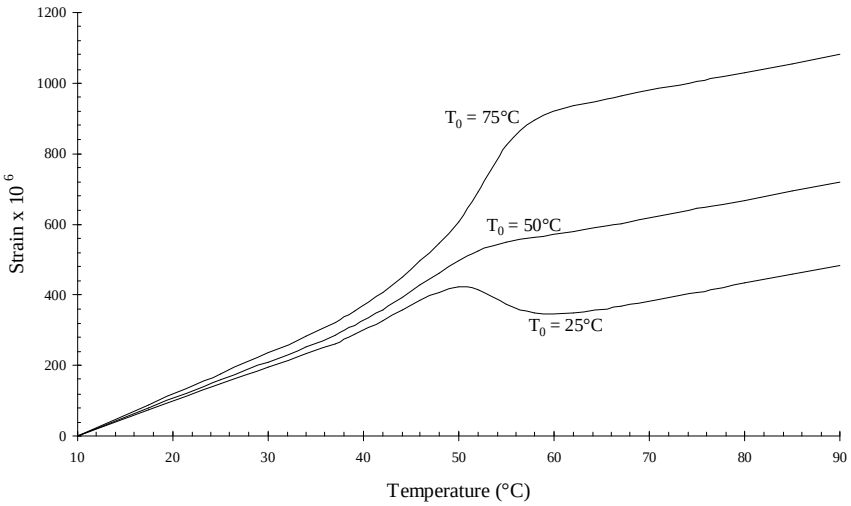


Figure A.5: Illustrative longitudinal thermal response of EPON 828/E-glass laminate

APPENDIX B Calculation of residual stresses

B.1 Elastic analysis

Although Hooke's Law can be used to predict the longitudinal residual stresses within a unidirectional laminate, proper calculation of these stresses requires that Poisson's effects are considered. For elastic systems, the magnitude of the Poisson's stresses can be estimated if the material properties are known. These stresses depend, however, on the origin of the longitudinal stresses. The Poisson's stresses arising from thermal strain and polymerization cure shrinkage are different to those arising from fibre pretension and so require a different analysis.

Residual stresses arising from all three of these effects are often present together and their effect must consequently be combined. The analysis appropriate to each effect is presented in turn, prior to their combination being considered.

B.1.1 Thermal stresses

B.1.1.1 Temperature independent material properties

A concise equation for considering Poisson's effects in thermal problems was developed by Ramamurty *et al.*.[115] The equation is based on a concentric cylinder model and gives the longitudinal residual stress in isotropic fibres, σ_f, as follows:

$$\sigma_f = \frac{E_f\,(E_f + E)}{E_f + E_c\,(1 - 2\nu)}\,\epsilon_f \tag{B.1}$$

where E_f and ϵ_f are the Young's modulus and longitudinal strain of the fibre. The

Poisson's ratio, ν, of both the fibre and matrix is assumed identical and the elastic modulus, E_c, of the composite is found using the rule of mixtures:

$$E_c = E_f V_f + E_m V_m$$

where E_m is the Young's modulus of the matrix and where V_f and V_m are the volume fractions of the fibre and matrix respectively.

Equation B.1 has been used in the analysis of residual stresses in titanium/silicon carbide composites. The Poisson's ratios of glass fibre and polymer matrices are quite different, however, and so this equation cannot be directly used for the current work.

A better estimate of the longitudinal fibre stress can, however, be obtained from the work of Nairn.[167] This work considers the thermal stresses acting on anisotropic fibres and so accommodates differences in the Poisson's ratios of the fibres and the matrix. It is consequently taken as the most accurate analytical method.

According to Nairn, the thermal stresses acting on a fibre within a unidirectional laminate can be found as follows:

$$\begin{bmatrix} \sigma_r \\ \sigma_\theta \\ \sigma_z \end{bmatrix} = \left(1 - \frac{1}{V_f}\right) \begin{bmatrix} A_1 \\ A_1 \\ A_3 \end{bmatrix} \tag{B.2}$$

where σ_r, σ_θ, and σ_z are the stresses aligned with the axes of a cylindrical coordinate system, V_f is the fibre volume fraction and where A_1 and A_3 are found from the following equation:

$$\begin{bmatrix} A_1 \\ A_3 \end{bmatrix} = \Delta T \, [A]^{-1} \begin{bmatrix} (\alpha_m - \alpha_{f_L}) \\ (\alpha_m - \alpha_{f_T}) \end{bmatrix} \tag{B.3}$$

where ΔT is the change in temperature, α_{f_L} and α_{f_T} are the longitudinal and transverse coefficients of thermal expansion of the fibre respectively and where

$$[A] = \begin{bmatrix} 2\left(\frac{\nu_m}{E_m} + \frac{\nu_{f_{LT}}}{E_{f_L}}\frac{V_m}{V_f}\right) & -\left(\frac{1}{E_{f_L}}\frac{V_m}{V_f} + \frac{1}{E_m}\right) \\ -\left(\frac{1-\nu_{f_{TT}}}{E_{f_T}}\frac{V_m}{V_f} + \frac{1-\nu_m}{E_m} + \frac{1+\nu_m}{E_m V_f}\right) & \left(\frac{\nu_m}{E_m} + \frac{\nu_{f_{LT}}}{E_{f_L}}\frac{V_m}{V_f}\right) \end{bmatrix}$$

where E_{f_L} and E_{f_T} are the longitudinal and transverse moduli of the fibre. The Poisson's ratios of the fibre when loaded in the longitudinal and transverse directions respectively are denoted by $\nu_{f_{LT}}$ and $\nu_{f_{TT}}$. ν_m is the Poisson's ratio of the matrix.

When equation B.3 is simplified for use with isotropic materials such as glass fibre it is no longer necessary to differentiate between the longitudinal and transverse directions and so the subscripts "L" and "T" can be deleted. The equation thus reduces to the following form:

$$\begin{bmatrix} A_1 \\ A_3 \end{bmatrix} = (\alpha_m - \alpha_f)\,\Delta T\,[A]^{-1} \begin{bmatrix} 1 \\ 1 \end{bmatrix} \tag{B.4}$$

where

$$[A] = \begin{bmatrix} 2\left(\frac{\nu_m}{E_m} + \frac{\nu_f}{E_f}\frac{V_m}{V_f}\right) & -\left(\frac{1}{E_f}\frac{V_m}{V_f} + \frac{1}{E_m}\right) \\ -\left(\frac{1-\nu_f}{E_f}\frac{V_m}{V_f} + \frac{1-\nu_m}{E_m} + \frac{1+\nu_m}{E_m V_f}\right) & \left(\frac{\nu_m}{E_m} + \frac{\nu_f}{E_f}\frac{V_m}{V_f}\right) \end{bmatrix}$$

It is apparent from equations B.2 and B.4 that for a given set of elastic properties of fibres and matrix, A_1 and A_3 and hence the ratio between the longitudinal stress and the circumferential and radial stress varies only with fibre volume fraction. The circumferential and radial stresses acting on the fibres can then be written as a fixed ratio, k_t, of the longitudinal stress and hence:

$$\sigma_r = \sigma_\theta = k_t \sigma_z \tag{B.5}$$

The way in which the ratio, k_t, varies as a function of fibre volume fraction can be examined. Assuming the use of Derakane 411-350, an epoxy vinyl-ester resin system commonly used in corrosion applications, the properties listed in Table A.1 apply at room temperature. The resulting data are presented in Figure B.1.

It can be seen from Figure B.1 that the radial and circumferential stresses have the

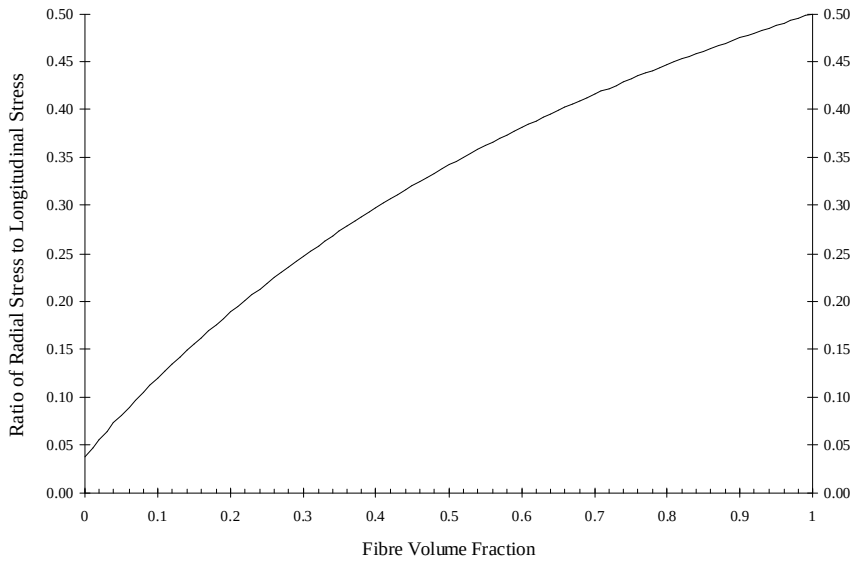


Figure B.1: Variation in ratio between radial and longitudinal stresses in the fibres

same sense as the longitudinal stress and are never zero[i].

The longitudinal stress in the glass fibre can be found using the relationship for an isotropic material:

$$\begin{bmatrix} \epsilon_r \\ \epsilon_\theta \\ \epsilon_z \end{bmatrix} = \begin{bmatrix} S_{11} & S_{12} & S_{12} \\ S_{12} & S_{11} & S_{12} \\ S_{12} & S_{12} & S_{11} \end{bmatrix} \begin{bmatrix} \sigma_r \\ \sigma_\theta \\ \sigma_z \end{bmatrix} \tag{B.6}$$

where $S_{11} = \frac{1}{E_f}$ and $S_{12} = \frac{-\nu_f}{E_f}$.

By incorporating equation B.5 to replace σ_r and σ_θ, equation B.6 can be rewritten as follows:

[i]The first statement can be verified for any matrix and isotropic fibre combination by considering the contents of the $[A]$ matrix used in equation B.4. If this matrix is represented as follows:

$$[A] = \begin{bmatrix} a & -b \\ -c & d \end{bmatrix}$$

then the ratio k_t, equal to $\frac{A_1}{A_3}$, is equivalent to $\frac{b+d}{a+c}$ which consists entirely of positive terms and hence is in turn positive. The second statement can also be verified by recognizing that for the radial and circumferential stresses to be zero, the sum of b and d must be zero. Since both of these terms consist entirely of positive terms, their sum is also positive and hence the ratio k_t cannot be zero.

$$\begin{bmatrix} \epsilon_r \\ \epsilon_\theta \\ \epsilon_z \end{bmatrix} = \frac{\sigma_z}{E_f} \begin{bmatrix} 1 & -\nu_f & -\nu_f \\ -\nu_f & 1 & -\nu_f \\ -\nu_f & -\nu_f & 1 \end{bmatrix} \begin{bmatrix} k_t \\ k_t \\ 1 \end{bmatrix} \tag{B.7}$$

The longitudinal fibre stress can hence be found in terms of the measured longitudinal strain as:

$$\sigma_z = \frac{E_f}{(1 - 2k_t\nu_f)}\,\epsilon_z \tag{B.8}$$

By defining

$$g_t = \frac{1}{(1 - 2k_t\nu_f)} \tag{B.9}$$

equation B.8 can be written more concisely as:

$$\sigma_z = g_t E_f \epsilon_z \tag{B.10}$$

where g_t corresponds to a gain or amplification factor relative to the stress calculated using Hooke's Law, $E_f\epsilon_z$.

Since the value of k_t is always greater than zero it is clear from equation B.9 that the gain factor for the longitudinal thermal stress is always greater than unity and hence that the longitudinal stress predicted using Nairn's method is greater than that predicted using Hooke's Law. The use of Hooke's Law thus defines a lower bound to the magnitude of the longitudinal thermal stress.

At this stage it is possible to compare the longitudinal thermal stresses predicted by the methods of Ramamurty *et al.* and Nairn. This can be done by plotting, as a function of fibre volume fraction, the factor by which the calculated stress obtained by the two methods is greater than that obtained using Hooke's Law. Since the method of Ramamurty *et al.* assumes that the Poisson's ratio of both the fibre and the matrix are the same, it is necessary to investigate which value to use. For this reason, results are calculated using the values corresponding to both constituents. The comparison is plotted in Figure B.2.

The use of the matrix Poisson's ratio, ν_m, in the equation of Ramamurty *et al.* clearly gives poor results. Using the fibre Poisson's ratio, ν_f, however gives results

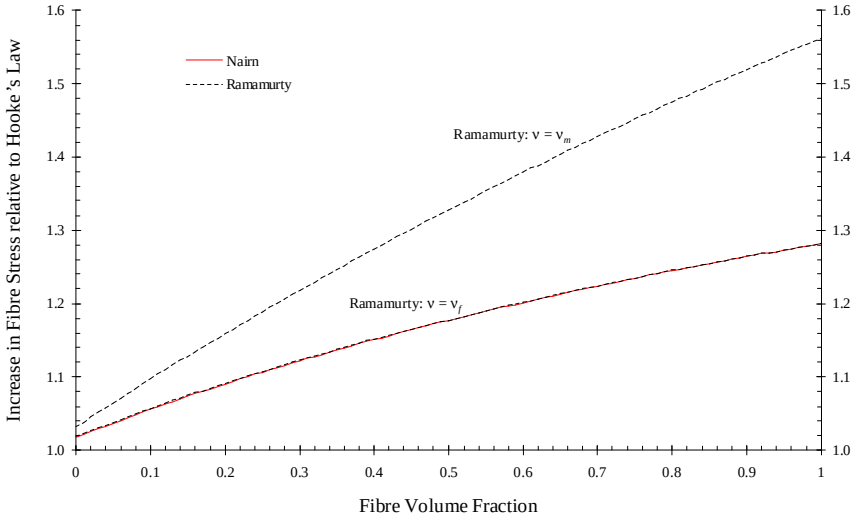


Figure B.2: Increase in fibre stress relative to that found using Hooke's Law

that are in extremely good agreement with the results obtained using the method of Nairn. The maximum discrepancy between the two methods never exceeds 0.2%. Either method can be used to calculate the longitudinal fibre stress, but since the method of Ramamurty *et al.* is much easier to implement it might be preferred.

B.1.1.2 Temperature dependent material properties

The methods described in Appendix B.1.1.1 can only be applied to material systems where the elastic and thermal expansion properties of the materials are invariant with temperature. Both the elastic stiffness and coefficient of thermal expansion of a polymer matrix varies with temperature, however. This means that account must be taken of these effects.

Nairn[167] provides the information required to find the stresses in these circumstances[ii]. The stresses acting on the fibre at temperature T_1 are found as follows:

$$\begin{bmatrix} \sigma_r \\ \sigma_\theta \\ \sigma_z \end{bmatrix} = \left(1 - \frac{1}{V_f}\right) \begin{bmatrix} A_1(T_1) \\ A_1(T_1) \\ A_3(T_1) \end{bmatrix} \tag{B.13}$$

where σ_r, σ_θ, and σ_z are the stresses aligned with the axes of a cylindrical coordinate system, V_f is the fibre volume fraction and $A_1(T_1)$ and $A_3(T_1)$ are constants evaluated at temperature T_1.

When allowance is made for the isotropy of glass fibre, the constants $A_1(T_1)$ and $A_3(T_1)$ can be found by means of the following equation:

[ii]The equation provided by Nairn[167] is incorrect. He provides an equation of the form:

$$\begin{bmatrix} \sigma_r \\ \sigma_\theta \\ \sigma_z \end{bmatrix} = \left(1 - \frac{1}{V_f}\right) \int_{T_0}^{T_1} \begin{bmatrix} A_1(T) \\ A_1(T) \\ A_3(T) \end{bmatrix} dT \tag{B.11}$$

where σ_r, σ_θ, and σ_z are the stresses aligned with the axes of a cylindrical coordinate system, V_f is the fibre volume fraction, T_0 is the stress-free temperature, T_1 is the temperature at which the stress is desired and $A_1(T)$ and $A_3(T)$ are constants evaluated at temperature T.

In this case, the constants $A_1(T)$ and $A_3(T)$ can be found at any temperature by means of the following equation:

$$\begin{bmatrix} A_1(T) \\ A_3(T) \end{bmatrix} = (\alpha_m - \alpha_f)\,[A]^{-1} \begin{bmatrix} 1 \\ 1 \end{bmatrix} \tag{B.12}$$

where α_f and α_m are the coefficients of thermal expansion of the fibre and matrix respectively at temperature T, and where $[A]$ is defined in equation B.15 using the material properties at temperature T.

Equation B.11 represents the integration of thermal stresses. It is not correct, however, to simply integrate stresses in this way. As an illustration, imagine a case where the stress-free temperature occurs at ambient conditions and where the matrix modulus remains constant up to 100℃ and then suddenly reduces to zero at higher temperatures. Clearly, the matrix cannot apply any constraints to the fibre when its modulus is zero, and so the resulting stress state must also be zero. Equation B.11, however, implies that the stress state does not reduce to zero above 100℃, but simply stops increasing. This is clearly incorrect.

The correct approach is to integrate the stress driver, in this case, the difference between the thermal expansions of the two constituents, and then determine the stress state using the material properties at the temperature of interest. This approach is embedded in equations B.13 through B.16.

$$\begin{bmatrix} A_1(T_1) \\ A_3(T_1) \end{bmatrix} = \int_{T_0}^{T_1} (\alpha_m - \alpha_f)\ dT\ [A]^{-1} \begin{bmatrix} 1 \\ 1 \end{bmatrix} \tag{B.14}$$

where T_0 is the stress-free temperature, α_f and α_m are the coefficients of thermal expansion of the fibre and matrix respectively at temperature T, and where

$$[A] = \begin{bmatrix} 2\left(\frac{\nu_m}{E_m} + \frac{\nu_f}{E_f}\frac{V_m}{V_f}\right) & -\left(\frac{1}{E_f}\frac{V_m}{V_f} + \frac{1}{E_m}\right) \\ -\left(\frac{1-\nu_f}{E_f}\frac{V_m}{V_f} + \frac{1-\nu_m}{E_m} + \frac{1+\nu_m}{E_m V_f}\right) & \left(\frac{\nu_m}{E_m} + \frac{\nu_f}{E_f}\frac{V_m}{V_f}\right) \end{bmatrix} \tag{B.15}$$

The terms in $[A]$ must be determined using the material properties at temperature T_1 where E_f, ν_f and E_m, ν_m are the elastic modulus and Poisson's ratio of the fibre and matrix respectively, and where V_m is the volume fraction of the matrix.

Since $\int_{T_0}^{T_1} (\alpha_m - \alpha_f)\ dT$ simply corresponds to the difference between the unconstrained thermal expansions of the matrix and glass between temperatures T_0 and T_1, equation B.14 can be rewritten as follows:

$$\begin{bmatrix} A_1(T_1) \\ A_3(T_1) \end{bmatrix} = \left(\epsilon_{m_{0-1}} - \epsilon_{f_{0-1}}\right)[A]^{-1} \begin{bmatrix} 1 \\ 1 \end{bmatrix} \tag{B.16}$$

where $\epsilon_{m_{0-1}}$ and $\epsilon_{f_{0-1}}$ are the unconstrained thermal expansions of the matrix and fibre respectively between temperatures T_0 and T_1.

Since E_f is constant over the operating temperatures of GFRP, the strain of the glass fibre can be related to the applied stresses as follows:

$$\begin{bmatrix} \epsilon_r \\ \epsilon_\theta \\ \epsilon_z \end{bmatrix} = \frac{1}{E_f} \begin{bmatrix} 1 & -\nu_f & -\nu_f \\ -\nu_f & 1 & -\nu_f \\ -\nu_f & -\nu_f & 1 \end{bmatrix} \begin{bmatrix} \sigma_r \\ \sigma_\theta \\ \sigma_z \end{bmatrix} \tag{B.17}$$

By incorporating Equation B.13 into equation B.17, and noting that $\sigma_r = \sigma_\theta$ the longitudinal strain in the fibres at T_1 can be written as follows:

$$\epsilon_z = \frac{V_f - 1}{E_f V_f}\Big(A_3(T_1) - 2\nu_f A_1(T_1)\Big) \tag{B.18}$$

Equation B.18 allows the residual stress state to be determined from the measured longitudinal strain at any temperature, T_1. Provided that the variation in $A_1(T)$ and $A_3(T)$ is known as a function of temperature[iii], it is possible to solve for the stress-free temperature, T_0, that results in the measured longitudinal strain, ϵ_z, at temperature T_1. Once T_0 is known, the stresses at T_1 or any other temperature can be calculated using equation B.13.

Even without knowing the temperature dependent matrix properties it is possible to assess the relative magnitude of the longitudinal thermal stresses against those obtained from Hooke's Law. The fibre stresses are proportional to the difference between the unconstrained matrix and fibre strains over the complete change in temperature. Irrespective of the matrix properties[iv], and hence at any temperature, the radial and circumferential stresses develop with the same sense as the longitudinal stress. Since the longitudinal stress increases progressively in magnitude, it is clear that the final radial and circumferential stresses also have the same sense as the longitudinal stress. It is thus apparent from equation B.17 that these stresses tend to reduce the magnitude of the longitudinal strain. As was found to be the case for constant material properties, the use of Hooke's Law provides a lower bound to the magnitude of the longitudinal thermal stress.

The longitudinal stress arising from thermal effects can thus be represented as follows:

$$\sigma_z = g_t^{'} E_f \epsilon_z \tag{B.19}$$

where $g_t^{'}$, having a magnitude greater than unity, corresponds to the gain or amplification factor relative to the stress calculated using Hooke's Law, $E_f \epsilon_z$.

B.1.2 Polymerization shrinkage stresses

Polymerization shrinkage of the matrix acts in all directions and is hence analogous to thermal contraction. As a result, the thermoelastic analysis of Nairn[167] used in Appendix B.1.1 can be used to study the residual stresses arising from polymerization cure shrinkage.

In order to make use of Nairn's equations it is useful to employ the method of Stone

[iii] This would typically require the use of both DMA tests to obtain the elastic properties of the matrix and TMA tests to measure the CTE of the matrix.

[iv] As shown in Appendix B.1.1.1

et al..[12] In this approach, the cure shrinkage of the matrix is substituted into the thermoelastic equations such that it replaces its thermal strain.

Even though polymerization cure shrinkage might take place at a constant temperature, the material properties vary with the degree of cure.[174] Since the shrinkage develops with cure,[174] the material properties vary as a function of shrinkage. This means that the simple form of Nairn's work described in Appendix B.1.1.1 cannot be used, and instead the more general equations used in Appendix B.1.1.2 must be used instead.

Equation B.16 is consequently modified so that the unconstrained thermal shrinkage of the matrix is replaced by the polymerization cure shrinkage, S. The fibre does not undergo polymerization shrinkage and so the strain term associated with the fibre is deleted.

The stresses resulting from cure shrinkage are consequently found as follows:

$$\begin{bmatrix} \sigma_r \\ \sigma_\theta \\ \sigma_z \end{bmatrix} = \left(1 - \frac{1}{V_f}\right) \begin{bmatrix} A_1(S) \\ A_1(S) \\ A_3(S) \end{bmatrix} \tag{B.20}$$

where S is the shrinkage state at which the stress is desired and $A_1(S)$ and $A_3(S)$ are constants evaluated at a particular state of shrinkage S.

The constants $A_1(S)$ and $A_3(S)$ can be found at any state of shrinkage by means of the following equation:

$$\begin{bmatrix} A_1(S) \\ A_3(S) \end{bmatrix} = S\,[A]^{-1} \begin{bmatrix} 1 \\ 1 \end{bmatrix} \tag{B.21}$$

and where

$$[A] = \begin{bmatrix} 2\left(\frac{\nu_m}{E_m} + \frac{\nu_f}{E_f}\frac{V_m}{V_f}\right) & -\left(\frac{1}{E_f}\frac{V_m}{V_f} + \frac{1}{E_m}\right) \\ -\left(\frac{1-\nu_f}{E_f}\frac{V_m}{V_f} + \frac{1-\nu_m}{E_m} + \frac{1+\nu_m}{E_m V_f}\right) & \left(\frac{\nu_m}{E_m} + \frac{\nu_f}{E_f}\frac{V_m}{V_f}\right) \end{bmatrix}$$

The terms in $[A]$ must be determined using the matrix properties at the shrinkage state S.

More typically, shrinkage takes place over a range of temperatures. In this case the material properties of the matrix vary both with state of shrinkage and also with temperature. In this situation, the stress state can be determined by including the effects of temperature on the material properties as the polymerization shrinkage develops. Equations B.20 through B.20 consequently take on the form:

$$\begin{bmatrix} \sigma_r \\ \sigma_\theta \\ \sigma_z \end{bmatrix} = \left(1 - \frac{1}{V_f}\right) \begin{bmatrix} A_1(S,T) \\ A_1(S,T) \\ A_3(S,T) \end{bmatrix} \tag{B.22}$$

where $A_1(S,T)$ and $A_3(S,T)$ are constants evaluated at a particular state of shrinkage, S, and temperature, T.

The constants $A_1(S,T)$ and $A_3(S,T)$ can be found at any state of shrinkage and temperature by means of the following equation:

$$\begin{bmatrix} A_1(S,T) \\ A_3(S,T) \end{bmatrix} = \left(\epsilon_{m_{0-1}} - \epsilon_{f_{0-1}}\right) [A]^{-1} \begin{bmatrix} 1 \\ 1 \end{bmatrix} \tag{B.23}$$

where $\epsilon_{m_{0-1}}$ is the matrix strain including both cure shrinkage and thermal effects as the temperature changes from the stress-free state, T_0, to that at shrinkage S, T_1. $\epsilon_{f_{0-1}}$ represents the fibre strain over the same temperature range[v]. The terms in $[A]$ are determined using the matrix properties at the shrinkage state S and temperature T_1.

Using the same technique described in Appendix B.1.1.2, it is possible to write the longitudinal strain in the fibre as follows:

$$\epsilon_z = \frac{V_f - 1}{E_f V_f}\left(A_3(S,T_1) - 2\nu_f A_1(S,T_1)\right) \tag{B.24}$$

Provided that the variation in matrix properties as a function of shrinkage and temperature are known[vi], it is possible to determine $A_1(S,T_1)$ and $A_3(S,T_1)$ and hence use equation B.24 to determine the state of shrinkage S that corresponds to the measured strain. Equation B.22 can then be used to determine the state of stress in the fibre.

[v] It is clear that equation B.23 has identical form to that of equation B.16.

[vi] Compilation of this information would require an extensive set of tests using both DMA and TMA and probably also differential scanning calorimetry.

Considering that the required matrix properties are not easy to compile, it is useful to have a sense of the effect that polymerization cure shrinkage has on the longitudinal residual stress. In the same manner as was performed in Appendix B.1.1.2 it is possible to assess the relative magnitude of the longitudinal thermal stresses against those obtained from Hooke's Law.

Since the cure shrinkage problem is analogous to that of thermal contraction, the stresses arising from shrinkage behave similarly to those arising from thermal effects. Consequently, the radial and circumferential stresses develop with the same sense as the longitudinal stress irrespective of the matrix properties[vii]. It is thus apparent from equation B.17 that, at any temperature or state of cure, these stresses tend to reduce the magnitude of the longitudinal strain. The use of Hooke's Law thus again provides a lower bound to the magnitude of the longitudinal residual stress.

The longitudinal stress arising from polymerization shrinkage of the resin can thus be represented as follows:

$$\sigma_z = g_s^{'} E_f \epsilon_z \tag{B.25}$$

where $g_s^{'}$ having a magnitude greater than unity, corresponds to the gain or amplification factor relative to the stress calculated using Hooke's Law.

B.1.3 Preload stresses

Although the thermoelastic analysis of Nairn[167] used in Appendix B.1.1 was not intended for this purpose, it can be readily adapted to calculate the residual stresses arising from fibre preload.

Both thermal stresses and the stresses resulting from the release of fibre prestrain arise from the fibres and matrix acting against each other. The set of equations used for a thermoelastic analysis can thus also be applied to an analysis of the residual stresses arising from the release of fibre preload. This can be achieved using a similar approach to that of Stone *et al.*.[12] By adjusting the coefficients of thermal expansion of the fibre and matrix and applying a "dummy" change in temperature, the effects of fibre preload can be replicated. Unconstrained thermal strains can thus be replaced by the strains that would result from the unconstrained release of the preload.

[vii] As shown in Appendix B.1.1.1.

The product of change in temperature and coefficient of thermal expansion must therefore be replaced by the corresponding free strains experienced during the release of the preload. By recognizing that the matrix is not preloaded and hence that its free response to the release of the fibre preload is zero, the matrix coefficient of thermal expansion, α_m, can be set to zero. The change in temperature, ΔT, can be replaced by the fibre prestrain, P, allowing the fibre longitudinal coefficient of thermal expansion to be replaced by -1. The unconstrained Poisson's strain of the fibre can be replicated by replacing its transverse coefficient of thermal expansion with the Poisson's ratio $\nu_{f_{LT}}$.

The preload is taken as known and hence no integration of strains is required. The simple form of Nairn's work, described in Appendix B.1.1.1, is thus applicable. Once the appropriate substitutions are made, the stresses acting on a fibre within a unidirectional laminate as a result of fibre preload can be found from equation B.2, repeated below as equation B.26 for clarity:

$$\begin{bmatrix} \sigma_r \\ \sigma_\theta \\ \sigma_z \end{bmatrix} = \left(1 - \frac{1}{V_f}\right) \begin{bmatrix} A_1 \\ A_1 \\ A_3 \end{bmatrix} \tag{B.26}$$

where A_1 and A_3 can be found from a rewritten form of equation B.3 as follows:

$$\begin{bmatrix} A_1 \\ A_3 \end{bmatrix} = P\,[A]^{-1} \begin{bmatrix} 1 \\ -\nu_{f_{LT}} \end{bmatrix} \tag{B.27}$$

and where $[A]$ has the same form as that of equation B.3. Since the fibres have isotropic elastic properties, equation B.27 can be simplified to the following form:

$$\begin{bmatrix} A_1 \\ A_3 \end{bmatrix} = P\,[A]^{-1} \begin{bmatrix} 1 \\ -\nu_f \end{bmatrix} \tag{B.28}$$

with $[A]$ having the same form as that of equation B.4. The material properties required to calculate $[A]$ are those at the temperature of interest.

It is apparent from equations B.28 and B.26 that, for a given set of elastic properties of fibres and matrix, A_1 and A_3 and hence the ratio between the longitudinal stress and the circumferential and radial stresses varies only with fibre volume fraction. The circumferential and radial stresses can then be written as a fixed ratio, k_p, of the longitudinal stress and hence:

$$\sigma_r = \sigma_\theta = k_p \sigma_z \tag{B.29}$$

The way in which the ratio, k_p, varies as a function of fibre volume fraction can now be examined. Assuming the use of Derakane 411-350, an epoxy vinyl-ester resin system frequently used in corrosion applications, the properties listed in Table A.1 apply at room temperature. The resulting data are presented in Figure B.3.

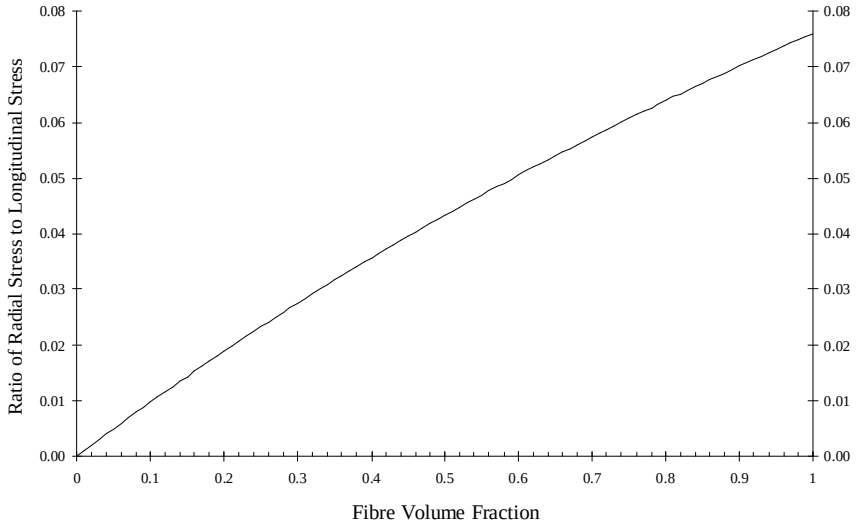


Figure B.3: Variation in ratio between radial and longitudinal stress in the fibres

It can be seen from Figure B.3 that the radial and circumferential stresses are small in comparison to the longitudinal stress. Interestingly, numerical calculations reveal that, for a given fibre volume fraction, the change in k_p is negligibly small as the elastic modulus of the matrix, E_m, reduces towards zero. As a consequence, provided the temperatures are sufficiently far below T_g that ν_m can be taken as constant[viii], Figure B.3 is also valid above room temperature.

Following the same approach as used in Appendix B.1.1, it is possible to calculate the longitudinal fibre stress in terms of the measured strain:

$$\sigma_z = \frac{E_f}{(1 - 2k_p\nu_f)}\,\epsilon_z \tag{B.30}$$

By defining

$$g_p = \frac{1}{(1 - 2k_p\nu_f)} \tag{B.31}$$

[viii] The value of ν_m is expected to tend towards 0.5 as the rubbery state is approached.[174]

equation B.30 can be written more concisely as:

$$\sigma_z = g_p E_f \epsilon_z \tag{B.32}$$

where g_p corresponds to a gain or amplification factor relative to the stress calculated using Hooke's Law, $E_f \epsilon_z$.

From Figure B.1 it is apparent that the value of k_p increases from zero with increasing fibre volume fraction. It is consequently clear from equation B.31 that the gain factor for the longitudinal stress in practical laminates is greater than unity and hence that the longitudinal stress predicted using Nairn's method is greater than that predicted using Hooke's Law. As has been found for thermal and shrinkage stresses, the use of Hooke's Law defines a lower bound to the magnitude of the longitudinal stress. When dealing with fibre preload, however, the fibre is always loaded into longitudinal tension. The longitudinal stress arising from fibre preload is thus more tensile than Hooke's Law would indicate.

The ratio between the stress predicted using Nairn's method and that obtained from Hooke's Law is plotted as a function of fibre volume fraction in Figure B.4. Since the value of k_p is negligibly affected by a reduction in the fibre modulus, Figure B.4 is also applicable between room temperature and the temperature at which the Poisson's ratio of the matrix begins to change appreciably.

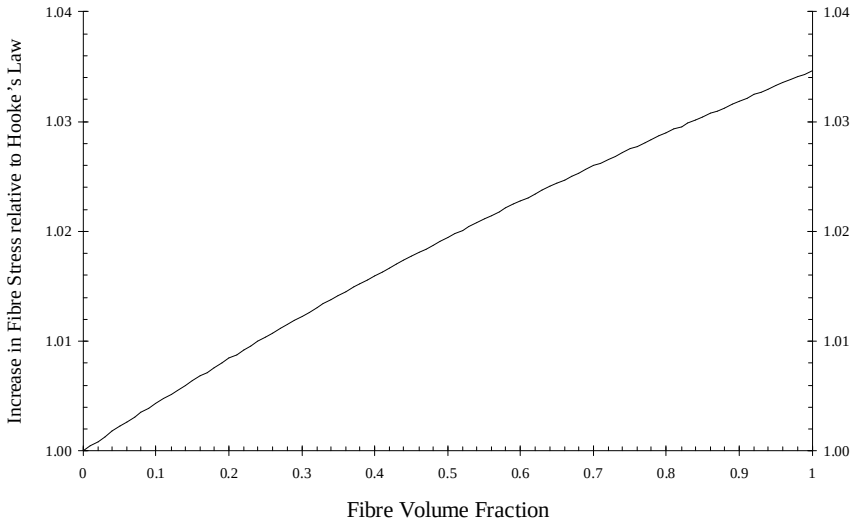


Figure B.4: Increase in fibre stress relative to that found using Hooke's Law

Figure B.4 allows the errors associated with the use of Hooke's Law to be evaluated for laminates manufactured from Derakane 411-350 epoxy vinyl-ester resin. It is

evident that the error never exceeds 3.5% and in practical laminates is significantly smaller.

B.1.4 Combined thermal, shrinkage and preload stresses

The residual stresses within a unidirectional laminate can consist of thermal stresses, polymerization shrinkage stresses and preload stresses. Using the methods described earlier in this Appendix it is possible to take account of Poisson's effects and hence calculate, for each of these effects, the longitudinal elastic stress associated with a particular longitudinal strain.

When stresses resulting from these effects are present simultaneously, however, the situation is not as neatly resolved. The total longitudinal stress, σ_z, comprises stresses from thermal, shrinkage and preload stresses:

$$\sigma_z = \sigma_{z_t} + \sigma_{z_s} + \sigma_{z_p} \tag{B.33}$$

where the subscripts t, s and p refer respectively to the stresses arising from thermal effects, cure shrinkage and fibre prestrain.

By incorporating equations B.19, B.25 and B.32 it is possible to rewrite equation B.33 as follows:

$$\sigma_z = E_f \left(\epsilon_{z_t} g_t^{'} + \epsilon_{z_s} g_s^{'} + \epsilon_{z_p} g_p \right) \tag{B.34}$$

where the g terms are gain factors relating actual stresses to those found using Hooke's Law. It is clear from equation B.34 that it is necessary to know each of the strains ϵ_{z_t}, ϵ_{z_s} and ϵ_{z_p} in order to properly calculate the longitudinal stress in the fibres.

The overall longitudinal strain, ϵ_z, consists of the sum of the thermal, shrinkage and preload strains, however:

$$\epsilon_z = \epsilon_{z_t} + \epsilon_{z_s} + \epsilon_{z_p} \tag{B.35}$$

It is only possible to measure the combined sum of these strains and so they cannot be isolated from each other. Depending on the temperature of measurement, the

thermal strains can be positive or negative (although they will usually be negative at room temperature), the shrinkage strains are negative and the preload strains are positive. As a consequence, for any measured longitudinal strain there are an infinite number of combinations of ϵ_{z_t}, ϵ_{z_s} and ϵ_{z_p} that can result in this value. An unlimited number of longitudinal stress combinations can thus result in the same longitudinal strain.

If for instance it is assumed that thermal strains are the most significant, ϵ_{z_t} in equation B.35 can be substituted into equation B.34 to yield the following:

$$\sigma_z = E_f \left(\epsilon_z g_t^{'} + \epsilon_{z_s}(g_s^{'} - g_t^{'}) + \epsilon_{z_p}(g_p - g_t^{'}) \right) \tag{B.36}$$

Unless ϵ_{z_s} and ϵ_{z_p} are explicitly known, or are rendered irrelevant because either $g_s^{'} = g_t^{'}$ or $g_p = g_t^{'}$ which is not likely, it is not possible to make further progress and the actual fibre stress cannot be determined. Similar equations can be obtained by substituting ϵ_{z_s} and ϵ_{z_p} into equation B.34 but these equations have the same limitations as equation B.36.

In general, in an arbitrary laminate where the prior history is unknown, the strains ϵ_{z_t}, ϵ_{z_s} and ϵ_{z_p} can have any values that add to ϵ_z. Since the relationship between the constituent strains is unknown, it is not possible to account for the individual contributions of Poisson's effects and so stress estimates obtained using Hooke's Law cannot be improved on.

If an estimate of the constituent strains in equation B.34 can be made, however, it is possible to improve on the accuracy of Hooke's Law. Such a situation might arise where the manufacturing and loading history are fairly well known.

B.2 Accounting for stress relaxation

It has been shown in Appendix B.1.4 that for a laminate with unknown history it is not possible to properly account for Poisson's effects and so there is little point in attempting analyses more sophisticated than the use of Hooke's Law. If, however, estimates can be made of the thermal, shrinkage and preload strains it is possible to account for Poisson's effects and hence to make improved estimates of longitudinal fibre stress. These stresses are based on the assumption of matrix elasticity. The matrix exhibits viscous behaviour, however, and so the effects of stress relaxation through viscous flow need to be considered.

At low stresses, the polymer matrix of GFRP can be described using linear viscoelasticity. Residual stresses acting between the fibre and matrix relax over time as viscous stresses dissipate. Once the viscous stresses have dissipated, however, elastic stresses remain. It is these stresses that are determined with the theory[167] used in this work. The calculated stress results are those that remain after all viscous stresses have dissipated.

At higher stresses the assumption of linear viscoelasticity is not valid, and the matrix behaviour becomes non-linear. Relaxation now occurs as a result of non-linear creep. Since inelastic strains develop, stresses can no longer be calculated using the elasticity approach of Nairn.[167]

In order to accurately estimate the stress state after non-linear creep, it is necessary to model the loading over time. The model clearly needs to accommodate non-linear processes in a radially varying triaxial stress field. In addition, the non-linear rheological properties of the matrix must be known as a function of temperature and cure state. Even if a suitable model is readily available, the effort required to obtain the necessary matrix information renders this approach impractical unless this is the focus of the investigation.

Although it is tempting to try to use logical analysis to determine boundaries within which the ratio of transverse and longitudinal stresses exist, and so find limits within which the stress state exists after non-linear creep, this is not really possible. It must be appreciated that the transverse stresses vary radially and are linked to longitudinal strains through Poisson's effects. In addition, the stress limits at which non-linear creep become apparent are different in tension and compression.[201] These factors conspire to prevent a simplified approach and it is consequently not possible to make any useful estimate of the radial and circumferential stresses. Depending on the loading and relaxation history, it is possible that they exceed the longitudinal stress or have an opposite sense. Unless the transverse stresses are approximately known, it is not possible to obtain an accurate estimate of the longitudinal stresses, and the only resort is to rely on the use of Hooke's Law with its limitations. Although this is not a desirable situation, this problem is not unique to this particular measurement technique. No measurement technique that does not measure all three components of the triaxial stress state can estimate the longitudinal stress state under these conditions.

APPENDIX C Calculation of strain gauge results

The measured data were logged in two channels; temperature and strain. Both channels were recorded in the form of a voltage and required conversion to physical values. Each of the two channels is considered in turn.

C.1 Temperature

The temperature within the oven was obtained using the following equation:

$$T = 10V \tag{C.1}$$

where T corresponds to the temperature (in °C) and V corresponds to the output voltage of the LM35D temperature sensor (in V). The equation presented above has an accuracy of ±0.9°C.[186]

C.2 Strain

It was not possible to measure the thermal strain of a specimen directly and so the method of Jeronimidis and Parkyn[21] was used. Strains were measured relative to the thermal strain of an AISI 4340 steel specimen. The measured strain was then added to the known thermal strain of the steel to determine the overall thermal strain of the specimens.

C.2.1 Thermal strain of AISI 4340 steel

The coefficient of thermal expansion of the steel specimen is not constant with temperature. The data describing this variation[187] are given in the form of average coefficients of thermal expansion between 20°C and a range of additional temperatures and are presented in Table C.1.

Table C.1: Coefficients of thermal expansion for AISI 4340 steel

Initial temperature (°C)	Final temperature (°C)	Average CTE over range ($\mu\epsilon$/°C)
20	-150	10.4
20	-100	11.2
20	200	12.4
20	400	13.6
20	600	14.3

By multiplying the average coefficient of thermal expansion between 20°C and any temperature by the difference in these temperatures, it is possible to obtain the thermal strain relative to that at 20°C. The results for the temperatures presented in Table C.1 are presented in Table C.2 .

Table C.2: Thermal expansion of AISI 4340 steel

Final temperature (°C)	Change in temperature relative to 20°C (°C)	Average CTE over range ($\mu\epsilon$/°C)	Thermal strain relative to 20°C ($\mu\epsilon$)
-150	-170	10.4	-1777
-100	-120	11.2	-1328
20	0	—	0
200	180	12.4	2232
400	380	13.6	5170
600	580	14.3	8293

The thermal strain at any temperature, relative to that at 20°C, can be estimated by fitting a curve through the data presented in the first and last columns of Table C.2. A cubic equation of the form shown in equation C.2 results in a coefficient of determination, R^2 of 0.999995.

$$\epsilon_{st_{thermal}} = -3.435 \cdot 10^{-6} \cdot T^3 + 7.008 \cdot 10^{-3} \cdot T^2 + 11.29 \cdot T - 258.1 \qquad \text{(C.2)}$$

where $\epsilon_{st_{thermal}}$ corresponds to the thermal strain of the steel (in $\mu\epsilon$) and T corresponds to the temperature (in °C). In order to determine the strain at any temperature, T, relative to a reference temperature of 25°C, equation C.2 must be evaluated at a temperature of 25°C and then subtracted from equation C.2, yielding the following equation:

$$\epsilon_{st_{thermal}} = -3.435 \cdot 10^{-6} \cdot T^3 + 7.008 \cdot 10^{-3} \cdot T^2 + 11.29 \cdot T - 286.5 \qquad \text{(C.3)}$$

C.2.2 Strain of specimen relative to AISI 4340

Prior to converting the measured voltages to strain values, the voltage corresponding to the measured strain was offset to give 0.0 mV at the reference temperature of 25°C. This was achieved by performing a linear regression through the voltage against temperature data at temperatures less than 50°C, where the data display good linearity. The best fit value of the voltage at 25°C [i] was consequentially determined and hence subtracted from all voltage measurements prior to processing.

The change in measured voltage relative to that at 25°C was then converted to strain using the following equation:

$$\epsilon_{measured} = \frac{V}{2 \cdot 10} \cdot \epsilon_{max} \qquad \text{(C.4)}$$

where $\epsilon_{measured}$ corresponds to the measured strain (in $\mu\epsilon$), V corresponds to the amplifier output voltage (in Volts) and ϵ_{max} corresponds to a calibrated value at an amplifier output of 10.000V. ϵ_{max} is equal to 1000 $\mu\epsilon$ for all specimens except those of cast resin, which has high thermal expansion and thus required the use of a different setting on the amplifier, in which case the value corresponds to 10000 $\mu\epsilon$. The overall value of strain is divided by 2 because the bridge has two active gauges on the material under investigation.

The output from the strain-gauge amplifier was calibrated by the manufacturer using a gauge factor of 2.05. In reality, gauges with a nominal gauge factor of 2.11 at 24°C were used. This value changes with temperature, the temperature coefficient of the gauge factor being listed as 0.8±0.5%/100°C. This information can be readily incorporated into equation C.4 in the following form:

[i] As a result of experimental scatter, this value did not necessarily correspond to a measured value at 25°C.

$$\epsilon_{measured} = \frac{V}{2 \cdot 10} \cdot \epsilon_{max} \cdot \frac{2.05}{2.11 \cdot (1 + \frac{T-24}{100} \cdot 0.008)} \tag{C.5}$$

where T corresponds to the temperature at which measurement is taking place.

C.2.3 Overall strain

The overall strain of the specimens was found by adding the measured strain relative to that of AISI 4340 steel to the calculated thermal response of the steel at any temperature. The overall thermal response of the specimens was consequently found by adding equations C.3 and C.5 as follows:

$$\epsilon = \epsilon_{st_{thermal}} + \epsilon_{measured} \tag{C.6}$$

APPENDIX D Calibration of test rig

Calibration of the test rig relied on the assumption that the measured specimen strain could be related to the output voltage of the displacement sensor and the oven temperature through equation 5.1, repeated below for clarity:

$$\Delta\epsilon_{cal} = C_1(\Delta V_{cal}) + C_2(\Delta T_{cal}) + C_3(\Delta V_{cal})(\Delta T_{cal}) + C_4(\Delta V_{cal})^2 + C_5(\Delta T_{cal})^2$$

where $\Delta\epsilon_{cal}$ corresponds to the measured change in thermal strain (in $\mu\epsilon$) relative to the strain at the reference temperature of 25°C, ΔT_{cal} corresponds to the change in temperature (in °C) relative to the reference temperature and ΔV_{cal} corresponds to the change in displacement sensor output voltage (in mV) relative to that at the reference temperature. The coefficients C_1 to C_5 correspond to calibration constants. Since the sample length of each specimen was the same, it was not necessary to directly account for specimen length in the calibration process.

Reference specimens of commercially pure copper (C10200), commercially pure aluminium (1100), AISI 4340 steel and graphite (Ellor+20) were tested within the rig and the unknown values of the coefficients C_1 to C_5 were then adjusted to obtain the best fit to the thermal expansion data for these materials. Clearly, the thermal expansion of each of the reference materials at any temperature is required for this process. The method whereby these data were obtained is discussed in the next section.

D.1 Thermal strain of reference materials

The method of obtaining the relationship between thermal strain and temperature has been illustrated in detail for AISI 4340 steel in Appendix C.2.1. The relevant

information required to obtain the results for the remaining reference materials is given in the following sections.

D.1.1 Aluminium

The variation in coefficient of thermal expansion for commercially pure aluminium (1100)[195] is presented in Table D.1.

Table D.1: Coefficients of thermal expansion for Aluminium 1100

Initial temperature (°C)	Final temperature (°C)	Average CTE over range ($\mu\epsilon$/°C)
20	-50	21.8
20	100	23.6
20	200	24.5
20	300	25.5

The data presented in Table D.1 allow the calculation of the thermal strain relative to 20°C. This information is presented in Table D.2 .

Table D.2: Thermal expansion of Aluminium 1100

Temperature (°C)	Thermal strain relative to 20°C ($\mu\epsilon$)
-50	-1526
20	0
100	1888
200	4410
300	7140

Fitting a cubic equation to the data presented in Table D.2 allows the thermal strain at any temperature relative to 20°C to be estimated:

$$\epsilon_{al_{thermal}} = -1.435 \cdot 10^{-6} \cdot T^3 + 1.065 \cdot 10^{-2} \cdot T^2 + 22.21 \cdot T - 443.7 \qquad \text{(D.1)}$$

where $\epsilon_{al_{thermal}}$ corresponds to the thermal strain of the aluminium (in $\mu\epsilon$) and T corresponds to the temperature (in °C). This equation results in a coefficient of determination, R^2 of 0.999999. By evaluating equation D.1 at a temperature of

25°C and then subtracting the result from the same equation, the strain at any temperature, T, relative to a reference temperature of 25°C can be calculated:

$$\epsilon_{al_{thermal}} = -1.435 \cdot 10^{-6} \cdot T^3 + 1.065 \cdot 10^{-2} \cdot T^2 + 22.21 \cdot T - 561.9 \qquad \text{(D.2)}$$

D.1.2 Copper

Table D.3 presents the variation in coefficient of thermal expansion for commercially pure copper (C10200).[195]

Table D.3: Coefficients of thermal expansion for Copper C10200

Initial temperature (°C)	Final temperature (°C)	Average CTE over range ($\mu\epsilon$/°C)
20	100	17.0
20	200	17.3
20	300	17.7

The data presented in Table D.3 allow the calculation of the thermal strain relative to 20°C. This information is presented in Table D.4 .

Table D.4: Thermal expansion of Copper C10200

Temperature (°C)	Thermal strain relative to 20°C ($\mu\epsilon$)
20	0
100	1360
200	3114
300	4956

Fitting a cubic equation to the data presented in Table D.4 allows the thermal strain at any temperature relative to 20°C to be estimated:

$$\epsilon_{cu_{thermal}} = 5.000 \cdot 10^{-6} \cdot T^3 + 1.400 \cdot 10^{-3} \cdot T^2 + 16.77 \cdot T - 336.0 \qquad \text{(D.3)}$$

where $\epsilon_{cu_{thermal}}$ corresponds to the thermal strain of the copper (in $\mu\epsilon$) and T corresponds to the temperature (in °C). By evaluating equation D.3 at a temperature

of 25°C and then subtracting the result from the same equation, the strain at any temperature, T, relative to a reference temperature of 25°C can be calculated:

$$\epsilon_{cu_{thermal}} = 5.000 \cdot 10^{-6} \cdot T^3 + 1.400 \cdot 10^{-3} \cdot T^2 + 16.77 \cdot T - 420.0 \tag{D.4}$$

D.1.3 Graphite

The manufacturer's data-sheet[202] lists the linear coefficient of thermal expansion for Ellor+20 graphite as 5.0 $\mu\epsilon$/°C between 20°C and 1000°C. The operating region of the test rig occupied only a small part of this temperature range and consequently it was decided that a more accurate value would be obtained by measuring the thermal expansion by means of strain gauges.

Two strain gauges were affixed to opposite sides of a sample of Ellor+20 graphite using Kyowa PC-6 high temperature strain gauge adhesive. The gauges were connected to the bridge used for the work described in section 5.2.2.3. Again, the strain gauges were connected so as to eliminate a bending response.

The specimen was then tested according to the method described in section 5.2.3. Results were processed according to the method described in Appendix C except that the strain gauge measurements were corrected to incorporate the effects of transverse sensitivity prior to being added to the known thermal response of the AISI 4340 steel.

The correction factor associated with transverse sensitivity can be obtained by considering two strain gauges mounted orthogonal to each other. In this case, the actual strains can be related to the measured strains as follows:[188]

$$\begin{aligned} \epsilon_{x_{relative}} &= \frac{(1 - \mu_\circ K)(\epsilon_{x_{measured}} - K\epsilon_{y_{measured}})}{1 - K^2} \\ \epsilon_{y_{relative}} &= \frac{(1 - \mu_\circ K)(\epsilon_{y_{measured}} - K\epsilon_{x_{measured}})}{1 - K^2} \end{aligned} \tag{D.5}$$

where $\epsilon_{x_{relative}}$ and $\epsilon_{y_{relative}}$ correspond to the relative thermal strains relative to those of AISI 4340 steel in the x and y directions respectively, $\epsilon_{x_{measured}}$ and $\epsilon_{y_{measured}}$ correspond to the measured strains in the x and y directions respectively. K corresponds to the transverse sensitivity coefficient of the gauge, in this case 0.4%, and $\mu_\circ$ is equal to the Poisson's ratio of the standard calibration material used by the

manufacturer, in this case, 0.285. Since the material is isotropic,[202] the thermal strain in both the x and y directions is the same and so equation D.5 can be written as follows:

$$\epsilon_{relative} = \frac{(1 - \mu_{\circ} K)\epsilon_{measured}}{1 + K} \tag{D.6}$$

or simplified to:

$$\epsilon_{relative} = 0.99488\epsilon_{measured} \tag{D.7}$$

The strain gauge measurements obtained from equation C.5 were thus corrected using equation D.7 and added to the thermal response of the steel given by equation C.3. A cubic equation was then fitted to the thermal strain and temperature data yielding the following relationship:

$$\epsilon_{graphite_{thermal}} = -7.367 \cdot 10^{-6} \cdot T^3 + 4.958 \cdot 10^{-3} \cdot T^2 + 3.780 \cdot T - 97.55 \tag{D.8}$$

where $\epsilon_{graphite_{thermal}}$ corresponds to the thermal strain of the graphite (in $\mu\epsilon$) and T corresponds to the temperature (in °C). This equation results in a coefficient of determination, R^2 of 0.999990.

D.2 Calculation of coefficients C_1 to C_5 for the initial rig

A set of values for the coefficients C_1 to C_5 was initially assumed. Using the assumed set of coefficients, the error between the known strain and the strain calculated using equation 5.1 was determined for every datum point of each reference material. These errors were then squared and summed together. By adjusting the values of the coefficients, the value of the sum varied. The best fit was taken to correspond to the minimum value of the sum. The values of coefficients C_1 to C_5 that resulted in the best fit are listed in Table D.5.

A comparison between the known thermal expansion of the reference specimens and calibrated measurements obtained from equation 5.1 using the calibration coefficients of Table D.5 is illustrated in Figure 5.14.

Table D.5: Best-fit calibration coefficients for the initial test rig

$$
\begin{aligned}
C_1 &= \text{-}9.6790\mu\epsilon/\text{mV} \\
C_2 &= 19.879\mu\epsilon/^{\circ}\text{C} \\
C_3 &= 6.7400{\cdot}10^{-3}\mu\epsilon/^{\circ}\text{C/mV} \\
C_4 &= 4.8826{\cdot}10^{-4}\mu\epsilon/\text{mV}^2 \\
C_5 &= \text{-}1.0488{\cdot}10^{-5}\mu\epsilon/^{\circ}\text{C}^2
\end{aligned}
$$

D.3 Accuracy of calibration of the initial test rig

The calibration was performed using a total of 6973 datum points. Its accuracy can be assessed by comparing the measured strain at each datum point to its corresponding reference strain. A perfect fit should yield a one-to-one correspondence. It can be seen from Figure D.1 that although a perfect correspondence does not exist, the fit is extremely good and the two sets of data are almost indistinguishable. The coefficient of determination, R^2, of the fit is 0.999967. The standard deviation from the reference strain is calculated as 4.5 $\mu\epsilon$. The maximum and minimum residuals are +9 $\mu\epsilon$ and -11 $\mu\epsilon$ respectively.

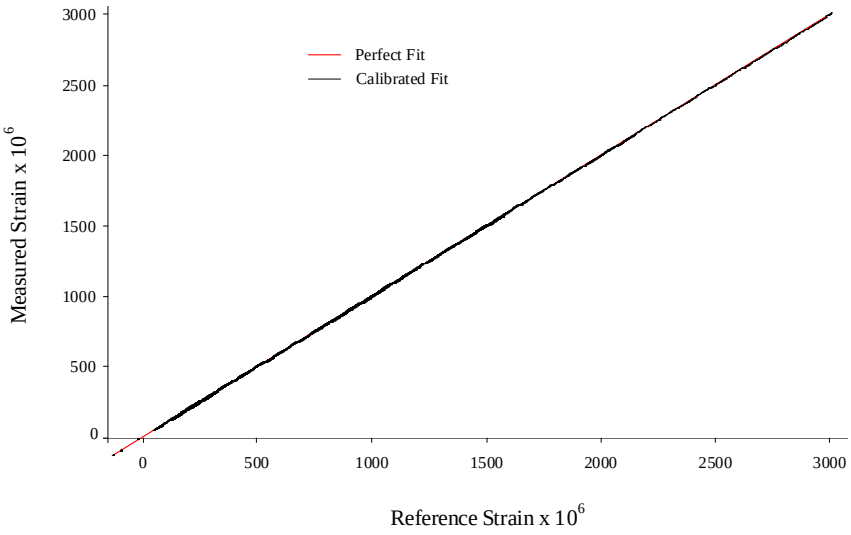


Figure D.1: Comparison of measured strains with reference strains

D.4 Calculation of coefficients C_1 to C_5 for the final rig

In exactly the same way as was done for the initial test rig, a set of values for the coefficients C_1 to C_5 was assumed. Using these values, the error between the

known strain and the strain calculated using equation 5.1 was determined for every datum point of each reference material. These errors were then squared and summed together. By adjusting the values of the coefficients, the value of the sum varied. The best fit was taken to correspond to the minimum value of the sum. The values of coefficients C_1 to C_5 that resulted in the best fit are listed in Table D.6.

Table D.6: Best-fit calibration coefficients for the final test rig

$$
\begin{aligned}
C_1 &= \text{-}8.7695\mu\epsilon/\text{mV} \\
C_2 &= 21.033\mu\epsilon/^\circ\text{C} \\
C_3 &= 5.5874{\cdot}10^{-3}\mu\epsilon/^\circ\text{C/mV} \\
C_4 &= 1.2930{\cdot}10^{-3}\mu\epsilon/\text{mV}^2 \\
C_5 &= \text{-}1.2467{\cdot}10^{-3}\mu\epsilon/^\circ\text{C}^2
\end{aligned}
$$

A comparison between the known thermal expansion of the reference specimens and calibrated measurements obtained from equation 5.1 using the calibration coefficients of Table D.6 is illustrated in Figure 5.33.

D.5 Accuracy of calibration of the final test rig

In this case the calibration was performed using a total of 17651 datum points. The accuracy of the resulting calibration function can be assessed by comparing the measured strain at each datum point to its corresponding reference strain. A perfect fit should yield a one-to-one correspondence. It can be seen from Figure D.2 that a perfect correspondence does not exist, but that the fit is very good. The measured data generally obscure the underlying line corresponding to a perfect fit. The coefficient of determination, R^2, of the fit is 0.999845. The standard deviation from the reference strain is calculated as 9.0 $\mu\epsilon$. The maximum and minimum residuals are +27 $\mu\epsilon$ and -35 $\mu\epsilon$ respectively.

The fit of this calibration is not as good as that of the calibration for the initial version of the test rig. This is expected, because each reference specimen was tested three times and was removed and refitted between tests. Slight inaccuracies are introduced by this process, and consequently every test of a particular reference material does not yield identical results. In addition, the measured strains of the Ellor+20 graphite show more variability than those of the other reference materials. This is because this material is brittle and the clamping pressure in the grips was lower than that of the other specimen types to prevent specimen fracture. The low pressure combined with the "lubricating" properties of graphite are believed to have

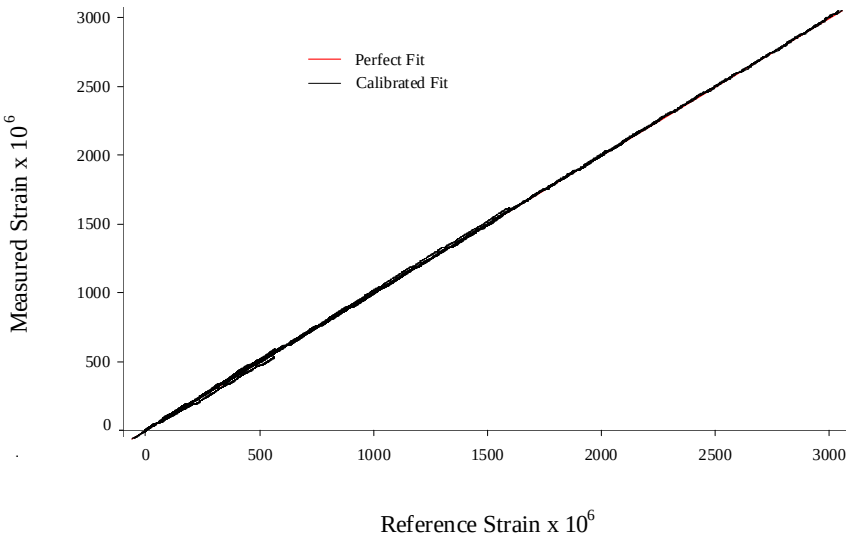


Figure D.2: Comparison of measured strains with reference strains

resulted in a small amount of specimen misalignment with resultant variability in the measured results. Overall the variability caused by these effects is not significant, however, and the correlation of the calibration with reference data is very good.

APPENDIX E Shear-lag analysis

A method of supporting the target in a way that enabled accurate measurements was required. It was known that dimpling of the specimen end faces resulted from the transfer of compatibility loads between the fibres and resin system near the ends of the specimen. Inclusion of the dimpling displacements in the change in specimen length resulted in erroneous strain measurements. It was thus necessary to predict the distance over which the compatibility loads acted so that a proper support mechanism could be designed that excluded the dimpling displacements from measurement.

An analytical solution to this problem allows a rapid understanding and facilitates parametric studies. The "shear lag" analysis presented by Nairn[54] was used for this purpose. The method considers the interaction of multiple concentric cylinders. In its simplest form the method considers two cylinders, the innermost of which has zero internal radius and represents the fibre whilst the outer cylinder represents the surrounding matrix. The specimen configuration used in the current work does not match that assumed in the analysis. Each specimen can, however, be considered to consist of a large number of approximately cylindrical elements packed together. As a result, the analysis method is adequate for obtaining approximate solutions. Due to necessary assumptions in the formulation of the analysis, the analytical technique is accurate to within 20% when calculating the average longitudinal stress in the fibre.[54]

Nairn considers the problem of concentric fibre and matrix cylinders of length L with an average applied longitudinal stress of σ_0. The fibre ends are treated as fibre breaks and therefore the end surfaces of the fibres are stress free. The entire applied longitudinal stress is assumed to be applied uniformly over the matrix at a stress level of

$$\sigma_m = \frac{\sigma_0}{V_m} \tag{E.1}$$

where V_m is the volume fraction of the matrix material. The relationship between the average fibre stress σ_f at some longitudinal position z, varying from $-L/2$ to $L/2$, along the fibre and that an infinite distance from the fibre ends, σ_{f_∞}, is given by:

$$\frac{\sigma_f}{\sigma_{f_\infty}} = 1 - \frac{\cosh \beta z}{\cosh(\beta L/2)} \tag{E.2}$$

where β is defined as follows:

$$\beta^2 = \frac{2}{r^2 E_f E_m} \left[\frac{E_f V_f + E_m V_m}{V_m/(4G_f) + 1/(2G_m)((1/V_m)\ln(1/V_f) - 1 - (V_m/2))} \right] \tag{E.3}$$

and E_f, G_f, E_m, G_m are the longitudinal and shear moduli of the fibre and matrix respectively. V_f is the volume fraction of the fibre and r is the fibre radius.

The situation described above does not correspond to the situation faced in reality. In this case there is no external loading and the fibres and matrix hold each other in equilibrium. The solution to the actual problem can, however, be recovered by superposition with the "far-field" stresses.[54] The stress transfer mechanism is identical in either situation and consequently, equations E.2 and E.3 can be applied to the current problem.

To customize Equation E.2 to the purposes required for this analysis it can be reformulated so that z varies from 0 to L as follows:

$$\frac{\sigma_f}{\sigma_{f_\infty}} = 1 - \frac{\cosh(\beta(z - L/2))}{\cosh(\beta L/2)} \tag{E.4}$$

The z term of equation E.4 can now be interpreted as the distance from one end of the fibre. The value of z at which 99% of the load has been introduced into the fibres is defined as z_{99}. This can be determined by setting the left hand side of equation E.4 equal to 0.99 and solving for the unknown value of z.

$$z_{99} = L/2 - \frac{1}{\beta} \cosh^{-1} \left[(1 - 0.99) \cosh(\beta L/2) \right] \tag{E.5}$$

Equation E.3 can be reformulated as:

$$\beta = \frac{\gamma}{r} \tag{E.6}$$

which requires that γ, corresponding to a measure of the ratio of shear and longitudinal stiffness, is defined as:

$$\gamma = \sqrt{\frac{2}{E_f E_m}\left[\frac{E_f V_f + E_m V_m}{V_m/(4G_f) + 1/(2G_m)((1/V_m)\ln(1/V_f) - 1 - (V_m/2))}\right]} \tag{E.7}$$

Substituting equation E.6 into equation E.5 allows z_{99} to be written in terms of the fibre diameter d and aspect ratio $\Re$, defined as L/d, as follows:

$$z_{99} = d\,\frac{1}{2}\left[\Re - \frac{1}{\gamma}\cosh^{-1}(0.01\cosh(\gamma\,\Re))\right] \tag{E.8}$$

Equation E.8 can then be used to define, in fibre diameters, the distance from the fibre end at which "far-field" conditions are achieved.

The choice of analysis approach depends to a very large extent on the degree of fibre dispersion within the laminate. In the case of uniformly distributed fibres, each fibre can be considered to act in isolation and shear lag effects are thus local to the fibre. The directly measured fibre properties can then be used in the analysis. If the fibres within the rovings are unable to disperse properly, however, it is not possible to use the measured fibre properties in equations E.7 and E.8 unchanged. In the limit, it can be assumed that each roving is unable to disperse at all, and in fact remains as a fibre bundle of maximum fibre packing. Under these conditions, it is more appropriate to determine equivalent properties for the fibre bundle as a whole and perform the shear lag analysis with equivalent properties for the fibre bundle.

By performing the analysis at both limits of fibre dispersion it is possible to calculate the possible range over which "shear-lag" effects have an effect.

E.1 Analysis of laminate with maximum fibre dispersion

In the case of the ideal unidirectional laminate, the fibres are uniformly dispersed throughout the laminate. Shear lag effects are thus local to the surrounds of each

fibre and equations E.7 and E.8 can be applied directly once the material properties, fibre volume fraction and fibre aspect ratio are known. The elastic properties of the E-glass fibres do not change significantly in the temperature range under consideration and can be found as:

$E_f = 72000$ MPa[185]

$\nu_f = 0.22$[191]

Since E-glass is isotropic, the shear modulus can be found as:

$G_f = \frac{E_f}{2(1+\nu_f)} = 29508$ MPa

The fibre volume fraction is taken as the nominal value for all specimens, 0.4.

E.1.1 Ambient temperature

At ambient temperature the longitudinal modulus of the resin system in question (Derakane 411-350) is:

$E_m = 3200$ MPa[178]

The resin system is isotropic and so using a Poisson's ratio of 0.411[203] the shear modulus is calculated as:

$G_m = \frac{E_m}{2(1+\nu_m)} = 1134$ MPa

All the terms in equation E.7 are now known and so γ can be determined:

$\gamma = 1.592$

The value of z_{99} as defined in equation E.8 clearly depends on the aspect ratio of the fibre, $\Re$. The fibres are continuous and so their aspect ratio is high. By considering a range of aspect ratios it is found that z_{99} is not sensitive to the aspect ratio at values greater than about 6. For all realistic values of the aspect ratio, the value of z_{99} is thus invariant:

$$z_{99} = 1.445d$$

For the nominal 15 μm fibre diameter used to manufacture the specimens, this means that 99% of the compatibility load between fibre and matrix is transferred within 21.7 μm.

E.1.2 Elevated temperatures

At temperatures around T_g the resin system exhibits viscoelastic behaviour. The analysis of Nairn[54] is based on elasticity and cannot properly consider this type of behaviour. The rate at which the specimen temperature was increased (6°C per hour), however, was chosen to be low enough that viscous effects could largely dissipate as they developed. It is thus possible to assume that the constraint loads transferred between the fibres and the matrix by viscous effects are negligible and that the only forces acting within the specimen are the remaining elastic loads. These loads can be considered using Nairn's analysis provided that the correct elastic properties of the resin system are used at the temperature of analysis.

At temperatures well above the glass transition temperature of the resin system, its modulus decreases considerably:

$$E_m \approx 20 \text{ MPa}$$

Assuming that the Poisson's ratio of 0.411 at ambient conditions remains unchanged, the shear modulus is calculated as:

$$G_m = \frac{E_m}{2(1+\nu_m)} \approx 7 \text{ MPa}$$

and hence γ can be determined as:

$$\gamma = 1.580$$

Again it is found that z_{99} is not sensitive to the aspect ratio at values greater than about 6. For all realistic values of the aspect ratio, the value of z_{99} is thus invariant:

$$z_{99} = 1.456d$$

For the nominal 15 μm fibre diameter used to manufacture the specimens, this means that 99% of the compatibility load between fibre and matrix is transferred within 21.9 μm.

It is interesting to note that the distance over which the load is transferred does not change significantly, even though the properties of the resin system are significantly lower at high temperatures. Although this seems counterintuitive, Nairn[54] discusses this effect and shows that a shear-lag analysis predicts the existence of an "iso-transfer" fibre volume fraction of 42% where the load transfer rate is independent of the ratio between fibre and resin moduli. Since the fibre modulus is constant with temperature, the load transfer rate is independent of resin modulus at this fibre volume fraction. The specimens in question have a nominal fibre volume fraction of 40% and it is therefore not surprising that the load transfer distance is not significantly affected by the drop in resin stiffness.

E.2 Analysis of laminate with minimum fibre dispersion

In this analysis it is assumed that the fibres of each roving are bunched together as densely as possible so that the effects of minimum fibre dispersion can be assessed. The analysis technique assumes that each fibre bundle can be treated as a single fibre as long as the mechanical properties of the bundle are calculated correctly and as long as the correct bundle volume fraction is used. Prediction of the mechanical properties and bundle volume fraction requires that the fibre volume fraction within each bundle is known.

E.2.1 Fibre volume fraction within each roving bundle

Under the conditions of maximum fibre packing the fibres exist in a hexagonal packing arrangement. The maximum fibre volume fraction within the fibre bundle is found by considering a hexagonal unit cell as shown in Figure E.1:

The area of the equilateral triangle A_Δ having sides of length l shown in Figure E.1 is calculated as follows:

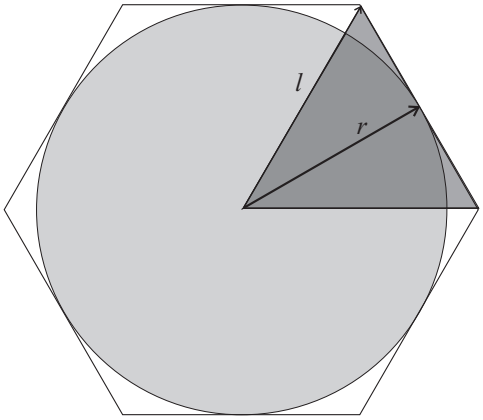


Figure E.1: Fibre within hexagonal unit cell

$$\begin{aligned} A_\Delta &= \frac{1}{2} \cdot l \cdot l \cos 30^\circ \\ &= \frac{1}{2}\frac{\sqrt{3}}{2} l^2 \\ &= \frac{\sqrt{3}}{4} l^2 \end{aligned}$$

But

$$r = l \cos 30^\circ$$

and so

$$l = r \frac{2}{\sqrt{3}}$$

The area of the equilateral triangle A_Δ can therefore be written as:

$$A_\Delta = \frac{1}{\sqrt{3}} r^2$$

The area of the circle $A_\circ$ inscribed within the hexagon shown in Figure E.1 is given by:

$$A_\circ = \pi r^2$$

The hexagonal unit cell consists of six equilateral triangles and so the maximum volume fraction $V_{f_{max}}$ of the fibre within the cell can be found as follows:

$$\begin{aligned} V_{f_{max}} &= \frac{A_\circ}{6A_\Delta} \\ &= \frac{\pi r^2}{\frac{6}{\sqrt{3}} r^2} \\ &= \frac{\pi}{2\sqrt{3}} \\ &\approx 0.9069 \end{aligned}$$

E.2.2 Volume fraction of roving bundles within specimen

The overall quantity of glass fibre is constant, no matter how it is distributed within the specimen. This information is used to determine the volume fraction of the roving bundles within the specimen. Each of these fibres has a fibre volume fraction of 0.9069 and so the following relationship holds:

$$V_f = 0.9069 \bar{V}_b$$

where V_f refers to the nominal fibre volume fraction of the specimens and $\bar{V}_b$ refers to the bundle volume fraction within the specimens. Equation E.9 leads to:

$$\begin{aligned} \bar{V}_b &= \frac{V_f}{0.9069} \\ &= \frac{0.4}{0.9069} \\ &= 0.441 \end{aligned}$$

The volume fraction of the fibre bundles within the specimen is thus 44.1% and consequently the volume fraction of the matrix $\bar{V}_m$ around the bundles is found as follows:

$$\begin{aligned} \bar{V}_m &= 1 - 0.441 \\ &= 0.559 \end{aligned}$$

E.2.3 Diameter of fibre bundles

The diameter of each fibre bundle or roving is found by first determining its cross sectional area. The cross sectional area of each roving can be found by considering its linear mass or "tex" value, denoted by t. The tex value of glass fibre rovings relates to the mass, in grams, of a kilometre of roving. The density of glass is taken as 2600 kg/m^3 [185] and so the cross sectional area of the glass fibres within each roving, A_g, can thus be found as:

$$\begin{aligned} A_g &= \frac{t \cdot 10^{-6}}{2600} \text{ m}^2 \\ A_g &= \frac{t}{2600} \text{ mm}^2 \end{aligned}$$

The effective area, $\bar{A}$, of the roving bundle can be obtained by dividing the cross sectional area of the glass by the fibre volume fraction within the bundle:

$$\begin{aligned} \bar{A} &= \frac{t}{2600 \cdot 0.9069} \text{ mm}^2 \\ &= \frac{t}{2358} \text{ mm}^2 \end{aligned}$$

The effective diameter, $\bar{D}$, of the roving bundle can be found by considering the relationship for the area of a circle:

$$\bar{A} = \pi \frac{\bar{D}^2}{4}$$

and so

$$\bar{D} = \sqrt{\frac{4\bar{A}}{\pi}}$$

By including the expression for the effective area of the roving bundle, $\bar{A}$, we get:

$$\begin{aligned} \bar{D} &= \sqrt{\frac{4t}{2358\pi}} \text{ mm} \\ &= \frac{\sqrt{t}}{43.03} \text{ mm} \end{aligned}$$

The Owens-Corning T111A rovings used in in the manufacture of the specimens have a linear mass of 400 tex. Consequently the effective diameter of the glass roving can be found as:

$$\begin{aligned} \bar{D} &= \frac{\sqrt{400}}{43.03} \text{ mm} \\ &= 0.465 \text{ mm} \end{aligned}$$

E.2.4 Ambient temperature

The elastic properties of the E-glass fibres at ambient temperatures are determined in Appendix E.1 as:

$E_f = 72000$ MPa

$G_f = 29508$ MPa

At ambient temperature the longitudinal and shear moduli of Derakane 411-350 epoxy vinyl-ester resin are determined in Appendix E.1.1 as:

$E_m = 3200$ MPa

$G_m = 1134$ MPa

The resin properties must be combined with those of the glass to determine the effective elastic properties of the roving bundle. Using "rule of mixtures" approximations,[191] estimates of the effective longitudinal and shear moduli of the fibre bundles, $\bar{E}_b$ and $\bar{G}_b$ respectively, can be obtained for the maximum possible fibre volume fraction of 0.9069:

$$\begin{aligned}\bar{E_b} &= E_f V_{f_{max}} + E_m(1 - V_{f_{max}}) \\ &= 72000 \cdot 0.9069 + 3200 \cdot (1 - 0.9069) \text{ MPa} \\ &= 65595 \text{ MPa}\end{aligned}$$

$$\begin{aligned}\bar{G_b} &= \left(\frac{V_{f_{max}}}{G_f} + \frac{1 - V_{f_{max}}}{G_m}\right)^{-1} \\ &= \left(\frac{0.9069}{29508} + \frac{1 - 0.9069}{1134}\right)^{-1} \text{ MPa} \\ &= 8863 \text{ MPa}\end{aligned}$$

The elastic properties of the unreinforced resin are known, and the effective volume fraction for the fibre bundles $\bar{V_b}$ and unreinforced resin $\bar{V_m}$ are known from Appendix E.2.2 to be 0.441 and 0.559 respectively. All necessary terms in equation E.7 are now known and so γ can be determined:

$$\gamma = 1.733$$

The value of z_{99} as defined in equation E.8 depends on the aspect ratio of the fibre bundle, $\Re$. The fibre bundles are continuous and so their aspect ratio is high. By considering a range of aspect ratios it is found that z_{99} is not sensitive to the aspect ratio of the bundle at values greater than about 6. For all realistic values of the aspect ratio, the value of z_{99} is thus invariant:

$$z_{99} = 1.328\bar{D}$$

For the estimated diameter of the fibre bundles, 0.465 mm, this means that 99% of the compatibility load between fibre and matrix is transferred within 0.62 mm.

E.2.5 Elevated temperature

As discussed in Appendix E.1.2, the analysis of Nairn cannot strictly be used at high temperatures due to the presence of viscous flow in the polymer matrix. Since the rate of temperature increase is very low, however, it is possible to assume that the viscous loads transferring constraints between fibre and matrix largely dissipate

as they develop. The only loads acting between the fibres and matrix are thus the remaining elastic loads. These can be considered using Nairn's approach if the elastic properties appropriate for the matrix at the analysis temperature are used.

At temperatures well above the glass transition temperature of the resin, the elastic properties drop considerably to those estimated in Appendix E.1.2:

$$E_m \approx 20 \text{ MPa}$$

$$G_m \approx 7 \text{ MPa}$$

The elastic properties of the E-glass fibres do not change significantly in the temperature range under consideration and remain the same as those determined in Appendix E.1:

$$E_f = 72000 \text{ MPa}$$

$$G_f = 29508 \text{ MPa}$$

The resin properties must be combined with those of the glass to determine the effective elastic properties of the roving bundle. Using "rule of mixtures" approximations,[191] estimates of the longitudinal and shear moduli of the fibre bundles can be obtained for the maximum possible fibre volume fraction of 0.9069:

$$\begin{aligned} \bar{E_b} &= E_f V_{f_{max}} + E_m(1 - V_{f_{max}}) \\ &= 72000 \cdot 0.9069 + 20 \cdot (1 - 0.9069) \text{ MPa} \\ &= 65299 \text{ MPa} \end{aligned}$$

$$\begin{aligned} \bar{G_b} &= \left(\frac{V_{f_{max}}}{G_f} + \frac{1 - V_{f_{max}}}{G_m} \right)^{-1} \\ &= \left(\frac{0.9069}{29508} + \frac{1 - 0.9069}{7} \right)^{-1} \text{ MPa} \\ &= 75 \text{ MPa} \end{aligned}$$

The elastic properties of the unreinforced resin are known, and the effective volume fraction for the fibre bundles $\bar{V_b}$ and unreinforced resin $\bar{V_m}$ are known from Appendix E.2.2 to be 0.441 and 0.559 respectively. All necessary terms in equation E.7 are now known and so γ can be determined:

$$\gamma = 1.719$$

Again it is found that the value of z_{99} is not sensitive to the aspect ratio at values greater than about 6. For all realistic values of the aspect ratio, the value of z_{99} is thus invariant:

$$z_{99} = 1.339\bar{D}$$

For the estimated diameter of the fibre bundles, 0.465 mm, this means that 99% of the compatibility load between fibre and matrix is transferred within 0.63 mm.

Again it is interesting to note that the distance over which the load is transferred does not change significantly, even though the properties of the resin system are significantly lower at high temperatures. This effect is, however, expected since the effective volume fraction of the fibre bundles within the laminate is 44.1%. This value is fairly close to the "iso-stress" fibre volume fraction of 42%, calculated by Nairn,[54] at which the load transfer rate is independent of resin stiffness.

E.3 Selection of results for design purposes

The "shear-lag" analysis used to estimate the load transfer distance has been performed at the two possible limits of fibre dispersion. When the fibres are fully dispersed, it is possible to consider each fibre acting in isolation within the matrix. When the fibres have minimum dispersion, each roving can be considered to act as a fibre bundle with maximum packing density. In either case, the load transfer distance is less than one and a half diameters. The difference is that the effective diameter of the fibre bundle is approximately thirty times greater than that of a single fibre. As a consequence, the load transfer distance increases accordingly. Load transfer occurs within 22 μm for a laminate with uniformly dispersed fibres but this distance increases to to 0.63 mm with minimal fibre dispersion.

The glass rovings used in the manufacture of the specimens were drawn from the inner diameter of the creel and were consequently twisted along their length. The twist in the rovings prevented the uniform dispersion of the fibres throughout the specimen. Tensioning of the rovings during the manufacture of the preloaded and annealed specimens exacerbated this effect and caused the fibres of each roving to be tightly bunched together. As a consequence, it is probably more appropriate to

make use of the results for minimal fibre dispersion rather than to assume that the fibres were uniformly dispersed.

In either case, however, these results are the more conservative and should be used for the purposes of design estimates.

APPENDIX F Calculation of residual fibre strain

The residual fibre strain can be determined directly if the assumption is made that the response of the composite coincides with that of unstressed glass fibre at high temperatures. It is possible however, to improve on the accuracy of the measured strains if the actual matrix properties are considered. When this done, the measured strains in the composite are shifted upwards relative to the locus of zero stress in the glass fibre. The offset, $\Delta\epsilon$, is measured relative to the strain at T_2, and can be found using equation 4.4:

$$\Delta\epsilon \approx \left(\frac{E_{m_2}}{E_f}\frac{V_m}{V_f}\right)\Big((\alpha_{m_{02}} - \alpha_f)\,(T_2 - T_0) - s_{0-2}\Big)$$

where E_{m_2} is the matrix modulus at T_2, and T_0 is the stress-free temperature. E_f, α_f, V_m and V_f have their usual meanings. The effective coefficient of thermal expansion of the matrix between T_0 and T_2 is denoted by $\alpha_{m_{02}}$. The polymerization shrinkage of the matrix between T_0 and T_2 is represented by s_{0-2}.

T_2 must be located within the region where the modulus of the resin has reduced to low values. For the purposes of this work, the temperature at which the locus of zero stress is tangent to the measured data of each specimen, as indicated in Figure 6.12, is taken as T_2. The offset, $\Delta\epsilon$, of the measured strains is taken relative to the measured strain at the point of tangency.

Since $\alpha_{m_{02}}$ is defined as $\frac{\epsilon_{0-2}}{T_2-T_0}$, where ϵ_{0-2} is the change in thermal strain of the matrix between T_0 and T_2, equation 4.4 can be rewritten as follows:

$$\Delta\epsilon \approx \left(\frac{E_{m_2}}{E_f}\frac{V_m}{V_f}\right)\Big(\epsilon_{0-2} - s_{0-2} - \alpha_f\,(T_2 - T_0)\Big) \tag{F.1}$$

The polymerization shrinkage of the matrix, s_{0-2}, can be defined as the difference

in its strain response between the first and subsequent heatings. This concept is illustrated in Figure F.1 for a material previously post-cured at $T_{post-cure}$.

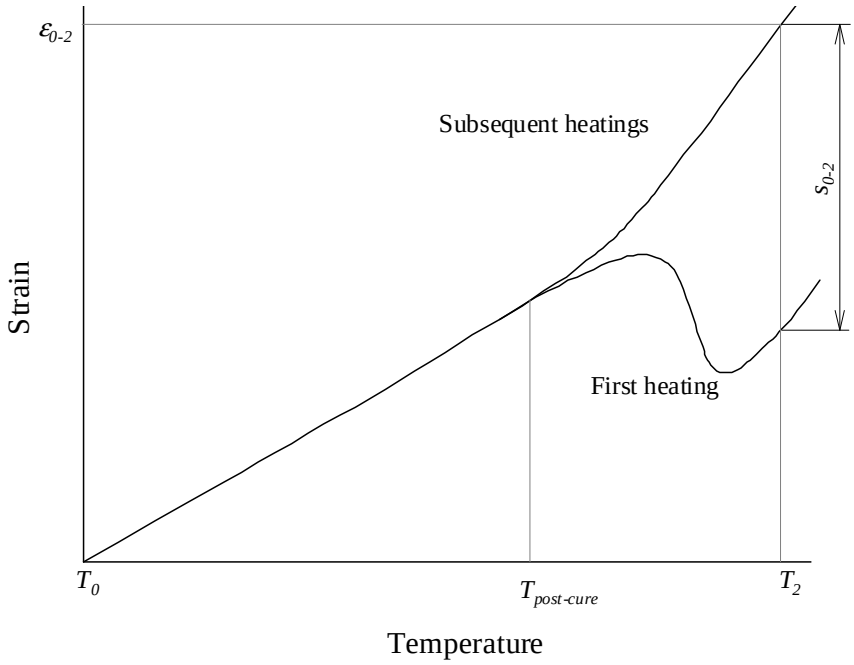


Figure F.1: Definition of ϵ_{0-2} and s_{0-2}

It is thus apparent from Figure F.1 that the term $\epsilon_{0-2} - s_{0-2}$ in equation F.1 simply defines the strain of the matrix during its first heating from T_0 to T_2. This information is consequently required for use in equation F.1.

F.1 Matrix strain between T_0 and T_2

Measurements of the matrix strain were made the first time it was heated above the post-cure temperature. This information has been presented in Figure 6.1. To facilitate calculation of the strain offset of each specimen, curves were fitted to the experimental data in two temperature ranges. The first range, from 0℃ up to 95℃, encompasses the entirety of the expected stress-free temperatures, T_0[i]. The second range, from 108℃ up to 120℃, includes the temperature at the point of tangency of every specimen and thereby the full range of T_2. Since measured data only exist from 17.3℃ upwards, the fitted curve below this value is extrapolated from the measured data. The fitted curves are shown with the measured data in Figure F.2.

The curve fitted to the experimental data between 17.3℃ and 95℃ can be written

[i]Initial estimates of T_0 can be obtained from Figure 6.16.

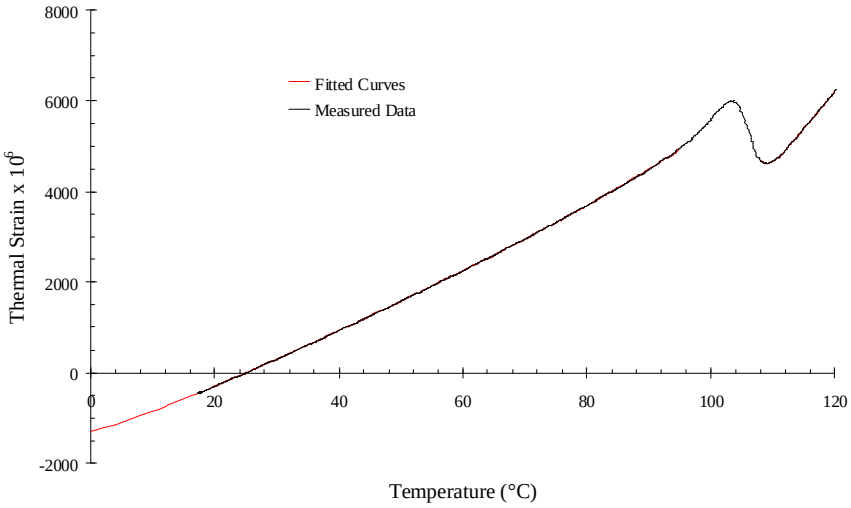


Figure F.2: Correlation between measured strains and fitted curves

as a polynomial series as follows:

$$\epsilon_0 = \sum_{m=0}^{4} C_m \left(\frac{T_0}{100} \right)^m \tag{F.2}$$

where T_0 is in ℃ and where the constants, C_m, are defined as follows:

C_0 = -1310.15 $\mu\epsilon$
C_1 = 4202.39 $\mu\epsilon$
C_2 = 5496.15 $\mu\epsilon$
C_3 = -6342.76 $\mu\epsilon$
C_4 = 3341.78 $\mu\epsilon$

The curve fitted to the experimental data between 108℃ and 120℃ can be written as a trigonometric series as follows:

$$\epsilon_2 = C_0 - \sum_{m=1}^{6} C_m \sin \left(\frac{m\pi}{2} \frac{120 - T_2}{120 - 108} \right) \tag{F.3}$$

where T_2 is in ℃ and where the constants, C_m, are as follows:

C_0 = 6209.20 $\mu\epsilon$
C_1 = 903.14 $\mu\epsilon$
C_2 = 769.15 $\mu\epsilon$
C_3 = -597.13 $\mu\epsilon$
C_4 = 137.74 $\mu\epsilon$
C_5 = 34.66 $\mu\epsilon$
C_6 = -21.20 $\mu\epsilon$

The term $\epsilon_{0-2} - s_{0-2}$ in equation F.1 can now be found by subtracting the strain at T_0, given by equation F.2, from the strain at T_2, given by equation F.3, resulting in an equation in terms of T_0 and T_2.

F.2 Matrix modulus at T_2

The variation in the modulus of Derakane 411-350 epoxy vinyl-ester was measured by Mr. K.M. Midor and is presented in Figure 4.1. To aid in the calculation of E_{m_2}, a curve was fitted to these data between 110°C and 140°C. The fitted curve is shown with the measured data in Figure F.3.

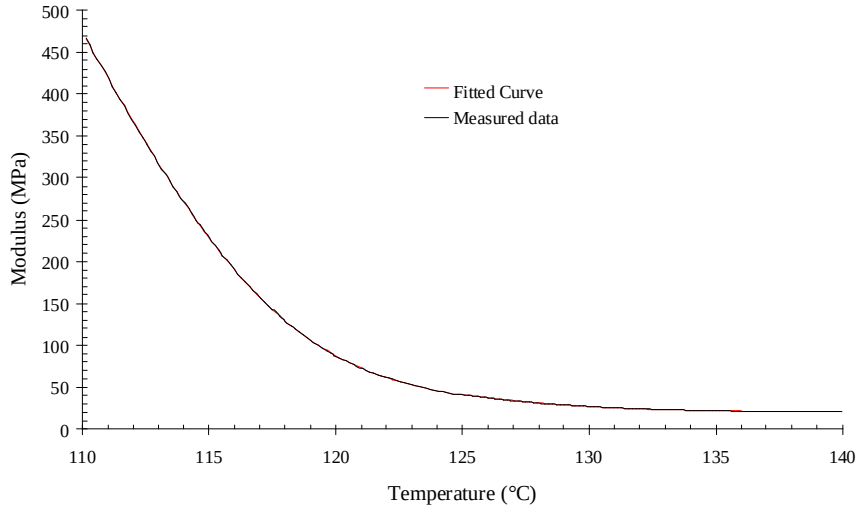


Figure F.3: Correlation between measured matrix modulus and fitted curve

The fitted curve is represented by the following trigonometric series:

$$E_{m_2} = C_0 - \sum_{m=1}^{6} C_m \sin\left(\frac{m\pi}{2} \frac{T_2 - 110}{140 - 110}\right) \tag{F.4}$$

where T_2 is in ℃ and where the constants, C_m, are as follows:

$C_0 = 472.94\ \mu\epsilon$
$C_1 = 322.43\ \mu\epsilon$
$C_2 = 327.16\ \mu\epsilon$
$C_3 = -203.50\ \mu\epsilon$
$C_4 = 209.39\ \mu\epsilon$
$C_5 = -74.32\ \mu\epsilon$
$C_6 = 31.96\ \mu\epsilon$

The data in Figure F.3 were measured using DMA equipment at an oscillation frequency of 2.0 Hz. The rate of temperature increase used in the current work is only 6℃ per hour, however. Since the measured material properties of a polymer depend on the time scales (or frequency) used in testing,[180] it is not appropriate to use the data presented in Figure 4.1 to estimate the modulus of the matrix at T_2.

The time-temperature superposition principle, however, implies that there is a direct correspondence between time (or frequency) and temperature. This means that the data measured at one time scale can be used at another time scale if they are shifted by a constant amount along the temperature axis.[19] Provided that an estimate can be obtained for the appropriate temperature shift, it is possible to use DMA data to estimate the matrix modulus when it is heated at 6℃ per hour.

The temperature shift can be estimated by comparing T_g measurements obtained from the two testing methods. If the assumption is made that the difference in measured T_g is only a consequence of differing time scales it is possible to find the temperature through which the DMA measurements should be shifted.

Tan δ measurements were obtained during the DMA test and are presented in Figure F.4. The maximum value of tan δ occurs around 121.5℃, indicating that T_g is in this region also.[180]

T_g can also be determined from measurements of the coefficient of thermal expansion. The rate of thermal expansion changes considerably at temperatures around T_g.[180] T_g is usually taken as the temperature at the intersection of linear fits to thermal strain data each side of the curved region near T_g.[182] Although Figure 6.1 presents thermal strain measurements for unreinforced resin, these data are inappropriate for use in finding the T_g because these measurements were taken as the resin was heated. Customarily T_g measurements are obtained as the material is cooled, allowing it to tend towards thermodynamic equilibrium. Measurements taken as the material is

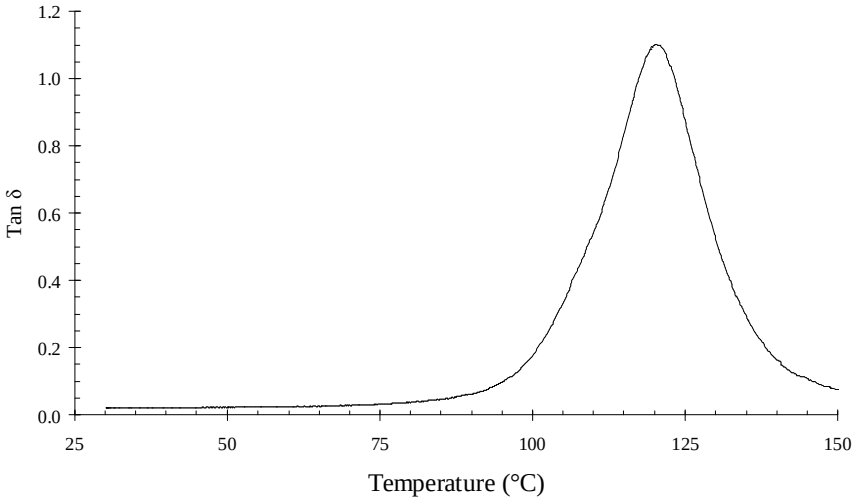


Figure F.4: Temperature variation of tan δ in Derakane 411-350

heated reflect the molecular state frozen in as the resin was previously cooled. Since the rate of cooling was not monitored, the thermal expansion data presented in Figure 6.1 are of no use in finding the appropriate temperature shift to allow the DMA data to be used in the current work.

The temperature offset can still be estimated, however, if it is assumed that the measured thermal response of the composite becomes linear at temperatures greater than T_g. This assumption seems reasonable since the elastic modulus, as measured using DMA, is less than 2% of its room temperature value above 121.5℃. The resin consequently cannot significantly affect the thermal response of the composite in this region. The temperature at which the measured thermal response of the composite becomes linear has been determined, and corresponds to the temperature at which the thermal response is tangent to the locus of zero fibre stress. The average value of this temperature is found to be approximately 112.5℃. The difference between these two temperatures is 9℃, taken to correspond to the temperature shift required to make use of time-temperature equivalence. When the composite is heated at a rate of 6℃ per hour, the elastic modulus can thus be found by modifying equation F.4 as follows:

$$E_{m_2} = C_0 - \sum_{m=1}^{6} C_m \sin\left(\frac{m\pi}{2} \frac{T_2 - 110 + \Delta T_{shift}}{140 - 110}\right) \tag{F.5}$$

where the constants, C_m, are the same as those defined for equation F.4 and where ΔT_{shift} is 9℃.

F.3 Calculation of $\Delta\epsilon$

Equation F.1 can be broken into two components. The first corresponds to the difference in the strains of the matrix and fibre:

$$\epsilon_{0-2} - s_{0-2} - \alpha_f (T_2 - T_0) \tag{F.6}$$

Here, $\epsilon_{0-2} - s_{0-2}$ corresponds to the combined change in thermal and shrinkage strains of the matrix between the stress-free temperature, T_0, and the temperature, T_2. The term $\alpha_f (T_2 - T_0)$ corresponds to the change in thermal strain in the fibre between the same temperature limits.

The second component of equation F.1 corresponds to a scaling factor arising from the ratio of fibre and matrix stiffnesses at temperature T_2:

$$\frac{E_{m_2}}{E_f}\frac{V_m}{V_f} \tag{F.7}$$

To find the difference in the fibre and matrix strains (equation F.6) it is necessary to know the stress-free temperature, T_0. The matrix strain, $\epsilon_{0-2} - s_{0-2}$, is equal to the difference between ϵ_2 and ϵ_0 found using equations F.3 and F.2 respectively. It is necessary to know T_0 to evaluate ϵ_0 and also to find the fibre strain. In general though, T_0 is not known but can be found using iterative techniques.

It is initially assumed that $\Delta\epsilon$ is zero, which easily allows the variation in the residual fibre strain with temperature to be obtained for each specimen. This information has been determined and is presented in Figures 6.13 through 6.15. An initial estimate of the stress-free temperature is obtained by finding the temperature at which the measured fibre strain is zero. This is readily done by using linear regression techniques in the region where the residual strain is small[ii].

Once an estimate of T_0 is known, an estimate of the mismatch in fibre and matrix strains can be obtained using equation F.6. When this is combined with the scaling factor of equation F.7, the offset, $\Delta\epsilon$, can be estimated. The scaling factor requires that the matrix modulus, E_{m_2} is known at temperature T_2. This can be found using equation F.5, and so a first estimate of $\Delta\epsilon$ can be obtained from equation F.1.

[ii] The measured residual strain of some of the preloaded specimens does not cut the temperature axis. As a consequence, a quadratic curve is fitted to the data so that it can be extrapolated to obtain an estimate of T_0.

The measured specimen strains are then moved upwards relative to the locus of zero fibre stress by an amount corresponding to $\Delta\epsilon$ and the residual fibre strains are recalculated. An improved estimate of T_0 is thus obtained, allowing an improved estimate of $\Delta\epsilon$. This new estimate of $\Delta\epsilon$ can be used to obtain an even better estimate of T_0. The calculated values of T_0 and $\Delta\epsilon$ converge rapidly to constant values, thereby defining the solution to the problem.

Calculated values of T_0 and $\Delta\epsilon$ for each specimen are presented in Table F.1. T_2 data are also presented since they were required in the calculation of T_0 and $\Delta\epsilon$.

Table F.1: T_0 and $\Delta\epsilon$

	Unloaded			Preloaded			Annealed		
	T_2 (℃)	T_0 (℃)	$\Delta\epsilon$ ($\mu\epsilon$)	T_2 (℃)	T_0 (℃)	$\Delta\epsilon$ ($\mu\epsilon$)	T_2 (℃)	T_0 (℃)	$\Delta\epsilon$ ($\mu\epsilon$)
	112.8	82.2	1.4	110.0	24.8	9.4	112.6	43.1	4.8
	113.7	87.6	0.9	109.7	15.5	11.1	114.4	51.1	3.5
	114.3	82.8	1.3	109.5	7.0	12.5	110.4	38.6	7.2
	112.7	79.5	1.6	109.3	4.1	13.3	114.6	37.4	4.2
	114.2	79.3	1.6	110.2	13.7	10.3	119.5	30.1	3.4
Average		**82.3**	**1.3**		**13.0**	**11.3**		**40.1**	**4.6**
Std deviation		3.0	0.3		7.2	1.4		6.9	1.4

These results are used to correct the measured variation in residual fibre strain. The data presented in Figures 6.13 through 6.15 are accordingly offset upwards by the $\Delta\epsilon$ values presented in Table F.1. The corrected data are presented in Figures F.5 through F.7.

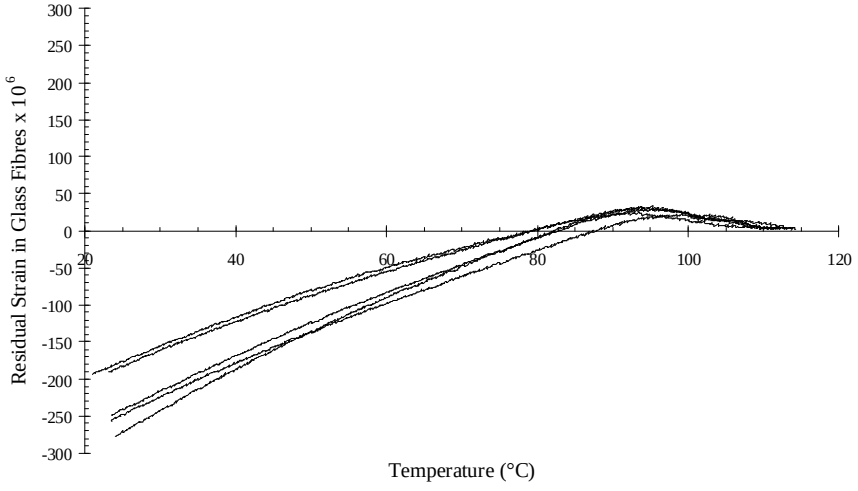


Figure F.5: Residual strain in glass fibres of unloaded specimens

The residual strain at 25℃ is found by performing a linear regression analysis on the data presented in Figures F.5 through F.7 between temperatures of 23℃ and

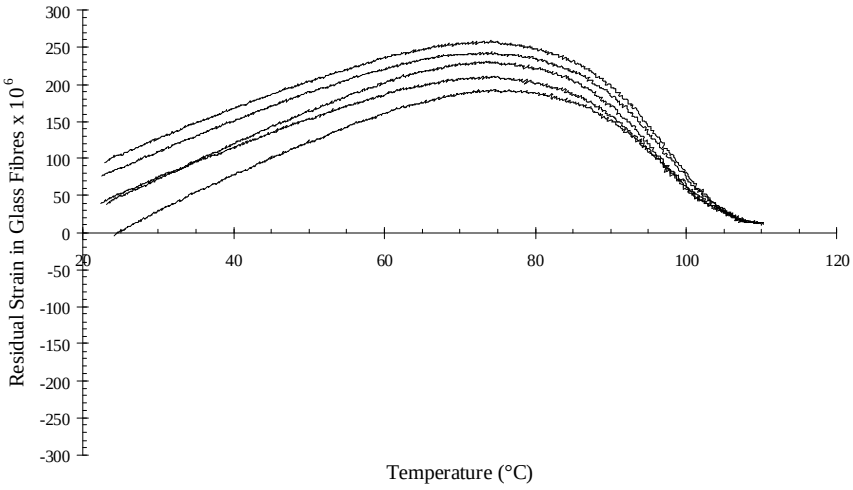


Figure F.6: Residual strain in glass fibres of preloaded specimens

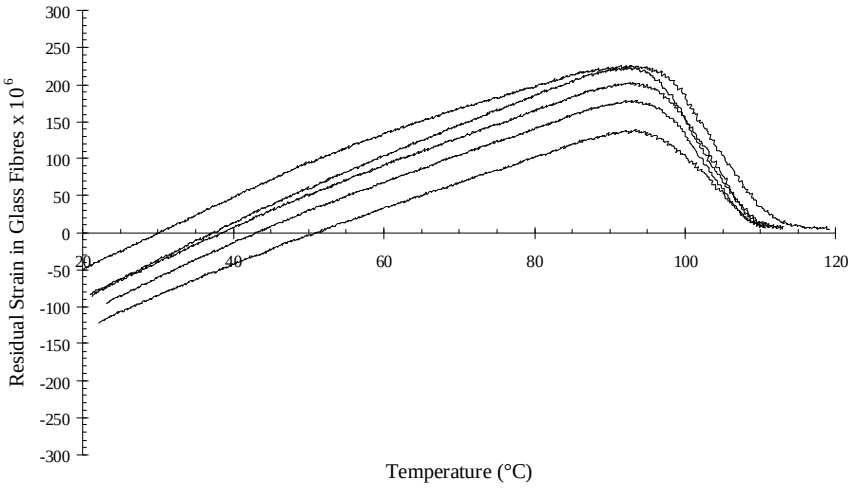


Figure F.7: Residual strain in glass fibres of annealed specimens

27℃. This information is presented in Table F.2.

Table F.2: Residual strain in glass fibres at 25℃

	Unloaded specimens ($\mu\epsilon$)	Preloaded specimens ($\mu\epsilon$)	Annealed specimens ($\mu\epsilon$)
	-272	0	-86
	-248	49	-108
	-242	87	-65
	-183	105	-63
	-176	52	-25
Average	**−224**	**59**	**−69**
Std deviation	42	40	31

APPENDIX G Calculation of measured longitudinal stress at 25°C

Unless the loading and thermal history of a composite laminate is known, it is not possible to obtain estimates of Poisson's effects and hence the stress estimates obtained using Hooke's Law cannot be improved upon. Since the manufacturing process of the specimens used in this work is known, an attempt is made in this appendix to estimate the residual stresses in the fibres and matrix.

Neither the modulus nor Poisson's ratio of the matrix are properly known however, and so some element of uncertainty in the calculated stress values exists. The modulus of the matrix has been measured, but at an oscillation frequency of 2.0 Hz. These data are not appropriate for use when the loading increases only slowly as a consequence of rising temperature. The measured data can be used, however, if the principle of time-temperature equivalence is used. The measured data are thus shifted along the temperature axis by a constant offset.[19] The temperature offset has been estimated in Appendix F as approximately 9°C but this value is not precisely known. The Poisson's ratio of the epoxy vinyl-ester matrix is also not known. It is assumed similar to that of an epoxy and so a value of 0.36[191] is used at room temperature. As the matrix approaches the rubbery state at high temperatures, the value of the Poisson's ratio is expected to tend towards 0.50[174] however. Ideally this analysis should incorporate changes to the Poisson's ratio with temperature. It has been found though, that variations in Poisson's ratio do not play an important role and that a constant value can be used.[174]

G.1 Material properties

Material properties are required before any analysis can be performed and so these are determined first.

The matrix modulus was measured using DMA and curves were fitted to these data over the complete range of testing. Three functions chosen to have identical value and slope at their junction are used. The first function, valid from 25℃ to 70℃, is described as follows:

$$E_m = \sum_{m=0}^{2} C_m \left(\frac{T - 25}{90} \right)^m \tag{G.1}$$

where T is in ℃ and where the constants, C_m, are defined as follows:

C_0 = 3200.00 MPa
C_1 = -484.41 MPa
C_2 = -677.35 MPa

The second function, valid from 70℃ to 115℃ is:

$$E_m = \sum_{m=0}^{2} C_m \left(\frac{T - 25}{90} \right)^m + \sum_{m=0}^{3} C_m \left(1 - \cos \left(\frac{(2m+1)\pi}{2} \, \frac{T - 70}{45} \right) \right) \tag{G.2}$$

where T is also in ℃ and where the constants, C_m, in the polynomial series are defined in equation G.1 and where the constants, C_m, in the trigonometric series are defined as follows:

C_0 = -1890.67 MPa
C_1 = -8.35 MPa
C_2 = 150.99 MPa
C_3 = -67.77 MPa

The third function, valid from 115℃ to 150℃ follows:

$$E_m = \sum_{m=0}^{2} C_m \left(\frac{T - 115}{35} \right)^m + \sum_{m=1}^{7} C_m \left(1 - \cos \left(\frac{m\pi}{2} \, \frac{T - 115}{35} \right) \right) \tag{G.3}$$

where T is also in ℃ and where the constants, C_m, in the polynomial series are defined as follows:

C_0 = 222.4 MPa
C_1 = -1492.6 MPa
C_2 = 746.30 MPa

The constants, C_m, in the trigonometric series are defined as follows:

C_1 = 257.76 MPa
C_2 = 43.79 MPa
C_3 = 11.94 MPa
C_4 = 4.02 MPa
C_5 = 1.64 MPa
C_6 = 0.97 MPa
C_7 = 0.86 MPa

The match between equations G.1 through G.3 and experimental measurements is shown in Figure G.1. It can be seen that the fitted curves represent the measured data extremely well.

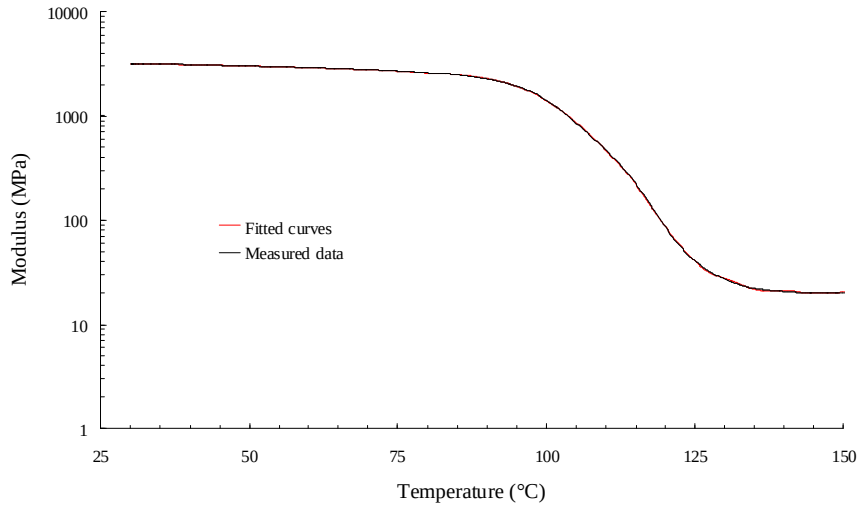


Figure G.1: Correlation between measured modulus and fitted curves

Equations G.1 through G.3 enable the modulus of the matrix, as determined by DMA testing, to be found at any temperature. The experimental data were obtained at an oscillation frequency of 2.0 Hz, however, and so it is not correct to use it for this work, where the loading arises from a slow increase in temperature. Time-temperature equivalence allows data collected at one temperature and time scale to be used at different time scale if the data are shifted along the temperature axis. A temperature shift of 9°C, as estimated in Appendix F, enables data collected using DMA to be used in this work. Equations G.1 through G.3 are consequently modified

such that the T terms in each of the equations are replaced by $T + \Delta T_{shift}$ where ΔT_{shift} is 9℃.

Thermal expansion data for the matrix are obtained by fitting curves to measured data over the complete range of testing. Three equations are used to describe the measured strain response. These equations are selected to have identical values and slopes at the transition point between their regions of validity.

Care must be taken is selecting the appropriate data for curve fitting at temperatures above 92℃. The first time that the matrix is heated above the post-cure temperature, the apparent strain response is a combination of thermal expansion and polymerization shrinkage. Since the specimens were not heated above the post-cure temperature prior to testing, it is expected that their strain response will be affected by polymerization shrinkage as the temperature is increased beyond 92℃. It is consequently necessary to use "thermal expansion" data corresponding to the first time that the matrix is heated into this region. Curves are consequently fitted to "Initial Heating" data in Figure 6.1.

The strain response at temperatures less than 92℃ is described by the following equation:

$$\epsilon = \sum_{m=0}^{4} C_m \left(\frac{T}{100} \right)^m \tag{G.4}$$

where T is in ℃ and where the constants, C_m, are defined as follows:

C_0 = -1310.15 $\mu\epsilon$
C_1 = 4202.39 $\mu\epsilon$
C_2 = 5496.15 $\mu\epsilon$
C_3 = -6342.76 $\mu\epsilon$
C_4 = 3341.78 $\mu\epsilon$

The strain response at temperatures greater than 112℃ is described as follows:

$$\epsilon = \sum_{m=0}^{3} C_m \left(\frac{140 - T}{28} \right)^m \tag{G.5}$$

where T is in ℃ and where the constants, C_m, are defined as follows:

$C_0 = 9655.20\ \mu\epsilon$
$C_1 = \text{-}5094.04\ \mu\epsilon$
$C_2 = 487.39\ \mu\epsilon$
$C_3 = \text{-}146.80\ \mu\epsilon$

From 92℃ to 112℃, the strain response is described by the following equation:

$$\epsilon = \sum_{m=0}^{3} C_m \left(\frac{T - 92}{20} \right)^m + \sum_{m=1}^{10} C_m \left(1 - \cos \left(m\pi \, \frac{T - 92}{20} \right) \right) \qquad \text{(G.6)}$$

where T is also in ℃ and where the constants, C_m, in the polynomial series are defined as follows:

$C_0 = 4662.98\ \mu\epsilon$
$C_1 = 1723.72\ \mu\epsilon$
$C_2 = \text{-}5988.05\ \mu\epsilon$
$C_3 = 4503.10\ \mu\epsilon$

The constants, C_m, in the trigonometric series are defined as follows:

$C_1 = 50.61\ \mu\epsilon$
$C_2 = 689.33\ \mu\epsilon$
$C_3 = \text{-}152.56\ \mu\epsilon$
$C_4 = \text{-}114.72\ \mu\epsilon$
$C_5 = 128.16\ \mu\epsilon$
$C_6 = \text{-}41.33\ \mu\epsilon$
$C_7 = \text{-}11.28\ \mu\epsilon$
$C_8 = 21.69\ \mu\epsilon$
$C_9 = \text{-}13.25\ \mu\epsilon$
$C_{10} = 3.08\ \mu\epsilon$

The correlation between equations G.4 through G.6 and the measured strain data is illustrated in Figure G.2. It is apparent that these equations provide a good approximation to the experimental data.

The Poisson's ratio of the matrix is assumed constant, $\nu_m = 0.36$.[191]

It is assumed that the fibre properties are invariant over the range of testing. The

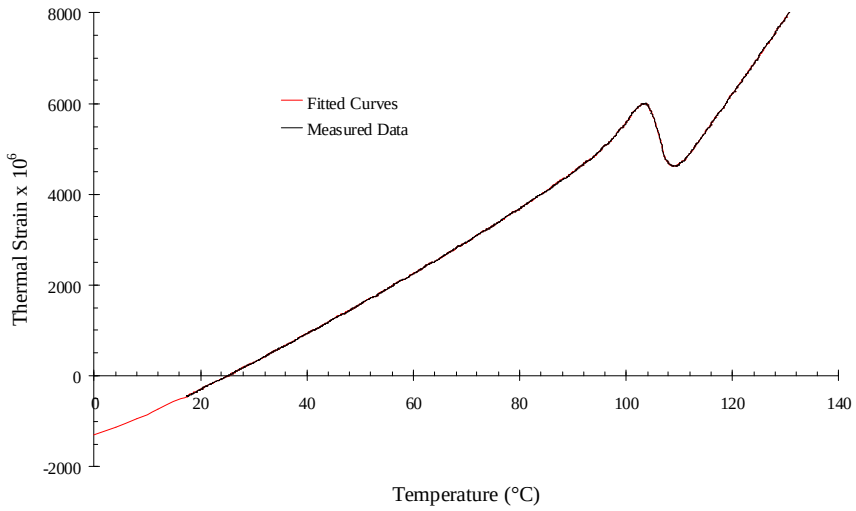


Figure G.2: Correlation between measured strain and fitted curves

elastic properties of the fibre are listed in Table G.1.

Table G.1: Elastic constants of E-glass fibre

E (MPa)	α ($\mu\epsilon$/°C)	ν
72000[185]	5.0[185]	0.22[191]

G.2 Effect of different loads

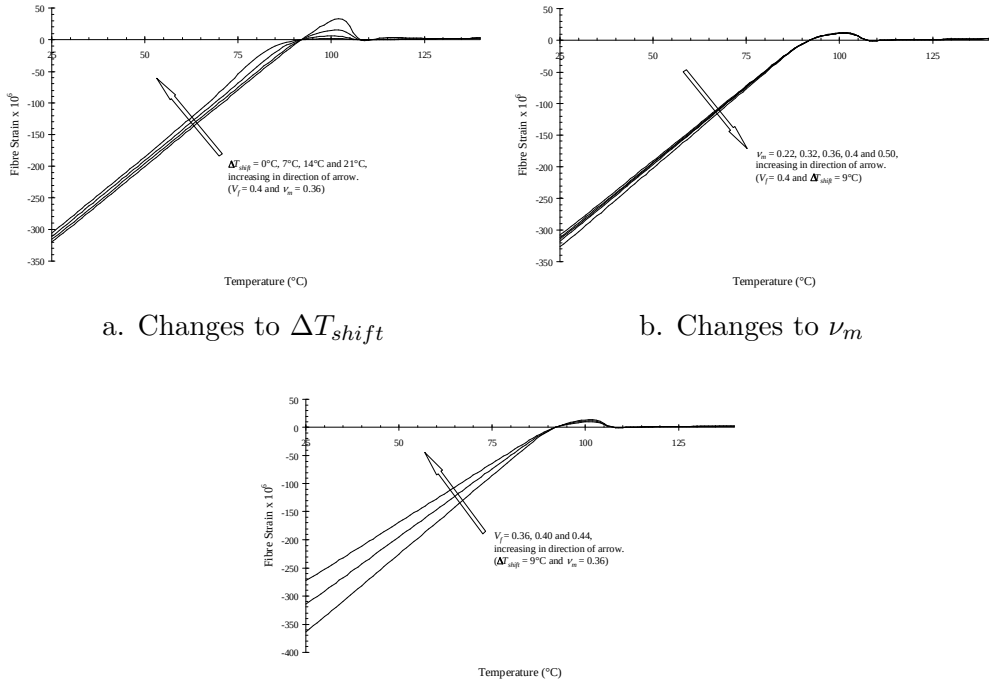
Residual stresses arise from thermal effects, preloading and cure shrinkage. The internal load state arising from each of these is different and is discussed before any attempt is made to estimate the residual stress in the different specimen types.

G.2.1 Thermal strains

The matrix was post-cured at 92°C and so thermal stresses are taken as zero at this temperature. The magnitude of the thermal stresses is larger below the cure temperature than above the cure temperature because the matrix modulus increases as the temperature reduces. These stresses can be calculated using equations B.13 and B.16. The corresponding strains can be determined from the stresses using equation B.17.

The sensitivity of the calculated fibre strain is determined for a range of ΔT_{shift},

ν_m and V_f values and presented in Figure G.3.



a. Changes to ΔT_{shift}

b. Changes to ν_m

c. Changes to V_f

Figure G.3: Response of the fibre strain to changes in matrix and laminate properties

It is apparent from Figure G.3 that thermal strains rapidly decay to negligible values at temperatures above the post-cure temperature. Fibre strains only really become significant at lower temperatures. Discussion of the effects of changes in ΔT_{shift}, ν_m and V_f is consequently limited to this region.

It can be observed from part a. of Figure G.3 that the thermal strain decreases with an increase in ΔT_{shift}. For the presented range of ΔT_{shift}, the slope of the response is independent of ΔT_{shift} at temperatures less than about 65°C. At higher temperatures, the shape of the curve changes for large values of ΔT_{shift}, reflecting the reduction in matrix modulus in this region.

As expected,[174] part b. of Figure G.3 indicates that the thermal response of the fibres is not significantly affected by changes in the matrix Poisson's ratio. Consequently, the lack of accurate knowledge of ν_m seems not to be important.

The effect of changes to V_f is presented in part c. of Figure G.3. It is apparent that the scaling of the response increases significantly with V_f .

By considering equation B.13 it is clear that the ratio between the transverse stresses and longitudinal stresses is simply equal to the ratio of the A_1 and A_3 terms of the

same equation. This ratio is plotted in Figure G.4 as a function of temperature.

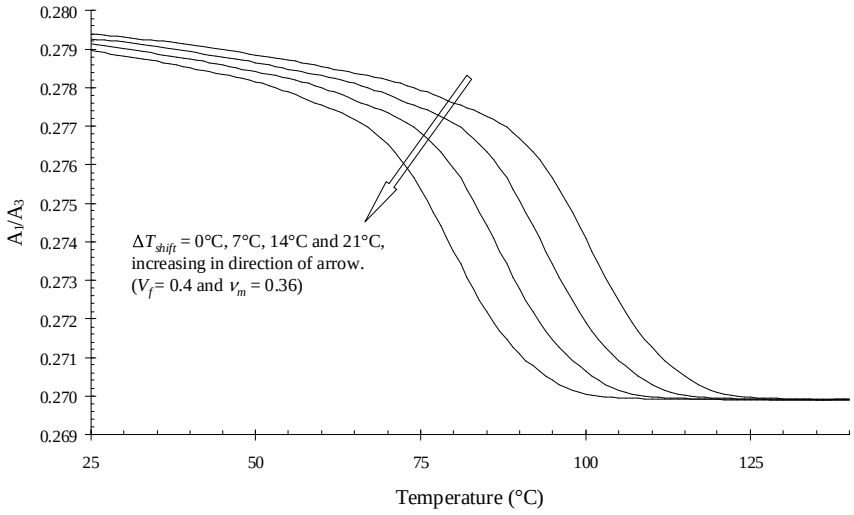


Figure G.4: Variation of $\frac{A_1}{A_3}$ as function of temperature and ΔT_{shift}

It is clear that ratio of A_1 and A_3 varies only slightly with changes in ΔT_{shift}. Between 25℃ and 140℃ the variation is only from 0.2794 to 0.2699. Since the ratio is approximately constant it is treated as such and is given the symbol κ. The ratio between the transverse stresses and the longitudinal stresses can hence be written as follows:

$$\frac{\sigma_r}{\sigma_z} = \frac{\sigma_\theta}{\sigma_z} = \kappa \tag{G.7}$$

where κ varies between 0.2794 and 0.2699.

Since the ratio between the transverse and longitudinal stresses is not significantly affected by changes to ΔT_{shift}, it is apparent that inaccuracies in the estimation of ΔT_{shift} are not material in determining this ratio.

G.2.2 Strains arising as laminate is heated from the cure temperature to the post-cure temperature

The matrix was cured at 60℃ before being post-cured at 92℃ to obtain better cross-linking. Since the matrix vitrified at 60℃, thermal stresses were introduced as the composite material was heated. The matrix coefficient of thermal expansion is greater than that of glass fibre and so tensile stresses were introduced to the fibre. Simultaneously, additional cross-linking took place as the available thermal

energy increased, and so shrinkage strains in the matrix placed additional compressive stresses onto the matrix.

Since the matrix was not fully cross-linked during the transition to the post-cure temperature, the variation in matrix modulus as described by equations G.1 through G.3 is not applicable in this temperature range. Additionally, neither the thermal response of the matrix nor its shrinkage behaviour are known in this region. These factors combine to prevent the prediction of strains that arise as the laminate is heated to the cure temperature.

It is possible to get around this problem by recognizing that cure shrinkage is analogous to thermal strain.[12] In the case of thermal loading, the driver in the development of thermal stresses is the $(\epsilon_{m_{0-1}} - \epsilon_{f_{0-1}})$ term in equation B.16. Since both constituents are isotropic, this term is identical when calculating either A_1 or A_3. When the ratio of A_1 to A_3 is determined, the stress driving term is cancelled and so the ratio is independent of the source of the residual stresses. Since the unconstrained cure shrinkage of the matrix is also isotropic, the same logic applies to cure stresses and consequently the ratio of A_1 to A_3 is identical for both cure stresses and thermal stresses.

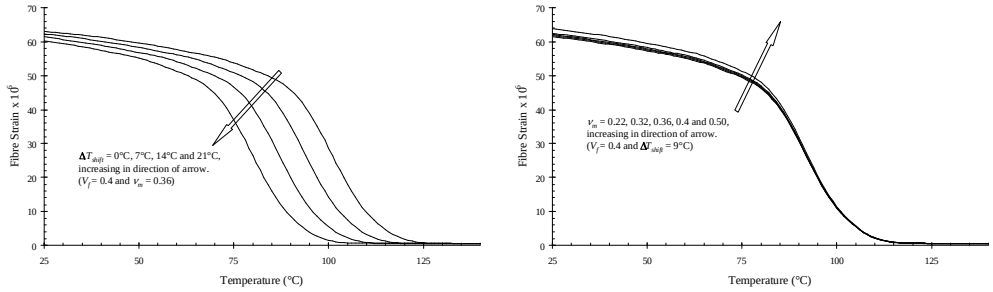
The relationship presented in equation G.7 can therefore be applied to cure stresses. Although the calculations are not presented, in the limit where the modulus of the matrix reduces to zero, the minimum value of $\frac{A_1}{A_3}$ reduces to 0.2698. Equation G.7 is consequently valid even for a matrix that is not fully cross-linked.

If the value of κ is adjusted to the range between 0.2698 to 0.2794, equation G.7 is valid for both curing and thermal stresses.

G.2.3 Preload strains

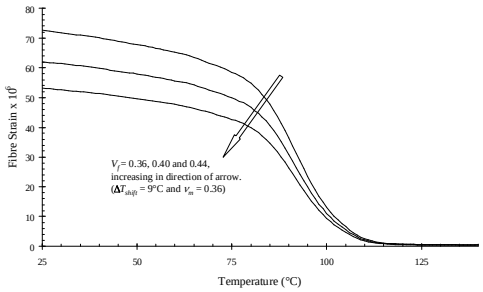
The glass fibres are much stiffer than the polymer matrix and so the release of a fibre preload is largely relieved by straining the matrix in compression. A small component remains, however, which results in fibre stresses that can be calculated using equations B.26 and B.28. Since the resin modulus changes with temperature, the internal equilibrium state varies also with temperature. Provided that the appropriate matrix modulus is used at the temperature of interest, the longitudinal and transverse stresses are easily calculated. The longitudinal strain at this temperature can then be calculated using equation B.17.

The temperature shift, ΔT_{shift}, for time-temperature equivalence and the Poisson's ratio, ν_m, of the matrix are not well known. The fibre volume fraction, V_f, is also not entirely constant. As a consequence it is necessary to estimate the effect that errors in these parameters have on the strain response of the fibres. Plots of the mechanical strain response of the fibres are consequently plotted for a range of different values of each of these parameters. Figure G.5 presents this information for a preload strain of 1000 $\mu\epsilon$ between 25℃ and 140℃.



a. Changes to ΔT_{shift}

b. Changes to ν_m



c. Changes to V_f

Figure G.5: Response of the fibre strain to changes in matrix and laminate properties

From part a. of Figure G.5 it can be seen that the strain response to changes in ΔT_{shift} is significant at temperatures where the matrix modulus varies rapidly with temperature. At temperatures outside this range, including ambient conditions, the strain response is not significant.

Part b. of Figure G.5 indicates that, as expected,[174] significant changes in the Poisson's ratio of the matrix do not have a significant effect on the strain response of the fibres. A similar lack of sensitivity was noted for the strain response resulting from thermal effects. It is thus apparent that the lack of accurate knowledge of the matrix Poisson's ratio does not affect calculated residual strains to any great degree.

As would be expected, part c. of Figure G.5 indicates that changes in V_f directly affect the scale of the strain response and so have a significant effect on its slope.

Interestingly, the ratio between the transverse and longitudinal stresses in the glass fibre is almost unaffected by temperature. To three decimal places the ratio is unaffected by changes to ΔT_{shift} and, for ν_m and V_f equal to 0.36 and 0.40 respectively, can be treated as a constant equal to 0.036. The fact that the temperature shift, ΔT_{shift}, is not precisely known is therefore of no consequence when assessing this ratio.

G.2.4 Relaxation strains

The matrix modulus used in this analysis, described by equations G.1 through G.3, corresponds to the storage modulus obtained from DMA testing. There is consequently an inherent assumption that the stress response of the matrix remains low enough that linear viscoelasticity applies.

The analysis is based purely on elastic stresses and so there is also the assumption that stress changes take place sufficiently slowly that all viscous stresses dissipate to zero. A slow rate of temperature increase, 6℃ per hour, was used in the experimental work to facilitate the dissipation of viscous stresses. The assumption that viscous stresses dissipate is reasonable at temperatures much above T_g since the rate of conformational change is high.[181] The analysis is therefore expected to yield good results in this region.

At temperatures well below T_g, the assumption that viscous stresses have dissipated is not valid since the viscous response is extremely slow in the glassy region. In this region though, the viscous stress is "frozen in" and cannot dissipate and so the response is again elastic.[181]

Between these two extremes however, the magnitude of the viscous modulus is comparatively large and the rates of conformational change are such that the viscous response cannot be neglected. As a consequence, some differences between the measured and predicted strain responses should be expected. It is important to emphasize, however, that differences arise not because viscous relaxation occurs, but rather because it has not fully dissipated.

G.3 Unloaded specimens

G.3.1 Residual fibre stresses at 25℃

To accurately determine the residual stresses in the unloaded specimens at 25℃, it is necessary to know the matrix properties and volume fraction of the composite. The matrix properties are determined by its elastic modulus and Poisson's ratio.

The elastic modulus has been measured, but depends on the temperature shift, ΔT_{shift}, required to use time-temperature equivalence. This value is not precisely known, but as discussed in Appendix G.2.3 the strain response to the release of a fibre preload is not significantly affected by ΔT_{shift} at ambient conditions. Additionally as shown in Appendices G.2.3 through G.2.2, the ratio of the transverse stresses to longitudinal stresses is not heavily dependent on ΔT_{shift}. This information can be used to obtain a reasonably accurate estimate of the residual stress state.

It is also shown in parts b. of Figures G.5 and G.3 that the residual strain is not significantly affected by the Poisson's ratio of the matrix. Errors arising from estimating this quantity are therefore not expected to be large.

Calculation of the residual stresses is determined for the average fibre volume fraction, measured at almost exactly its nominal value, 40%. The fibre volume fraction of individual specimens in this specimen group, however, varies between 36% and 44%.

A small fibre preload was applied to the unloaded specimens even though this was not intended. The fibres of the unloaded specimens were lightly tensioned around a substantial steel frame to prevent their displacement during infusion of the resin. After the resin had cured, it was post-cured overnight at 92℃. During heating of the specimens to the post-cure temperature, the steel frame was also heated. The frame expanded more than the fibres and so strained them in the process. Cross linking of the resin was thus completed with the fibres loaded in a state of tension.

As the specimens were cooled to room temperature, the strain mismatch between the glass fibre and steel frame reduced and the preload was progressively released. The released fibre load was thus increasingly applied to the matrix. At room temperature, the glass fibre and steel frame no longer loaded each other and the released preload was carried only by internal equilibrium within the specimen.

The magnitude of the preload strain, P, can be estimated by considering the differences in thermal strains of the steel frame and glass fibres.

$$P = (\alpha_{st} - \alpha_f)\Delta T \tag{G.8}$$

The temperature change from room temperature to the post-cure temperature, ΔT, is 67℃. Taking CTEs for steel, α_{st}, and glass fibre, α_f, of 12.0 $\mu\epsilon$/℃ and 5.0 $\mu\epsilon$/℃ respectively it is found that the preload strain is approximately 469 $\mu\epsilon$.

The fibre stress at room temperature can then be found by using equations B.26 and B.28 with V_f as 0.40. The matrix properties are those at 25℃, evaluated using equation G.1 where the temperature, T, is replaced by $T + \Delta T_{shift}$ where ΔT_{shift} is estimated as 9℃.

The calculated values of the longitudinal, σ_z, and transverse fibre stresses, σ_r and σ_θ, are 2.13 MPa and 0.08 MPa respectively. The corresponding longitudinal fibre strain is found to be 29 $\mu\epsilon$ using equation B.17.

The average residual strain in the unloaded specimens at 25℃ is listed in Table 6.5 as -224 $\mu\epsilon$. Provided that it is assumed that the residual stresses are small enough that linear viscoelasticity applies, the difference in these two values arises from the combination of thermal and curing strains.

The residual strain caused by this combination is consequently -253 $\mu\epsilon$.

As discussed in Appendix G.2.2, the relationship between the transverse fibre stresses and the longitudinal stresses is the same for both thermal stresses and cure stresses. As a consequence, it does not matter whether the fibre strain arises from thermal stresses or cure shrinkage. The stress state resulting from the combination of thermal effects and cure shrinkage can consequently be estimated by combining equations G.7 and B.17:

$$\sigma_z = \frac{\epsilon_z E_f}{(1 - 2\nu_f \kappa)} \tag{G.9}$$

and

$$\sigma_r = \sigma_\theta = \frac{\kappa \epsilon_z E_f}{(1 - 2\nu_f \kappa)} \tag{G.10}$$

where κ varies between 0.2698 and 0.2794.

Performing the appropriate calculations gives the longitudinal and transverse fibre stresses arising from thermal effects and cure shrinkage as follows:

-20.67 MPa $\geq \sigma_z \geq$ -20.77 MPa

-5.58 MPa $\geq \sigma_r = \sigma_\theta \geq$ -5.80 MPa

These stresses must be added to those arising from the fibre preload, resulting in the following stresses:

-18.54 MPa $\geq \sigma_z \geq$ -18.64 MPa

-5.50 MPa $\geq \sigma_r = \sigma_\theta \geq$ -5.72 MPa

G.3.2 Comparison between theoretical predictions and experiment

The strain response of the specimens is affected by the combination of thermal strains, cure shrinkage and strains resulting from fibre preload. The stress resulting from the preload strains is easily calculated as a function of temperature using equations B.26 and B.28 with P equal to 469 $\mu\epsilon$. The associated longitudinal strain is calculated using equation B.17.

Thermal stresses can be calculated using equations B.13 and B.16 if it is assumed that the temperature at which thermal stresses are zero corresponds to the post-cure temperature of 92℃. The corresponding longitudinal strains can again be calculated using equation B.17.

Insufficient material data are available, however, to directly calculate the stresses resulting from cure shrinkage. This prevents an *a priori* prediction of the fibre stresses and associated longitudinal strains. It is possible, however, to construct a reasonable estimate of such a prediction by incorporating a single strain measurement into the analysis.

Since the strains resulting from cure shrinkage are analogous to thermal strains[12] they can be treated together. Under these circumstances it is not reasonable to expect that the combined stresses are zero at the post-cure temperature. Since the resin cured at 60℃, thermal stresses developed as the material was heated to the post-cure temperature. These stresses are offset to some degree by cure shrinkage,

however, and so the temperature at which the combined thermal and shrinkage stresses are zero increases or decreases relative to the post-cure temperature, depending on whether the shrinkage stresses are greater than or less than the thermal stresses.

An estimate of this temperature can be found by considering the measured strains at 92℃. At this temperature, the average measured strain of the data presented in Figure 6.17 is 24 $\mu\epsilon$. The strain resulting from fibre preload is calculated as 12.4 $\mu\epsilon$. The difference corresponds to the combined effect of thermal strains and cure shrinkage strains. Since the purely thermal strains are zero at this temperature, the difference of 11.6 $\mu\epsilon$ corresponds to the strains introduced by cure shrinkage. Adjusting the temperature at which the combined thermal and shrinkage stresses are zero changes their strains at 92℃. A temperature of approximately 88℃ corresponds to cure strains of 11.6 $\mu\epsilon$. This value was used for further calculation.

The combined thermal and cure stresses are calculated using equations B.13 and B.16 by assuming that the "thermal" stresses are zero at 88℃. These stresses are added to those arising from the fibre preload and the longitudinal fibre strain is calculated using equation B.17.

The resulting variation in fibre strain is compared against experimental measurements in Figure G.6. Since the experimental data presented in Figure 6.17 do not exceed 115℃, data are presented for temperatures between 25℃ and 115℃ only. Results are plotted for a fibre volume fraction of 36%, 40% and 44% corresponding to the approximate minimum fibre volume fraction tested, the average volume fraction and the approximate maximum volume fraction respectively.

The theoretical results presented in Figure G.6 can also be used to obtain matching thermal strain predictions for the composite specimens. The measured strain at any temperature is simply the difference between that at 25℃ and that at the temperature of interest. The difference in strain measurements presented in Figure G.6 is added to the thermal expansion of glass fibre, referenced to 25℃, to obtain the strains corresponding to those that would be experimentally measured. These predictions are compared against actual measurements in Figure G.7.

G.3.3 Residual matrix stresses and strains at 25℃

The longitudinal matrix stress is found by considering force equilibrium in the longitudinal direction:

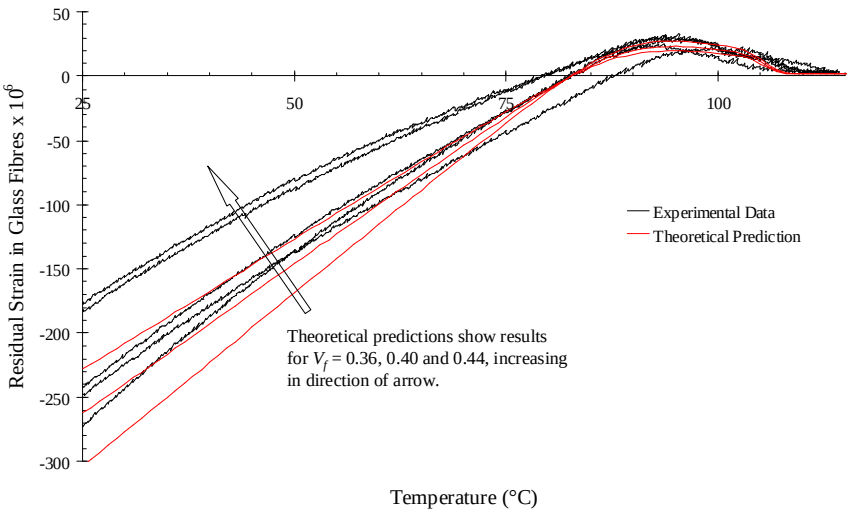


Figure G.6: Comparison between predicted residual strain variation and experimental data

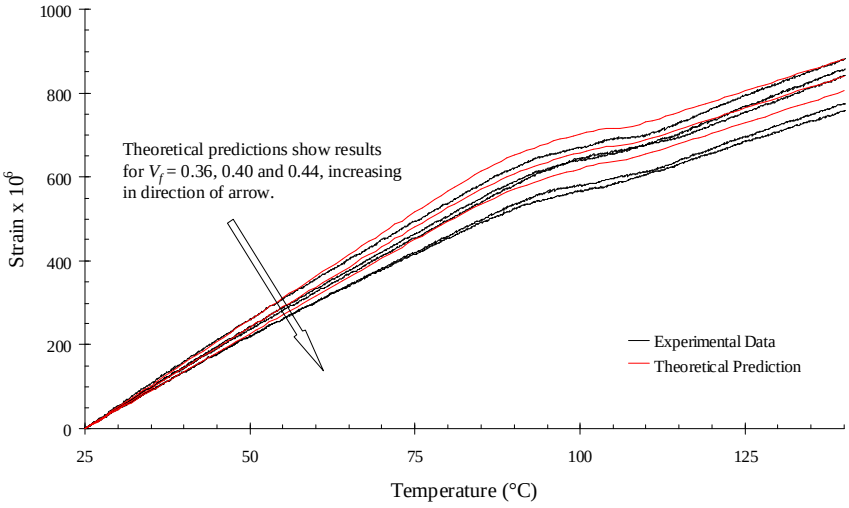


Figure G.7: Comparison between predicted strain variation and experimental data

$$\sigma_m = -\frac{V_f}{V_m}\sigma_f \tag{G.11}$$

By considering the longitudinal fibre stresses presented in Appendix G.3.1, the longitudinal matrix stress can be written as follows:

12.36 MPa $\leq \sigma_m \leq$ 12.43 MPa

The transverse stresses in the matrix are identical to those of the fibre at the fibre/matrix interface, presented in Appendix G.3.1. They vary logarithmically in opposite directions,[167] however, with increasing radial distance from the fibre.

The longitudinal matrix strain is found by considering the free fibre and matrix strains in combination with the known residual strain in the fibre. The stress-free temperature of the matrix has been estimated in Appendix G.3.2 as 88℃. By using equation G.4, the free thermal strain of the matrix on cooling to 25℃ is calculated as -4326 $\mu\epsilon$.

The free thermal strain of the fibre is similarly calculated as -315 $\mu\epsilon$ using its CTE of 5.0 $\mu\epsilon$/℃ and a change in temperature of -63℃. Additionally, a free fibre contraction of -469 $\mu\epsilon$ is expected as a result of releasing the fibre preload.

The mismatch in the free strains of the matrix and fibre is thus calculated as the difference in the free matrix strain and the free fibre strain, 3542 $\mu\epsilon$. Since the free matrix contraction is larger than that of the fibre, it is expected that the matrix is strained in tension and the fibre strained in compression, the sum of the two residual strain magnitudes being equal to the mismatch in free strains. The residual fibre strain has been measured as -224 $\mu\epsilon$ and so the residual strain in the matrix is equal to 3318 $\mu\epsilon$.

G.4 Preloaded specimens

G.4.1 Residual stresses at 25℃

The preloaded specimens are identical to the unloaded specimens except that they are subjected to the effects of an additional fibre preload. The extra preload increases the average measured residual strain in the fibre. The fibre strain, and hence stress, increases sufficiently that it is fair to assume that non-linear creep occurs in the

matrix during the testing of these specimens[i]. The calculated offset strain used to correct for the non-zero matrix properties at high temperatures is consequently incorrect and so cannot be used to improve the accuracy of the measured residual strains. It is thus chosen to use measured strain data that do not rely on the calculation of an offset strain. The data presented in Table 6.3 are consequently used in this analysis.

The value of the average tensile strain at 25℃ in the preloaded specimens is listed in Table 6.3 as 47 $\mu\epsilon$. The best estimate for the unloaded specimens, as presented in Table 6.5, is -224 $\mu\epsilon$. The change in average residual strain relative to the unloaded specimens is therefore 271 $\mu\epsilon$.

The stress state resulting from the additional fibre preload can be estimated using the same technique employed to find the contribution of thermal and cure stresses to the overall stress state of the unloaded specimens:

$$\sigma_z = \frac{\epsilon_z E_f}{(1 - 2\nu_f \kappa)} \tag{G.12}$$

and

$$\sigma_r = \sigma_\theta = \frac{\kappa \epsilon_z E_f}{(1 - 2\nu_f \kappa)} \tag{G.13}$$

where κ is found in Appendix G.2.3 to be 0.036.

Performing the appropriate calculations gives the longitudinal and transverse fibre stresses arising from the deliberate fibre prestrain as follows:

$\sigma_z = 19.82$ MPa

$\sigma_r = \sigma_\theta = 0.71$ MPa

These stresses must be added to those present in the unloaded specimens, resulting in the following stresses:

1.18 MPa $\leq \sigma_z \leq$ 1.28 MPa

-5.01 MPa $\leq \sigma_r = \sigma_\theta \leq$ -4.79 MPa

[i]The annealed specimens were manufactured by allowing non-linear creep to develop in the preloaded specimens. Since the annealing process took place at 80℃, it is fair to assume that non-linear creep can also develop in the preloaded specimens at this temperature.

G.4.2 Comparison between theoretical predictions and experiment

The stress in the fibres of the preloaded specimens can be predicted by adding theoretical estimates of the stresses caused by the fibre preload to the predicted stresses in the unloaded specimens. The stresses arising from the preload can be calculated once the fibre preload, P, is known.

It was attempted to measure P during manufacture of the preloaded specimens. Since the preload could not be measured in the dry fibres it was attempted to infer this value by measuring the contraction of the cured laminate when the preload was released by cutting the laminate from the tensioning frame. Two different methods were used to measure this strain. Strain was measured using five strain gauges mounted on the top surface of the laminate[ii] and also by directly measuring the change in length of the entire laminate over its length of 1560 mm. Unfortunately the strain measurements obtained using these approaches varied erratically with time and cannot be taken as valid.

It is consequently necessary to calculate a value of P that, if applied to the unloaded specimens, would result in the average longitudinal fibre strain measured experimentally. Table 6.5 indicates that the average residual strain in the preloaded fibres is measured as 59 $\mu\epsilon$ at 25°C[iii]. The calculated strain[iv] in the unloaded fibres is -262 $\mu\epsilon$ at the same temperature. The addition of the fibre preload consequently results in a change in longitudinal fibre strain of 321 $\mu\epsilon$.

From equation B.17, and recognizing that $\sigma_r = \sigma_\theta$ it is possible to write the longitudinal fibre strain as follows:

$$\epsilon_z = \frac{\sigma_z - 2\nu_f \sigma_r}{E_f} \tag{G.14}$$

Equation B.26 can be simplified and written so that the stresses are the subject as follows:

[ii] It was not possible to access the lower surface of the laminate to install additional strain gauges that would have eliminated bending sensitivity.

[iii] Table 6.5 is used rather than Table 6.3 since it is pointless to compare predicted results that do account for the non-zero matrix modulus at high temperatures against measurements that neglect this information. Material data used to obtain the predicted results must also be used to obtain the measured results if meaningful comparisons are to be made.

[iv] Theoretical values are used here since the predicted effects of the preload are added to the predicted response of the unloaded specimens.

$$\begin{bmatrix} \sigma_r \\ \sigma_z \end{bmatrix} = \left(\frac{V_f - 1}{V_f}\right) \begin{bmatrix} A_1 \\ A_3 \end{bmatrix} \tag{G.15}$$

If equation B.28 is substituted into equation G.15, the following is true:

$$\begin{bmatrix} \sigma_r \\ \sigma_z \end{bmatrix} = \left(\frac{V_f - 1}{V_f}\right) P \left[A\right]^{-1} \begin{bmatrix} 1 \\ -\nu_f \end{bmatrix} \tag{G.16}$$

For a fibre volume fraction of 40% and matrix properties at 25°C, equation G.16 can be written in the following form:

$$\begin{bmatrix} \sigma_r \\ \sigma_z \end{bmatrix} = \frac{-3P}{2} \begin{bmatrix} -288.7 & -821.5 \\ -3154.3 & -577.4 \end{bmatrix} \begin{bmatrix} 1 \\ -0.22 \end{bmatrix} \text{MPa} \tag{G.17}$$

which gives

$$\begin{bmatrix} \sigma_r \\ \sigma_z \end{bmatrix} = \begin{bmatrix} 161.9 \\ 4540.9 \end{bmatrix} P \text{ MPa} \tag{G.18}$$

Equation G.14 can now be written as follows:

$$\begin{aligned} \epsilon_z &= \frac{4540.9 - 2 \cdot 0.22 \cdot 161.9}{72000} P \\ &= \frac{P}{16.11} \end{aligned} \tag{G.19}$$

Since the change in longitudinal strain is 321 $\mu\epsilon$, the additional preload strain, P, can now be calculated as follows:

$$\begin{aligned} P &= 16.11 \cdot 321 \ \mu\epsilon \\ &= 5171 \ \mu\epsilon \end{aligned}$$

The preload strain is constant irrespective of fibre volume fraction, and so the additional stresses at any temperature can be found using equations B.26 and B.28. The associated fibre strains can be found using equation B.15 and added to those

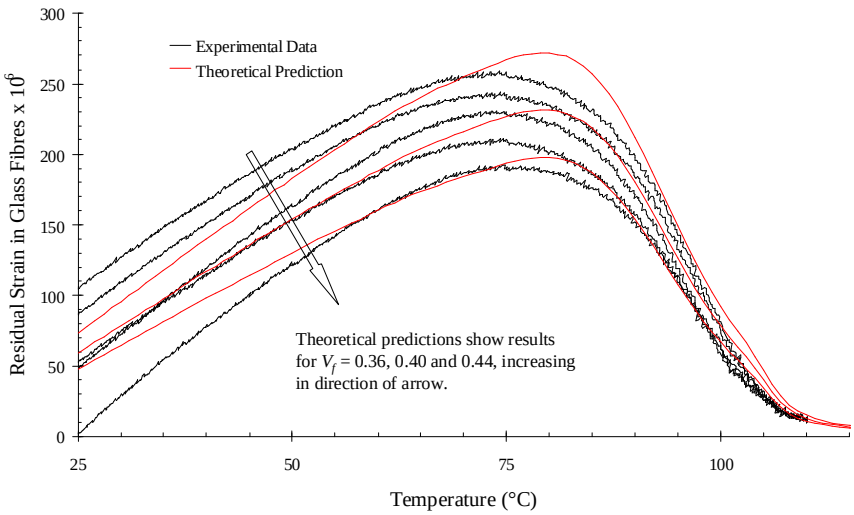


Figure G.8: Comparison between predicted residual strain variation and experimental data

calculated for the unloaded specimens. The resultant strain variation is presented in Figure G.8 alongside experimental data from Figure 6.18.

The overall strain response of the preloaded specimens is predicted by adding changes to the residual strain data presented in Figure G.8 to the strain response of unstressed glass fibre. Predicted strains are overlaid on experimental data in Figure G.9.

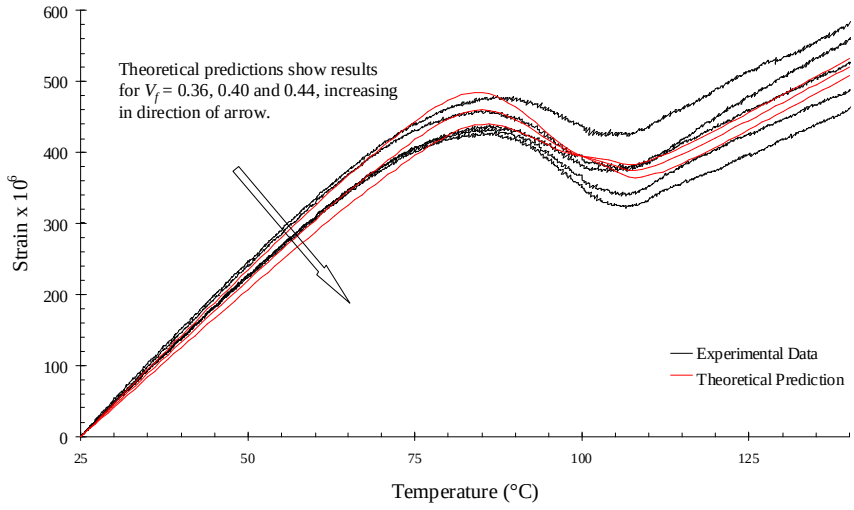


Figure G.9: Comparison between predicted strain variation and experimental data

G.4.3 Residual matrix stresses and strains at 25°C

The longitudinal matrix stress is found using the same approach presented Appendix G.3.3. By considering force equilibrium in the longitudinal direction and using the longitudinal fibre stresses presented in Appendix G.4.1, the longitudinal matrix stress follows:

-0.79 MPa $\geq \sigma_m \geq$ -0.85 MPa

The transverse stresses in the matrix are identical to those of the fibre at the fibre/matrix interface, presented in Appendix G.4.1. They vary logarithmically in opposite directions, however, with increasing radial distance from the fibre.

The longitudinal matrix strain is found by considering the free fibre and matrix strains in combination with the known residual strain in the fibre. The preloaded specimens are identical to the unloaded specimens apart from the deliberate application of a fibre prestrain. This prestrain was calculated in Appendix G.4.2 as 5171 $\mu\epsilon$. This value results in an average fibre strain of 59 $\mu\epsilon$ in the preloaded specimens. If the average fibre strain for the preloaded specimens is taken as 47 $\mu\epsilon$ however, to be consistent with analysis presented in Appendix G.4.1, the fibre preload can be scaled as follows:

$$P = \frac{47 + 224}{59 + 224} \, 5171 \; \mu\epsilon = 4952 \; \mu\epsilon$$

The mismatch in the free strains of the matrix and fibre in the unloaded specimens is calculated in Appendix G.3.3 as 3542 $\mu\epsilon$, with the free contraction of the matrix being larger than that of the fibre. Once the deliberate fibre preload is released, the free contraction of the fibre is larger than that of the matrix by 1410 $\mu\epsilon$. Since the free fibre contraction is larger than that of the matrix, it is expected that the fibre is strained in tension and the matrix strained in compression, the sum of the two residual strain magnitudes being equal to the mismatch in free strains. The residual fibre strain has been measured as 47 $\mu\epsilon$ and so the residual strain in the matrix is equal to -1363 $\mu\epsilon$.

G.5 Annealed specimens

The annealed specimens were manufactured by heating the preloaded specimens to 80℃ for 100 hours with the intention that residual stresses would relax through creep processes. There was thus the inherent assumption that linear viscoelasticity is not applicable under these conditions and that relaxation occurs through non-linear processes. The validity of this assumption must be investigated. This can be done by comparing the measured residual strain of annealed specimens against that of preloaded specimens at 80℃.

If linear viscoelasticity applies under these conditions, it is expected that viscous stresses relax until only elastic stresses remain. Since the rate of heating is deliberately kept low to facilitate the relaxation of viscous stresses, the measured residual strain of the preloaded and annealed specimens should be identical, or very similar, if linear viscoelastic conditions exist at 80℃.

Measured residual strain data indicate that the strains of the preloaded and annealed specimens are clearly different at 80℃. The average longitudinal strain of the preloaded specimens at 80℃ is measured as approximately 216 $\mu\epsilon$ whereas that of the unloaded specimens is only 157 $\mu\epsilon$. The strains in the annealed specimens have therefore relaxed through approximately 59 $\mu\epsilon$ relative to the preloaded specimens. Linear viscoelasticity clearly does not apply in the preloaded specimens at 80℃ and so the annealed specimens were created through non-linear creep processes.

These measured results are confirmed to some extent by the literature. Although no data could be found for vinyl-ester resin, it has been shown that the creep of a polyester resin loaded in compression at room temperature is no longer linearly dependent on stress above 19.6 MPa.[201] The mobility of the polymer chains in the resin is dependent on an Arrhenius type relationship,[204] and so the creep rate increases exponentially with temperature. It is therefore expected that linear viscoelasticity breaks down in polyester resin at compressive stresses significantly lower than 19.6 MPa at 80℃. Vinyl-ester resin is similar to polyester resin and so the stress at which linear viscoelasticity is no longer valid in vinyl-ester resin can be expected to be comparable to that in polyester resin.

The elastic stresses in the preloaded specimens can be determined at 80℃ through the use of equations B.26 and B.28. These equations predict the longitudinal fibre stress to be 16.63 MPa which corresponds to a longitudinal matrix stress of approximately -11.1 MPa. Although the longitudinal stress in the resin is not large, it is a

significant fraction of -19.6 MPa and so it is possible that it exceeds the limit applicable to linear viscoelasticity at 80℃ and that non-linear creep relaxation therefore occurs.

G.5.1 Residual stresses at 25℃

Although the stress state in the preloaded specimens can be estimated prior to annealing, the stresses that are present in the annealed specimens cannot be determined with the analysis technique used in this work. This technique is based on elasticity and cannot account for the strains that develop as a result of non-linear creep during the annealing process. Proper analysis of the annealing process requires a three-dimensional, non-linear solution that incorporates non-linear matrix rheology, and is consequently not feasible in this work.

It is tempting, however, to estimate limits to the stress state in the annealed specimens by evaluating logical constraints on the ratio of transverse and longitudinal stresses. This allows the relative importance of thermal and preload stresses to be assessed for each limiting state and consequently enables the corresponding stress limits at 25℃ to be calculated.

This approach was attempted, and it was found that the strain variation corresponding to all potential limiting stress states are indistinguishable from each other even though the longitudinal and transverse stresses vary significantly between stress limits. As an illustration of this effect, the strain variation arising from two different loading combinations is presented in Figure G.10 for a fibre volume fraction of 40%. One strain variation arbirarily assumes that the combined thermal and cure stresses are zero at 88℃ and that a preload strain of 4057 $\mu\epsilon$ exists. The other strain variation arbitrarily uses a temperature of 34.6℃ and zero preload strain. The calculated strain in both cases matches the measured longitudinal strain of 157 $\mu\epsilon$ at 80℃.

It is clear that the strain variations presented in Figure G.10 are identical and that neither matches the experimentally measured data particularly well. Even if reasonable estimates of the limits to the possible stress states are determined, the predicted strain variation will be identical to that shown in Figure G.10 and so will not correspond well with experimental data. There is is thus no point in spending much time in finding accurate limits to the possible stress states in the annealed specimens since it is clear that these estimates are not accurate.

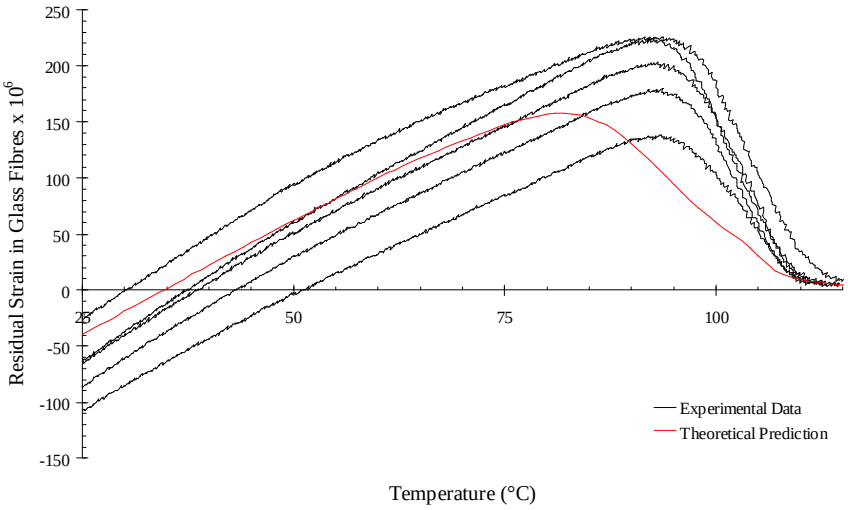


Figure G.10: Comparison between predicted residual strain variation and experimental data

The predicted residual strain response and the overall strain variation of the annealed specimens are however presented in Figures G.11 and G.12. These data are presented to provide figures that correspond to the data presented for the unloaded and preloaded specimens.

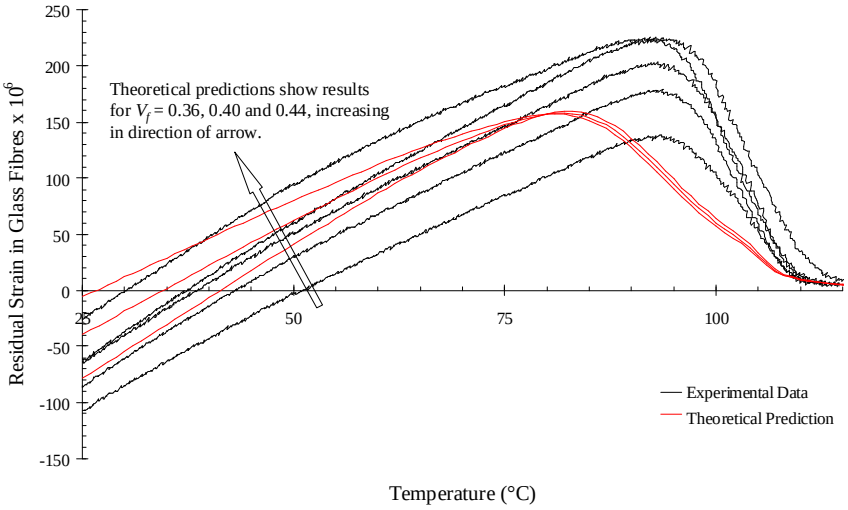


Figure G.11: Comparison between predicted residual strain variation and experimental data

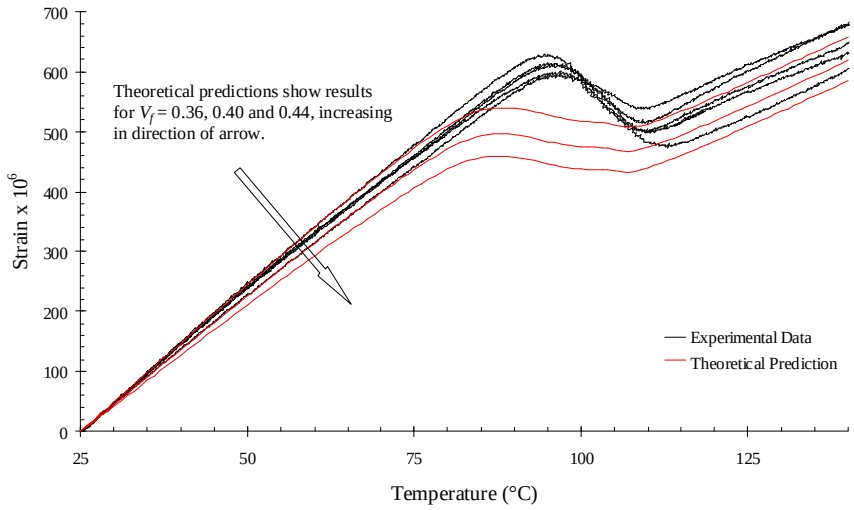


Figure G.12: Comparison between predicted residual strain variation and experimental data